College of Health and Life Sciences

Department of Life Sciences

Division of Biosciences

Investigation the Role of PARP Inhibitors in Ovarian Cancer Using *In vitro* Models and Clinical Samples

A thesis submitted for the degree of Doctor of Philosophy

by

Sayeh Saravi

Declaration

I hereby declare that all the research presented in this thesis is my own work, except where otherwise specified, and has not been submitted for any other degree.

Sayeh Saravi

Abstract

Ovarian cancer (OC) is the fifth most common cancer in women worldwide with 14.1 million incidences. Approximately 5 out of 10 women with ovarian cancer have BRCA mutations (BRCA-m) or other defects in DNA repair. The current management of BRCAm-associated ovarian cancer is not different from the treatment of the non-BRCA stage-matched cases. However, recent data suggest that these BRCA-m cancers should be treated as a distinct disease entity, since BRCA mutation status has a significant influence on OC patient outcomes. Poly (ADP-ribose) polymerase (PARP) inhibitors effectively can destroy tumour cells with defective BRCA1 or BRCA2 genes through the concept of synthetic lethality. Early results of phase I and II of clinical studies have shown that rucaparib -a new PARP inhibitor-, has an efficacy in BRCA-m OC cells with homologous recombination deficiency (HRD) loss of heterozygosity (LOH), although it might also exert a beneficial effect on non-BRCA-m ovarian cancer.

In this work, I evaluate the effects of BRCA2 mutation on homologous recombination (HR) efficiency by using immunofluorescence technique (γ-H2AX assay). Moreover, I report significantly higher levels of γ-H2AX staining in BRCA2-m OC cell lines, compared to control (BRCA2-wt) cell lines which shows that HR pathway can be affected by BRCA2 deficiency. My results indicate the lack of ability to fully repair of DNA damage in cancer cells with BRCA2-mutation.

In addition, I show a good connection between the phosphorylation level of γ-H2AX foci and the H2AX gene expression *in vitro*. I present a complete overview of the alterations at gene and protein level of H2AX in OC and propose its potential as a predictive biomarker. The TCGA databases revealed that H2AX is overexpressed in OC in comparison to controls. In terms of prognostic value, it has been showed that higher expression of H2AX is related to better overall survival (OS), whereas there is no apparent difference on disease free interval (DFI) in the ovarian cancer cohort. Moreover, I prove high level of H2AX expression in different type of OC while there is no correlation between H2AX overexpression and FIGO stage.

I also study the effects of Rucaparib *in vitro*. The BRCA2 mutant ovarian cancer cell line PEO1 exhibited higher PARP1 activity when treated with H_2O_2 compared to BRCA2 wild type cell lines (PEO4 and SKOV3). The migratory and proliferative capacity of PEO1 cells was compromised following treatment with rucaparib 10 μM compared to BRCA2 wild-type

cell lines. These results suggest that ovarian cancer patients with BRCA mutation have the higher likelihood of benefiting from treatment with PARP inhibitors.

Finally, I demonstrate that liquid biopsies offer a promising alternative to tissue samples, providing a non-invasive diagnostic approach or aid in serial monitoring of disease evolution. I assess the levels/staining patterns of γ-H2AX and WT1 in a clinical study (CICATRIx) of patients (BRCA-wt and BRCA-m); and analyse these data to identify the clinical validity of this staining with patient outcome. I determine the practicality of γ-H2AX quantification as a predictive biomarker of response in CTCs in OC patients. My results show that overall, the level of CTCs with positive γ-H2AX staining is highest prior to chemotherapy treatment and fell during treatment to the lowest at the end of treatment.

Collectively my data suggest that liquid biopsies can be used for monitoring of disease progression in OC patients treated with chemotherapeutic agents and/or PARP inhibitors. Preclinical models developed in this study can also be used in the future to identify effects of novel drugs.

To my mum, Mahnaz, my dad, Masoud, for all the sacrifices & to my brother, Sina

you are everything to me …

Acknowledgments

Firstly, I would like to express my deepest gratitude to my supervisor, Dr. Emmanouil Karteris for his continuous help and support throughout this study, especially during the challenging times, for believing in me and giving me this opportunity. I am incredibly grateful for your guidance, support and understanding at tough times. You have given me so much; experience, confidence in myself, emotional, and professional, thank you so much.

I also wanted to thank my second supervisor Dr Sabrina Tosi for encouragement and helping me with various needs during my degree, and I value all your support. I would like to extend my gratitude to Dr Marcia Hall, as a clinical supervisor, for her support and advice on how to improve my work. Your guidance as a clinical supervisor has been invaluable.

My continuous thanks also go to my research group, Rooban for all the help in the lab and more importantly, all the jokes and laughs, and Zena for helping me with clinical part of the project and her opinions and guidance were invaluable to this project.

Last but not least, I would like to say special appreciations to my wonderful family, for their love, support long-suffering listening to my difficulty throughout my PhD studies and always encouraging me to keep going. Words cannot describe how lucky I am to have your love and support and to know that you are always there by my side in happiness and grief. I love you all so much.

Publications

- Saravi S, Katsuta E, Jeyaneethi J, Amin HA, Kaspar M, Takabe K, Pados G, Drenos F, Hall M, Karteris E. H2A Histone Family Member X (H2AX) Is Upregulated in Ovarian Cancer and Demonstrates Utility as a Prognostic Biomarker in Terms of Overall Survival. J Clin Med. 2020 Sep 2;9(9):2844. doi: 10.3390/jcm9092844. PMID: 32887437; PMCID: PMC7565050
- Saravi, S.; Alizzi, Z.; Tosi, S.; Hall, M.; Karteris, E. Preclinical Studies on the Effect of Rucaparib in Ovarian Cancer: Impact of BRCA2 Status. *Cells* **2021**, *10*, 2434. https://doi.org/10.3390/cells10092434
- Clinical chapter, manuscript in preparation

Table of contents

List of figures

List of tables

Abbreviation

53BP1	p53-binding protein 1
AD	Auto-modification domain
AQ	Absolute quantification
AR	Androgen receptor
ARID1A	AT-Rich interaction domain 1A
ART	ADP-ribosyl transferase
ATM	Ataxia telangiectasia mutated kinase
ATR	ATM- and Rad3- related kinase
BARD1	BRCA1-associated ring domain protein 1
BAX	BCL2-associated X protein
BCL2	B-cell lymphoma 2
BER	Base excision repair
BME	Beta-mercaptoethanol
BRAF35	BRCA2-associated factor 35
BRCA	Breast cancer susceptibility gene
BRCT	BRCA1 C-terminal
BRIP1	BRCA1-interacting protein 1
BSA	Bovine serum albumin
CA125	Cancer antigen 125
CAT	Catalytic domain
CCNE1	Cyclin E1
CDK	Cyclin-dependent kinase
cDNA	Complementary DNA
CFI	Chemotherapy free interval
CHK1/2	Checkpoint kinase1/2
CHEK1/2	Checkpoint kinase ½
CT	Computed tomography
CTCs	Circulating tumour cells
ctDNA	Circulating tumour DNA
CtIP	C-terminal binding protein-1 interacting protein
ctNAs	Circulating nucleic acids
CTNNB1	beta-catenin 1

DAB	3,3’-Diaminobenzidine
DAF	Data analysis file
DDR	DNA damage response
DEPTOR	DEP domain-containing mTOR-interacting protein
DFI	Disease free interval
DFS	Disease free survival
DMEM	Dulbecoo’s modified eagle medium
DMSO	Dimethyl sulfoxide
DNA	Deoxy-ribonucleic acid
DNA-PK	DNA Protein kinase
dNTP	Nucleoside triphosphate
DPX	di-N-butyl phthalate in xylene
DSB	Double strand break
EGFR	Epidermal growth factor receptor
ELISA	Enzyme-linked immunosorbent assay
EOC	Epithelial ovarian cancer
EpCAM	Epithelial cell adhesion molecule
ERBB2	Erb-B2 receptor kinase 2
ERCC1	Excision repair cross-complementation 1
EMT	Epithelial to mesenchymal transition
FA	Fanconi anaemia
FACS	Fluorescence-activated cell sorting
FBS	Foetal bovine serum
FDA	Food and drug administration
FGF	Fibroblast growth factors
FITC	Fluorescein isothiocyanate
FSH	Follicle-stimulating hormone
GnRH	Gonadotropin-releasing hormone
GSEA	Gene set enrichment analysis
GTEX	Genotype-tissue expression
GWAS	Genome-wide association study
H2AFX	H2A histone family member X
H2AX	Histone H2AX phosphorylated on serine-139
H_2O_2	Hydrogen peroxide

HD	Helical subdomain
HER2	Human epidermal growth factor receptor 2
HGSC	High grade serous carcinoma
HIPEC	Heated intraperitoneal chemotherapy
HR	Homologous recombination
HRD	Homologous recombination deficiency
HRT	Hormone replacement therapy
HTA	Human tissue act
ICC	Immunocytochemistry
IDS	Interval debulking surgery
IGF	Insulin like growth factor
ITT	Intention to treat
IR	Ionizing radiation
LGSC	Low grade serous carcinoma
LH	Luteinizing hormone
LOH	Loss of heterozygosity
MDC1	Mediator of DNA damage checkpoint protein 1
MEFs	Mouse embryonic fibroblasts
MET	Mesenchymal to epithelial transition
MiRNA	MicroRNA
MMC	Mitomycin C
MMEJ	Microhomology-mediated end joining
MMS	Methane-sulfonate
mRNA	messenger ribonucleic acid
MTA	Material transfer agreements
mTORC1	Mammalian target of rapamycin complex 1
MUC1	Mucin 1 cell surface associated
NACT	Neo-adjuvant chemotherapy
NAD^+	Nicotinamide adenine dinucleotide
NAT	Normal adjacent tissue
NBN	Nibrin
NHEJ	Non-homologous end joining
NICE	National institute for health and care excellence
NLS	Nuclear localization signals

NRES	National research ethical authority
NTT	Normal tissue toxicity
OB	Oligonucleotide/oligosaccharide-binding
OC	Ovarian cancer
ORR	Objective response rate
OS	Overall survival
OSE	Ovarian surface epithelial
PALB2	Partner and localizer of BRCA2
PARP	Poly-adenosine diphosphate-ribose polymerase
PBS	Phosphate buffered saline
PCR	Polymerase chain reaction
PCS	Primary cytoreductive surgery
PD	Pharmacodynamics
PDGF	Platelet-derived growth factors
PFA	Paraformaldehyde
PFS	Progression-free survival
PI	Propidium iodide
PIK3CA	PI3kinase component
PP2A	Protein phosphatase 2A
pRb	Protein retinoblastoma
PS	Phosphatidylserine
PTEN	Phosphatase and tensin homolog
PTM	Post-translational modification
RBC	Red blood cell
RICTOR	Rapamycin-insensitive companion of mammalian target of rapamycin
RNA	Ribonucleic acid
ROS	Reactive oxygen species
RPA	Replication protein A
RPM	Revolutions per minute
RPMI	Roswell park memorial institute
RQ	Relative quantification
RT	Reverse transcriptase
RT-PCR	Reverse-transcriptase polymerase chain reaction
SDSA	Synthesis-dependent strand-annealing

SDS	Sodium dodecyl sulfate
SIR	Silent information regulator
SMC	Structural maintenance of chromosomes
SNP	Single-nucleotide polymorphism
SSA	Single strand annealing
SSB	Single strand break
TBST	Tris-buffered saline with tween
TE	Tryple express
TP53	Tumour protein 53
TNBC	Triple negative breast cancer
TSG	Tumour suppressor gene
TSGA	The cancer genome atlas
UV	Ultra-violet
VEGF	Vascular endothelial growth factor
WGR	Tryptophan-glycine-arginine-rich domain
WT1	Wilms tumour 1
XLF	XRCC4 like factor
XRCC	X-ray repair cross complementing protein

Chapter1: Introduction

1. Ovarian cancer

Ovarian cancer (OC) is the fifth most common cancer worldwide and the most lethal gynaecologic cancer which after diagnosis, less than 50% of patients can survive more than five years after diagnosis (Doubeni, Doubeni and Myers, 2016).The main problem is that more than 75% of women with ovarian cancer are diagnosed at late stage with symptoms that are nonspecific. Therefore, it is hard to diagnose early-stage disease which is usually asymptomatic. Moreover, the awareness of the risks and symptoms of OC between women universally is low. On the other hand, these symptoms can overlap with other signs of common abdominal and gastrointestinal diseases and it is one of the reasons regarding to disease diagnosis at advanced stage in almost 70% of patients (Gaitskell *et al.*, 2018). The rate of early diagnosis is low, although guidelines advise against routine screening for OC in average-risk women since screening such as routine pelvic examinations, is ineffective and combined with injury and harm (Doubeni, Doubeni and Myers, 2016). Consequently, it is necessary to embark on further studies on diagnostic and prognostic methods, evolution, and discovery of new biomarkers and future screening approaches using both tissue and liquid biopsies to help patients at high risk of disease.

1.1. Physiological function of the ovaries

There are two ovaries which are part of a woman's reproductive system. The role of ovaries includes hormonal secretion, production of oocytes during the monthly cycle (in women who are at the age of childbearing) and subsequent release for possible fertilisation (Huang *et al.*, 2018). Oestrogen and progesterone are the two principal hormones that control the reproductive cycle and are produced in the ovaries. Through every menstrual cycle, one or more oocytes are released in the ovulation process. The level of oestrogen before ovulation reaches high and after that, progesterone levels increase gradually. If the oocyte fails to fertilise, it will be flushed from the uterus and the level of hormones returns to normal (Tortora and Derrickson, 2017).

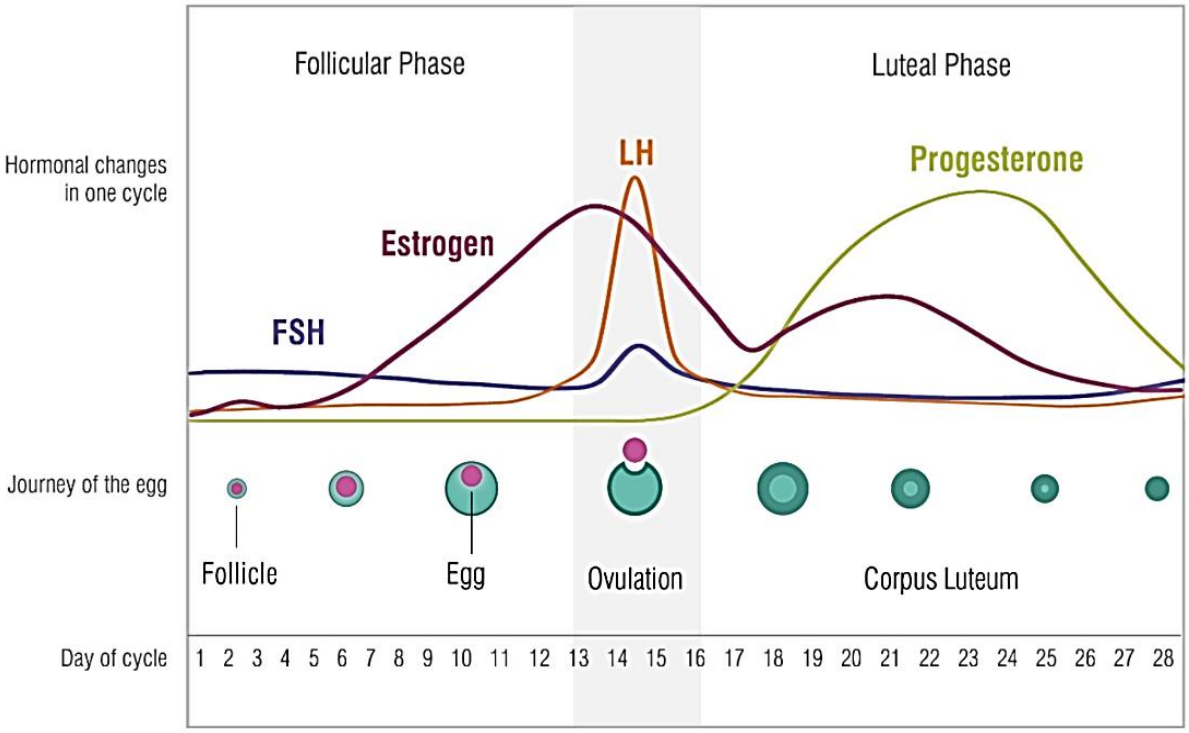

Figure 1. An example of a 28-days cycle. This figure displays the hormonal changes and day of ovulation which varies with cycle length. Credit: (Hauck, 2020).

The function of ovaries is controlled through a complicated control system which includes the ovaries, hypothalamus and pituitary. All these organs interact with each other through positive and negative feedback loops.

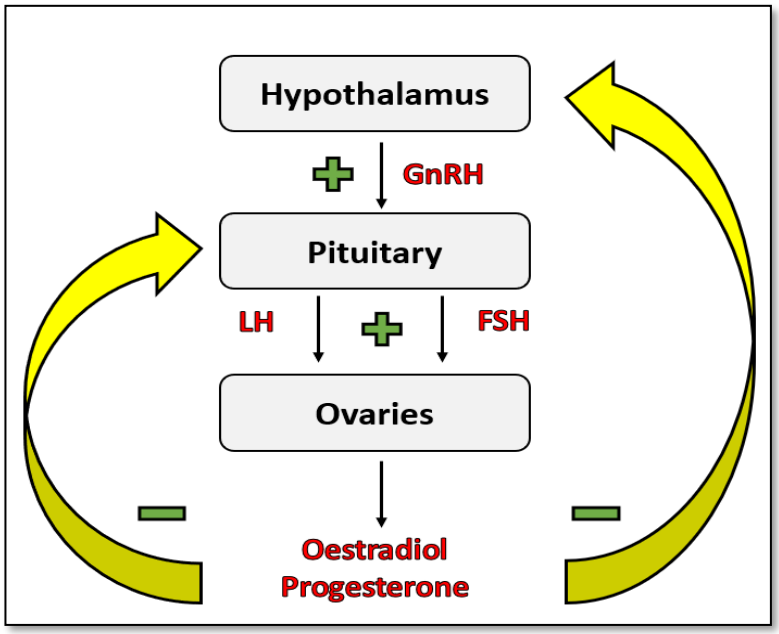

Figure 2. A diagrammatic figure of the hypothalamic-pituitary-ovarian axis. This figure displays the origins, target organs and response mechanisms of the main hormones involved in the hypothalamic-pituitary-ovarian axis. Adapted from (Sun *et al.*, 2013).

Neurons in the hypothalamus produce gonadotropin-releasing hormone (GnRH), and this hormone binds to particular receptors in the pituitary, comprising of gonadotropins follicle-stimulating hormone (FSH) and luteinizing hormone (LH) synthesis and thus release into the circulation. Once they bind to their individual receptors at the ovary, FSH and LH activate follicular maturation, ovulation and corpus luteum formation. Once the follicle becomes the corpus luteum, oestrogen and progesterone are produced which inhibit the production of FSH and LH by the pituitary. The level of progesterone drops when the egg is not fertilised and it is excreted alongside the uterine lining (Tortora, Derrickson and Nielsen, 2011).

1.2. Epidemiology of ovarian cancer

Every year, 7,400 new ovarian cancer (OC) cases are diagnosed in the UK and 28% of these cases affect women aged 75 and over. Although, the rate of ovarian cancer incidence in the UK have been remained stable since the 1990s. Ovarian cancer is ranked the 6th most common cancer in women in the UK (CRUK, 2018a). High rates of ovarian cancer are recorded in European countries and North America and lowest levels in Western Africa and Asia. This variation between geographical regions might be associated with a different prevalence of risk factors, use of screening, and diagnostic approaches (WorldAtlas, 2017).

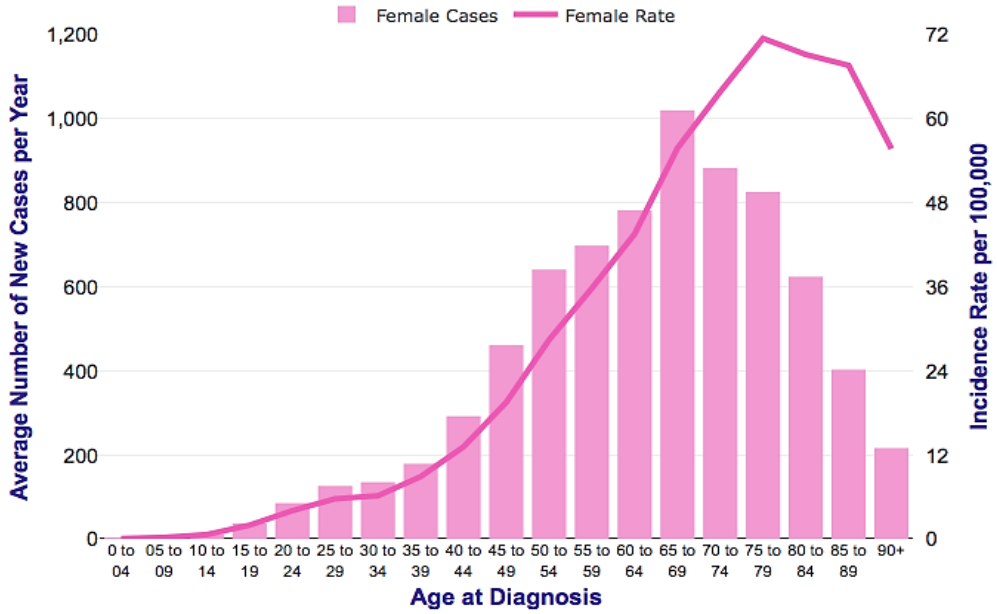

Figure 3.Average number of new cases per year and age-specific incidence rates per 100,000 population (Females, UK, 2013-2015). The figure above represents the number of new cases per year which the highest cases shown in the 65-69 aged females. For ovarian cancer, like most other cancer types, incidence increases with age. A drop or plateau in incidence in the oldest age clusters frequently shows reduced diagnostic activity possibly due to general ill health. Credit: (CRUK, 2018a).

1.3. Risks and causes of ovarian cancer

There are several risk factors for ovarian cancer, but age is the one which is strongly related to ovarian cancer which was displayed in previous section (Figure 4). Furthermore, incessant ovulation and level of sex hormones such as oestrogen, progesterone, and androgens can be associated with ovarian cancer causes (Ho, 2003). It has been estimated that 1% of ovarian cancer cases are related to oestrogen hormone replacement therapy (HRT) which is used to control the conditions of menopausal symptoms. This treatment is recommended for lowest effective dose and shortest time-period. There are other factors connected to ovarian cancer such as smoking and ionizing radiation (CRUK, 2018b), family history of ovarian cancer, a genetic condition (Lynch syndrome), obesity, diabetes and endometriosis (Rossi and La Vecchia, 2014). One of the most significant factors is related to hereditary cases with breast cancer gene type 1 and 2 (BRCA1/2). It has been established that these two genes cause 3-12% of all OCs. The risk of epithelial OC, associated with BRCA1 mutation is 40-50% and for those with BRCA2 mutation is 20-30% (Russo *et al.*, 2009).

1.4. Types of ovarian cancer

The most common type is epithelial ovarian cancer accounting for 90% of all cases. This cancer occurs on the surface layer covering the ovary. There are different types of epithelial ovarian cancers: (1) serous, (2) endometrioid, (3) clear cell, (4) mucinous, and (5) undifferentiated (Gaitskell *et al.*, 2018). 68-71% of the ovarian cancer is related to serous epithelial cancer. It has been proposed that the high-grade serous (HGS) actually starts with cells at the end part of fallopian tumor rather than the ovary surface and eventually spread to ovary (CRUK, 2019b). The low grade serous (LGS) carcinomas are relatively rare, grow slowly and often diagnosed in younger women (Webb and Jordan, 2017). Endometrioid tumor cells can be an independent separate endometrial tumor or endometrial hyperplasia which is a thickening of the inner lining of the uterus. Clear cell carcinoma is a rare type of ovarian cancer, 12-13% of all epithelial OC cases (Rojas *et al.*, 2016).

There are two types of mucinous cells including, primary ovarian cancer and metastatic from other sites. Many cases of epithelial ovarian cancer are undifferentiated due to several cancer cells which are underdeveloped, and it is hard to recognize their origin site (Hacker and Rao, 2017). In the remaining 10% of ovarian cancers, 5-8% are diagnosed with stromal cells tumor

and 3-5% of patients have germ cell ovarian cancer and commonly occurs in younger women (McCluggage, 2011).

There are some other rare types of ovarian cancer which do not start with these cells. For instance, sarcoma is a type of cancer that originates in connective tissue in the body. Some types of ovarian cancer are categorized as fallopian tube cancer which develops in the fallopian tubes. Symptoms of this cancer also may mimic those of other gynecological problems such as abnormal vaginal bleeding, abdominal pain or feeling of pressure in the abdomen. Therapeutic methods for this type of cancer are similar to ovarian cancer treatments. This type of cancer is very rare and accounts for only 1-2% of all gynecologic cancers (Kyo *et al.*, 2020). Figure 4 displays the different ovarian cancer subtypes.

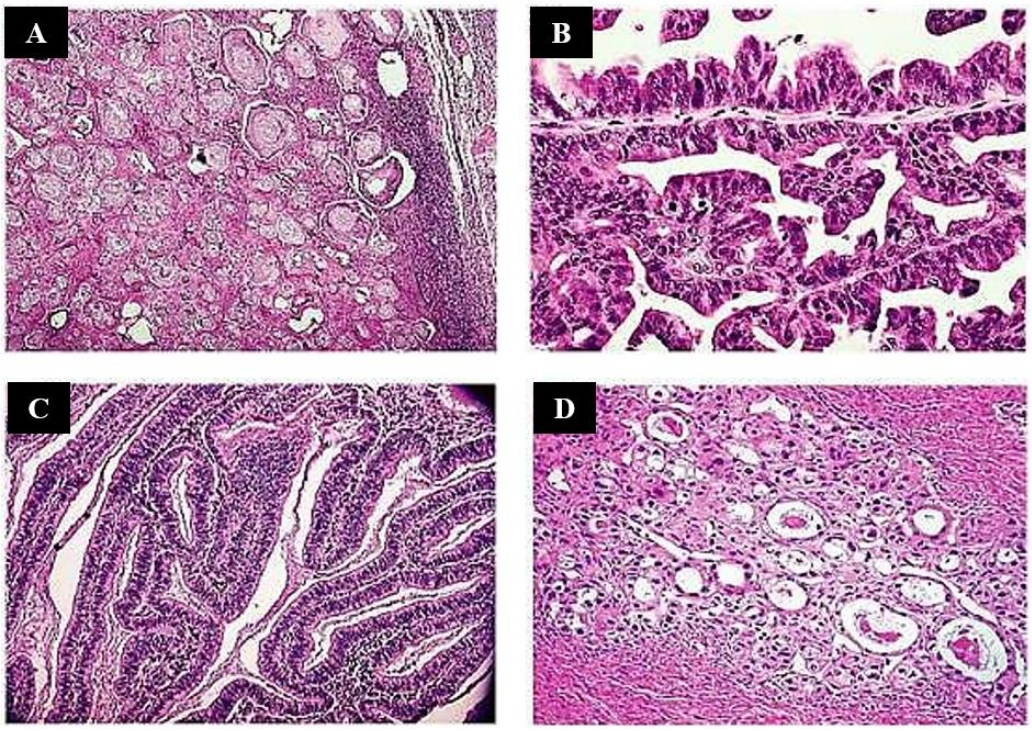

Figure 4.Histological preparations of haematoxylin and eosin-stained ovarian cancer subtypes. A. High-grade serous carcinoma. B. Mucinous carcinoma. C. Endometrioid carcinoma. D. Clear cell carcinoma. Credit: (WHEC, 2014).

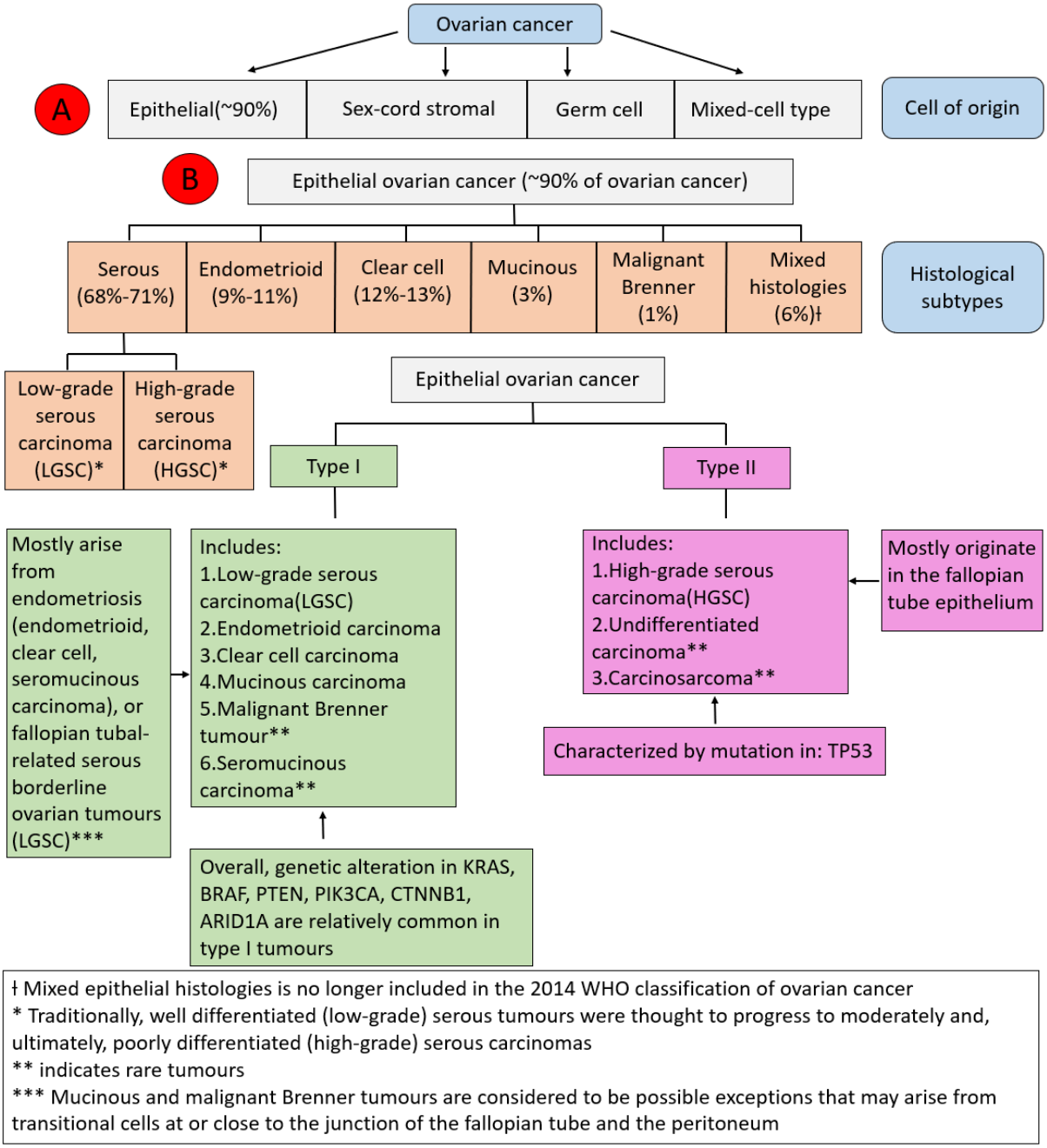

Figure 5. Histological subtypes of OC and widely accepted epithelial OC classification paradigm based on clinicopathologic and molecular evidence that type I and type II tumors develop through different pathways. Adapted from (Rojas *et al.*, 2016) (Kurman and Shih, 2016) (McCluggage, 2011).

1.5. Stages and grades

The stage of a cancer is about, how far it has grown and if it has spread in the vicinity or distant organs. Clinicians use a simple 1 to 4 staging system which is called the FIGO (Federation International of Gynaecological Oncologists) system for ovarian cancer (CRUK, 2019a).

Stage 1: In this stage, the tumour is only in the ovaries and divided into three groups.

1. **Stage 1A:** the cancer is completely inside one ovary.

2. **Stage 1B:** the cancer is completely inside both ovaries.
3. **Stage 1C:** as well as tumour cells in one or both ovaries, there is some tumour cells on the surface of an ovary. There are some tumour cells in fluid taken from inside abdomen during surgery or the ovary ruptures (bursts) before or during surgery.

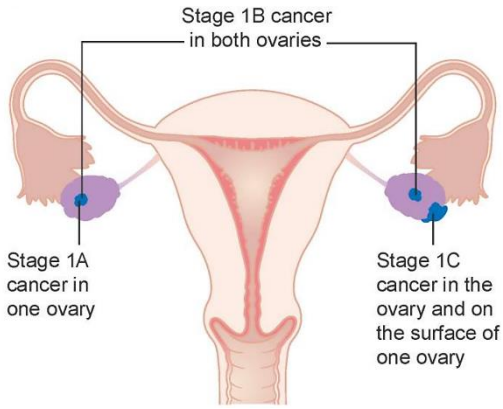

Figure 6. Schematic image of stage 1 in OC. The figure displays different stage 1 and where it is located. Credit: (CRUK, 2019d).

Stage 2: In this stage, tumour cells has grown outside the ovaries and are growing within the area circled by hip bones (the pelvic) and might also be in the abdomen. There are three groups for this stage.

1. **Stage 2A:** the tumour has grown into the fallopian tubes or the womb
2. **Stage 2B:** the tumour has grown into other tissues in the pelvis, for instance the bladder or rectum.
3. **Stage 2C:** the tumour has grown into other tissues in the pelvis and there are cancer cells in fluid taken from inside the abdomen.

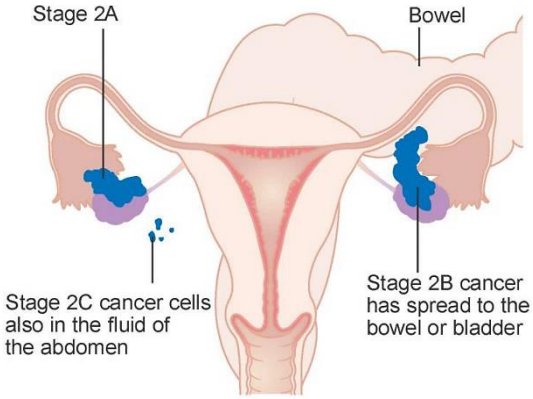

Figure 7.Schematic image of stage 2 in OC. The figure displays different stage 2 and where it is located. Credit: (CRUK, 2019e).

Stage 3: this stage means the tumour cells has spread outside the pelvis into the abdominal cavity, if is found in the lymph nodes in your upper abdomen, groin or behind the womb. There are three groups for this stage.

1. **Stage 3A:** tumour growths are found in tissue samples taken from the lining of the abdomen.
2. **Stage 3B:** tumour growths are found on the lining of the abdomen and their size is about 2cm or smaller.
3. **Stage 3C:** tumour growths bigger than 2cm and are found on the lining of the abdomen, and also it can be found in lymph nodes in the upper abdomen, groin and/or behind the womb.

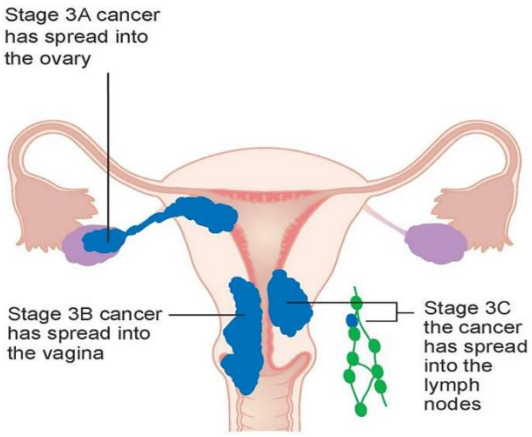

Figure 8. Schematic image of stage 3 in OC. The figure displays different stage 3 and where it is located. Credit: (CRUK, 2019f).

Stage 4: this stage means the tumour has spread to other body organs some distance away from the ovaries such as liver or lungs. There are two groups for this stage.

1. **Stage 4A:** tumour has caused a build-up of fluid in the lining of the lungs (called the pleura) and it is called pleural effusion.
2. **Stage 4B:** the tumour has spread to the inside of the liver or spleen, to the lymph nodes in the groin or outside the abdomen and/or to other organs such as the lungs.

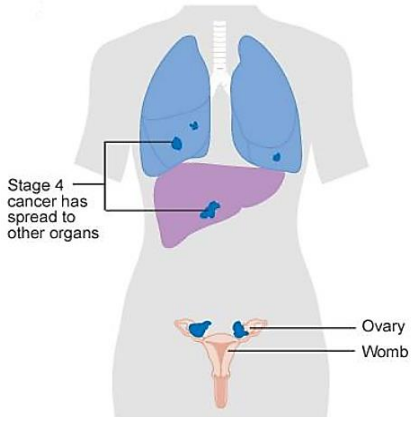

Figure 9. Schematic image of stage 4 in OC. The figure displays different stage 4 and where it is located. Credit: (CRUK, 2019g).

The grade is determined based on cell morphology: the lower the grade, the more similar the morphology to normal cells. Staging can give the clinician an idea of how the cancer might behave. There are 3 grades comprising of grade 1 or well differentiated, grade 2 or moderately differentiated and grade 3 or poorly differentiated (or undifferentiated) (CRUK, 2019a). Normal cells grow and mature specifically for their role through differentiation process. However, there are some cancer cells which looks like normal cells and are defined as well differentiated or low grade that are more likely to grow slowly. There are other kinds of cancer cells that look underdeveloped and nothing like a normal cell, known as undifferentiated or high grade that tend to grow and spread more quickly than low grade cancers (CRUK, 2019a).

1.6. Genetic mutations in ovarian cancer

It has been shown that there are five major subtypes of ovarian cancer with specific genetic profiles, and they should be treated as distinct diseases. 70% of ovarian cancer is HGS which is defined by TP53 mutation (96%), homologous recombination DNA repair defects (~50%), Cyclin-E1 (CCNE1) amplification and genomic instability. By contrast, LGS carcinoma represents TP53 wildtype and display frequently activating mutations of RAS pathway (Beaufort *et al.*, 2014). Additionally, RAS pathway mutations are found in 40% of the mucinous cancer cells. Moreover, it was reported that the frequency of BRAF mutations in LGSC varies from 2% to 33% (Moujaber *et al.*, 2018). However, endometrioid and clear cell type, show PIK3CA mutation with 12% and 31% respectively and for ARID1A mutation; 30% and 46% respectively (Beaufort *et al.*, 2014). Figure 10 displays the histological and molecular sub-types of epithelial ovarian cancer.

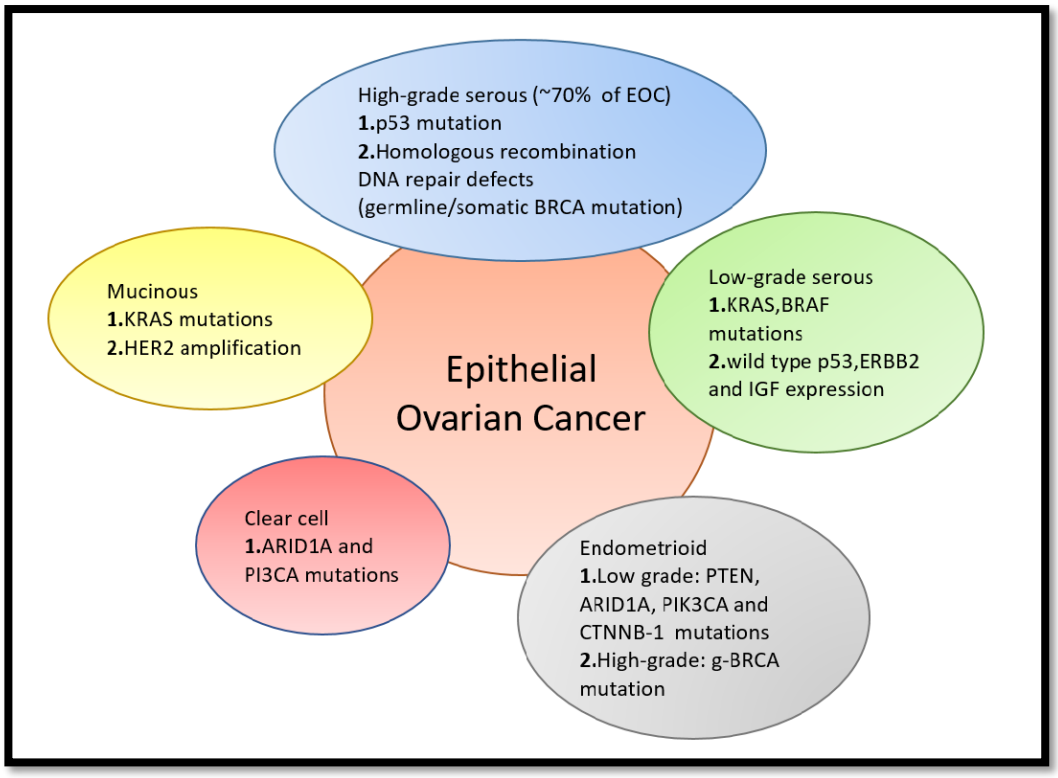

Figure 10. Histological and molecular sub-types of epithelial ovarian cancer. Adapted from (Ledermann, Drew and Kristeleit, 2016).

1.7. Symptoms

As mentioned, ovarian cancer symptoms can be non-specific, especially in the early stages of the disease. There are many signs that can be alarming such as, feeling full quickly, losing appetite, feeling pain in the abdomen or at the lower part of the abdomen continuously (NHS, 2020), increasing the size of abdomen and feeling bloating, feeling too tired without an explanation, losing weight unexpectedly (ACS, 2018), in the cases with irritable bowel syndrome changing the habit of bowel particularly if it begins after age of 50, needing to urinate more than usual, back pain, vaginal bleeding particularly after menopause (Smits *et al.*, 2017). If these symptoms are not normal it is necessary to be checked by a clinician. It has been recommended by the national institute for health and care excellence (NICE) if someone shows these signs 12 or more times in a month, need to do tests according to ovarian cancer (NICE, 2011).

1.8. Diagnosis

Ovarian cancer can be diagnosed using a number of different approaches. These include pelvic examination which is carried out by a specialist doctor who will look for symptoms of disease in an individual organ. Nonetheless, it is not an effective way to identify ovarian

cancer (Sun *et al.*, 2016). The most common screening tools used are measurement of the serum cancer antigen 125 (CA125) and transvaginal ultrasound. Unfortunately, as it has been shown recently, CA125 does not appear to have the required specificity and sensitivity for routine screening of the general population (Van Gorp *et al.*, 2011) (Sharma *et al.*, 2016). In a USA-based study that screened almost 40,000 women (randomized controlled trial) Buys and colleagues (2011) have found no statistically significant reduction in mortality from ovarian cancer in this cohort of women derived from the general population who were screened for ovarian cancer with 6 annual CA125 tests and 4 annual transvaginal ultrasound examinations (Buys *et al.*, 2011).

CA125 cannot be used as a standard method of detection as its levels are increased in all epithelial ovarian cancers (EOC) cases and those patients diagnosed with stage I of EOC, with the incidence of 80% and 50% respectively. Therefore, CA125 can be hardly used as a distinctive factor to predict tumour malignancy which generally can be distinguished from benign tumour through combination of medical history, clinical examination results, imaging data and profile of tumour marker (Van Gorp *et al.*, 2011).

Abdominal ultrasound or transvaginal ultrasound: this test can detect the size of a tumour and any cysts in ovaries. Transvaginal ultrasound can also define the cyst in ovaries and check if the ovaries contain a tumour or not. If the cyst has a substantial region, it is likely that it causes cancer (Sharma *et al.*, 2016). These methods currently fail to identify ovarian cancer at early stage (I and II).

Consequently, innovative approaches for detecting ovarian cancer at the early stage are required (Mahdian-shakib *et al.*, 2016).

1.9. Treatments

1.9.1 Chemotherapy:

A combination of one or two drugs can be used before or after surgery, depending on the stage and grade of cancer. In the first line setting, the chemotherapy drugs used include paclitaxel and carboplatin. With this regime, patients usually have chemotherapy once every three weeks (one cycle) and each session of treatment can take 3 to 4 hours (Clamp *et al.*, 2019). The aim for these patients is to complete six cycles in total. In addition there are some new chemotherapy drugs such as Trabectedin (Yondelis®) and Belotecan (Kang, 2015) which have not been used in general practice.

Despite the progress of first-line treatment in OC patients, it has been shown that some patients with advanced ovarian cancer will develop recurrent disease. Combination of

paclitaxel-platinum has been used as a superior treatment to platinum monotherapy in those patients who have recurrence of disease at least 6 months after initial therapy. Generally, OC patients who relapse after administration of platinum–paclitaxel therapy are at major risk of neurotoxicity after re-treating, due to the cumulative neurotoxicity of platinum and paclitaxel. Although, neurotoxicity can be developed in many patients, frequently resulting in discontinuation of treatment. There are several alternative regimens for those patients who relapse, including Carboplatin-Caelyx, Carboplatin-Gemcitabine, Cisplatin-Etoposide or Paclitaxel or Cyclophosphamide (Pfisterer *et al.*, 2005).

1.9.2. Targeted therapy: One of the successful treatments is shown in Figure 11 and targets the cancer cells while causing little damage to healthy cells. Each of these methods works in a different way. Bevacizumab (Avastin) is a selective inhibitor for vascular endothelial growth factor (VEGF) which plays a significant role in inducing angiogenesis that is crucial for the development of tumour cells. This molecule can shrink or slow the growth of advanced epithelial ovarian cancer cells, particularly when it is used in combination with chemotherapy such as paclitaxel and topotecan (Avastin, 2021). However, there are some side effects including tiredness, high blood pressure, low white blood cells count and bleeding (Grunewald and Ledermann, 2017). This treatment is usually given in the first line of treatment alongside chemotherapy, every 3 weeks for 18 cycles in total.

Approximately 50% of ovarian cancer patients harbour homologous recombination repair deficiencies (HRD) (The Cancer Genome Atlas Research Network, 2011). HRD has been successfully exploited using poly (ADP-ribose) polymerase inhibitors (PARPi) in patients with germline BRCA1/2 mutations (BRCAm) (Gelmon *et al.*, 2011) (Ledermann *et al.*, 2012). PARP inhibitors can be used as a new drug to treat advanced ovarian cancer patients. The use of PARP inhibitor first-line therapy or maintenance therapy can significantly delay the length of time between treatment. It was established in 2018, that using olaparib (PARP inhibitor) as maintenance therapy in OC patients with BRCA mutant gene, was effective and beneficial (NIH, 2019). Additionally, the food and drug administration (FDA) has expanded the indication of olaparib to be used as a first-line maintenance treatment, in combination with bevacizumab, in those patients with homologous recombination deficiency (HRD) (Arora *et al.*, 2021).

Several genetic abnormalities in PI3K/AKT/mTOR signalling genes have been discovered in EOC, including PTEN (5% of HGSOC cases), PIK3CA (in 20% of HGSOC cases), PIK3R1, AKT1/AKT2/AKT3 (in 10-15% of HGSOC cases) and mTOR (Katopodis *et al.*, 2019). The PI3K/AKT/mTOR is one of the main cellular signalling pathways involved in various

cellular activities including cell growth regulation, proliferation, protein synthesis, transcription, as well as angiogenesis. Consistent with its physiological role, it has been established that this pathway is hyperactivated in various cancers such as ovarian cancer and breast cancer which leads to increase the interest in developing inhibitors of this pathway as a treatment for EOC (Andorfer *et al.*, 2016). There are some mTOR inhibitors for OC treatment including Temsirolimus, everolimus, and ridaforolimus. The effects of the combination of mTOR and cytotoxic drugs has been investigated in some trials due to the evidence from preclinical studies which indicating an additional benefit of mTOR inhibitors when combined with chemotherapy, along with considering the use of mTOR inhibitors as monotherapy (Piha-Paul *et al.*, 2014).

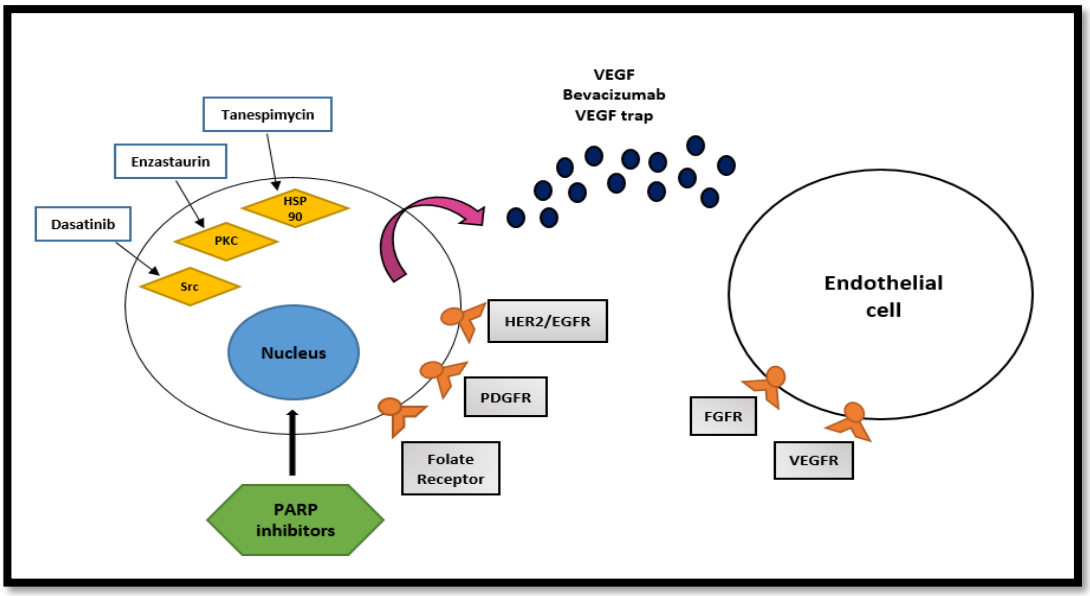

Figure 11.Targeted therapy. The figure above shows the targeted therapy agents which are used in the treatment of epithelial ovarian cancer. Vascular endothelial growth factor (VEGF) is one of the main genetic factors which control tumour angiogenesis and their function is mediated by binding to VEGF tyrosine kinase receptors (VEGFR). Targeting the VEGF pathway has proven to be a successful strategy in cancer treatment. Bevacizumab have demonstrated a benefit for VEGF inhibition. Platelet-derived growth factors (PDGF) and fibroblast growth factors (FGF) pathways have been improved in efficacy of anti-VEGF therapies. Targeting the base excision repair pathway with poly adenosine diphosphate-ribose polymerase (PARP) inhibitors appears promising in particular BRCA-associated subtype of OC. Another target is human epidermal growth factor receptor 2 (HER2). Both HER2 and EGFR are functional in epithelial OC. Adapted from (Banerjee and Gore, 2009).

2. DNA DAMAGE AND REPAIR

2.1. DNA damage

2.1.1 Introduction

Mammalian cells are continuously exposed to numerous agents which lead to DNA damage. These agents differ from toxic products of cell's own metabolic to external agents such as radiation and chemicals. Constant exposure to these agents will cause cells to develop various mechanisms to deal with subsequent DNA damage.

Due to the normal metabolic processes and environmental elements, there is 1,000 to 1,000,000 rate of molecular lesions per cell every day that could occur to DNA. In addition, around 0.000165% of these lesions are left unrepaired and most happen to essential genes such as tumour suppressor genes which potentially increase the risk of tumour formation (Hoeijmakers, 2001).

There are two primary types of DNA damage that can affect the primary structure: 1) DNA bases chemical modification and 2) generation of single strand breaks (SSB) or double strand breaks (DSB) in DNA. As these changes develop and repair pathways takes place, the normal DNA structure can be altered through the formation of non-native chemical bonds which cannot fit in the standard size DNA double helix (Chatterjee, N., Walker, 2017). Due to the absence of DNA tertiary structure, unlike RNA and proteins, the tertiary level of DNA organization will not be affected by DNA damage. Although, DNA is super coiled via proteins called "histone" which compact it into chromatin that is also vulnerable to the DNA damage effect (Kimura and Suzuki, 2009).

2.1.2 Source of DNA damage

There are two main types of DNA damage. First type is called "endogenous DNA damage" induced by reactive oxygen species as a result of normal metabolic process containing products of oxidative deamination and replication errors. Second type of DNA damage occurs through external factors, including:

- Sun ultraviolet (UV 200-300nm) radiation (Garm *et al.*, 2013); UV-A light generates mainly free radicals and is called indirect DNA damage, UV-B light induces crosslinking between adjacent cytosine and thymine bases building pyrimidine dimers which is referred to as direct DNA damage (Rastogi *et al.*, 2010).
- Ionizing radiation (IR) such as X and gamma rays that causes breaks in DNA strands including SSB and DSB (Garm *et al.*, 2013).

- Human-made mutagenic chemicals, specifically aromatic combinations act as DNA intercalating factors; and cancer chemotherapeutic agents such as alkylating agents including ethyl-methane sulfonate and N-methyl-N-nitrosourea which result in DNA point mutations (Lidder and Sonnino, 2012).
- Viruses including coronaviruses, hepatitis C virus (HCV), rabies and influenza (Ryan, Hollingworth and Grand, 2016).

2.1.3. Cell cycle

In active eukaryotic cell, cell cycle contains four different stages including, Gap 1 (G1), Synthesis (S), Gap 2 (G2) and Mitosis (M). The procedure between one mitosis and the next is known as interphase that comprising of G1, S and G2. Following to cell cycle, the cell either begins the process from G1 again or leaves the cycle through Gap 0 (G0) which can lead the cell to terminal differentiation (Cooper, 2000).

Table 1. Different stages of cell-cycle. Table represents different stages of cell cycle and explains the process of each phase.

G1 phase	• Increase in size of the cell • Duplication in cellular contents
S phase	• DNA replication
G2 phase	• Cell grows more • Development of organelles and proteins regarding to preparation for cell division
M phase	• Followed by cytokinesis to form to identical daughter cells
G0 phase	• Resting state which means cell perform its function without dividing

The progress of cell cycle is regulated by checkpoints at different stages, shown in Figure 12. Checkpoints distinguish damaged-DNA and prevent the cell to not replicate. The main checkpoint located in G1, is Restriction point (R). Most cells that pass the R point will result in finishing the entire cell cycle. There are other checkpoints positioned at the transitions between G1 and S, and G2 and M phase. Due to detection of damaged-DNA at any checkpoint, p53 protein becomes activated, leading to arrest of the cell cycle process and triggering of repair mechanisms. When DNA repair pathway fails, it triggers apoptosis

procedure. Moreover, cyclins are another regulator in cell cycle that become activated by cyclin-dependent kinase (CDK) enzymes (Cooper, 2000). During the S-phase of cell cycle, DNA damage could lead to duplication of damaged and incorporation of wrong bases which are a potential source of mutations. Essentially, cells cannot remove the mutations once they pass through DNA replication process (McGlynn and Lloyd, 2002).

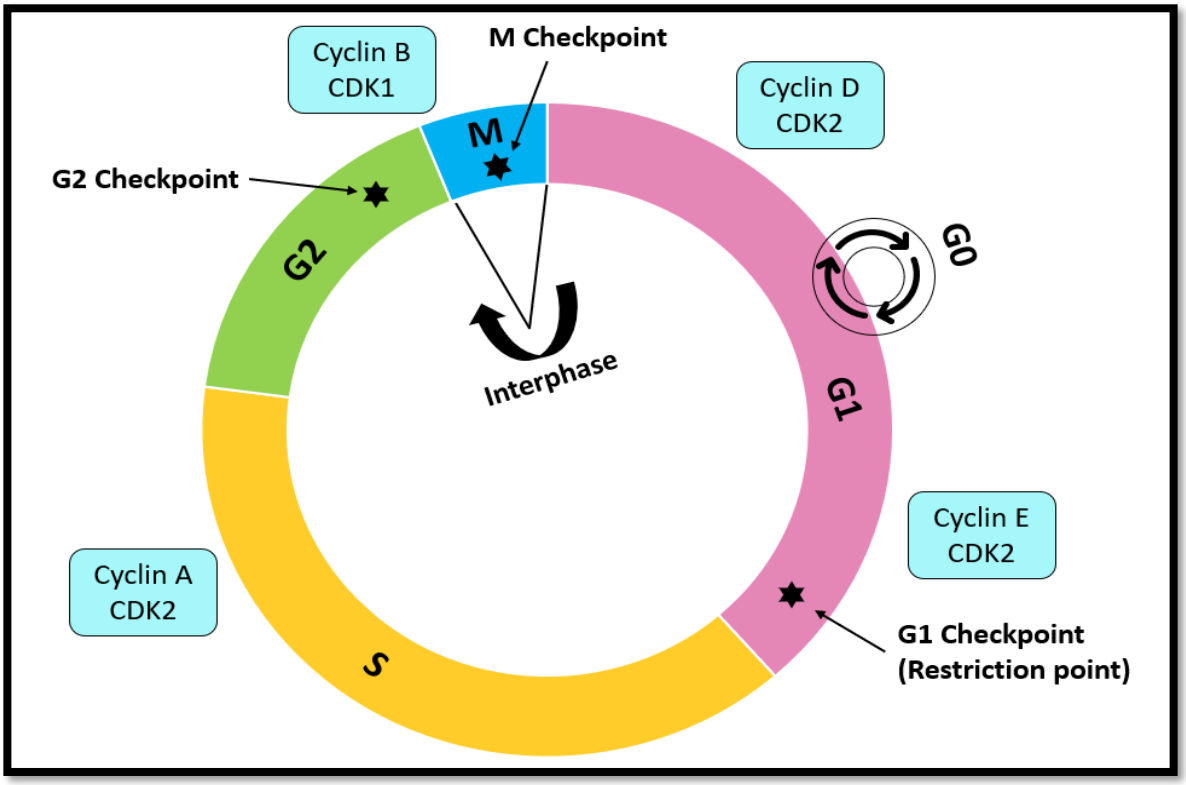

Figure 12. Cell cycle diagram. This figure shows the important checkpoints and regulators in different steps of cell cycle. In G1 phase, cell is prepared to divide. Then in the S phase all the DNA is copied and synthesized. G2 phase, is where genetic materials start to organize, condense, and prepare to divide. In M phase cell division occurs and makes two daughter cells.

2.1.4 DNA damage response and repair pathways

As a result of DNA damage, it is also likely that other biomolecules such as carbohydrates, lipids, RNA, and proteins will also be damaged. DNA damage accumulation, in particular DSBs or adducts which stall the replication fork, will lead to DNA damage response (DDR), triggering DNA repair pathways (Lord and Ashworth, 2012a).

It is essential for normal cellular function and maintenance of genomic stability to recognise and subsequent repair the DNA damage. An acquired or inherited deficiency in DNA repair pathways in human, can lead to an increased lifetime risk of cancer. DNA double strand break (DBS) is the most lethal insult to the genome and if left unrepaired, can result in genomic instability and cell death (Ledermann, Drew and Kristeleit, 2016). Figure 13 shows

the five distinct pathways of DNA damage responses and repairs, while there is some overlap in their functions.

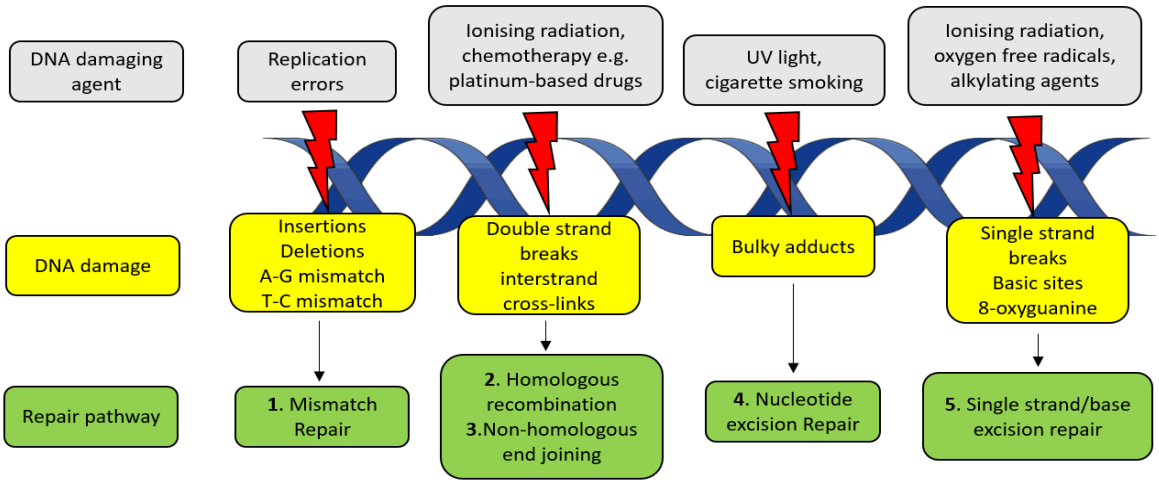

Figure 13.The five DNA repair pathways in eukaryotes. Adapted from (Ledermann, Drew and Kristeleit, 2016).

DNA double strand break can be repaired through several pathways. Homologous recombination (HR) pathway is an error-free pathway which is used when cells enter S and G2 phase during cell cycle. In the next section, HR will be discussed in more detail.

2.2 DNA repair and cancer

Normal cells naturally have efficient mechanisms for DNA repair, nevertheless, some people inherently have mutations that affect DNA repair pathways, and as a result, will be at a higher risk of cancer. For instance, people born with mutant a gene involved in non-homologous end joining (NHEJ) pathway are more sensitive to IR and have high risk of suffering from leukaemia and solid tumours (Sekiguchi and Ferguson, 2006). Other examples of mutations in DNA repair genes include BRCA1 and BRCA2. Mutations in these two well-characterized genes, could result in a significant risk of breast and ovarian cancer to carriers. Both genes are involved in homologous recombination (HR) which has a main role in DNA DSBs repair (O'Donovan and Livingston, 2010).

2.2.1 Non-homologous end joining pathway (NHEJ)

Most DSBs in eukaryotic cells are repaired by either NHEJ or HR. Recently, a third repair mechanism which is less characterized named microhomology-mediated end joining (MMEJ) has been proposed as an additional DNA DSB repair DNA DSB repair pathway (Mcvey *et al.*, 2017). HR take places in late S-G2 phases, whereas NHEJ occurs throughout the cell cycle, but mostly in the G1 phase (O'Driscoll and Jeggo, 2006).

The main proteins involved in the NHEJ pathway comprising of Ku complex (Ku70-Ku80), DNA-PKcs, XRCC4, Ligase IV, Artemis, and cernunnos/XLF core factor (Sekiguchi and Ferguson, 2006). The Ku dimers (Ku70/Ku80) play a role in the early detection of DNA DSBs due to their high affinity for DNA ends. As a result of the Ku hetero-dimmer attachment to the site of DSB, DNA-PKcs -which is a serine/threonine protein kinase- is attracted to DNA DSB site, with the Ku70/80/DNA-PKcs complex playing a role as a DNA damage sensor. Another protein called Artemis acts as a single-stranded 5' to 3'exonuclease enzyme. Artemis is phosphorylated via DNA-PKcs, resulting in increasing endonuclease activity on 5' and 3' overhangs as well as hairpins (Balmus *et al.*, 2019).

Artemis induces an important nucleolytic processing activity to prepare DNA ends for re-ligation. Following DNA ends protection, XRCC4 and Ligase IV cover the break, while other proteins including MRE11/RAD50/NSB1 (MRN complex) are required for further DNA ends processing before re-ligation. The other family member of NHEJ proteins, Cernunnos/XLF, appears to have a role in joining of DSB end alongside with XRCC4 and Ligase IV (Balmus *et al.*, 2019). The role of this protein is not fully elucidated, but Ahnesorg et al (2006) suggested some possible role(s) for Cernunnos-XLF including; 1) act as a bridge between XRCC4 and Ligase IV, 2) simplify the recruitments of other elements for DSB ends, 3) play a role in XRCC4-Ligase IV regulation (Sekiguchi and Ferguson, 2006). Moreover, there is another protein named as SIR (silent information regulator) which is recruited to decrease DNA ends accessibility and chromatin condensation with deacetylation of histone (Howard, Yanez and Stark, 2015). Figure 14 provides an overview of NHEJ pathway.

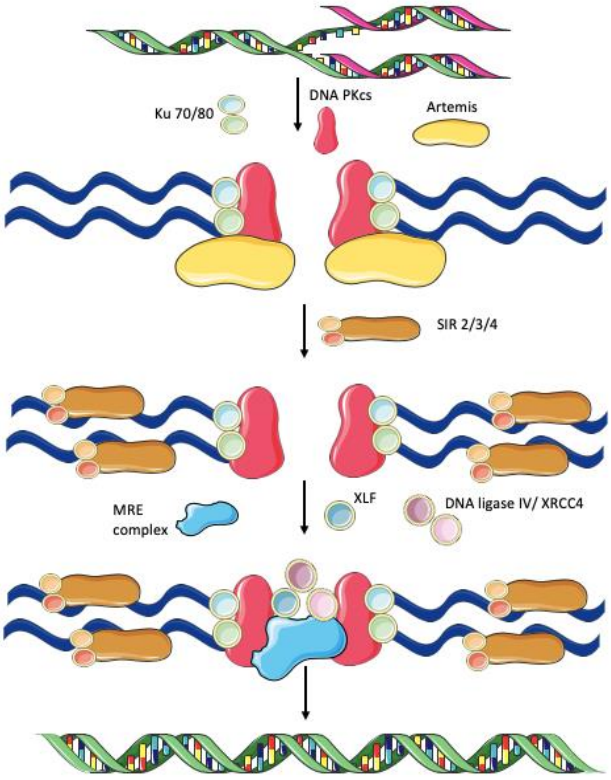

Figure 14. Schematic representation of DSB repair pathway through NHEJ. The two broken ends are processed directly through activation of the end-binding KU70/80 complex and then followed by ligation with DNA-PKcs and XRCC4-ligase4.

2.2.2 Homologous recombination pathway (HR)

DNA double strand breaks (DSBs) is a threatening kind of DNA lesions that effect on genome integrity, and another pathway that repairs these DSB is homologous recombination (HR). HR uses a homologous DNA template to repair DSBs which occurs through end resection from the ends of DNA breaks to produce a long stretch of single-strand DNA for strand invasion. Cyclin-dependent kinases (CDKs) are required to promote end resection and to activate HR (Ledermann, Drew and Kristeleit, 2016).

There are several proteins involved in HR, with RAD51 being central to the process. RAD51 plays a role as a DNA strand-exchange which binds to the single strand DNA (ssDNA) to form a nucleoprotein filament in order to promote strand invasion into a homologous duplex for initiation of repair synthesis (Morrical, 2015). Synthesis-dependent strand-annealing (SDSA) is a part of HR and during this, the new synthesized DNA detaches to anneal to the other DNA end and finally HR pathway is completed by ligation (Zelensky, Kanaar and Wyman, 2014).

There are some differences between HR and NHEJ that is the DNA ends, before becoming re-joined, are protected from resection in NHEJ. However, the risk of deletion and insertion during NHEJ can arise (Newman *et al.*, 2015). Another difference is that HR is restricted to

the S/G_2 phases during cell cycle, whereas NHEJ is effective throughout the cell cycle (Ceccaldi, Rondinelli and D'Andrea, 2016). Although, the identical sister chromatid is a preferred template for HR and leads to precise repair by rebuilding the original sequence.

In the past two decades, the increasing significance of HR in the conservation of mammalian genome integrity has emerged. HR is mostly responsible for DSBs repairing, as a result of replication fork stalling (in the late S phase). HR pathway includes nucleolytic processing, strand invasion, formation of Holliday junction and branch migration. The main proteins involved in HR contain: MRN complex, are: γ-H2AX, RAD51, RAD52, RPA, CtIP, BRCA1, BRCA2, XRCC2, XRCC3, RAD54, DNA polymerases, DNA ligases etc (Su *et al.*, 2017).

In the first step, RAD52 protein recognizes the broken DNA ends. Then, MRN (MRE11, RAD50, NBS1) heterotrimeric complex gathers with CtlP (interacting protein) and other exonucleases and to generate 3′- single stranded DNA (ssDNA). ssDNA tail is coated with replication protein A (RPA) to eliminate secondary structure as presented in Figure 15 (Cerbinskaite *et al.*, 2012). In the next stage, whereas BRCA1 is required as a regulatory mechanism, RAD51-BRCA2 with RAD54 assistance, is bonded to ssDNA overhangs to replace the RPA. According to this invasion, the non-matching integral strand is moved to form a D-loop that enlarges as new DNA synthesis developments in the site of DNA break (Huang and Mazin, 2014). Straight after getting paired of DNA strand at the homologous sequence, the activation of DNA polymerase will start to fill the gap in broken DNA by DNA ligase IV and XRCC4. This resolution step can be accomplished by two Holliday junction formation to resolve giving crossover or non-crossover products (Chun, Buechelmaier and Powell, 2013) (Drew, 2015). Figure 15 displays an overview of HR pathway.

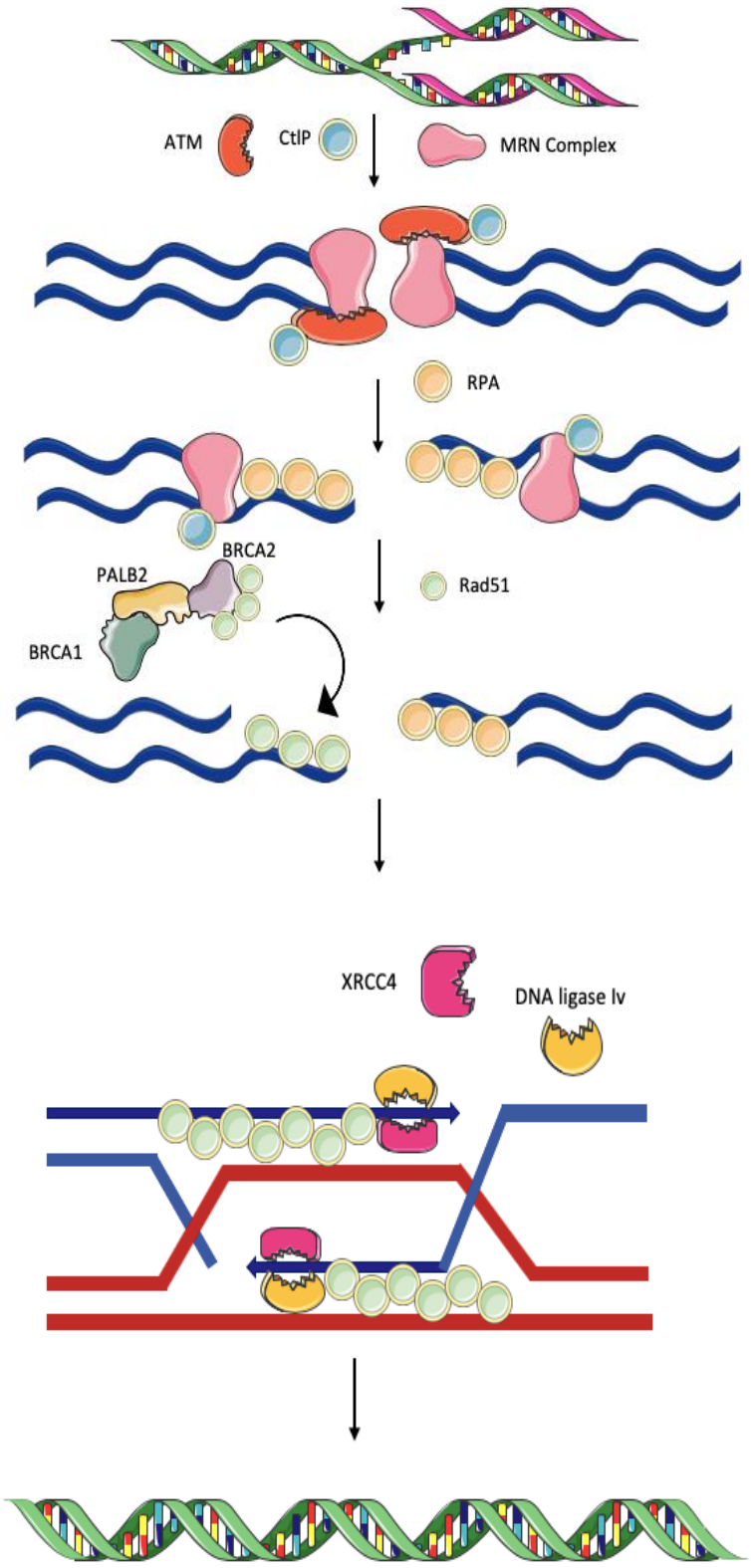

Figure 15 .Schematic representation of DSB repair pathway through HR. In HR pathway, after recognition of DSB, the overhangs are processed by MRN complex comprising of RAD50, MRE11 and NBS1 proteins. NBS1 activates ATM which is a serine/threonine kinase enzyme. ATM can phosphorylate H2AX histone, and its structure will be changed and then called γ-H2AX. In the next stage, the number of proteins, called RPA such as, RAD52, RAD54, ERCC1, go to load at the damage location. After that, RPA is replaced with RAD51 which is loaded by BRCA2. Finally, the new created strand is annealed to the broken one and DNA fills the gap, and the process is completed through Holliday junction.

2.2.3 Balancing HR and NHEJ

Normally, HR predominates in organisms with a small genome which have low abundance of repetitive sequences, while mammals mostly rely on NHEJ for DSB repair. Due to the large numbers of highly repetitive sequences in higher eukaryotes DNA, HR take place between sister chromatids to prevent misalignment of the homologous sequences. Although, even in highly complex genomes, to deal with the DSBs formed during replication, HR pathway will be used as the preferred repair mechanism for DSB.

As it has been mentioned previously, HR is used to repair breaks in the S and G2 phases during cell cycle (Brandsma and Gent, 2012).

The first mechanism to control it, depends on S/G2 specific CDKs. They play a role in CtlP phosphorylation which is required for DNA end resection. Moreover, CDK1/CyclinB complex causes phosphorylation of NBS1 component in the MRN complex on Serine 432 during the S, G2 and M phases, which is necessary for resection and efficient HR (Brandsma and Gent, 2012). Due to cell cycle dependent manner, the protein activation is restricted in HR. When replication is ongoing in the S phase, some parts of the genome have not yet been replicated and recombination of these parts needs to be avoided to inhibit loss of heterozygosity and non-allelic recombination. Therefore, another regulatory factor is provided by the structural maintenance of chromosomes (SMC) proteins including Cohesin, Condensin and SMC5/6. These SMC proteins are able to restrict repair to the sister chromatid and stop HR between other sequences (Brandsma and Gent, 2012).

2.3 γ-H2AX

DSBs can be visualized as local spots of repair protein accumulation which called foci in the nucleus. These certain proteins which accumulate in foci, including 53BP1, RPA, RAD51 and γ-H2AX around the DSB. However, not all the proteins involved in repair can accumulate in sufficient numbers to form foci such as Ku70/80. Changes in the foci number inside the nucleus in time can be quantified for DNA repair analysis (Brandsma and Gent, 2012).

In the last decade, a new biomarker, the phosphorylated histone H2AX, has emerged as a powerful tool to monitor DNA DSBs in cancer. H2AX is one of the isoforms from the Histone H2A family protein which is distinguished from other isoforms through the presence of a short COOH terminal tail. Cellular H2AX content varies from 2% in lymphocytes to 20% in SF268 glioma cells. total H2A protein (Bonner *et al.*, 2008) (Ji *et al.*, 2017). Before stop codon, the tail has a highly conserved sequence containing one serine at position 139

and one glutamine residue at position 140, known as the SQ motif. The phosphorylated form of H2AX on the Serine 139 residue located in the COOH tail, was named gamma H2AX (γ-H2AX) because it was first detected in cells exposed to γ-rays and accumulated around the break in a 2Mb region (Kuo and Yang, 2008).

The histones are a group of proteins which are responsible for compacting DNA into the nucleus. They are found as an octamer comprising of 2 molecules of H2A, H2B, H3 and H4. Due to their positive charge, they can bind to DNA very tightly, resulting in the formation of 100kDa protein complex. For further DNA condensation, histone H1 act as a linker to compresses the nucleosomes into chromatin fibres (Podhorecka, Skladanowski and Bozko, 2010).

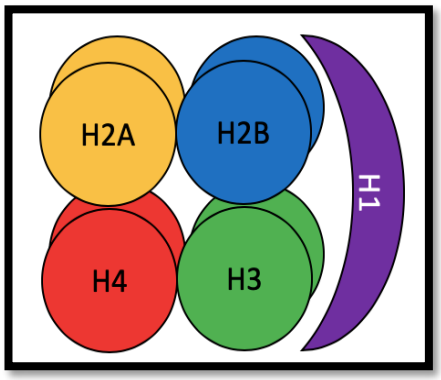

Figure 16.Structure of histones in chromatin. The figure above represents the histone structure in chromatin, comprising of a histone octamer; two copies of each of the histones H2A, H2B, H3, H4 and single H1 which is on top of the structure.

Once DSB has taken place, H2AX molecules are rapidly phosphorylated via PI3-kinases, including kinases like ATM, ATR and DNA-PK, depending on the cause of DNA damage and timing. γ-H2AX generation is one of the earliest events discovered in cells due to exposure to DNA damaging agents. It appears within minutes and reaches maximum levels after 30 min (Ivashkevich *et al.*, 2012).

Some proteins such as BRCA1, 53BP1 and MDC1 (mediator of DNA damage checkpoint), all have the BRCT (BRCA1 C Terminus) domain which co-localizes with γ-H2AX. Also, γ-H2AX MDC1 has been shown to be a bridging factor between γ-H2AX and the MRN complex. Furthermore, cohesion complexes are found to localize with γ-H2AX by binding MRE11. Once DNA is repaired, is dephosphorylated, by the phosphatase PP2A. (Kuo and Yang, 2008).

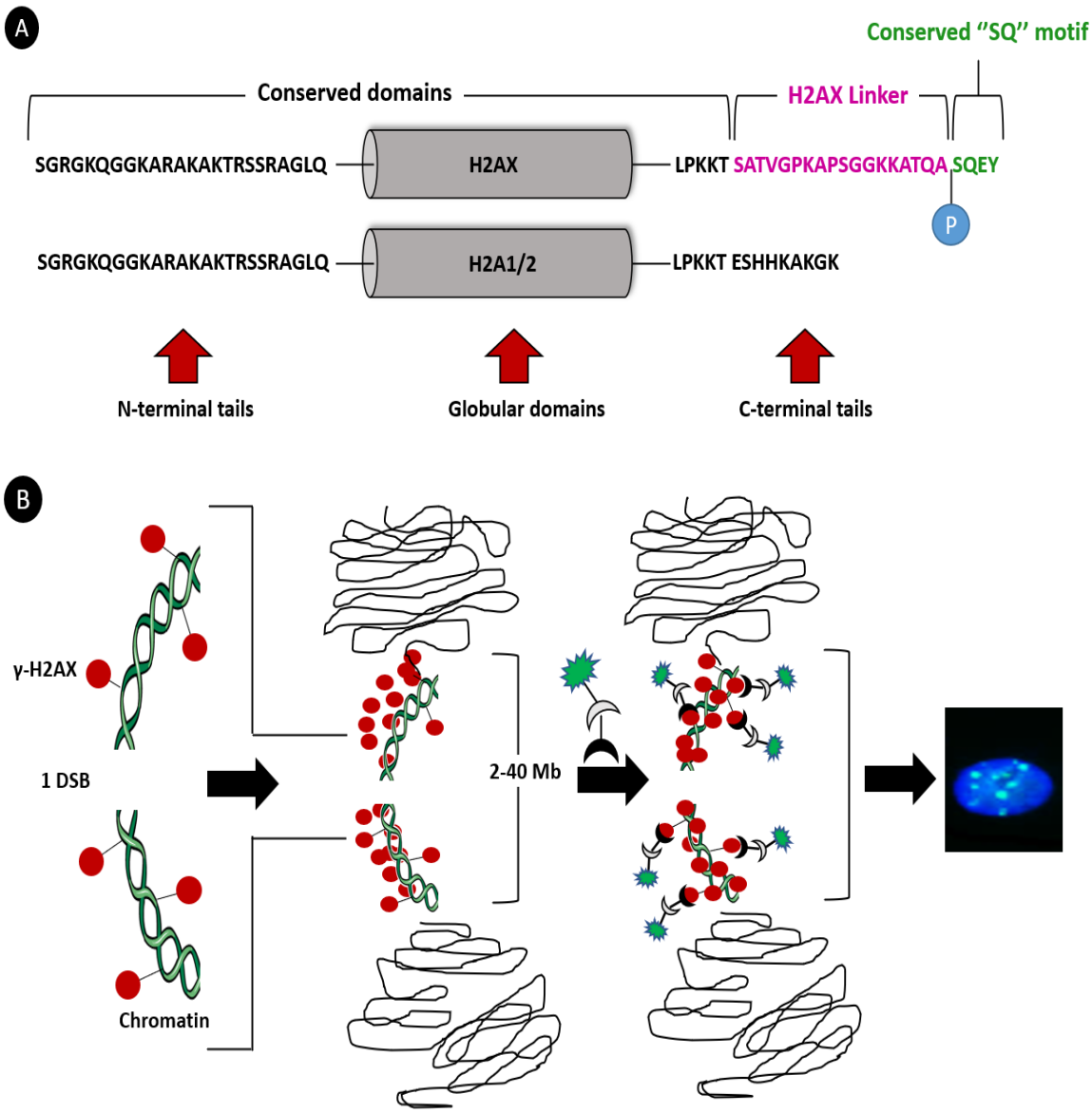

Figure 17.γ-H2AX formation in human cells and/or tissues. The figure above represents (A) H2AX which is a variant of histone H2A. It can replace other subtypes of H2A in a subset of nucleosomes. There are two identical domains between H2AX and other H2As comprising of the globular domain and the N-terminal tail, while H2AX has a unique C-terminal tail holding an evolutionarily conserved "SQ" motif (green) connected by a "linker" that is different in sequence and length, through phosphorylation (blue). The conserved "SQ" motif contains the C-4 serine that is phosphorylated due to DNA DSB induction. (B) as a result of DSB induction, the H2AX C-4 serine is phosphorylated (γ-H2AX). Phosphorylation of H2AX extends from the original site of DNA break and can be located within a 2–40 Mb region surrounding the DSB site. Therefore, using of a specific γ-H2AX antibody allows to visualize the DSBs in cells. Adapted from (Redon *et al.*, 2012).

3. BRCA2 ROLE IN DSB-DNA REPAIR

3.1. Role of BRCA1/2 in HR

3.1.1. BRCA1

Several breast cancers and engineered BRCA1 mutated cells have been under experimentation to confer HR deficiency and display the connection of HR and tumor suppressor roles of BRCA1 (Drost *et al.*, 2011). BRCA1-deficient cells are considerably

more sensitive to poly (ADP-ribose) polymerase (PARP), which plays an important function in repair of SSB DNA and other cellular processes including gene transcription. There are two distinct function proposed for BRCA1 including (1) 5′ to 3′ resection of DSBs to generate 3′ ssDNA overhangs and (2) RAD51 recombinase loading onto ssDNA (Towler *et al.*, 2013).

Furthermore, following DNA damage, BRCA1 interacts with the MRN complex comprising of MRE11, RAD50, and NBS. BRCA1 directly interacts with phosphorylated CtIP, a resection factor, in BRCA-C complex by its BRCT domain to band with the MRN nuclease to catalyze resection (Yun and Hiom, 2009). For CtIP activation and BRCA-CtIP interaction, CDK-dependent phosphorylation of CtIP is required. It has been suggested that BRCA1 elevates resection through recruiting CDK-phosphorylated/activated CtIP to DSB sites (Buis *et al.*, 2012).

Distinct fork restart pathways, which are antagonistically controlled by 53BP1 and BRCA1 in a DSB repair-independent manner (Xu *et al.*, 2017). The 53BP1 accumulates in the absence of BRCA1, leads to block resection and HR, genomic instability and finally cell death. It has been suggested that BRCA1 spatially excludes 53BP1 from the DSB complex during S phase (Chapman *et al.*, 2013) (Reczek *et al.*, 2013). According to the mutual exclusiveness of the BRCA1 complexes, it is shown that the absence of BRCA1-A complex leads to more functional BRCA1 to interact with other complexes which develop resection (Coleman and Greenberg, 2011).

Resected DNA is initially bound to the ssDNA binding replication protein A (RPA) and to RAD51. For this binding, mediator proteins like BRCA2 are required to help the RAD51 loading into ssDNA, associated with the eviction of RPA (Zelensky, Kanaar and Wyman, 2014). Additionally, BRCA1 can enhance the recruitment of BRCA2 to DSB by connecting to PALB2 protein. Disruption of BRCA1 reduces the PALB2, BRCA2, and RAD51 foci. On the other hand, PALB2 disruption can diminish BRCA2 and RAD51 but not BRCA1 foci. Disruption of BRCA2 can only affect RAD51 foci after DNA-damaging treatment (Li *et al.*, 2016). Consistently to the idea which is BRCA1 can facilitate the loading of RAD51 via PALB2, clinical BRCA1-m with defective BRCA1-PALB2 interaction consequence in a deficiency of HR (Bunting *et al.*, 2012).

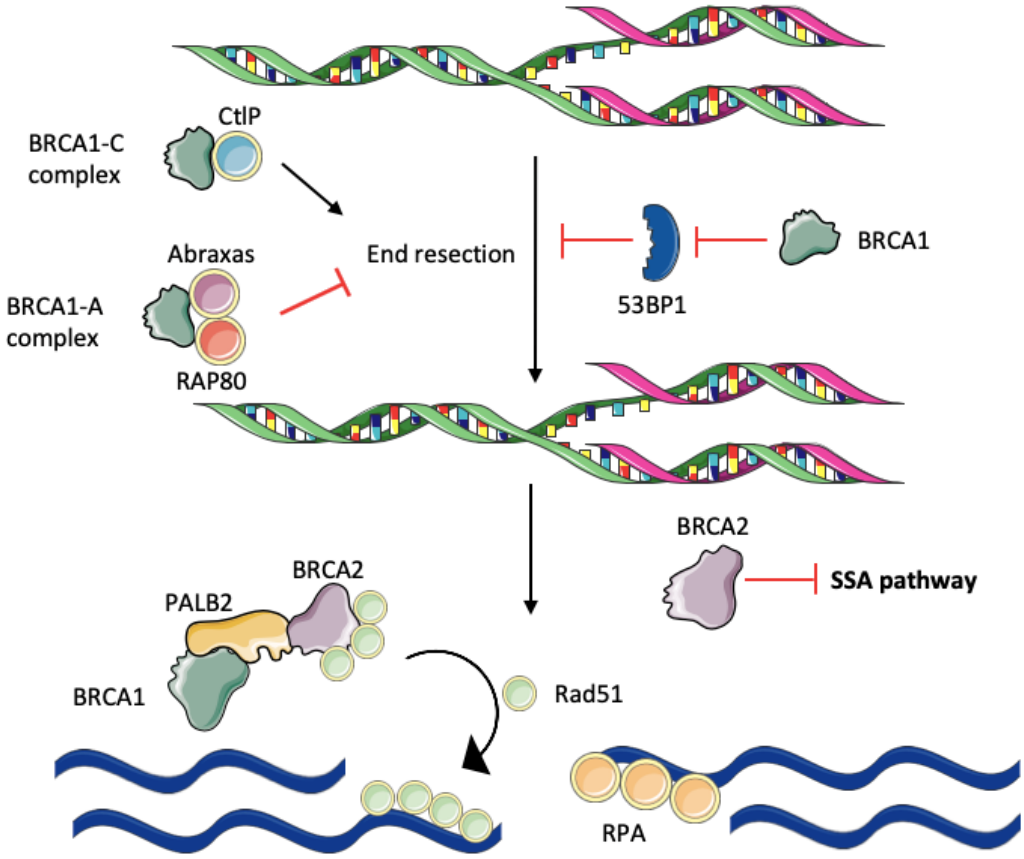

Figure 18. Schematic figure of BRCA1 role in HR. Both BRCA1 and BRCA2 play a distinct role in homologous recombination DNA repair pathway. The role of BRCA1 is at an early step of HR, which promotes end resection and, at a later step to recruit PALB2 regarding increase localization of BRCA2 chromatin. BRCA1 performance is through antagonizing the resection inhibitor 53BP1. It has been suggested that BRCA1 can have a role to regulate resection by recruiting CtIP (blue ball) in the BRCA1-C complex, while inhibition of end resection in the BRCA1-A complex comprising of Abraxas and RAP80 (red and purple); otherwise, Abraxas-RAP80 might inhibit resection, independently of BRCA1. BRCA2 facilitate the loading of RAD51 recombinase onto the resection product to create a RAD51-ssDNA filament that is important for HR and blocks the engagement of the 3′-ssDNA into the deleterious single-strand annealing (SSA) pathway. SSA plays a role when homologous repeats are represented and result in the deletion of sequences between the repeats (Prakash *et al.*, 2015).

3.1.2 BRCA2

3.1.2.1. Chromosomal location and structure

The BRCA2 gene is located on chromosome 13 and has a complex genomic structure comprising of 27 exons. The gene is translated into a large nuclear protein containing of 3418 amino acids with a predicted molecular weight of 460 kDa. There are certain regions which are highly conserved in BRCA2 genome, an indicator of its importance in mammalian cells. In human cells, there are eight BRC repeats which are located within exon 11, residing in the central portion of the protein. The BRC repeats extend over 1200 amino acids, whereas each BRC repeat is about 70 amino acids in length with the core sequence contained of 26 amino

acids. All eight BRC repeats in BRCA2 protein, have the ability of binding to RAD51 protein.

However, each repeat of BRC shows a different affinity for binding to RAD51. For instance, the four BRC repeats positioned at the 5' region of exon 11 bind RAD51 more strongly than the four repeats at the 3' end of the exon (Kim *et al.*, 2003).

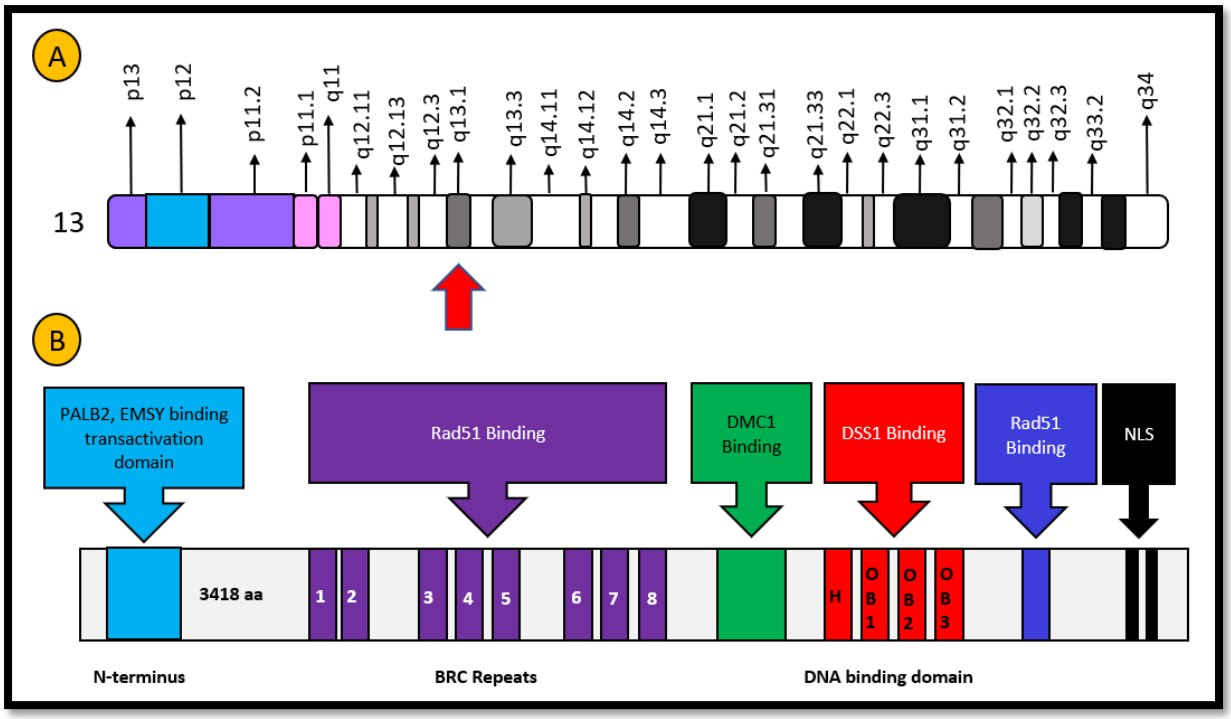

Figure 19. (A) BRCA2 genome decoration: this figure shows the cytogenetic location of BRCA2 on long arm of chromosome 13, at position 13.1 (13q13.1) Adapted from (National Institutes of Health, 2015). (B) Schematic structure of the BRCA2 protein comprising of N-terminus interacting region, eight BRC repeat motifs, H, helical domain, OB oligonucleotide binding fold, RAD51 binding site at the c-terminus and NLS nuclear localization signal. At the extreme C-terminus, there are at least two nuclear localization signals (NLS) which has an important role for BRCA2's function as a nuclear protein. BRCA2, in cooperation with the BRC repeats and the OB domains, can target RAD51 to dsDNA/ssDNA junction at double strand breaks HR pathway. BRCA2 can interact with PALB2 via the N-terminal section with RAD51 by the 8 BRC motifs and with a connection between SS-DNA and duplex DNA through DBD which is including three oligonucleotide/oligosaccharide-binding (OB) folds, following high rate of RAD51polymerization at resected DSBs through the BRCA1-PALB2 complex together with BRCA2 protein. Adapted from (Powell and Kachnic, 2003).

3.1.2.2. BRCA2 function

The original evidence about the importance of BRCA2 in genome integrity maintenance was presented in BRCA2 mutant (BRCA2-m) mice which had early embryonic lethality and deficiency in DNA repair similar to RAD51 mutant mice (Lim and Hasty, 1996). BRCA2 plays a distinct role in HR from that of BRCA1. BRCA1-BARD1 stimulate repair through HR and single-strand annealing (SSA), while BRCA2 can promote HR by suppressing SSA. In BRCA2-m cells, normally end resection start appearing but ssDNA overhangs cannot be

channeled into HR; instead, they anneal to each other complementary at the place where they present, ending in deletion of one repeat and consequently intervening sequences. As a result of the gene deletion by SSA , it initiates an error-prone HR (Abaji, Cousineau and Belmaaza, 2005).

Disruption of RAD51 results in the same phenotype as a BRCA2 mutation demonstrating that, BRCA2 acts at the same step during HR process as RAD51. Then, not surprisingly, a 53BP1 loss cannot lead to rescue the viability of BRCA2 mutant cells, similar to BRCA1 mutant cells (Jacot *et al.*, 2013). Consistently with its main role in HR, cells with defective BRCA2 are selectively sensitive to DNA damaging agents comprising of cross-linking agents and PARP inhibitors that normally causes lesions repaired through HR (Francis *et al.*, 2010) (Telli and Ford, 2010).

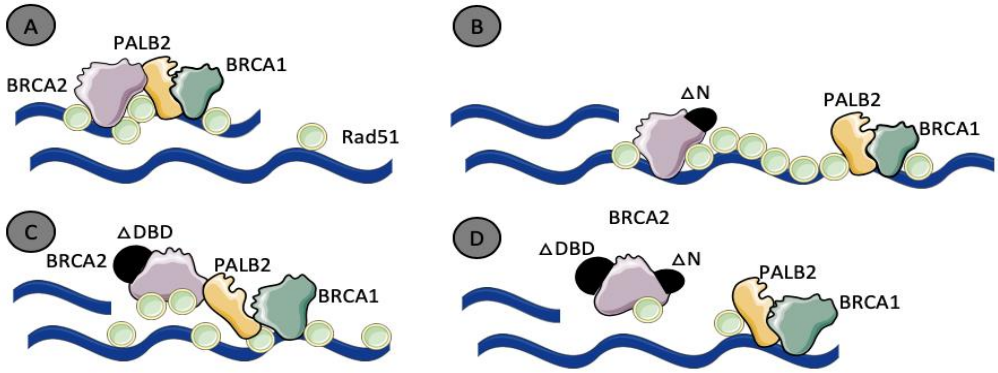

Figure 20. Schematic model of collaboration between BRCA1, BRCA2, and PALB2. BRCA2 wild-type (A) and different mutant types including (B) $BRCA2^{\Delta N}$, (C) $BRCA2^{\Delta DBD}$ and (D) $BRCA2^{\Delta N+\Delta DBD}$. (A) BRCA2 wild-type protein can efficiently increase the RAD51 loading on SS-DNA. (B) The DBD is able to compensate due to the disruption of the stable interaction between BRCA2 and the BRCA1-PALB2 complex and consequently induce a slight deficiency in RAD51 loading in $BRCA2^{\Delta}N$ cells while the BRCA1-PALB2 complex is still capable of facilitating the RAD51 loading. (B) The BRCA1-PALB2-BRCA2 complex compensates for the interruption of the DBD of BRCA2. (C) The $BRCA2^{\Delta N+\Delta DBD}$ protein cannot connect to damage DNA sites or to increase RAD51 loading. Adapted from (Al Abo *et al.*, 2014).

3.2. BRCA2 mutations

Over 100 different germline mutations have been identified in BRCA2, which are related to cancer susceptibility. Looking at cBioPortal, there are 683 mutations recorded in BRCA2 genome (Figure 21).

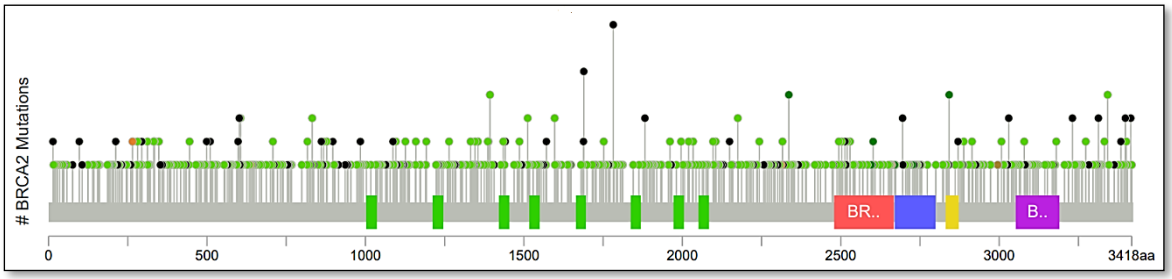

Figure 21. Mutation diagram in BRCA2. This figure represents different types of mutation which the majority of mutation in BRCA2 is missense mutation. In case of different mutation types at a single position, colour of the circle is defined regarding to the most frequent mutation type. Credit for cBioPortal (cBioPortal, 2021).

Most BRCA2 mutations are caused by small deletions or insertion, resulting in truncated BRCA2 protein, and followed by generation of translation frameshift, or faulty splice sites. More than 70% of these mutations contain one or two nucleotides, located in a repetitive sequence (Murray and Davies, 2013).

There are some common BRCA2 mutations in specific populations. For instance, in Ashkenazi Jews, the germline 6174delt mutation leads to truncated BRCA2 protein as a result of insertion of premature stop codon. It is estimated to be present in 1% of the population and is reported to correlate with breast, ovarian and prostate cancer (Murray and Davies, 2013).

Another example is the Icelandic population which have BRCA2 mutation 999del5, that accounts for 40% of male breast cancer and approximately 8% of female breast cancer (Cassidy, Liau and Venkitaraman, 2014). More than 75% of families with more than four breast cancer cases have this type of mutation. This deletion generates an unstable protein which increases the risk of breast cancer, as it causes haploinsufficiency at the BRCA2 locus (Thorlacius *et al.*, 1997).

Further common BRCA2 mutations include 5579insA (insertion) in selected populations or groups such as Dutch (Verhoog *et al.*, 2001), 8765delAG (deletion) in French Canadian and Italian (Pisano *et al.*, 2000), 6503delTT in Scottish and Northern Irish (Steel, 2003) and 3337C>T point mutation in Pakistani population (Liede *et al.*, 2002).

Mutations in tumour suppressor genes are mostly recessive in nature, as one intact allele is normally enough to compensate. Therefore, for neoplastic transformation, mutation in both alleles within a single cell is required. Several mechanisms cause cell to lose its normal gene

and be predisposed for tumour developing and may result in loss of heterozygosity (LOH) (Nowacka-Zawisza *et al.*, 2008). It was established that 30-40% of sporadic breast and ovarian cancers display LOH on chromosome 13q12-q13 (Deb *et al.*, 2014). LOH on chromosome 13q12-q13 in 50 BRCA2 tumours cases has been studied and outcomes revealed a high frequency of LOH in tumours of the prostate, ovary, cervix, colon, male breast cancer and urethra and also BRCA2 function as TSG in these cancers (Cassidy, Liau and Venkitaraman, 2014).

3.3. BRCA2 absence in cancer treatment

The most important aim when using chemotherapeutic agents, as well as radiotherapy, is to induce DNA damage and subsequent cell death. Cells respond to DNA damage by activating multiple pathways including DNA repair, cell cycle arrest and apoptosis, depending on the damage extent and the types of DNA damage. Cancer is a genetic multistep disease, usually arise due to mutational activation or inactivation of oncogenes and/or TSGs respectively.

Several of these mutations lead to alteration and dysfunction of proteins which contribute to DNA repair pathways, as a central mechanism of maintaining genomic integrity. Consequently, designing treatment(s) for targeting cells with deficiency in repair pathway may be lethal to cancer cells while sparing normal cells. An impaired BRCA2 gene and an absence of error-free DSB repair pathway was proven to be the Achilles' heel of BRCA2 deficient tumours (Rigakos and Razis, 2012). Therapeutic approaches designed to target the DSB repair pathway as useful therapeutic approach. PARP is an enzyme which has critical role in base excision repair (BER), an essential pathway in the repair of DNA Single Strand Breaks (SSBs). The PARP inhibition leads to increase the DNA SSBs which encounter the replication fork and then consequently could be the creation of DNA DSBs (Zhang *et al.*, 2015). PARP inhibition in cells containing defective BRCA2, will result in chromosomal instability and subsequent cell death.

Naturally, these DSBs are repaired by error-free HR repair pathway, in which BRCA2 and Rad51 are involved. In the absence of BRCA2, the replication fork cannot be restarted (i.e. Collapsed), leading to failed DSB repair, followed by alternative error-prone mechanisms including single-strand annealing and/or NHEJ, numerous chromosomal aberrations and finally cell death (Patel, Sarkaria and Kaufmann, 2011). PARP inhibitors through the concept of synthetic lethality have a strong effect in BRCA2 deficient cells (Lord and Ashworth, 2017).

3.4. Interacting proteins of BRCA2

The N-terminal region in BRCA2 contain an interaction site for two proteins including partner and localiser of BRCA2 which is PALB2 (also known as FANCN) and EMSY, the putative oncogene. PALB2 has a significant role as a nuclear partner of BRCA2 due to the formation of strong and stable associations with certain nuclear structures. PALB2 facilitates BRCA2 localisation, accumulation and function in the nucleus which allows BRCA2 to escape from proteasome-mediated degradation (Nepomuceno *et al.*, 2020).

Furthermore, PALB2 has been displayed to play a role in HR repair through its ability to recruit BRCA2 and RAD51 to DNA breaks. Additional data expanded PALB2's role by presenting that PALB2 interact with BRCA1 and BRCA2 to create a functional complex and target DNA damage site. Moreover, PALB2 form BRCA1-PALB2-BRCA2 complex as a molecular scaffold that is involved in HR repair and cell survival. It has been showed that, PALB2 interaction with BRCA1, can affect on BRCA2-RAD51 function in HR, hence contributing to genomic stability (Xia *et al.*, 2006).

According to this suggestion, several germline BRCA2 missense mutations were identified in breast cancer that established disability of binding PALB2, as well as a failure to apply functional HR. The EMSY protein can bind to transactivation domain of BRCA2 on exon 3, including the transactivation domain which lead to silence the activation role of BRCA2 through chromatin remodelling proteins. Interestingly, EMSY amplification has been seen in many cases of sporadic breast cancer and high-grade ovarian cancer. Despite all the data regarding to linkage between BRCA2, EMSY and their localisation at DNA damage site, the EMSY role in the repair mechanism is still unclear (Cousineau and Belmaaza, 2011).

3.5. BRCA2 function during cell cycle

Loss of BRCA2 results in increased error-prone DSB repair pathways, including gene conversion with unequal cross-over or single strand annealing, as well as increasing intra-strand cross-linking following to a considerable genomic instability and contributes to tumorigenesis (Powell and Kachnic, 2003). Various studies have established that replication fork stalling is a regular event at DNA lesion sites and HR is required to initiate blocked replication. Due to the high incidence of DSBs in BRCA2-m cells, it is suggested that

BRCA2 play an important role in the stabilization of stalled DNA replication forks and HR (O'Donovan and Livingston, 2010).

Furthermore, BRCA2 has been displayed to form a high molecular weight protein complex with the evolutionary conserved protein BRCA2-Associated Factor 35 (BRAF35). BRAF35 is a DNA binding protein which has a similar pattern of expression to BRCA2 during embryogenesis. Moreover, it was found that an antibody which inhibits BRCA2 caused delayed in metaphase progression which suggests BRCA2 role in mitosis. Regarding to BRCA2 role in meiosis, DMC1 which is a meiosis-specific recombinase interacts with BRCA2 and occurs within a highly conserved region in BRCA2, containing 26 amino acids and is separated from the RAD51 interaction domain. As a result of two distinct interaction regions for RAD51 and DMC1, the interaction of both recombinases with BRCA2 during meiosis is enabled (Venkitaraman, 2001).

4. Poly (ADP-ribose) Polymerase (PARP) Enzyme

4.1 The PARP family of enzyme and their function

DNA damage or lack of repair is the major cause of mutation that leads to the development of cancer. Normal cells can defend themselves via DNA damage response (DDR) that recognises the damage, stalling the cell cycle and mediating DNA repair accordingly, to maintain genome integrity. One of the key factors in DDR are poly (ADP-ribose) polymerase (PARP). PARP family is comprised of 17 proteins involved in several cellular processes, largely DNA repair and programmed cell death. It has been confirmed only members with PARP enzyme activity includes PARP1, PARP2, PARP4, PARP-5a and PARP-5b. The others are mono ADP ribosylators and/or with undetermined function. However, PARP-1 is the most widely studied which is encoded by ADPRT- 1 (PARP1) gene located on 1q41-q42 (Li *et al.*, 2006).

The PARP1 enzyme binds damaged SSB DNA and other kinds of DNA lesions. After that, it leads to make a number of allosteric changes in the PARP1 structure and activate its catalytic domain (Lord and Ashworth, 2017). It leads to PARylation (synthesizing branched poly (ADP-ribose) chains), and recruitment of DNA repair effectors including XRCC1 and affects chromatin structure remodelling around the DNA which is part of the DNA repair progression. Eventually, PARP1 can auto-PARylate itself. Researching about PARP1/2 function during the DDR has led to developing small molecule called PARP inhibitors (PARPi). The basic justification about these inhibitors is that can sensitize tumour cells to

conventional treatment which trigger DNA damage and finally cause cell death (Benafif and Hall, 2015).

PARP-1 and PARP-2 are the only well-known members of the PARP family, which their activity is stimulated through DNA strand interruptions. The main targeted proteins have a role in chromatin structure and DNA metabolism as well as PARP-1 and PARP-2 themselves. The PARP-1 and PARP-2 activity is associated with dramatic PAR formation stimulated by DNA- damage. PARP-1 is the most active protein in DNA damage and responsible for about 90% of cellular PAR formation under these conditions. The PARP-2 discovery was in PARP-1- deficient (Parp-1$^{-/-}$) mouse embryonic fibroblasts (MEFs), as a result of the presence of residual DNA-dependent PARP activity (Yelamos *et al.*, 2011).

Poly-(ADP-ribosyl)-ation mediated by PARP-1 and PARP-2 lead to chromatin de-condensation around damage sites, recruitment of DNA damage repair pathways. It has been indicated a dual role for PARP-1 and PARP-2 in the DNA damage response including DNA damage sensors and signal transducers to down-stream effectors. A full- understanding of the mechanistic involvement of PARP-1 and PARP-2 proteins in DNA repair and genomic instability is likely to provide valuable evidences for development of specific inhibitor drugs to design a new therapeutic approach in cancer (Yelamos *et al.*, 2011).

4.2. PARP1 structure

PARP-1 generates poly (ADP-ribose) (PAR) covalently linked onto target proteins which mediate gene transcription, DNA damage repair, and cell death signalling. It has identified as a promising drug target cancer therapy due to its role in maintaining genome stability. The primary target for PARP-1 initiated poly (ADP-ribosylation is PARP-1 itself. As a result of PARP-1 binding to DNA strand breaks, PAR synthesis activity will be dramatically elevated, over a low basal level (Langelier *et al.*, 2012). PAR production is a tightly controlled process and can induce dramatic consequences in cellular physiology. Therefore, the regulation of PARPs activation is significant for their function as shown in Figure 23 (Langelier *et al.*, 2012).

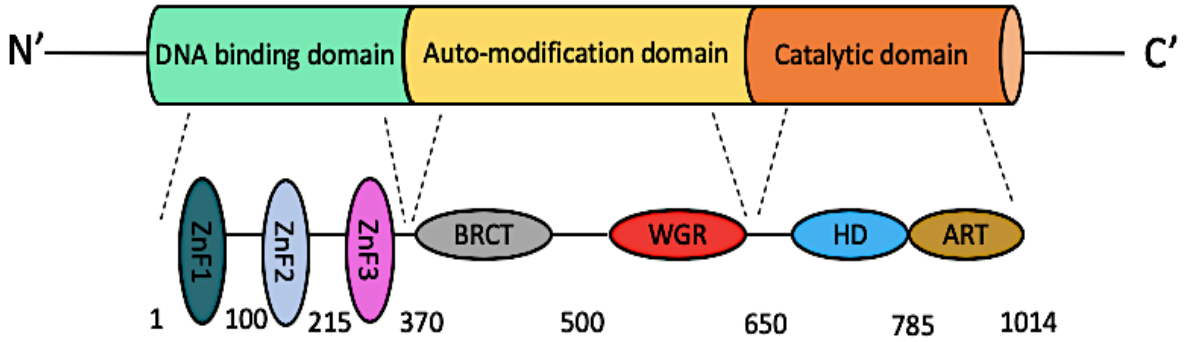

Figure 22.Modular domain architecture of human PARP-1. The structure of PARP-1 contains three main domains, DNA binding domain, auto-modification domain, and catalytic domain. In DNA binding domain, two zinc-binding domains, Zn1 and Zn2, that enable PARP-1 to distinguish particular DNA structures. A third zinc-binding domain, Zn3, has a different structure and function from that of Zn1 and Zn2. The auto-modification domain (AD) carries the main region for auto-modification which comprises of BRCT (BRCA1 C–terminus) fold and WGR, a critical area of unknown function. The catalytic domain (CAT) is contained two subdomains, the helical subdomain (HD) and the ART subdomain, that is conserved in other ADP-ribosyl transferases (ARTs) and has some kind of amino acids involved in catalysis and binding of NAD^+. Adapted from (Langelier et al., 2012).

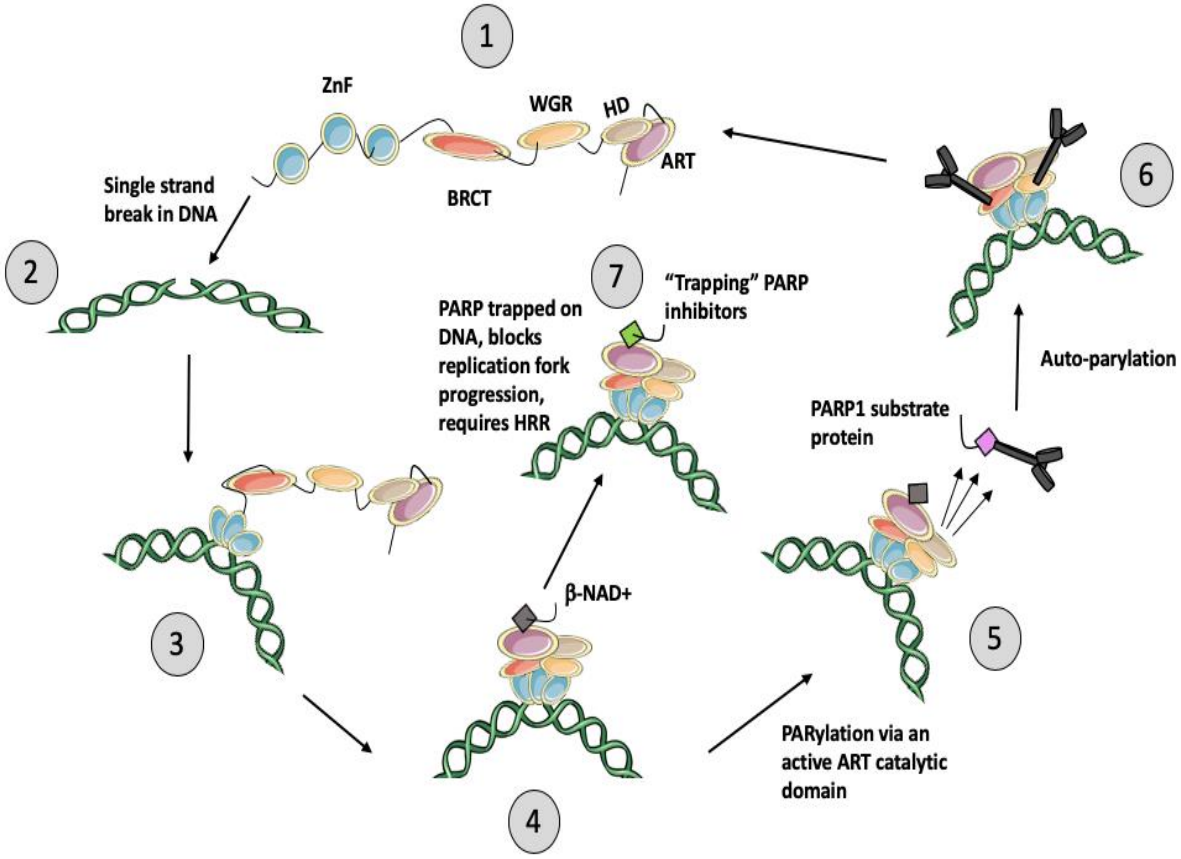

Figure 23. Schematic figure of the PARP1 catalytic cycle. (1) This step is a non-DNA bound state and PARP1 occur in a relatively disordered conformation, generally mentioned to as "beads on a string". The structure of domain in PARP1 is exposed, comprising of three zinc finger–related domains: the BRCA1 C-terminus domain (BRCT); the tryptophan-, glycine-, arginine-rich domain (WGR); and the catalytic region that contains two subdomains; a helical domain (HD) and an ADP- ribosyltransferase (ART) catalytic domain. In this non-DNA bound state, HD acts as an auto-inhibitory region which stops binding of the PARP-superfamily co-factor, β-NAD+, to its ART binding site. (2) the Damage happened in the DNA double helix frequently results in the formation of SSBs (pre-damaged and damaged in a structure of DNA are revealed); SSBs leads to an alteration in the standard orientation of the double helix, which, in turn, (3) makes a binding site for DNA binding PARP1 ZnF areas. The interaction of ZnF 1, 2, and 3 with DNA start a stepwise assembly of the PARP1 protein domains that are remained onto the PARP1/DNA nucleoprotein structure, presented in (4); this pathway results in the alteration in HD conformation, and subsequent loss of auto-inhibitory function, therefore allosterically activating PARP1 catalytic activity. (5) The catalytic activation of ART triggers the PARylation of PARP1 substrate proteins (branched PAR chains are displayed on a target protein), mediation of the recruitment of DNA repair effectors (such as BRCA1/2), remodelling of chromatin, and finally DNA repair. (6) PARP1 auto-PARylation (likely in cis at SSBs but possibly in trans at other DNA lesions lastly induce the release of PARP1 from DNA and the restoration of a catalytically inactive state [presented in (1)]. (7) Different clinical PARP inhibitors, each of them is able to bind the catalytic site, stop releasing of PARP1 from DNA, "trapping" PARP1 at the damage site, potentially PARP1 is removed from its common catalytic cycle. Adapted from (Lord and Ashworth, 2017).

4.3. PARP1, PARP2 and DNA DSB repair

An early signalling protein kinase for initiation of transduction cascade at DNA DSBs sites is Ataxia telangiectasia mutated (ATM). In early embryonic lethality of Parp-1$^{-/-}$ATM$^{-/-}$ and Parp-2$^{-/-}$ATM$^{-/-}$ mice, the consequence of inefficient SSBR/BER of several lesions due to the absence of PARP-1 or PARP-2, is conversion of unrepaired SSB to DSB during

replication which result in cell death. It has described the functional interaction of PARP-1 with different NHEJ proteins, which suggesting a role of PARP-1 in NHEJ. For example, latest studies have demonstrated an interaction between PARP- 1 and DNA-PK in response to ionizing radiation suggest that PARP-1 and DNA-PK cooperate within the same pathway to develop DSB repair whereas the role of PARP-2 in NHEJ, remains elusive. Regarding to HR, PARP-1 and PARP-2 detect disrupted replication forks and attract Mre11 for end processing that is necessary for subsequent recombination repair and renew the replication forks. Lately, has also been described that disruption of PARP-1 can inhibit HR by suppressing expression of BRCA1 and RAD51.

4.4. PARP inhibitors and the concept of synthetic lethality

HR deficiencies present sensitivity to certain agents for DNA damaging, that they are being exploited in therapeutic methods in cancer. Drugs such as PARP inhibitors which induce synthetic lethality in the context of HR deficiency have shown promise as therapeutic agents (Mehta and Haber, 2014).

The concept of synthetic lethality was established from genetic research in model organisms including fruit flies and yeast (Nijman, 2011). Synthetic lethality interaction happens between two genes when either one gene perturbation is viable, while a deficiency in both gene functions can lead to losing viability. In cancer studies, the interaction of synthetic lethality which involves a specific mutation that caused cancer is indicated to as "non-oncogenic addiction". In this situation of abnormal cancer cells, it is needed for an act of the synthetic lethal partner gene for viability (O'Neil, Bailey and Hieter, 2017). The identification and the mechanistic characterization of normal synthetic lethal interactions are the significant part for the exploitation of synthetic lethality in cancer therapy approaches. Innovation in next generation of sequencing technologies is capable of identification of different mutations in several cancer cells and alteration in gene expression which can be targeted via synthetic lethality methods (Leung *et al.*, 2016).

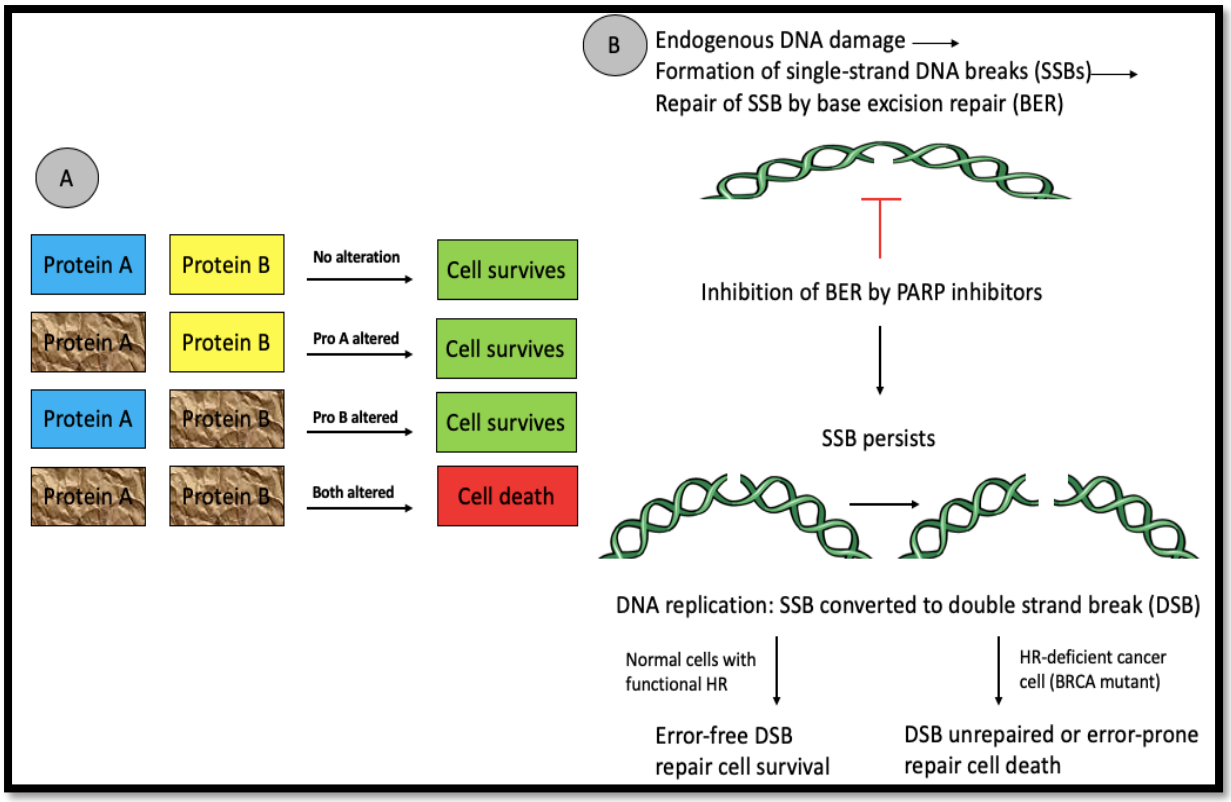

Figure 24. Schematic of synthetic lethality. (A) This is a very simple form of synthetic lethality interaction, the simultaneous variation in two genes or proteins (displayed here as A and B) leads to cell death, whereas alteration of either gene/protein alone does not. When the theory is related to cancer therapy approaches, where gene A presents an oncogene, tumour suppressor gene, or oncogenic process or pathway, gene B, once recognized, becomes a target of therapeutic, which can be used to target cancer cells with dysfunction in A. (B) Synthetic lethality of PARP inhibitors in BRCA-deficient cells. Adapted from (Drew, 2015).

4.4.1. Targeting PARP1/2 in cancer

PARP inhibitors show cytotoxicity in proliferating tumour cells, treated with genotoxic agents. Some main features such as potency pharmacokinetic properties have increased through three generations of inhibitors which evaluate the benefit of these inhibitors in cancer and clinical trials. On the other hand, current PARP inhibitors can target the catalytic site of PARP enzymes which due to its similarity amongst PARPs family members and no isoform-specific PARP inhibitors are available (Grignani *et al.*, 2020).

Two strategies for PARP inhibitors have been discovered in cancer therapy including their use (1) as chemo/radio- potentiator and (2) as a stand-alone therapy for tumour types with deficiency in certain types of DNA repair elements. In the first method, the combination of PARP inhibitors and DNA damaging chemotherapeutics or radiation can lead to genomic dysfunction in cancer cell DNA repair mechanisms and finally cell death. The first phase I clinical trial of a PARP inhibitor was carried out between 2003 and 2005 with AGO14699 in

combination with the temozolomide which is a methylating agent, in patients with advanced solid tumours (Plummer *et al.*, 2013).

The main breakthrough in this field was in 2005 when two independent groups demonstrated the sensitivity of BRCA1 and BRCA2-deficient cell lines toward PARP inhibitors. Following to this data, it supports the potential use of PARP inhibitors as single therapeutic agents in cancer cell types with defective DNA repair pathways. This method is based on the concept meaning that PARP inhibition result in accumulation of SSB which convert to DSB and eventually lead to DSB via replication fork collapse. In tumour cells with mutant BRCA1 or BRCA2, critical factors for the HR pathway, using PARP inhibitors lead to chromosomal aberrations, instability and consequently cell death (Curtin, 2014).

4.4.2. PARP-inhibitors function

Each PARP inhibitor is different in its ability for PARP1 trapping, in clinically use. These different level of PARP1 trapping, in comparison to their ability of PARylation inhibition, might be a better predictor of *in-vitro* cytotoxicity in cells with BRCA mutation (Curtin, 2014). All these PARP inhibitors interact with the binding region on the PARP enzyme co-factor which is β-NAD+ (nicotinamide adenine dinucleotide) in the catalytic site of PARP1/2, while, they have a different effect due to their cytotoxic potency and ability to trap the PARP on DNA damage site (Bunnell *et al.*, 2017).

Two groups of researchers, in 2005, identified the synthetic lethal interaction between PARP inhibition and BRCA1/2 mutation and suggested an innovative strategy for the treatment of patients with BRCA mutation cancer cells. It was established that BRCA-m cancer cells were 1000 times more sensitive to PARP inhibitors than those tumour cells with wild-type BRCA gene, but also it depends on the PARP inhibitors which is used, the format and condition provided in the experiment (Ledermann, Drew and Kristeleit, 2016).

Additionally, any tumour cells which have deficiency in other proteins of HR pathway can be sensitive to PARP inhibitors. Recent studies have revealed that cells carrying PTEN (phosphatase and tensin homologue) mutations are sensitive to PARP inhibitors. Similarly, PALB2-deficient cells are also sensitive to PARP inhibitors. There is a concept called ‘BRCAness’ which characterises the phenotype that some sporadic tumours share with those occurring in either BRCA1- or BRCA2-mutation carriers. These properties reflect the defective DNA-repair, due to mutation in other genes involved in HR, such as RAD51. The ability to discover other mutations in these genes would have significant implications in

clinical management, in terms of treatment decisions and prognosis determination (Turner, Tutt and Ashworth, 2004).

Moreover, in using of PARP inhibitors as therapeutic drugs in cancer, several major challenges should be addressed, including development of isoform-specific PARP inhibitors, understanding of PARP1/2 specific involvement in the DNA damage response and genome surveillance which provide a basis for the logical development of isoform-specific PARP inhibitors, clarification of the details of the DNA damage response strategy to overcame PARP inhibitor resistance due to reactivation of BRCA1 or BRCA2 by secondary mutations (Drew, 2015).

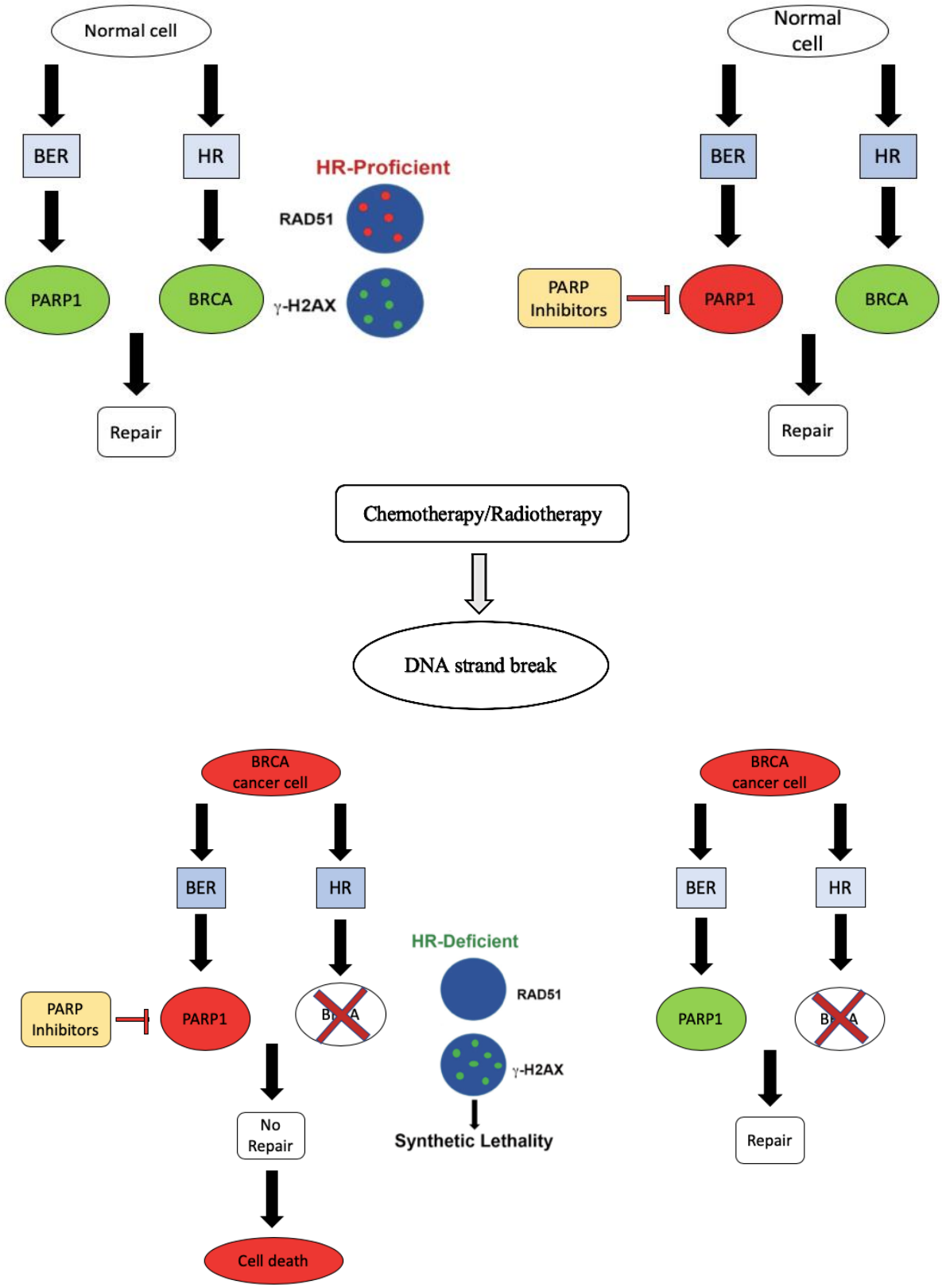

Figure 25.Schematic of synthetic lethality in ovarian cancer cells vs normal cells. Despite the PARP1-enzyme inhibition, normal cells with BRCA-wt have effective repair pathway after inducing DNA damage, whereas in BRCA-m cells, it leads to cell death.

4.3.3 Different types of PARP inhibitors

It has been identified that through inhibition of PARP-mediated repair of DNA lesions formed via chemo- or radiotherapy, potential therapeutic might be developed. Nearly 30 years ago, small molecules were detected as nicotinamide analogs which prevent PARylation and improve the cytotoxicity of dimethyl sulfate, known as DNA damaging agent. The latest discovery in a drug development area has come up with the innovative clinical PARP inhibitors including Veliparib (Abbvie), Rucaparib (Pfizer/Clovis), Olaparib (KuDOS/AstraZeneca), and Niraparib (Merck/Tesaro). More recently, the second generation of PARPi with more potential inhibitory features such as Talazoparib (Lead/Biomarin/Medivation/Pfizer) and has been developed (Brown, Kaye and Yap, 2016).

Table 2. Different types of PARP inhibitors and their status in clinical development. Adapted from (Hou, Chen and Yu, 2019).

PARP Inhibitors	Status in clinical development
Olaparib	FDA approved for advanced ovarian cancer with gBRCAmut with ≥ 3 prior lines of chemotherapy
Niraparib	FDA approved for recurrent epithelial ovarian, fallopian tube, or primary peritoneal cancer who have complete or partial response to platinum chemotherapy
Rucaparib	FDA approved for advanced ovarian cancer with gBRCAmut or sBRCAmut with ≥ 2 lines of chemotherapy
Veliparib	In Phase III studies as combination therapy with chemotherapy in patients with breast and ovarian cancer with gBRCAmut or sBRCAmut and lung cancer
Talazoparib	In Phase III study as monotherapy in patients with locally advanced or metastatic breast cancer with gBRCAmut

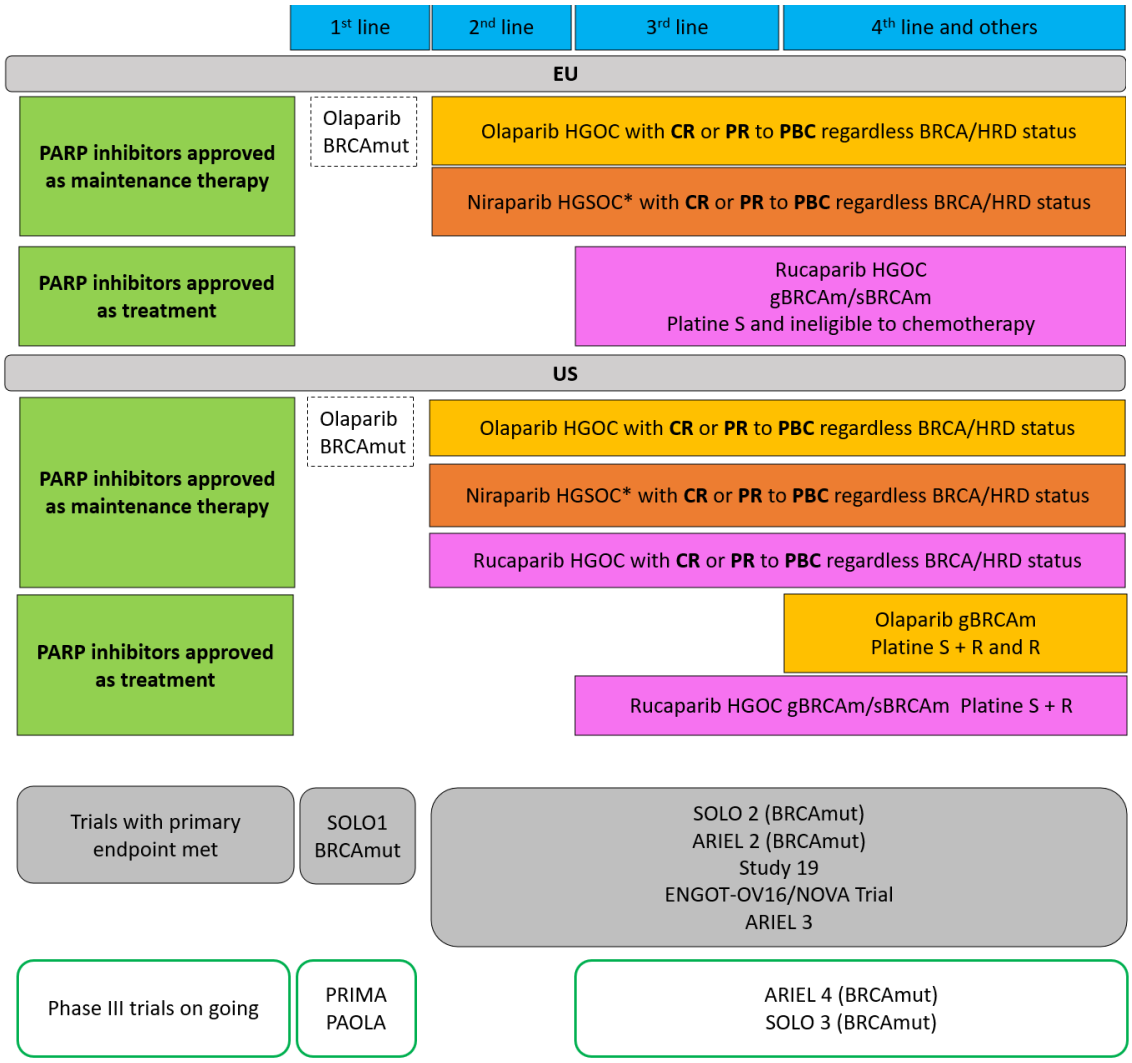

Figure 26. Landscape of PARP inhibitors in ovarian cancer. HGOC: high grade ovarian carcinoma; HGSOC*: high grade serous ovarian carcinoma; BID: twice a day; gBRCAm: BRCA1/2 germinal mutation; sBRCAm: BRCA1/2 somatic mutation; PR: partial response; CR: complete response; PBS: platine based chemotherapy; Platine S:in platine sensitive relapse: Platine S+R: in platine sensitive and resistant relapse; ----------: not currently approved. Adapted from (Colomba et al., 2019).

5. Biomarker development using liquid biopsies

5.1. introduction

Over the last few decades, the concept of liquid biopsies has been identified as an alternative to a conventional needle (tissue) biopsy for different type of cancers. There are many advantages regarding to using liquid biopsies, including the use of different biofluids such as blood, urine, sputum and saliva, early warning of pending resistance, consecutive patient's monitoring, those with many cycles of treatment, less risk to patients, particularly for those who cannot have invasive biopsy (Huang *et al.*, 2017) (Khoo *et al.*, 2016). For instance, tests

can be performed on a blood sample to assess circulating tumour cells (CTCs) or circulating tumour DNA (ctDNA) and can offer a better insight into the real-time tumour dynamics. A sub-population of CTCs have the ability to move into distant organs and develop metastatic events which characterized as disseminated tumour cells (DTCs) (Dasgupta, Lim and Ghajar, 2017). Additional area where improvements have been made is the use of ctDNA, which originates directly from the cancer cell. Further investigation connect ctDNA to progression of cancer cells, level of tumour cell changes and a biological rate of tumour aggressiveness (Chudasama *et al.*, 2019).

5.2. Circulating tumour cells (CTCs)

CTCs are cancer cells which developed from primary or metastatic site of tumour, then shed into the blood circulation and express tumour-specific characteristics. They are detected in different metastatic carcinomas and have capability to form metastasis in other secondary organs. It has been suggested that only 0.01% of these cells will survive and get metastatic. The most described transition of cancer cells is epithelial to mesenchymal, whereby they lose their epithelial characteristic and develop mesenchymal features comprises of invasiveness, motility, and resistance to apoptosis.

CTCs have potential prognostic value in several cancers, while their clinical value is still under investigation. Using CTCs as a liquid biopsy is favourable for continuous evaluation of tumour progression through systemic treatment in a less aggressive and real-time manner, by a simple blood draw (Alix-Panabières and Pantel, 2016). Moreover, it offers potential for the early diagnosis of cancer and significant insights into tumour heterogeneity and genomic multiplicity for the early diagnosis of disease and management of clinical treatment (Alix-Panabières and Pantel, 2013). Therefore, a sensitive and unbiased isolation method is essential to capture CTCs which can provide a tumoral information for analysis and possibly lead treatment decisions (Kapeleris *et al.*, 2018). It has been found that the levels of CTCs are related to therapeutic response and survival (Munzone *et al.*, 2010). By separation and analyzation of CTCs, it has showed a promising technique for non-invasive diagnosis, prognosis, and real-time monitoring to analyse the efficiency of treatment and drug resistance (Munzone *et al.*, 2010).

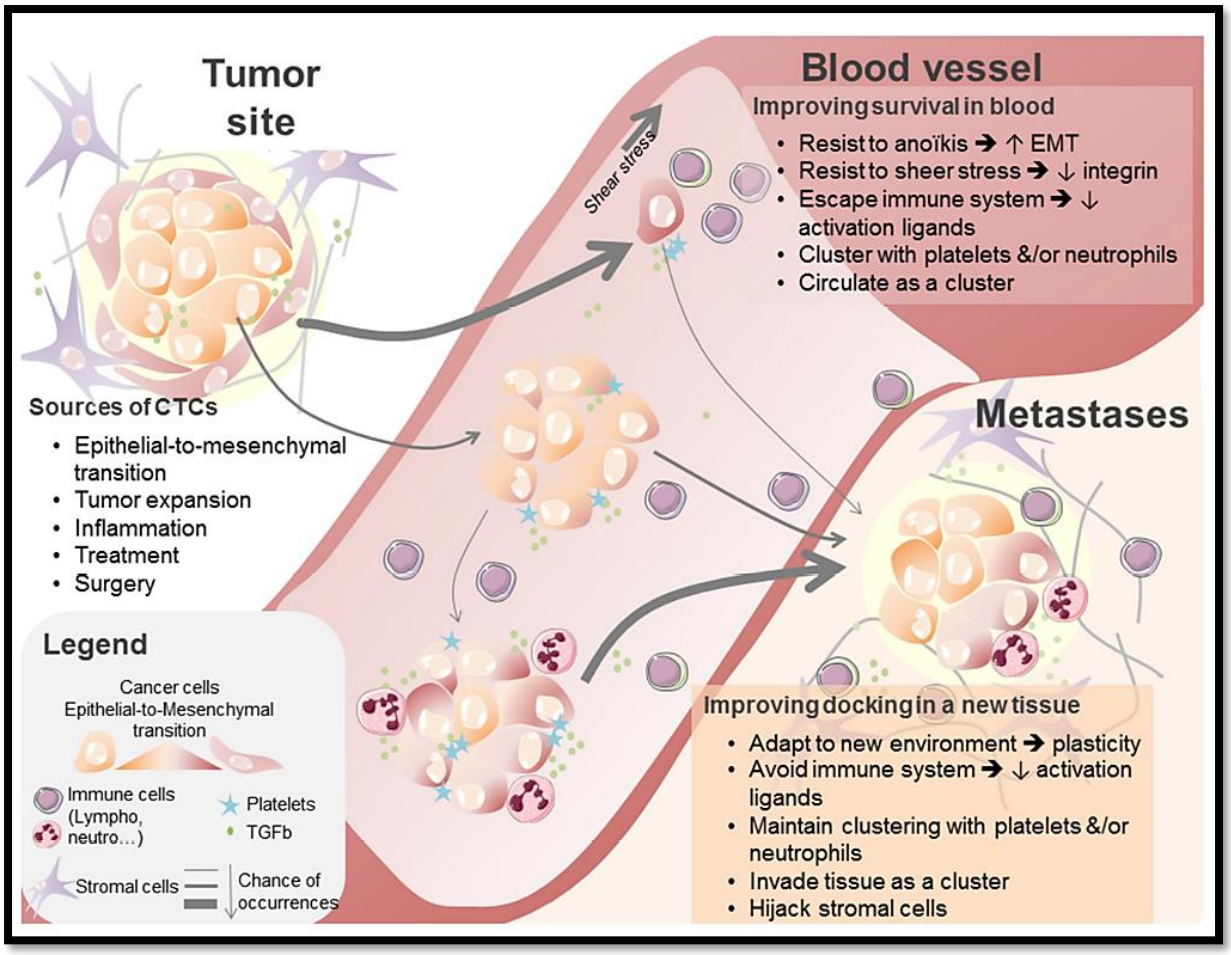

Figure 27. Description of CTCs origins, biological characteristics, and their abilities to facilitate metastases development. CTCs flow into the blood circulation. Illustrative picture of the process of CTCs entering the blood circulation, with highlights on the role of EMT and MET in the spread of cancer. Credit: (Mari *et al.*, 2019).

Table 3. Different techniques used to separate CTCs via different criteria. Depending on the circumstances different technique will be better suited for the separation of CTCs.

Label-Free		**Affinity-Based**		
Function	**Platform**	**Function**		**Platform**
Gradient Based	Ficoll Paque RareCyte	Immunomagnetic		CellSearch Adna Test MACS
Size Based	Circulogix ISET ScreenCell Parsortix	Microfluidic		GEDI Chip OncoCEE Clearbridge BioMedics
Dielectrophoresis	ApoSTream DEPArray	Surface Based		ImageStream HD Imaging

Despite the fact that CTCs play an important role in metastatic disease, (Hiltermann, van der Wekken and Groen, 2012), the basic features of tumour cells in the bloodstream are fully

understood, including their ability to avoid apoptosis, the facility in migration, mostly to specific secondary sites (i.e. ovarian metastasis arises mainly in the bowel, bladder, and abdomen (Hong, Fang and Zhang, 2016).

In the past decade, there has been substantial technological developments in identification and characterisation of CTCs (Table 3). CTCs can be detected using specific antibodies such as epithelial cell adhesion molecule (EpCAM) that is expressed in several cancer types of CTCs including breast , ovarian, pancreatic, prostate and lung cancers (Lorente, Mateo and de Bono, 2014). The most widely used method to detect CTCs to date, is EpCAM detection.

However, due to EMT transition, this poses a limitation in detecting CTCs using this antibody (Wicha and Hayes, 2011). Thus, reliable CTCs detection based on morphological antigen is still challenging.

Epithelial to mesenchymal transition, is a process to generate cells with stem cell-like features from differentiated epithelial cells. EMT is a crucial procedure for embryonic development, while has a role in tumour progression and metastasis as well (Brabletz, 2012). Through EMT process, epithelial cells of the primary tumour trigger upregulation of mesenchymal genes which lead them to lose their cell-to-cell adhesions ability and apicobasal cell polarity. As a result, the cells mobility and invasiveness are increased. It is hypothesised, that in some cases the combination of EMT and stem cell features might make tumour cells to evade from the primary tumour, enter the blood stream and play a role as potential metastasis initiating cell (Blassl *et al.*, 2016). Recent studies have revealed that EMT helps the spread of a single carcinoma cell from origin tumour sites and allows them to adhere and develop into distant metastases (Krebs *et al.*, 2014).

On the other hand, marker independent methods of separating CTCs are not limited to the expression of certain cell surface markers, but are included biophysical features of CTCs, comprising of size, deformability, or dielectric susceptibility (Miyamoto *et al.*, 2012). There are some efforts with notable results which seem to be promising, but it continues to be a necessary techniques to assess the potential role of CTCs as biomarkers in ovarian cancer (Cheng *et al.*, 2017).

5.3. Current CTC Data in ovarian cancer

Due to the vague symptoms and screening technique limitations, most of the patients are diagnosed at late stage. In such a setting, it is crucial to identify prognostic indicators for OC patients. The common biomarker used in OC is CA125, while some non-malignant

gynaecological conditions can cause increasing serum CA125 concentrations. (Sevinc *et al.*, 2007). Therefore, additional prognostic markers are necessary for OC patients.

It has been showed that CTCs have prognostic value among patients with breast, colorectal, gastric, lung and pancreatic cancers. Many studies have reported the prognostic value of CTCs in patients with ovarian cancer, such as Zhou et al., 2015 which revealed that patients in CTC-positive group displayed a worse OS and PFS/DFS compared to CTC- negative group (Zhou *et al.*, 2015). Moreover, Poveda et al., 2011 discovered CTCs in OC patients, and reported a significantly decreased progression-free and overall survival in CTC-positive patients (Poveda *et al.*, 2011). In the study by Zhang et al., 2018 CTC counts declined during adjuvant and neoadjuvant therapy as well (Zhang *et al.*, 2018). Additionally, in Banys-Paluchowaski et al., 2020 study, the level of CTC positivity was dropped rapidly during treatment and no patient revealed CTCs at the end of sixth cycle of chemotherapy. They demonstrated that positive CTC status associated with shorter OS and PFS (Banys-Paluchowski *et al.*, 2020).

Although, the importance of CTCs in ovarian cancer remains debated. There was no correlation between CTC status and prognosis in some researcher (Aktas *et al.*, 2011). The analysis of single cell of CTC can allow us to classify cells with various expression profiles to give a hint regarding to the CTC development during treatment. In That Way, single CTC analysis displays a 'liquid biopsy' for the collection of an applicable therapy and for real time monitoring of its effectiveness (Blassl *et al.*, 2016).

5.4. Gamma H2AX as PD Biomarkers to Monitor Drug Activity in CTCs

There are numerous reasons to explore the clinical potential of γ-H2AX as it can be be used as a biomarker to predict outcomes of patient and latest studies have determined γ-H2AX as a biomarker for clinical diagnosis in cancer development (Sedelnikova and Bonner, 2006).

CTCs separated from peripheral blood of patients with metastatic breast cancer has an increased in positive γ-H2AX count in CTCs from 2% at baseline to 38% after a single day of treatment, regardless of decreases in the total number of CTC (Wang *et al.*, 2010a). Consequently, this measurement can be used to improve the assessment of drug effectiveness in cancer treatments (Krebs *et al.*, 2010). However, chemotherapeutic agents also target normal cells in patients and in comparison, the response of γ-H2AX in normal cells might be more informative and reproducible. The γ-H2AX levels can be assessed using fluorescent microscopy or flow cytometry which present low level of background and improve the detection of DNA damage even in low level (Wang *et al.*, 2010b).

5.5. Circulating nucleic acids

Circulating cell-free DNA (ccfDNA) released from apoptotic cells which is usually found to be in 160-200bp fragments whereas ccfDNA from necrotic cells varies in length (Kustanovich *et al.*, 2019). In both scenarios, ccfDNA concentration in the plasma or serum is increased in cancer patients than healthy subjects just like the CTC number. In numbers, normal subjects have an average mean of 13 ng/ml ccfDNA concentration, whereas cancer patients' mean is around 180ng/ml (Vymetalkova *et al.*, 2018). Stroun et al. showed that free DNA of cancer patients is originated from the tumour cells and many mutations in oncogenes and/or tumour suppressor genes have been found in the ccfDNA in plasma (Stroun *et al.*, 1989).

To date, several successful studies have been performed to validate this concept, in a variety of cancers, including lung, breast, pancreatic, bladder, gastroesophageal, colorectal, melanoma, hepatocellular, and head and neck cancers, by comparing both CTCs and ctDNA. Circulating nucleic acids (ctNAs) are another form of liquid biopsy which include DNA (ctDNA) and RNA. It is not well understood how ctDNA enter the blood, but the evidence indicates that apoptosis could be one of these. Figure 28 represent a schematic of this process. There is evidence which shows ctDNA has a fragment length comparable to the classic apoptotic fragment length pattern, with a range from 145 to 180 bp. Moreover, Moulier et al., 2018 was showed that cfDNA derived from cancer patients had a different size distribution in cfDNA in comparison to length of ctDNA fragments. In particular, an enrichment in fragments size < 150bp in mutant ctDNA (41%) compared to non-mutant cfDNA (21%) was displayed which leads to demonstrating the highly fragmented profile of ctDNA versus cfDNA (Mouliere *et al.*, 2018). However, there is no studies which has estimated the accurate half-life of cfDNA/ctDNA in the bloodstream. It is generally accepted that its half-life in circulation can change from 15 min to 2.5 hours. Despite the short half-life of ctDNA, they can be detected in plasma due to continuum process of its release to bloodstream (Paracchini, D'incalci and Marchini, 2021).

All the studies report higher detection and concordance with tissue results using ctDNA over CTCs. The percentage of ctDNA originating from tumour cells, however, has been estimated to range from 10 to 90% of the total cfDNA (Lanman *et al.*, 2015). Thus, the applicability of measuring the cfDNA length (i.e., DNA integrity) in plasma may therefore depend on the type of disease. Detection of these longer ctDNA fragments and quantification of their

relative abundance in plasma compared to short cfDNA fragments and the calculation of a DNA Integrity Index has been explored as a potential cancer monitoring technique (Elazezy and Joosse, 2018). ctDNA analysis is currently used as the most promising circulating biomarker with potential clinical utility in the near future. Additionally, the ctDNA analysis leads to have a better and complete view of the general biological features to characterize the disease, and finally overcoming the issue of spatial heterogeneity (Paracchini, D'incalci and Marchini, 2021).

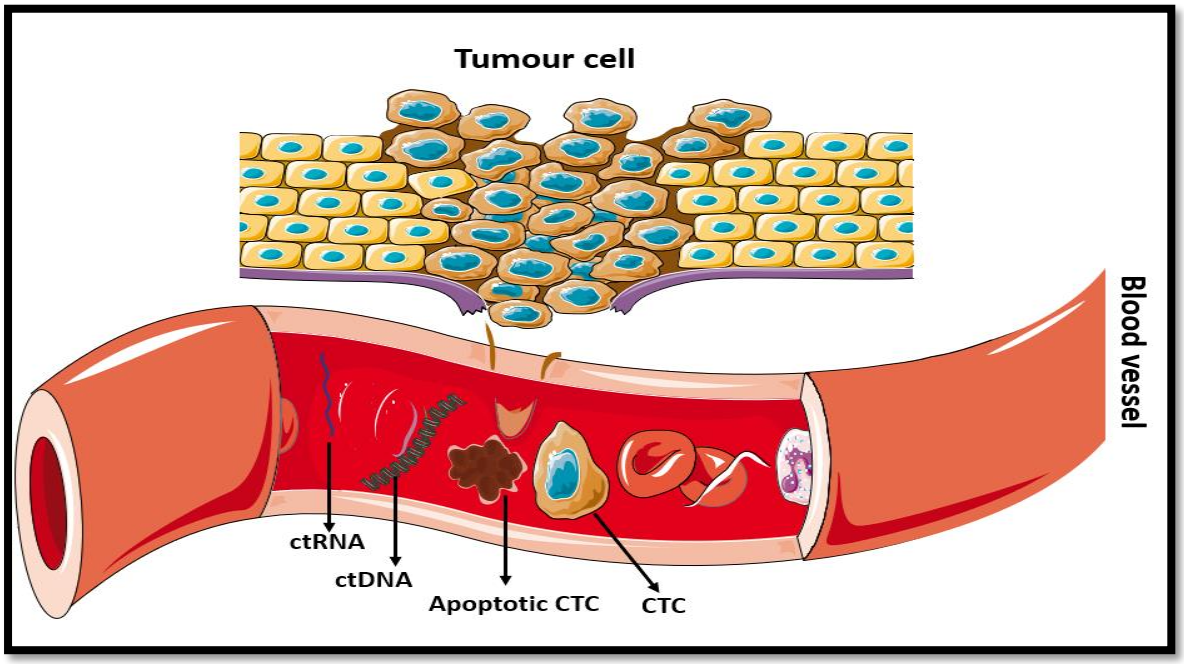

Figure 28. Source and process of some circulating liquid biomarkers formed from the primary tumour to their migration into the bloodstream. Adapted from (Medicalexpress, 2017).

The exact nature of ctDNA and CTCs shedding is unidentified, but it is assumed to happen due to apoptosis and necrosis of cancer cells. Apoptosis of normal cells make larger truncated cfDNA fragments, while ctDNA are smaller fragmented DNA and made when cancerous cells undergo necrosis and mitotic (Huang *et al.*, 2018). Currently, ctDNA can be found in several bodily fluids, including blood, urine, stools, milk, bronchial lavages and ascites. The new field, genomic profiling for ctDNA has developed a popular research, based on the assumption that ctDNA has the same profile of somatic mutations and genomic characterization as the tumour itself (Freidin *et al.*, 2015). Due to reliance of cancer cells on the oncogene's activation for proliferation and survival, the existence of these particular gene alterations and mutations can be of diagnostic value and also reflect responsiveness of patients to the therapy, and predict survival (Wang *et al.*, 2013).

The total amount of cfDNA in EOC patients was evaluated and compared to healthy controls and patients with benign ovarian tumours. It was demonstrated that the level of cfDNA was increased in plasma of cancer patients. Additionally, there was a significance difference in the amount of cfDNA between patients with early and late stages of the disease (Bettegowda *et al.*, 2014) (Capizzi *et al.*, 2008). In the last few years, using next generation sequencing technologies and developing new bioinformatics tools, leads to improvement of ctDNA analysis despite the short ctDNA fragment length which make it possible to examine the genomic features of HGS-EOC, including the clonal pathogenic TP53 mutation, other genes such as BRCA1 and BRCA2, involved in treatment response, and the chromosomal abnormalities which characterized HGS-EOC (Dann *et al.*, 2012) (Adalsteinsson *et al.*, 2017).

Currently, there are two phase of clinical trials which are registered, including CLIO trial (ClinicalTrials.gov Identifier: NCT02822157) that is concentrated on the ctDNA analysis to guide Olaparib treatment in recurrent epithelial carcinoma of the ovary, fallopian tubes, primary peritoneum cancers, whereas the second one (ClinicalTrials.gov Identifier: NCT04175470) aims to assess the different level of methylated HOXA9 ctDNA in platinum resistant EOC patients receiving bevacizumab. The outcomes of these ongoing researches will be available, starting from 2023 (Paracchini, D'incalci and Marchini, 2021).

5.6. The Role of CTCs in Clinical Trials

CTC evaluations offer an opportunity to develop new biomarkers to monitor drug efficiency while reducing the need of biopsies and its risk related to the process. In addition, assessment of CTCs is merged into clinical trials as prognostic, predictive and intermediate biomarkers to response of therapy (Attard and de Bono, 2011) . This approach might also enable to detect the molecular changes in CTCs indicating tumour genotype which can lead to drug-resistant in disease progression. The number of CTC has been currently used in metastatic breast cancer regarding to treatment decision algorithm in several phase III to select between chemotherapy vs endocrine therapy, as well as help to change of treatment at early stage. In this method they are evaluating HER2-positive CTCs in HER2-negative primary tumours and analysing the role of HER2-directed therapies in these patients (Alemar and Schuur, 2013).

6. Aims

This PhD project aims to evaluate the use of Rucaparib-new PARP inhibitors- on BRCA-m ovarian cancer cells with homologous recombination deficiency (HRD). It is broadly accepted that formation of γ-H2AX in response to DNA double stranded breaks (DSBs) can provide the basis for a sensitive assay of DNA damage in human liquid biopsies. Moreover, liquid biopsies offer a promising alternative to tissue samples, providing non-invasive diagnostic approaches or serial monitoring of disease evolution. Based on preliminary data, the hypothesis at the basis of this project is that γ-H2Ax staining in non-haematopoietic circulating cancer-related cells (CCs) and H2AX gene expression can act as surrogate biomarkers for patients with advanced epithelial OC (aEOC) undergoing treatment.

Hypothesis

- Homologous recombination (HR) pathway can be affected by BRCA2 deficiency.
- H2AX can potentially be used as a predictive biomarker.
- Cancer cells with BRCA2 mutation are more sensitive to PARP inhibitors treatment.
- γ-H2AX quantification can be used as a predictive biomarker of response in CTCs in OC patients.

Aims

- The expression of BRCA2 protein in OC cell lines.
- The effects of BRCA2 mutation on efficiency of HR by using immunofluorescence technique (γ-H2AX assay).
- Look at the H2AX expression in OC using TCGA and validating our cancer patients' sample through qPCR.
- Using gene set enrichment analysis (GSEA) to study gene association of some genes involved in OC patients with high level of H2AX.
- Genome-wide association study in order to identify any associations of SNPs with cancer as well as 5-year overall survival,
- Study of H2AX prognostic value by using KM plot in OC patients
- Assess the expression of H2AX in different type of OC with different stage by using tissue microarray.
- Compare the level of H2AX phosphorylation with gene expression.
- Use different ovarian cancer cell lines that are BRCA2-wildtype (SKOV3), BRCA2-m (PEO1) and BRCA2-silent mutant (PEO4, MDAH) to assess the effects of Rucaparib *in vitro.*

- Use liquid biopsies from a clinical trial of ovarian cancer patients treated with Rucaparib (in collaboration with MVCC) to assess the effect of Rucaparib on CTC enumeration and expression of key proteins.
- To study the γ-H2AX expression and assess γ-H2AX in CTCs as a predictive biomarker of treatment response.
- To assess any correlations between γ-H2AX foci, WT1 and CA125 levels and clinical outcomes of OC patients receiving chemotherapy.

Objectives

- To assess the effects of Rucaparib *in vitro* by using different ovarian cancer cell lines with wild-type or mutant BRCA2 gene.
- To assess the effect of PARP inhibitors on CTC enumeration and expression of key protein using liquid biopsies from ovarian cancer patients treated with Rucaparib as part of a clinical trial.
- To assess the γ-H2AX expression in CTCs and evaluate this as a predictive biomarker of treatment response by establishing any correlations between γ-H2AX foci, WT1 and CA125 levels and clinical outcomes of OC patients receiving chemotherapy.

Chapter2: Materials and method

1. Cell maintenance

1.1. Cell lines

SKOV3 (ATCC, 2016), PEO1 (Ximbio, 2018a), PEO4 (Ximbio, 2018b) and MDAH-2774 (Expasy, 2020) cell lines were used as *in vitro* models of human OC. All cells were cultured in proper media comprising of 10% FBS (foetal bovine serum, Gibco) and 1% penicillin-streptomycin (Gibco) to avoid contamination. Cells were grown in T75 flasks, and the growth temperature was 37°C and 5% CO2. Media was changed 2 or 3 times a week. A standard technique for cell culture aseptic was carried out in a controlled temperature, class m2 Laminar Flow Hood. Cell line detail are summarised in Table 4.

Table 4. List of all cell lines, used in my study and their details.

Cell line	Gene mutation	Morphology	Disease	Media	Histology
SKOV3	P53 null PIK3CA	Epithelial	Adenocarcinoma	DMEM	Clear cell
PEO1	BRCA2 TP53	Epithelial	Adenocarcinoma	RPMI-1640	High grade serous
PEO4	BRCA2 (silent) TP53	Epithelial	Adenocarcinoma	RPMI-1640	High grade serous
MDAH-2774	TP53 PIK3CA KRAS BRCA2(silent)	Epithelial	Adenocarcinoma	DMEM	Endometrioid

1.2. Cell culture methodology

Before start working, all solutions were warmed up in the warming water bath, at 37° C for 30 minutes. All cells were frozen and kept in liquid nitrogen. After thawing the frozen vials, they were transferred to 15mL falcon tube with 3ml media. Next, to remove the DMSO, they were centrifuged at 1500 RPM for five minutes and then the supernatant was aspirated. The pellet was mixed with 5mL of media, transferred to a T25 flask with a filter head (Nunc) to avoid contamination. Depends on their doubling time, they were sub-cultured every two or three days at 80-90% confluency, through using TE (TrypLE Express, Gibco) for cell detachment. All the hood, incubator and water-bath were constantly cleaned and disinfected.

1.3. Cryopreserving cells

Cells were frozen to be used for the future experiment. 90-100% confluent flask was chosen and checked for contamination. To begin, the old media was aspirated, and the cells were washed in 10mL phosphate buffered saline (PBS, 1x PH7.4, Severn Biotech Ltd). As described before, cells were trypsinized, resuspended in 5ml media. Next, moved into a 15mL falcon tube and centrifuged for 5 min at 1500 RPM, followed by mixing the cell pellet with proper amount of freezing medium (Recovery Cell Culture Freezing Medium, DMSO (10%), Gibco). Finally, 1ml of cell suspension was transferred to cryogenic vials and placed in a cell freezing container at the temperature of -80^{0}C for at least 24 hours before transferring them into the liquid nitrogen dewar.

1.4. Cell counting

Prior to using cell line in an experiment or sub-culture, cells in each flask were counted by using cell countess device which is presented in Figure 29. First, cells were detached from the flask with TE as previously described and re-suspended with 1mL media. After recovering the cells in growth media, 10µL of cell suspension was added to another 10µL of Trypan blue dye in new Eppendorf tube. Finally, 10µL of the new mix was loaded onto the Countess™ cell counting chamber slide (Invitrogen). Trypan blue dye was added to detect the dead cells and colour them blue whereas the live cells were not coloured due to their intact cell membrane (Alphametrix, 2015).

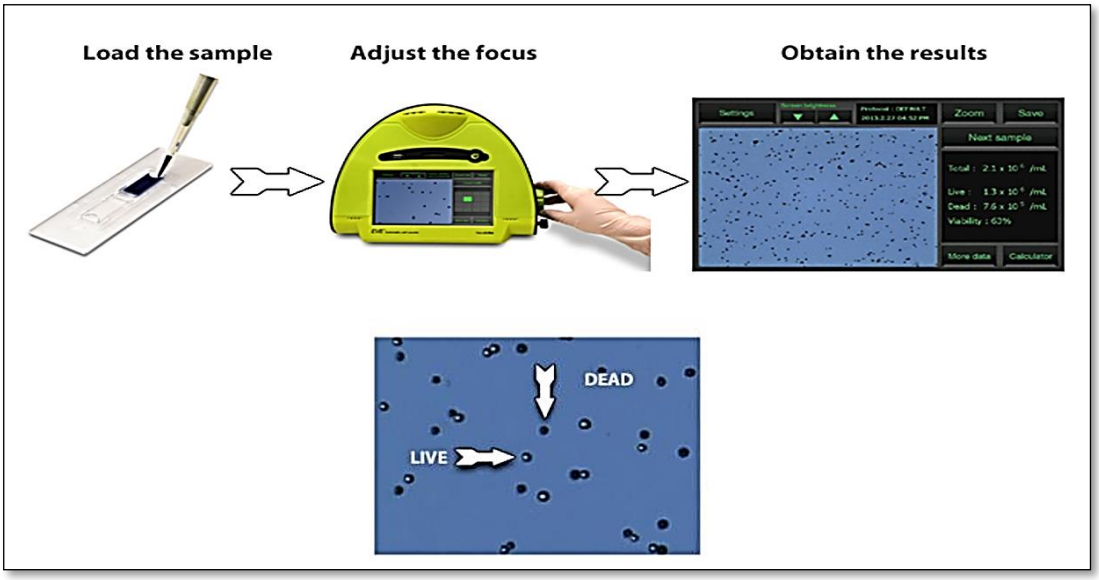

Figure 29.Counting cells with a cell Countess. The figures show the progress of cell counting by using the countess machine that demonstrates the number of living cells, dead cells and the cell viability. The numbers can help to determine the total number of cells in each flask (Alphametrix, 2015).

2. Hydrogen peroxide (H_2O_2) concentration

Hydrogen peroxide solution (H_2O_2 30% (w/w) in H_2O, contain stabilizer, Sigma-Aldrich), can be used as an oxidizer, bleaching agent, antiseptic. Concentrated H_2O_2 is known as reactive oxygen species (ROS), can produce hydroxyl radical in the presence of iron and converted to a strong oxidizing agent. H_2O_2 modifies several cellular macromolecules such as proteins, polyunsaturated fatty acids, and DNA. Despite the fact that damage to each cellular component is responsible for lethal cell injury, there are some components that may be more important than others (Lee, Ha and Kim, 2001). H_2O_2 can induce the double strand break in genome which can lead to cell death. It has been established that the high concentration of H_2O_2 can kill the cells and it is necessary to optimize the H_2O_2 concentration at levels which induce the DSB but not kill all the cells. Two 6-well plates were used to seed $1x10^6$ cells/well. After specific time points, the old media was discarded, cells were trypsinized and counted by countess slide, as described before in section-1.4. The H_2O_2 kill curve was generated for each cell line to choose the appropriate concentration.

3. Immunocytochemistry (γ-H2AX assay)

There are several techniques to detect the DSB-DNA and γ-H2AX assay is one of the most popular ones which detect damage sites of DNA in interphase nuclei by using a monoclonal antibody against the γ-H2AX protein.

3.1. H_2O_2 treatment to induce DSB

To detect the DNA damage, I needed to induce the DSB on DNA. All cell lines were exposed to H_2O_2 in time- and dose-dependent manner. Additionally, it was required to make two more flasks including AlexaFluor-488 and DRAQ5, for ImageStream^{TM} to be used as compensation sample. After specific time-points, all flasks were washed with 5ml PBS to remove extra H_2O_2. Next, they were trypsinized, transferred to 15mL falcon tube and centrifuged for 10 minutes at 2500 RPM. The supernatant was discarded, and the pellet was used for the next step which is explained later in section 3.2 and 3.3.

3.2. γ-H2AX detection in cell lines

First, cells need to be fixed with 1-mL 4% paraformaldehyde (PFA) (Sigma-Aldrich) and kept for approximately 5 minutes on ice. Following fixation, cells were washed with PBS to rehydrate them. They were centrifuged, then permeabilized with 0.5% TritonX100 (Sigma-Aldrich) in PBS and incubated for further 10 minutes on ice. Cells were centrifuged and washed with PBS prior to blocking step. One mL blocking buffer (10% Bovine Serum Albumin (BSA, Gibco) in PBS) was added to cell pellet to prevent non-specific binding and

incubated for 1-hour at room temperature. All samples except for the DRAQ5 compensation one, were incubated with γ-H2AX antibody conjugated with AlexaFluor-488 (Millipore), at the relevant concentration (1:100), overnight in cold room with gentle agitation and covered with foil to prevent the light absorption. Next day, cells were re-centrifuged, washed with 1-mL washing buffer including 0.1% Tween (Sigma-Aldrich) in PBS. Then, 99µL of Accumax (Cell detachment solution, STEMCELL technologies) was added to all tubes. At the final step, all samples except for the AlexaFuor-488 compensation one, 1.0µL of DRAQ5 (Biostatus Ltd) was added to stain the nucleus, covered from light and ready to Imagestream image capture.

3.3. γ-H2AX detection in clinical samples

For the blood samples, it is required to separate the red blood cells (RBC) from plasma. First, 1ml of blood was added to 9mL of RBC lysis buffer (G Biosciences). It was inverted 5 times and then incubated at shaker for 10 minutes. After that, it was centrifuged at 2500 RPM for 10 minutes, the supernatant was discarded, and the pellet was suspended with 3mL of RBC lysis buffer. It was incubated at shaker and re-centrifuge, followed by fixation and other steps which were described previously at section 3.2.

4. Immunofluorescence (γ-H2AX assay)

4.1. γ-H2AX detection in cell lines

Another popular method of detecting DSB-DNA damage is cell staining on slide and analyse it under the fluorescence microscope. It detects DSB in interphase cells using a monoclonal anti-body against the γ-H2AX protein. For γ-H2AX assay on adherent cells, they must be seeded on poly-prep slides (Poly-L-lysine coated glass slide, Sigma-Aldrich) for 24 hours prior to treatment with DNA damaging agent which in our case was H_2O_2. All the cell lines were treated with H_2O_2 in time- and dose-dependent manner and the plan is shown in the Figure 30.

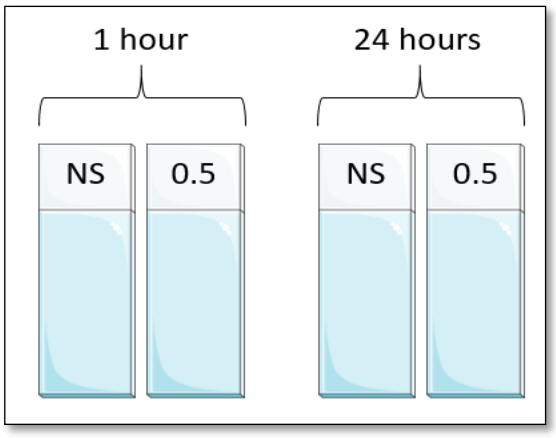

Figure 30. Schematic figure of the plan for γ-H2AX assay with Leica microscope. The figure shows the concentration of used H_2O_2 (0.5mM) and the time points. After 1-hour exposure to 0.5mM H_2O_2, old media was replaced with fresh one, then after 1- and 24-hrs, cells needed to be fixed and go through other steps of the experiment (Authors' adaptation).

After indicated time-points, cells were fixed using 4% PFA in PBS for 15 min. In the next step, cells were permeabilized using 0.2% Triton-X solution (Sigma-Aldrich) in dH_2O for 10 min at 4°C. Then, non-specific sites on the cells were blocked using 2.5% BSA blocking buffer which 100µL of it was added to each slide and then slides were covered with parafilm and placed in a humidified dark box for one hour. Next, a total of 100µL of diluted γ-H2AX antibody conjugated with AlexaFluor-488 (Merckmillipore), at the relevant concentration (1:100) (following manufacturer's instructions), was added to the slides and slides were covered with parafilm and placed in a humidified dark box for one hour. After that, the slides were washed 3x 5 min in TBST (Tris-buffered saline with Tween 20, PH7.5, Sigma-Aldrich) and then PBS. The slides were de-hydrated in ethanol series ((70%, 90% and 100%) for 5 minutes each time. Once the slides were air dry, a total of 15µL DAPI (Vector Laboratories) was added to each slide and covered with a cover slip and sealed using clear nail varnish. The slides were ready to analyse under the Leica DM4000 microscope.

4.2. γ-H2AX and WT1 detection in clinical samples

4.2.1. Whole blood

Ovarian cancer blood samples were collected from ovarian cancer patients joined on a clinical trial at Mount Vernon Hospital, London, known as the CICATRIX and Centurion trial (with appropriate ethical approval). Normal control blood samples were collected from volunteers. All patients were stage III & IV, participated on the CICATRIX and Centurion trial with chemotherapy and targeted therapy treatment, respectively. All blood samples were collected in Roche tubes to stop coagulation of the blood. Plasma was collected after 10 min

spinning at 1500 rpm and stored at -80°C until use. To use blood's RNA, 0.5mL of whole blood was collected, 1.0mL of RNAlater® (Life Technologies) added and stored at -20°C.

4.2.2. Process

For the blood sample processing, there is a need to separate the red blood cells from the remaining sample containing CTCs and white blood cells. Firstly, 1mL of blood sample was added to 9mL of RBC lysis buffer. It was inverted 10 times and then incubated at shaker for 10 minutes. After that, it was centrifuged at 2500 RPM for 10 minutes. Next, the supernatant was discarded and again 3mL of RBC lysis buffer was added and mixed with pellet. It was incubated again at shaker and re-centrifuge. Next, the pellet was re-suspended in one mL PBS and cytospined for 5min/800 rpm to attach the blood cells to slide. In the following step, slides were fixed in 4% PFA and then permeabilized with 0.5% Triton-X on ice. After 1-hour blocking step, I added γ-H2AX antibody conjugated Alexa Fluor (488), and WT1 antibody conjugated Alexa Fluor (647) (abcam) to detect CTC in cell pellet and left overnight. Then the pellet was washed three times with 0.1% Tween in PBS for 5 minutes. Finally, after dehydrating steps with ethanol (70%, 90% and 100%), 15µL DAPI was added and slides were covered with a cover slip, sealed using clear nail varnish and were ready to analyse under the Leica DM4000 microscope.

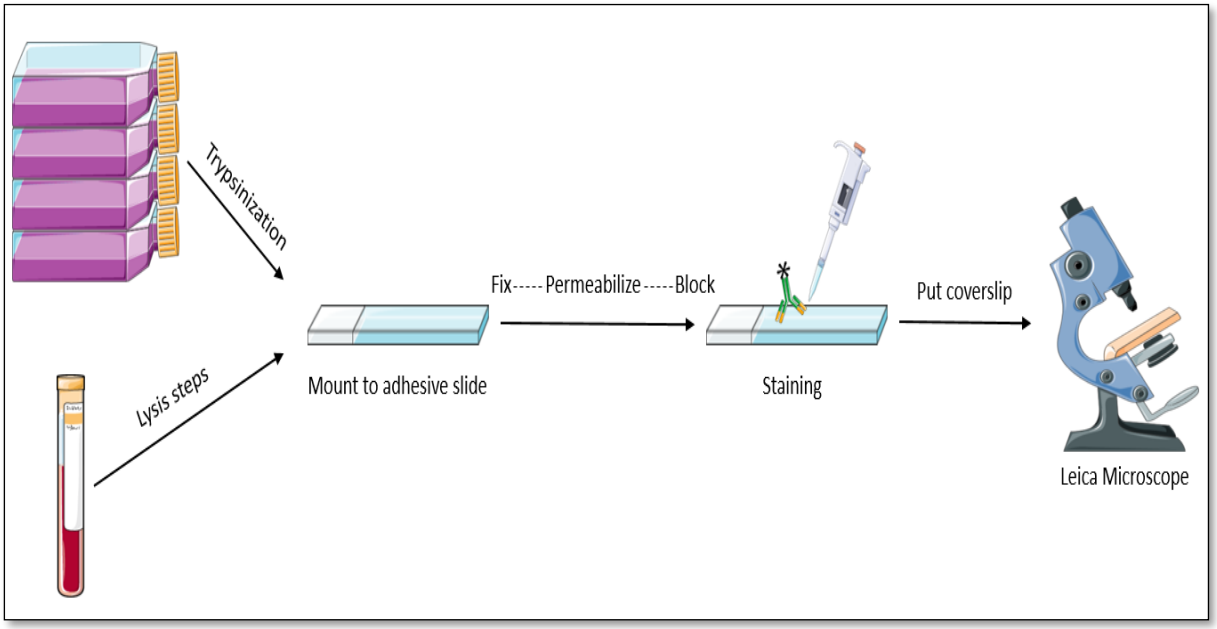

Figure 31. Schematic figure of immunofluorescence technique.

5. Western Blot

BRCA2 protein lysates was analysed by Western blot in all OC cell line including PEO1 (BRCA2-m), SKOV3 (BRCA2-w/t), PEO4 (BRCA2-silent mutation) and MDAH-2774 (BRCA2-silent mutation).

5.1. Protein sample preparation

Cells were seeded to 80-90% confluence and plates were washed three times with PBS. Excess liquid was removed and 250µL of laemmli buffer (Merkmillipore) containing 10% (v/v) sodium dodecyl sulfate (SDS), 250mM Tris pH 8.0, 50% (v/v) glycerol and 0.01% (w/v) bromophenol blue plus 10µL of protease Inhibitor (x7) and 10µL of beta-mercaptoethanol (BME) were added for at least one minute on to each well. Then, cells were scraped off using a cell scraper. Samples were collected into an Eppendorf tube. The samples were boiled on heating block at 90°C for 10 min to denature the protein followed by storing at -80°C. It is important to avoid repeated thawing and freezing of the protein sample.

5.2. Protein Gel Electrophoresis

In this step, 10µL of samples were added into the well, along with the 3µL protein ladder. The higher the molecular weight of a protein of interest, the lower the percentage of gel that is required. In my experiments where heavy proteins such as BRCA2 (molecular weight of 460kDa) were involved, a 4-15% precast gel (Bio-Rad) was used. Eventually the protein samples were loaded carefully onto each well. The ladder (protein marker) was normally loaded on the first wells. The interior and exterior of the tank was filled with 1x running buffer made with 3.02g (w/v) of Tris base, 14.4g (w/v) of glycine, 1g of SDS in 1L of distilled water. After that, the gel was placed in the tank to run at 40mA (80mA if there are 2 gels) constant and 300V for approximately 40 minutes. The samples were checked regularly to prevent running off from the protein samples.

5.3. Blotting and Transfer

Heavier proteins move slower and hence were at the top of the gel, whereas smaller proteins move faster and were found near the bottom of the gel. Once proteins were separated based on their size and mobility, transferred onto a blotting paper. Nitrocellulose membranes have a high protein-binding affinity. The cassette “sandwich” was then prepared as displayed in Figure 32.

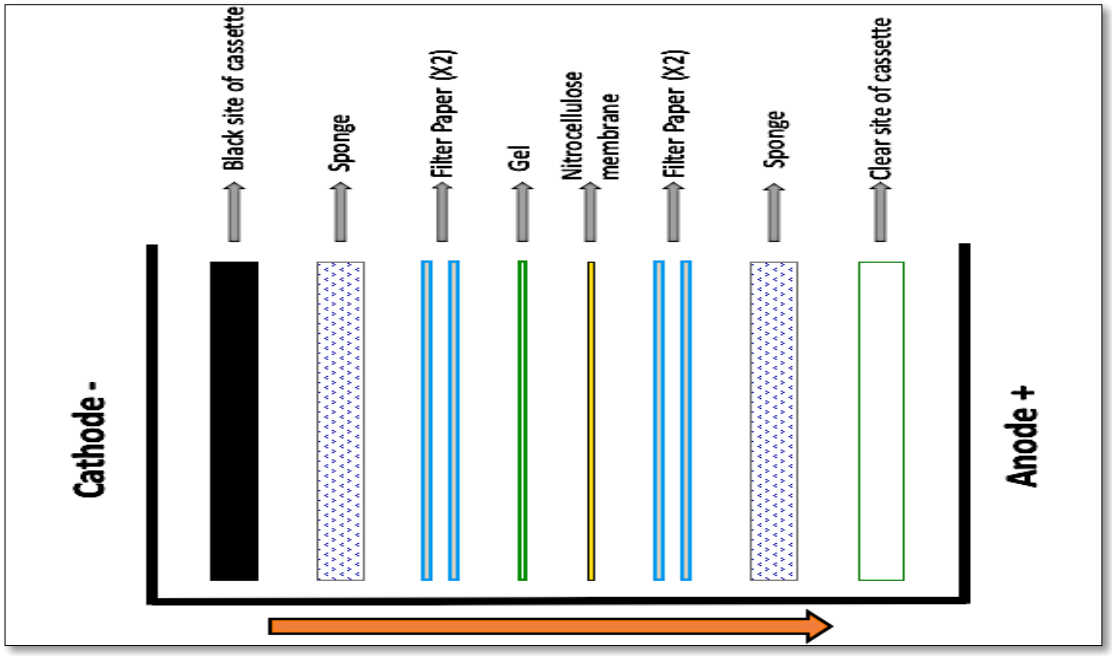

Figure 32. Schematic figure of the electro blot transfer process using an immersion procedure. Arrow at the bottom of the tank indicates transfer direction.

A small magnetic stirrer was placed in the tank, topped with 1 X transfer buffer made with 11.25g (w/v) of glycine, 2.41g (w/v) of TRIS base, in 800ml of distilled water. The blotter was placed inside the tank and the tank was run at 400mA and 300V for 1 hour and 30 min on a magnetic stirrer to create an even distribution of the electrolysis. An ice block was also placed inside the tank, next to the red side of the holder to raise the level of buffer solution and to prevent over-heating of the buffer solution. The tank is then transferred to the tray and surrounded in ice.

5.4. Blocking and antibody incubation

Once the transfer of protein from gel onto the nitrocellulose membrane was completed the proteins were blocked with blocking buffer including 1g of milk powder in 20mL of Tris buffer saline-Tween (TBST). The membrane was left in 30ml of blocking solution for about one hour on a shaking platform at room temperature. The milk mixture blocks unspecific binding of an antibody with the membrane. After one hour of blocking, the membrane was rinsed with TBST and then the primary antibody (anti BRCA2 (Ab-1) mouse (Merkmillipore), diluted 1/100) was added which was prepared in 5 % BSA in 1x TBST and kept overnight on the orbital shaker at 4°C. The following day, the membrane was washed three times with 1x TBST for 15 minutes each and incubated with a secondary antibody,

which is anti-mouse IgG in rabbit (Sigma-Aldrich), diluted 1/2000) which was prepared same way as the primary antibody on a shaker for one hour.

5.5. Protein detection with chemiluminescence

After one-hour incubation with a secondary antibody the membrane was washed as before. During the final wash, the development solutions were made in centrifuge tubes labelled A (including 5mL 100mM TRIS pH 8.0, 22µL Coumaric acid and 50µL Luminol) and B (including 5mL 100mM TRIS pH 8.0, 3µL 30% H_2O_2). From this step, everything needed to be taken to dark room. Solution A and B were mixed and added to the tray with membrane and put on shaker (gently) for 2 min. Next, the membrane was blotted on filter paper and exposed to X-ray film within a light impermeable cassette for 30 seconds to 3 minutes (dependent on strength of antibody), followed by developing on a Curix60 (AGFA) automatic developing machine.

6. Reverse Transcriptase Polymerase Chain Reaction (RT-PCR) analysis

6.1. Sample preparation

First, I used one 80-100% confluent T75 flask to get enough number of cells. After trypsinization, the cells with TE were moved to 15mL falcon tube to centrifuge at 1500 RPM for 5 minutes. After removing the TE, the pellet was re-suspended with 1mL media. Before placing them in the 6-well plate, it was necessary to count the cells to make sure enough cells needed for extraction, is placed. As described earlier about cell counting process in the section 1.4, the proper number of cells was calculated. Next, the rest of the solution (cells with media) was diluted within 3ml media and then 1mL of it was transferred to each well. It was required to give the cells time to attach the surface; therefore, I kept them overnight in the incubator. In the next day, to harvest the cells, they were trypsinized with 1.5mL of TE and then centrifuged at 1500 rpm for 5 minutes (to extract RNA) or 190 rpm for 5 minutes (to extract DNA). They were ready to use for the next process.

6.2. RNA extraction

RNA extraction was performed by using the RNeasy® Mini Kit (Qiagen) following instructions of manufactures that was provided in the kit. The maximum number of cells which was recommended for this process was 1 x10^7. Firstly, the supernatant was discarded, and the pellet washed with PBS 3 times. After removing the PBS, the pellet was re-suspended in 350µL of RLT buffer (guanidium thiocyanate lysis buffer) in the Eppendorf tube. Next, 1mL of 70% ethanol was added to the lysate, the Eppendorf was inverted 10 times and

pipetting technique was done. A total of 700µl of the solution was transferred into a RNeasy spin column placed in 2mL collection tube and then centrifuged for 15 seconds at 10000 rpm. The flow-through was discarded and 700µL Buffer RW1 was added to the RNeasy spin column. Again, it was re-centrifuged for 15 seconds at 10000 rpm, followed by discarding flow through. In the next step, 500µL Buffer RPE was added to the RNeasy spin column and re-centrifuged for 15 seconds at 10000 rpm. The flow-through was discarded and again 500µL Buffer RPE was added to the RNeasy spin column and re-centrifuged for 2 minutes at 10000 rpm. In the following step, the spin column was placed into the new 1.5mL collection tube and 30-50µL of RNase-free water was added directly to the spin column membrane. Then it was centrifuged for 1 minute at 10000 rpm to elute the RNA. It was crucial to keep the RNA in the -80°C.

6.3. Measurement of RNA quality

The quality of the RNA was checked through a Nano-Drop 2000C (Thermo-Fisher Scientific) which its function is based on an absorbance measurement of all molecules in the sample at the wavelength of interest. At 260 nm, nucleotides, RNA, ssDNA, and dsDNA will contribute to the total absorbance of the sample. Therefore, to confirm the correct results via using Nano-Drop™, the purification of a nucleic acid sample is required (Desjardins & Conklin, 2010). To assess the purity of RNA, the 260 nm and 280 nm wavelength is used. The accepted "pure" ratio for RNA is ~2.0. The other ratio significantly lower, in either case, can be related to the presence of protein, phenol or other contaminants which absorb strongly at or near 280nm (Ponti, et al., 2018).

Before using the Nano-Drop device, the lens (top and bottom) needs to be cleaned gently with clean “lens tissue”. Then, 1µL of appropriate diluent was added, depending on the solution used to dissolve the DNA/RNA and the spectrophotometer was blanked. After measurement of blank which should be zero, the lens was cleaned again and then 1µL of samples was added and then measured. Once all the samples were finished, the lens was cleaned by adding 1µL of PURITE water and then gently wiped and the pedestal was closed.

6.4. Reverse Transcription (cDNA synthesis)

cDNA synthesis was performed by using the high-capacity cDNA reverse transcription Kits (Applied-Biosystems) following instructions of manufactures that was provided in the kit. A summary of this procedure can be seen in table6. The quantity of cDNA which was indicated for this experiment was 1000ng. For the first step, I prepared the RT master mix using the kit

components before preparing the reaction plate. The kit components were put on ice to thaw. By referring to the Table 5, I calculated the sufficient volume of components, all reagents were prepared and kept on ice.

Table 5.The volume of components to make master mix.

Components	Volume/Reaction (µL) Kit without RNase Inhibitor
10X RT Buffer	2.0
25X dNTP mix (100 mM)	0.8
10X RT Random Primers	2.0
MultiScribe™ Reverse Transcriptase	1.0
Nuclease-free H2O	4.2
Total per Reaction	**10.0**

In the next step, I calculated and prepared all the RNA samples. After that, 10µL of master mix was added to 10µL of each RNA sample and briefly spun down to eliminate any air bubbles. At the final step, the thermal cycler conditions were programmed based on the Table 6 and then all reactions were loaded into the thermal cycler.

Table 6.The condition of thermal cycler.

	Step1	Step2	Step3	Step4
Temperature(°C)	25	37	85	4
Time	10 min	120 min	5 min	∞

The cDNA RT tubes can be stored short-term which is up to 24-hrs before use and the storage temperature are 2-6°C. For the long-term condition, it is essential to be placed in -15 to -25°C.

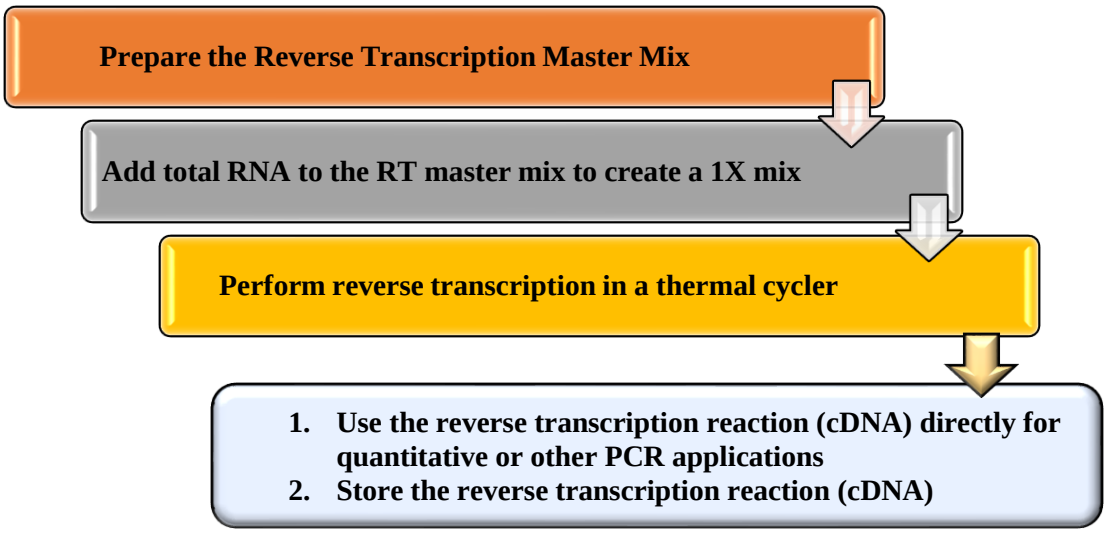

Figure 33. Schematic overview of synthesize single-strand cDNA from total RNA.

6.5. Primers used for rt-qPCR

All the primers, used in my study can be found in Table 7.

Table 7. List of the human primers used for RT-PCR.

Gene name	Orientation	Sequence
YWHAZ	Forward	5´-AGACGGAAGGTGCTGAGAAA-3´
	Reverse	5´-GAAGCATTGGGGATCAAGAA-3´
H2AX	Forward	5´-CGGGCGTCTGTTCTAGTGTT-3´
	Reverse	5´-GGTGTACACGGCCCACTG-3´
Snai1	Forward	5´-GAGCTGAACCTCCCTGTCAGA-3´
	Reverse	5´-GTTGAAGGCCTTTCGAGCCT-3´
BAX	Forward	5´-TGCTTCAGGGTTTCATCCA-3´
	Reverse	5´-GGAAAAAGACCTCTCGGGG-3´
mTOR	Forward	5´-TGCCAACTACCTTCGGAACC-3´
	Reverse	5´-GCTCGCTTCACCTCAATTC-3´
Rictor	Forward	5´-GGAAGCCTGTTGATGGTGAT-3´
	Reverse	5´-GGCAGCCTTTTTATGGTGT-3´
Raptor	Forward	5´-ACTGATGGAGTCCGAATGC-3´
	Reverse	5´-TCATCCGATCCTTCATC-3´

7. Real-time PCR (Q-PCR)

7.1. Q-PCR process

The expression of genes of interest was measured on an ABI Prism 7900HT Sequence Detection System (Applied-Biosystems) using SYBR® Green PCR Master Mix (Applied-Biosystems). SYBR® Green dye is attached to the cDNA and generates a fluorescent signal. The intensity of signal is relative to the quantity of the cDNA involved in the reaction. Therefore, in each step of the PCR reaction, the intensity of the signal increases due to increasing amount of product. Each PCR- reaction was performed in triplicate on a MicroAmp optical 96-well PCR plate (Applied-Biosystems). Each reaction well comprised of 2 µL of diluted cDNA products, 0.5 µL of each 10 µM optimised respective forward and reverse primers, 7 µL of nuclease free water and 10 µL of SYBR® Green Master Mix (2x concentration). Different master mixes were made separately for target and endogenous and then added to the plate. Finally, the plate was sealed with a real time plate sealer (MicroAmp, Applied-Biosystems), centrifuged for 1 minute/1000 rpm to bring all the contents to the bottom of the well and then put in the QPCR QuantStudio 7 Flex Real-Time PCR machine. The real time PCR reactions were run by applying the program as displayed in Figure 34.

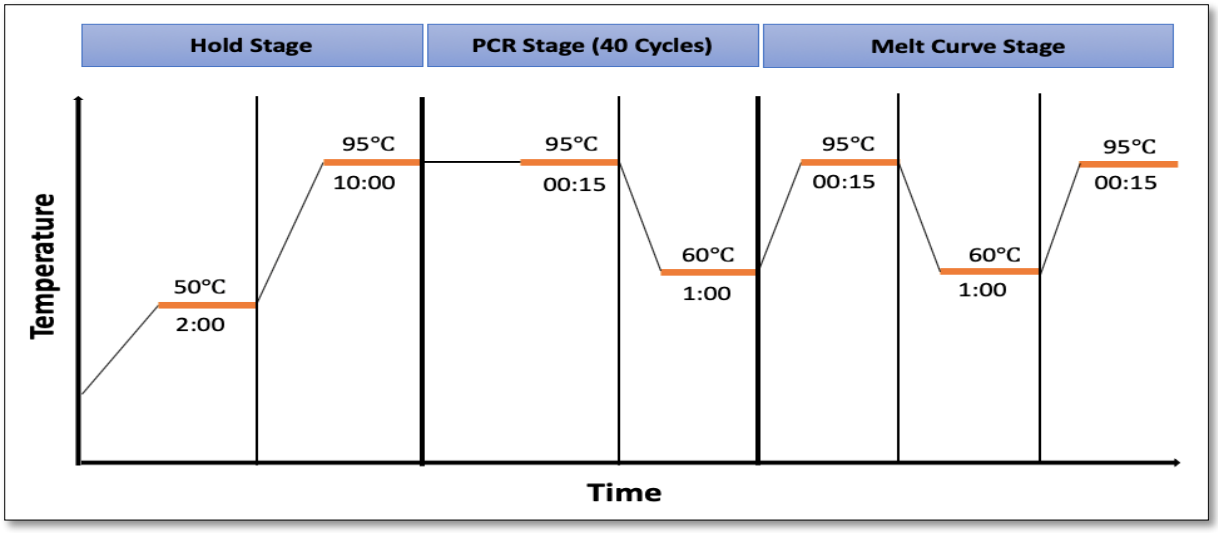

Figure 34. Schematic diagram of the real-time PCR program.

7.2. Q-PCR analysis

Gene expression can be measured through either absolute or relative quantification. Absolute quantification (AQ) measurement is based on amplification of absolute gene copy number. Relative quantification (RQ) measures an amplification according to a reference gene which is stably expressed under the experiment conditions (for instance after drug treatment). The most common way for analysis of qPCR data is the ΔCt or ΔΔCt method which is explained below:

ΔCt = Ct (gene test) - Ct (endogenous control)

ΔΔCt=ΔCt (sample) - ΔCq (calibrator/''untreated cell'')

$RQ = 2^{-\Delta\Delta ct}$

The ΔΔCt method shows fold change in expression when compared to a calibrator and is only acceptable when a valid calibrator is presented; for instance, for drug treatment, the cells under basal conditions can be used as calibrator. In the case of clinical samples, due to the different gene expression from person to person and it is not acceptable to match the ΔCq value from one patient to that of a different patient, the ΔCt method is used. However, in case of each sample is matched to non-affected adjacent-tissue and based on the assumption that tissue is 'normal', the ΔCq method can be used to make a comparison between samples and calibrators.

8. Cell treatment

8.1. Seeding cells

Based on recent studies, the proper concentration for each cell line was indicated which is shown in the table8. Three 6-well plates were used to seed 1 $x10^6$ cells/well. One 90-100%

confluent T75 flask was chosen, the old media was aspirated and, cells were trypsinized and re-suspended in fresh media. Finally, 2mL of the mixture were placed in each well and put in the incubator for 24-hrs to let the cells for attachment.

8.2. Scratch assay (wound healing assay)

Scratch assay was performed to assess the ability of cells to close a created gap in cell growth area. After seeding cells in 6-well plate, a 'scratch' was made vertically, as a line drawn on one part of well, by using a 200 µL pipette tip in growth area. In the following step, the scratch was monitored, and images were taken after 24-, 48- and 72-hrs using a Leica DMi1 inverted microscope (40x magnifications). The perpendicular line of marker was used as a landmark to ensure that an image of the same area was taken at each time point. All images were analysed with ImageJ.

8.3. Adding drug

All cell lines were treated with indicated dose of Rucaparib (PARP inhibitor) which can be found in Table 8. Then they kept in the incubator for 48- and 72-hrs. At the end, the old media was aspirated; cells were washed with PBS and trypsinized, followed by RNA extraction and finally qPCR.

Table 8.The indicated concentration of Rucaparib for each cell line.

Cell line	Rucaparib concentration (µM)
PEO1	10
PEO4	10
MDAH	10
SKOV3	25

8.4. Proliferation assay

By using countess cell counting chamber slide (Countess® Automated Cell Counter, Invitrogen) and Trypan blue staining, I assessed proliferation, death, and cell viability following Rucaparib exposures. After each time-point (24-hrs, 48- hrs and 72- hrs) cells were counted. First old media was aspirated, and cells were trypsinized and then re-suspended in appropriate media to make 1mL of cell suspension totally. An equal volume of cell suspension (10µL) was mixed with trypan blue dye and applied to a slide. Three readings were taken per sample and an average value calculated.

8.5. Flow cytometry

In the first step, cells were seeded in a 6-well plate and incubated with DMSO, Rucaparib and some samples with no treatment to be used as an untreated control, for 48 and 72-H, followed by cell detachment using TE and centrifugation at $1500 \times g$ for 5 min. For cell apoptosis

analysis, FITC annexin V apoptosis detection kit with PI (BioLegend) was used. After trypsinizing, the cells were washed twice with cell staining buffer and then re-suspended in 100µl Annexin V binding buffer. In the next step, 5 µL of FITC Annexin V (488nm) and 10µ of Propidium Iodide solution (610nm) were added to each tube, followed by incubation for 15 minutes in room temperature (25°C) in the dark. Compensation samples were made using unstained, untreated FITC stained, and untreated PI-stained cells. At the end, 400µL of Annexin V binding buffer was added to each sample and then analysed by Flow Cytometry ACEA Novocyte Flow Cytometer. 12,000 cells were then acquired for both treated and untreated samples and the FITC and PI histograms were plotted using the set markers within the analysis program of Novoexpress™ software (Figure 35).

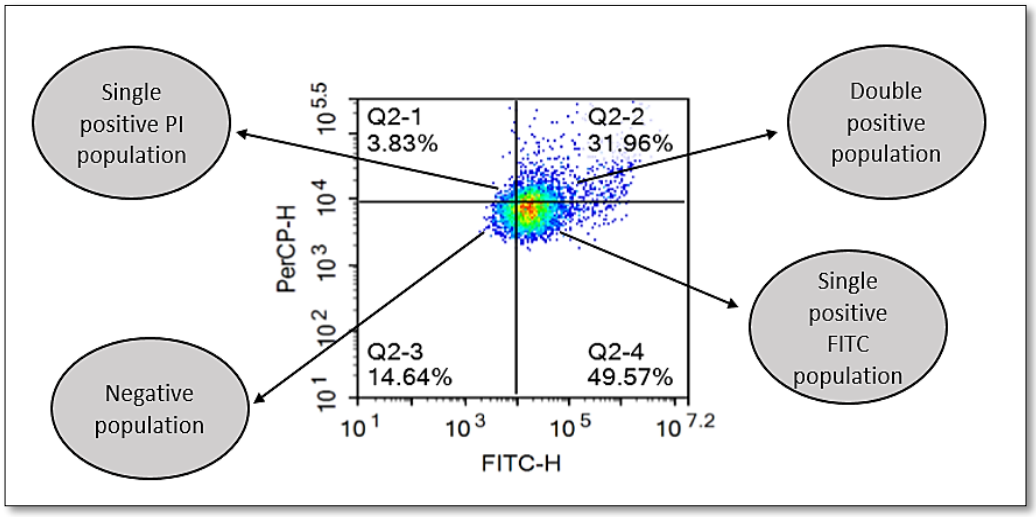

Figure 35. Tow-Parameter histogram from flow cytometry. This figure explained each section of histogram regarding to PI/FITC staining.

Annexin V is an intracellular protein which binds to phosphatidylserine (PS). PS can be normally found in healthy cells, on the intracellular leaflet of the plasma membrane. During early apoptosis, due to lose of membrane asymmetry, PS translocate to the external leaflet. Fluorochrome-labelled Annexin V can be used to precisely target and identify apoptotic cells. It is important to distinguish between necrotic and apoptotic cell. Propidium Iodide Solution (PI) is used to stain necrotic cells and late-stage apoptotic cells, while early apoptotic cells will exclude PI due to the passage of these dyes into the nucleus to bind DNA. Live cells show only a low level of fluorescent, whereas apoptotic cells show green and dead cells display both red and green.

8.6. PARP1 activity assay

Cells were attached on poly-prep slide and kept in incubator. After 24-hrs, fresh media was added containing rucaparib or DMSO (as a negative control) and incubated for 1.5-hrs at

37°C. PARP-1 activity was stimulated through treatment with 20 mM H_2O_2 for 20 min at room temperature in the dark. Cells were fixed in 4% PFA for 10 min, then permeabilized with 0.5% Triton-X for 10 min prior to blocking with 5% BSA for 1-hr at room temperature. In the following step, cells were incubated for 1-hr, with a 1:200 dilution of mouse anti-PADPR monoclonal antibody (Abcam). Bound anti-PADPR primary antibody was visualised after 1-h incubation using goat anti-mouse Alexa Fluor 488-conjugated secondary antibody (Abcam), at a dilution of 1:500. After that, the slides were washed 3x 5 min in TBST (Tris-buffered saline with Tween 20, PH7.5, Sigma-Aldrich) and then PBS. The slides were de-hydrated in ethanol series ((70%, 90% and 100%) for 3-5 minutes each time. Once the slides were air dry, a total of 10µL DAPI (Vector Laboratories) was added to each slide and covered with a cover slip and sealed using clear nail varnish. The slides were ready to analyse under the Leica DM4000 microscope. Fluorescence intensity for AF-488 was calculated by applying ImageJ software and normalised to DAPI fluorescence intensity in all cell lines.

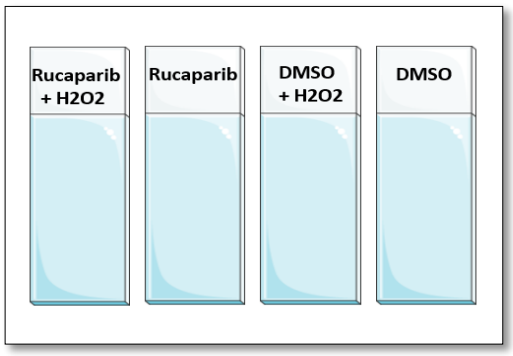

Figure 36. Schematic figure of the plan for PARP1-activity assay. DMSO was used as a vehicle sample (Authors' adaptation).

9. Immunohistochemistry

Immunohistochemistry and DAB (3,3'-Diaminobenzidine) staining was used to visualise H_2AX protein expression in paraffin embedded ovarian cancer tissue samples. The slides were provided from US Biomax, Inc. They contain of ovary carcinoma with adjacent normal tissue microarray, including 5 cases of clear cell carcinoma, 62 serous carcinoma, 10 mucinous adenocarcinoma, 3 endometrioid adenocarcinoma, 10 lymph node metastatic carcinoma, 10 adjacent normal ovary tissues (single core per case) (Figure 37) (US Biomax, Inc, 2019).

Figure 37. Microarray panel of ovarian cancer tissue. **Gre** - Greater omentum, **Lym** - Lymph node, **Ova** - Ovary, **Pel** - Pelvic cavity, **Adr** – Adrenal Gland, used as a negative control, - Malignant tumour, - Malignant tumour (stage I), - Malignant tumour (stage IA), - Malignant tumour (stage IB), - Malignant tumour (stage IC), - Malignant tumour (stage II), - Malignant tumour (stage IIA), - Malignant tumour (stage IIB), - Malignant tumour (stage III), - Malignant tumour (stage IIIA), - Malignant tumour (stage IIIC), - Malignant tumour (stage IV), - Metastasis, - NAT (US Biomax, Inc, 2019).

9.1. Process

The slide was already deparaffinised, and I started with rehydration step through incubation in HistoClear (National Diagnostics) and decreasing concentrations of ethanol as follows in table below.

Table 9. The incubation times and solution to deparaffinise and rehydrate paraffin embedded tissue.

Solution	Time
Histoclear	2 x 5 min
Histoclear:Ethanol (1:1)	3 min
100% Ethanol	3 min
95% Ethanol	3 min
70% Ethanol	3 min
50% Ethanol	3 min
Running Tap Water	1 min

Next step was antigen retrieval which was achieved by boiling slides in sodium citrate (2.94 g Sodium Citrate in 1L distilled water, 500µL Tween 20, pH 6) for 20 minutes (considering avoiding the slides boiling dry). The slides were then washed in running tap water for 10 minutes and then PBS 0.025% Triton-X (50µl Triton-X in 200mL PBS) 2 times for 5 minutes to remove excess sodium citrate. Endogenous hydrogen peroxidase activity was blocked through incubation with 3% hydrogen peroxide (150µl in 50mL PBS) for 15 minutes. After that, slides were washed with 0.025% Triton-X 3 times for 5 minutes each. For the blocking step, a humidity chamber was made by placing water-soaked tissue in a container and covering with foil. The slide was added 200µL of 5% BSA in PBS blocking buffer (2.5g in 50mL of PBS) for 1 hour at room temperature. For the next step, the primary antibody, H2AX (Millipore) (1:500 dilution) was applied, slide was covered with a small square of parafilm to ensure that antibody spreads over all area and incubated over one night at 4°C. In the second day, the slides were washed 3x / 5 minutes in PBS 0.025% Triton-X on a shaker to remove any unbound primary antibody. Then, it was incubated for 1-hr at room temperature in the humidity chamber with secondary antibody 1:200 in 1% rabbit serum (ZytoChem Plus HRP-DAB Kit). After washing step with 0.025% Triton-X, to remove any unbound secondary antibody, streptavidin-HRP conjugate was added to allow the visibility of the antibody along with the secondary antibody and incubated for 30 minutes in the humidity chamber. After washing step, DAB solution (VectorLabs) was prepared in 2.5ml distilled water as follows: 2 drops of buffer stock solution, 4 drops of DAB stock solution, and 2 drops of hydrogen peroxide solution. In the following step, 200 µL of DAB solution was applied to the tissue and incubated at room temperature for 2-10 minutes until a brown colour develops. DAB solution was washed off the slide by incubation in dH_2O/5 minutes. For nucleus staining, Haematoxylin (Fisher Scientific) was used to provide contrast to the brown DAB staining. The tissue was incubated in haematoxylin for 15-30 second and washed off with distilled water. Slide was covered with few drops of haematoxylin and parafilm on top. Slides were then incubated in 0.1% sodium bicarbonate (1g sodium bicarbonate in 1L distilled water) for 30-60 seconds and rinsed in running tap water. Tissue was dehydrated by performing the following washes displayed in Table 10.

Table 10. Incubations process to dehydrate stained tissue samples.

Solution	**Time**
50% Ethanol	3 min
70% Ethanol	3 min
95% Ethanol	3 min
100% Ethanol	3 min
Histoclear:Ethanol (1:1)	3 min
Histoclear	3 min

Coverslips were mounted with di-N-butyl phthalate in xylene (DPX) to protect the tissue. DPX was dried overnight at 4°C before observation.

9.2. Scoring

In order to score the slide staining, it was first determined how well the slide has stained overall, using the following parameters.

Table 11.Table of scoring pattern for stained slides.

Staining	Negative	<25% stained	25-50% stained	50-75% stained	>75% stained
Score	0	1	2	3	4

The slide was then positioned under a light microscope so that the whole circle of tissue was visible. Each circle was analysed as if it has been split into 3 sections (Figure 38):

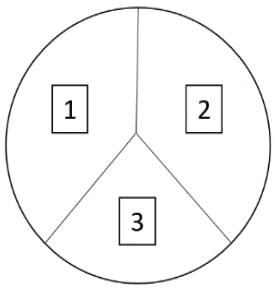

Figure 38. Schematic figure of microarray slide under the microscope. This figure shows how to split the cell into three sections.

Each section was scored so that 3 scores were got (one for each score) which an average score was calculated from Table 12.

Table 12. An example of the scoring and average score.

Location	1st Section	2nd Section	3rd Section	Average Score
A1	1	3	2	2

This process was repeated for the next two days in order to reduce bias. Images were taken using a Leica DMi1 inverted microscope (10x magnification).

10. *In silico* analysis using online tools

In silico analysis was carried out on several subsections of results. I used an online tool, Oncomine website, for the purposes of gene expression levels of existing microarray data for genes in both cancer and normal tissues, based on cancer types. In addition, I used another online tool known as Kaplan Meier Plotter which can be used to determine gene expression connections with prognosis and overall survival.

11. Bioinformatic analysis

The ovarian cancer cohort of TCGA was downloaded through cBioPortal (Gao *et al.*, 2013) and UCSC Xena (UCSC Xena, 2021). This cohort contains tissues of primary cancer, recurrent cancer, and normal ovarian tissue, with number of 568, 17, and 8 respectively and gene expression from microarray in TCGA. OC patients with primary cancer were split into high and low expression groups by H2AX expression using median cut-off. Gene Set Enrichment Analysis (GSEA) was performed to compare H2AX high and low groups using Hallmark gene sets, in software provided by the Broad Institute (GSEA, 2021).

12. Population sample and genotyping

The UK Biobank is a huge population study, around 500,000 individuals. These were enrolled between 2006 and 2011 from 22 UK Biobank assessment centres throughout England, Wales and Scotland. The range of the participant's age at the time of recruitment in the study was from 40 to 69 years, with a mean age of 56.5 years old. The 54.4% of sample was contained by female participants (Sudlow *et al.*, 2015). Existing health records have been associated with the remaining data from the participants. These involve several information about deaths, cancer registration and hospital inpatient episodes (Biobank, 2014) .

For this project we applied the ICD10 definition of ovarian cancer under code C56 with 1232 cases. To define the five-year survival, we used the dates of diagnosis of the incident cases with five-year follow up records and data from the death register for the next five years. The

UKB Axiom array (438,427 participants) or the UK BiLEVE Axiom array (49,950 participants) were used to genotype approximately 812,428 variants in 488,377 individuals. These variants were ascribed using the 1000 Genomes phase 3 dataset as a reference (Bycroft *et al.*, 2018). There was some variants with a minor allele frequency of frequency of <0.8, that did not pass standard quality control checks (Bycroft *et al.*, 2018), and were excluded from the analysis. All current polymorphisms which passed our QC filters and situated on chromosome 11 between positions 118,944,675 and 118,986,118, in total 108 genetic variants, were obtained from the genotyping data to be used in our study. The UK Biobank provided the sample genotyping quality control metrics. There were many samples, excluded from the analysis, including those outliers for missingness and/or PC-corrected heterozygosity and/or those with any sex chromosome aneuploidies as well as if the genetically inferred sex differed from the reported sex. Additionally, those samples which did not have a genetically verified White British ancestry were excluded. A list of related individuals was given by the UK Biobank and one individual from each linked pair was randomly excluded. The use of the UK Biobank data was covered under project 44,556.

13. Statistical analysis

Changes detected in experiments were measured for statistical significance using the Student's t-test and ANOVA (Analysis of Variance) test. The survival changes were analysed using Kaplan-Meier curves with log-rank test. A logistic regression model was used to examine the correlation between the genetic variants and OC risk or five-year survival, altering for the first four principle components of all genotyped variants, the genotyping array used, and the age at recruitment for OC risk, or the age at OC diagnosis for the five-year survival. All statistical tests were analysed using GraphPad Prism® (GraphPad Software, San Diego, CA, USA) and R software (R Project, 2021). Plot for the genetic connections were assembled through LocusZoom (Pruim *et al.*, 2011). Values were considered as significant when $p < 0.05$.

Chapter3: Validation

Introduction

Ovarian cancer, specifically high-grade serous is a highly mutated cancer. Most remarkable mutated gene in ovarian cancer is p53 which is mutated in approximately 96% of HGSOC. Additionally, it was found that BRCA1/2 genes have a role in many HGSOC, regardless of germline status. Women who carry mutation in BRCA2 gene, have a nearly 12-25% chance of developing ovarian cancer in their lifetimes, when compared to women without gene mutation with a rate of 1.6% in the general population (BetterthanBRCA, 2019). Moreover, BRCA2 mutation can increase the risk of some other types of cancer, containing breast cancer, pancreatic cancer, and melanoma (National Institutes of Health, 2015). Women with inherent deleterious BRCA1 or BRCA2 mutation have up to a 40% and 20% lifetime risk, respectively, of developing ovarian cancer and higher risks of developing breast cancer (Chen and Parmigiani, 2007). The prevalence of BRCA germline mutation is around 10-15% (Risch *et al.*, 2001). It has been established that 17% of patients with HGSOC were found to carry a BRCA mutation gene and 44% of these patients had no family history of cancer. Regarding to these data, use of BRCA mutation testing in all HGSOC patients is supported, regardless of family history (Alsop *et al.*, 2012).

In the UK, it is becoming increasingly crucial for ovarian cancer patients to undertake testing for germline BRCA1/2 mutation. Over the last few years, the demand for testing has been increased due to greater public awareness of breast and ovarian cancer genetic component. Recent findings have established that approximately 15% of all patients with OC, harbour a germline mutation in BRCA1/2 (George, 2015). There are no standard rules for testing ovarian cancer patients in case of BRCA1/2 germline mutations, whereby the National Institute for Health and Care Excellence (NICE) advises that all women with a 10% chance of having mutated BRCA1/2 gene should be recommended testing (NICE, 2013).

There are many proteins involved in homologous recombination pathway to repair DNA-DSB, such as BRCA1 and BRCA2. BRCA1 has a significant role in response to signalling pathway of DSB-DNA damage and leads to HR repair pathway. Moreover, BRCA2 has an extra straight part of repair in HR through its Rad51 regulation (Gudmundsdottir and Ashworth, 2006). It is suggested that the BRCA2–Rad51 complex binds to the defective DNA, and this binding can induce the Rad51 loading onto the break and creation of the presynaptic filament. By discovering more functions of BRCA1 and BRCA2, it might be reasonable to propose that deficiency of genes involving in HR repair pathway will lead to

HRD (Drew, 2015). Extra analysis on cellular pathways has discovered that almost half of all tumours carried a mutation in one gene, associated to HR pathway in DNA repair. These discoveries point to a significant role of HR deficiency in cancer development, as well as therapeutic potential to achieve (Neff, Senter and Salani, 2017).

Germline mutations in BRCA1/2 have been widely explored in the population to impute a risk related to carriers for the development of breast and ovarian cancer. It has showed that after analysing over 8000 unselected cases of patients with breast or ovarian cancer, the average increasing risk of developing ovarian cancer with a BRCA1/2 mutation was 39% and 11% respectively. Additionally, the convincing evidence was found regarding to the age discrepancy for onset of disease between BRCA1/2, which BRCA1 patients showed an increased risk after age 40 and BRCA2 patients after age 50. Over 15% of all patients diagnosed with serous ovarian carcinoma present a germline BRCA mutation (Neff, Senter and Salani, 2017). Following to these data, it suggests that BRCA mutation will have a significant impact on ovarian cancer progression and should be treated as an individual disease. Reliable indicator of HR deficiency in ovarian cancers was identified, based on quantification of immunofluorescent γ-H2AX nuclear foci formation due to DNA damage (Kukolj *et al.*, 2017).

I used four OC cell lines, including BRCA2-m (PEO1), BRCA2-wildtype (SKOV3) and BRCA2-silent mutation (PEO4, MDAH-2774). The PEO1 cell line is derived from the peritoneal ascites of a patient who had a poorly differentiated serous adenocarcinoma (ECACC, 2020a). PEO4 is derived from the same patient as the PEO1 and was collected after clinical resistance developed to chemotherapy (ECACC, 2020b). SKOV3 is an epithelial adenocarcinoma cell line with wild-type BRCA2 gene. Another ovarian cell line that I used was MDAH-2774 which is endometrioid adenocarcinoma carrying BRCA2 gene with silent mutation as expected to have a normal function, same as PEO4 cell line. As it can be seen in Figure 39, a nonsense mutation was detected in PEO1 (5193C>G) which lead to stop codon in exons 11 of BRCA2, and create truncated proteins (shown in Figure 40) (Sakai *et al.*, 2009), while it was converted to a silent mutation on the same base in PEO4 (5193C>T) in exon 11 which makes a normal BRCA2 protein (Sakai *et al.*, 2009).

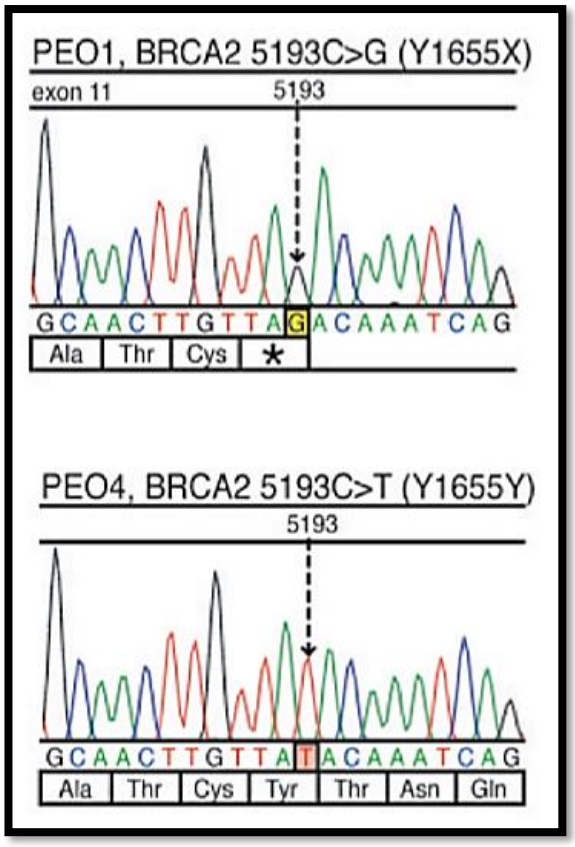

Figure 39. DNA sequences of BRCA2 in PEO1 and PEO4 (Sakai et al., 2010).

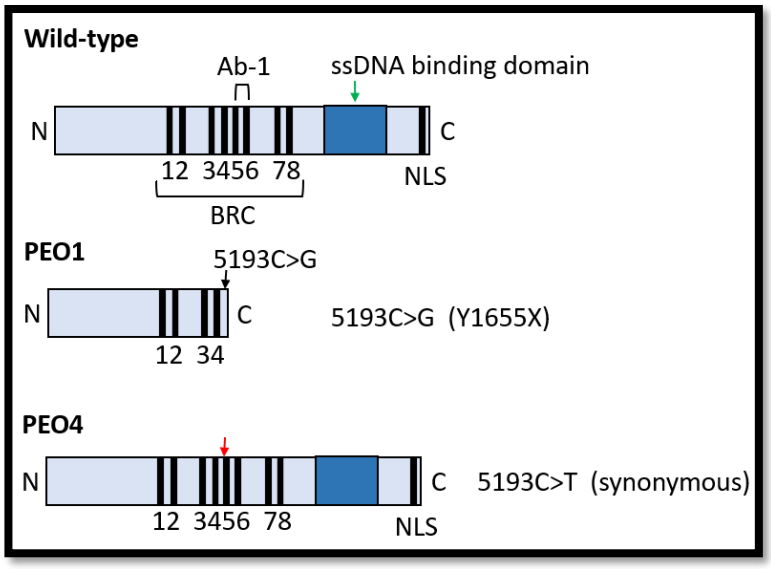

Figure 40. Schematic figure of BRCA2 proteins encoded by transcripts in PEO1 and PEO4. The secondary genetic changes (presented as red arrow heads) stop the nonsense mutation induced by the original mutation (5193C>G, black arrow heads), and the encoded BRCA2 proteins have complete C-terminal areas holding a single strand DNA (ssDNA) binding domain (green arrow) and nuclear localization signals (NLS). The regions that the BRCA2 antibodies (Ab-1) recognize are shown. Adapted from (Sakai et al., 2010).

Aims

Using different ovarian cancer cell lines including BRCA2-wildtype (SKOV3), BRCA2-m (PEO1) and BRCA2-silent mutant (PEO4, MDAH) to assess:

- The expression of BRCA2 protein in OC cell lines.
- The effects of BRCA2 mutation on efficiency of HR by using immunofluorescence technique (γ-H2AX assay).

Result

1. BRCA2 detection-Validation of cell lines

For the first part, I showed that whether the BRCA2 protein is expressed or not, through western blot technique which was performed for 4 different cell lines to detect expression of BRCA2 protein. The result is displayed in Figure 41. As it can be seen, PEO4, MDAH-2774 and SKOV3 cell lines express the full-length BRCA2 protein. However, in PEO1 cell line, BRCA2 protein is a truncated form of the wild-type protein due to the point mutation (5193C>G) which lead to a stop codon amino-acid, and therefore appears as a lower band in the gel. In addition, GAPDH was used as a house keeping control protein as it expresses at high level in most tissues, and it is valuable as protein loading control in Western Blot analysis.

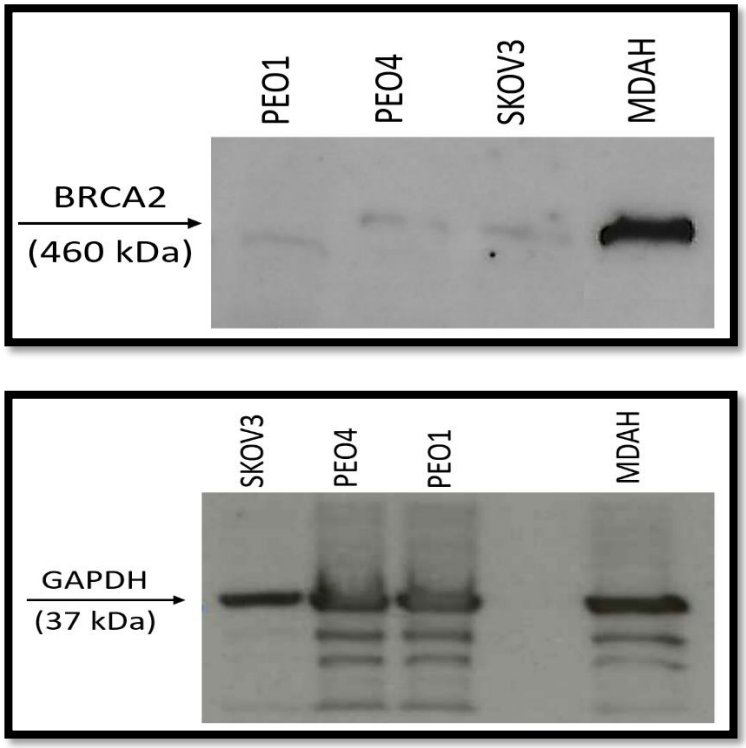

Figure 41. GAPDH and BRCA2 western blotting of PEO1, PEO4, MDAH-2774 and SKOV3. This result was provided in the lab.

2. Use of H_2O_2 to validate DSB *in vitro*

To assess the role of BRCA2 protein in HR pathway, I needed to activate the DNA-DSB repair pathways by inducing DNA damage. I used hydrogen peroxide (H_2O_2) to induce double strand breaks DNA damage that can be repaired through HR pathway. I started by choosing proper concentration and time-points for H_2O_2 exposure to induce double strand break in DNA, then analysis of DNA damage in each cell line. All cell lines were exposed to

H_2O_2 at different time points (1- and 24-hrs) and different concentrations (0.3-4 mM) to choose a suitable concentration and time point. Result can be found in Figure 42.

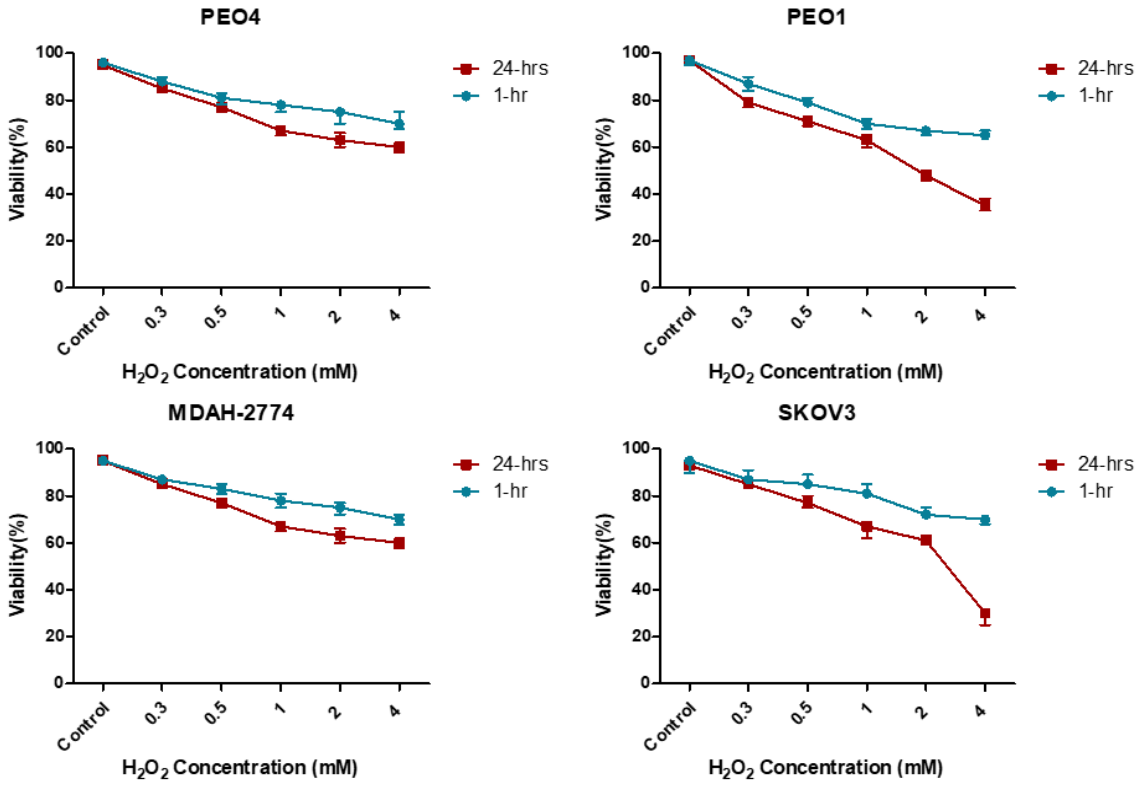

Figure 42. H_2O_2 Cell death curve. These graphs represent the cell viability for each cell line in different concentrations. As it is displayed in the graphs, by increasing the dose of H_2O_2, the level of cell viability was decreased. Maximum dose of H_2O_2 which kill 20-30% number of cells was selected. Therefore, 0.5 mM of H_2O_2 concentration for one hour was selected for all cell line.

3. Sample acquisition and analysis using image flow cytometry

3.1. ImageStream™

ImageStream™ (Amnis Inc., Seattle, Washington) was conducted to capture a picture on up to 6 optical channels and has power of obtaining 1000 cells per second. Based on different cells, images were achieved by using a 20X, 40X and 60X objective. This device has a different range of laser including 800 nm used to capture bright field (BF) (channel 1), the 488 nm for Alexa Fluor (channel 2) and 642 nm for DRAQ5 (channel 5). Alexa Fluor represents γ-H2AX foci by showing green dye. DRAQ5 is used to stain the nuclear region of each cell and show the red colour (Adam-Zahir *et al.*, 2015). Figure 43 is a sample of the captured image using image stream X.

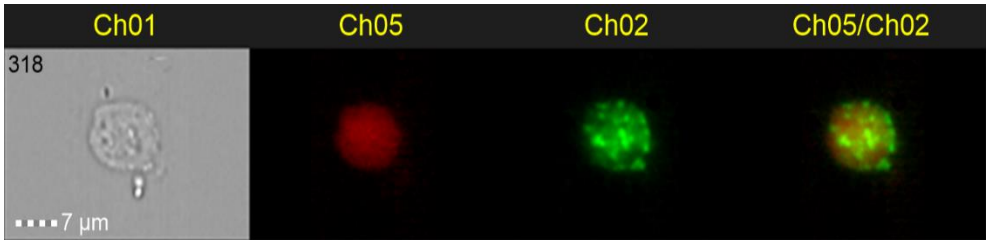

Figure 43.Captured images of PEO1 cell, using the ImageStream™. The figure above represents the captured image of the cell by using ImageStream™. Ch01 shows the bright field images of cells, Ch02 represents γ-H2A antibody staining and Ch05 displays the nuclear staining with DRAQ5 (provided in the lab).

3.2. Image compensation

This device is used to define specific fluorescence staining related to use of two or more masks. As described before, the cells were stained with AF-488 and DRAQ5. For data analysis and acquire an accurate data, it is important to display the right intensity of specific fluorescence light from each image. The software used for data analysis of ImageStream™ is called IDEAS®. The taken light from images was placed on the quantities table (shown in Table 13), related to the channels (e.g., Ch05 for DRAQ5). Operator displays two truth populations with a minimum of 25 cells, one to show a low number of foci (<2) and the other one present the high number of foci (>5-6). These numbers display the range of staining that allowed the software to select the most sensitive mask to measure the foci accurately (Adam-Zahir *et al.*, 2015).

Table 13. An example of a table for compensation matrix that is created by the analysis software IDEAS® in order to analyse the sample. Values presented in this table show coefficient numbers of leakage into adjacent channels. The coefficient of leakage reduces as it develops distant from the main channel specified with a 1 value. The values that were used in this research were adjusted to have a border of error which is less than 0.001.

	Ch01	Ch02	Ch03	Ch04	Ch05	Ch06
Ch01	1	0	0.061	0	0.036	0
Ch02	0	1	0.277	0	0.125	0
Ch03	0	0	1	0	0.100	0
Ch04	0	0	0.518	1	0.143	0
Ch05	0	0	0.208	0	1	0
Ch06	0.02	0	0.087	0	0.352	1

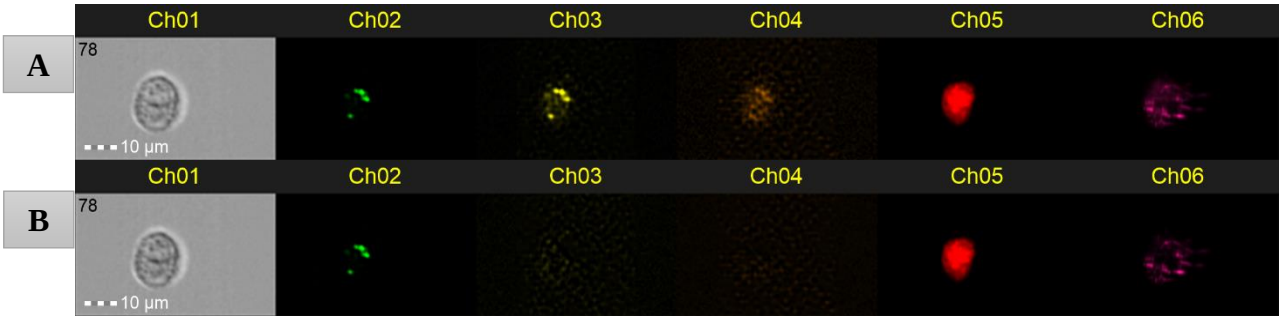

Figure 44. Example of uncompensated image compared to compensated one. The above figure displays an example of uncompensated (A) images compared to compensated one (B) from SKOV3 cell line. Ch02 shows γ-H2AX staining, while fluorochrome leaks can be seen on nearby channels (e.g., Ch03). The IDEAS software with compensation tool, allows for the correction of this leakage. Ch02 shows γ-H2AX foci, stained with AF-488 and Ch05 shows nucleus, stained with DRAQ5.

3.3. INSPIRE®

For ImageStream^x analysis, samples containing no less than 20µL were made. Before running samples on the ImageStream^x, pallet was gently re-suspended to break cell clumps. The captured image of many cells may differ to other ones. During some experiments, cells were not many at the beginning or accidentally lost in washes steps. Additionally, there is an option to extend the EDF (extended depth of field) that help to increase focus and image clarity. The focus and centring part are automatically measured by the machine and if it requires device at sometimes can adjust to acquire the optimal results. The size of cells was set to minimum 50 to maximum 900. Cells were captured from Ch01 which is a normal image, Ch02 which is about AF staining and Ch05 for the DRAQ5 staining. Moreover, the settings for the compensation samples must be set before loading them. All files were saved onto the computer as raw image file (RIF) and then used for analysis through the IDEAS® analysis software.

3.4. IDEAS®

ImageStream is a novel technique, and its software (IDEAS®) is constantly being upgraded with new features that being added to help swift and proficient in data analysis. One of these new features called “Spot wizard” that choose the best mask for foci measurement and show a more reliable and improved method to analyse the DNA damage foci in cells. At first, Spot wizard make a gate of single and focused cells according to the parameters which will be described later in this section. Then wizard need to identify if two populations; one population of cells with low number of foci (0 or 1) and another population which has a high number of foci. The IDEAS® software can be used for data analysis of samples captured with the machine, to make data analysis files (DAF). In the first step, the software analyses all the captured objects comprising of cells and debris

and also allows the user to make gate for specific region of them (based on manual examination of these objects) and label them as single viable cells, the analysis can then proceed using only single cells (shown in Figure 45). The considerable feature about this software is, the ability of isolation of captured single cells; though, it is important to consider the careful examination of collected cells, exclude minor clusters of cells which might be accidentally included into the main image.

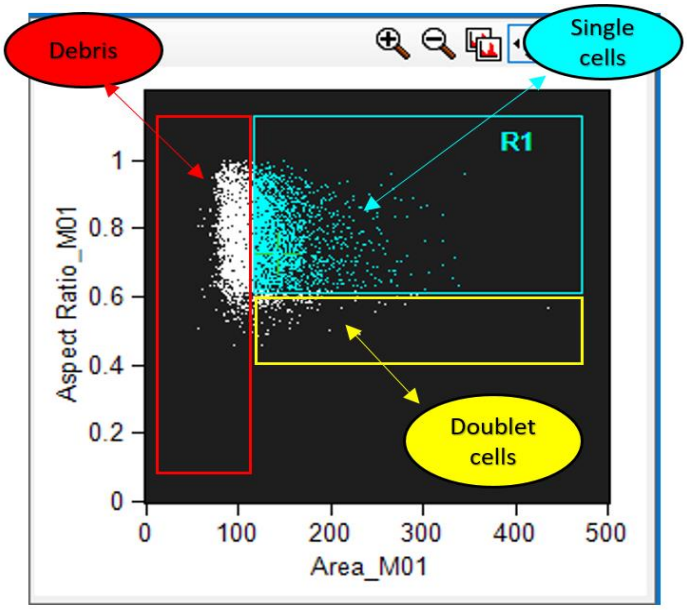

Figure 45. Example of gating for single cells using IDEAS®. The Y-axis displays the cell spreading according to their aspect ratio. However, the X-axis represents their distribution according to their size. All the single blue dots show one captured object which is including cell, debris and cell clusters. The "_M01" at the end of the axis' tag indicates the channel it applies to. This software mechanically makes statistics about the taken data comprising of the cell number, mean and more and these statistics are represented in a table that is created below the graph. Careful examination of these single blue dots or cells was monitored through making a gate for single cells to do the analysis totally.

Figure 46 displays the following stage which is to continue the analysis only on cells in focussed with clear morphology and structure for the cells.

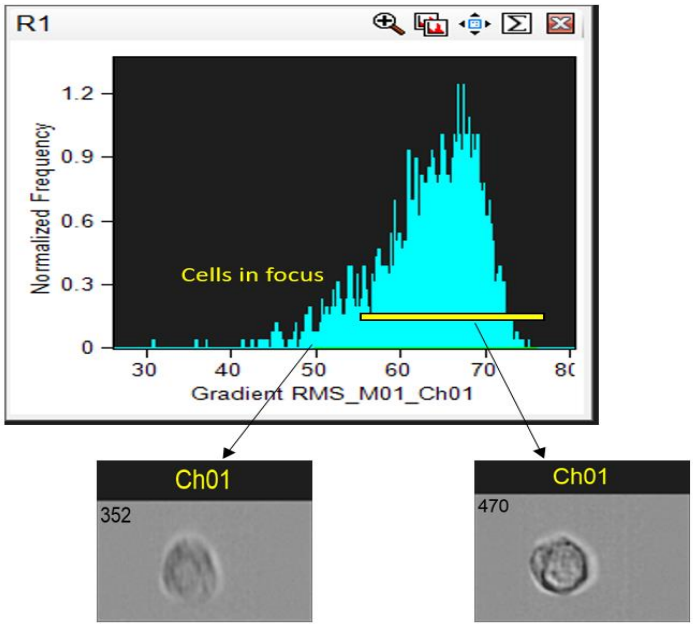

Figure 46. Identification of focused cells using IDEAS®. When the graph was generated from the single cells which were gated to detect the focused cells which were clear and not to choose any blurred cells from further analysis. On the X-axis, a gradient of cells is used based on focussed image, whereas the Y-axis displayed the normalised frequency. Subsequent examination, a line gate was shaped (in yellow) dividing single focused cells from blurred unclear cells. The table which was made below the graph is automatically produced through the data analysis after gating some cells in the graph. It is completed to represent the number and percentage of cells comprised in that range.

When the focused cells were chosen, the software made a gradient based on the intensity of staining for γ-H2AX in all cell lines. After creating the graphs by IDEAS® software, it is needed to examine the different section to decide points at which cells can be categorized as positively stained. After that, the statistic table according to percentage of every section for the graph and cell numbers can be acquired from this table. It generates the accurate numbers related to cell staining based on dilution of antibody that I used. It was required to detect the number of γ-H2AX foci within the nucleus of each cell, therefore, a series of masks were made which played a role to identify the region of interest (Figure 47).

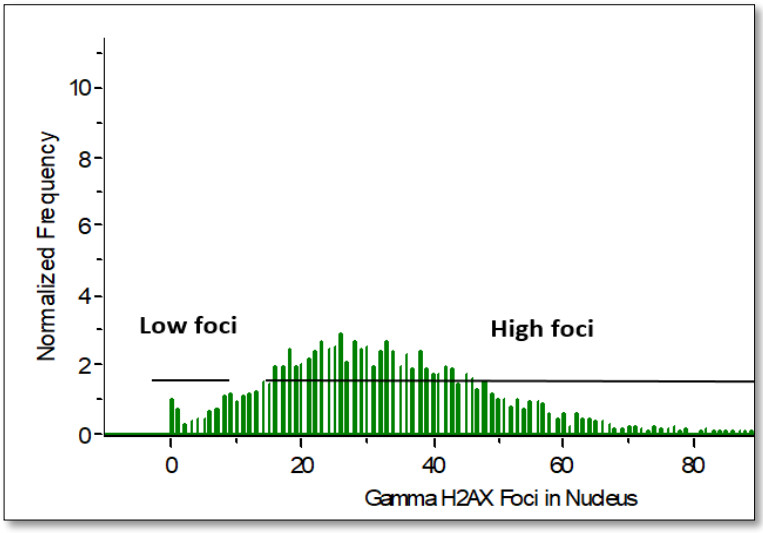

Figure 47.Typical foci distribution of γ-H2AX in the experiment after treatment with H_2O_2. The figure above displays a typical distribution plot for γ-H2AX foci for a sample fixed after 1-hour exposure to 0.5mM H_2O_2.

I chose treated sample with 0.5mM H_2O_2 after 1-hr exposure, to capture the high level of γ-H2AX foci which started to be formed after 30 minutes of exposure. After completing the analysis for 1-hr/0.5-mM sample, to be used as a template for the analysis, the data analysis file (DAF) was made and saved which can allow to apply the same spot mask and intensity mask to all other samples with different time point and concentration of H_2O_2. For each cell line, it was required to create a separate template file.

4. γ-H2AX foci induction in cell line (ImageStream^{TM})

To examine the role of BRCA2 in HR pathway and impact of BRCA2 mutation in HRD, I induced DSB in DNA to analyse the number of γ-H2AX foci which represents the DNA damage. Here I used 4 different types of ovarian cancer cell line including SKOV3 with BRCA2-wildtype, PEO1 with BRCA2 mutation, PEO4 and MDAH-2774 cell lines with silent mutation in BRCA2 gene. In the next step, all cells were exposed to H_2O_2 for 1- and 24-hrs and then finally γ-H2AX foci were analysed and quantified through applying a morphology and peak mask within IDEAS® software.

In brief, PEO1 which is a BRCA2-m, showed significantly higher number of γ-H2AX foci following 1-hr and 24-hrs exposures to H_2O_2, comparing to control samples. However, PEO4 cell line displayed a different pattern which was a similar level of γ-H2AX foci between control and after 24-hrs H_2O_2 treatment. Additionally, there was a significant difference between control and after 1-hr H_2O_2 exposures. In SKOV3 cell line, similar pattern as PEO1 was observed which showed a significant increase following 1- and 24-hrs exposures to H_2O_2. The reason for this can be related to a concept of ‘’BRCAness’’ which is referred to deficiency in other genes involved in HR pathway.

This experiment was done 3 times for all cell lines. Figures 48-50 show the data and p-value for all cell lines.

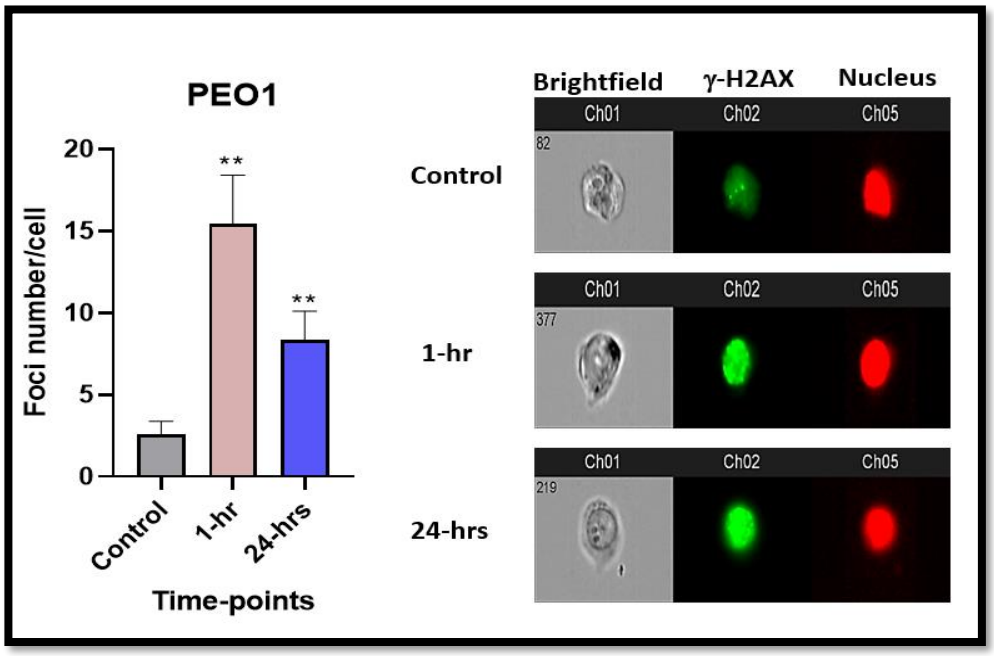

Figure 48. Number of γ-H2AX foci per cell in PEO1 after H_2O_2 treatment. Figure above displays the number of γ-H2AX foci per cell in PEO1, based on different condition of treatment. Error bars represent standard error of the mean (SEM). Significant change was seen between control and after 1-hr (p=0.0019), control and after 24-hrs (p=0.0064). ** Significantly higher than wild type (P<0.01).

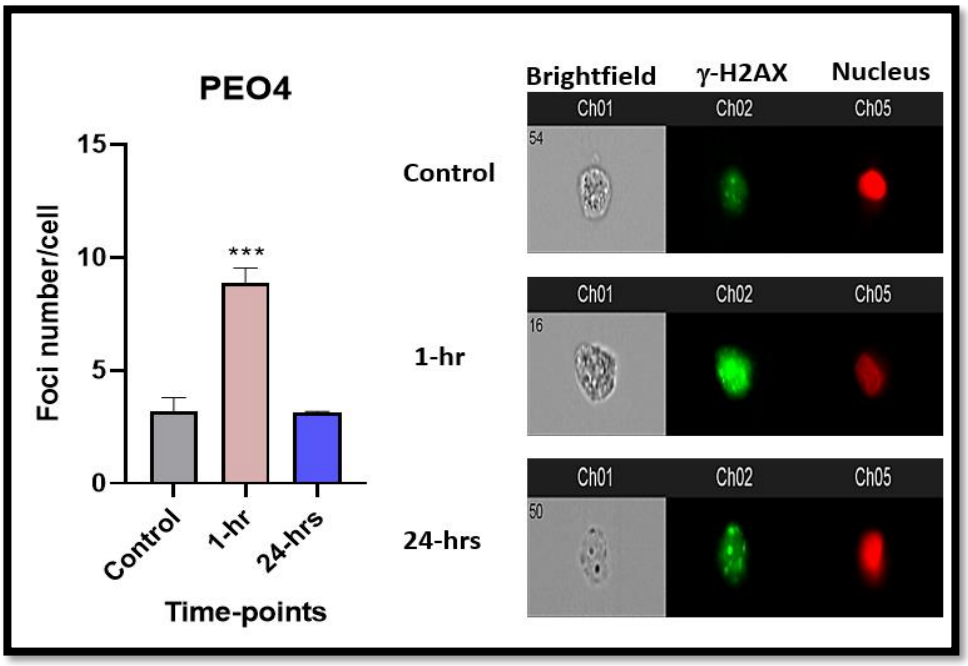

Figure 49. Number of γ-H2AX foci per cell in PEO4 after H_2O_2 treatment. Figure above shows the number of γ-H2AX foci per cell in PEO4 based on different condition of treatment. Error bars represent standard error of the mean (SEM). Significant change was seen between control and after 1-hr (p=0.0004) but no significant difference between control and after 24-hrs (p=0.8270). *** Significantly higher than wild type (P<0.001).

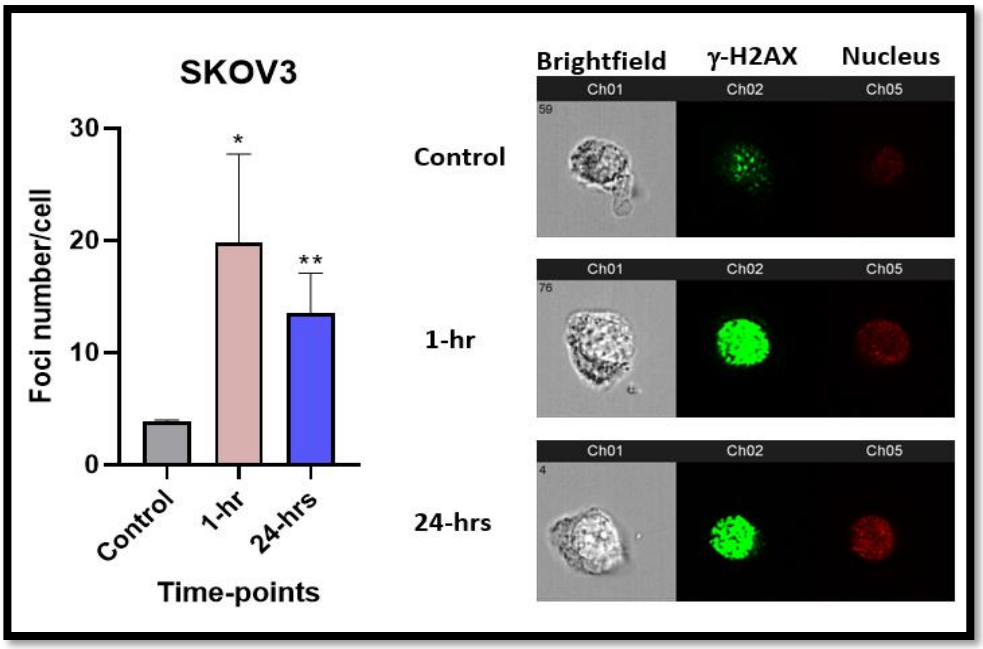

Figure 50. Number of γ-H2AX foci per cell in SKOV3 after H_2O_2 treatment. Figure above shows the number of γ-H2AX foci per cell in SKOV3 based on different condition of treatment. Error bars represent standard error of the mean (SEM). Significant change was seen between control and after 1-hr (p=0.0246), control and after 24-hrs (p=0.0098). ∗ Significantly higher than wild type (P<0.05), ∗∗ Significantly higher than wild type (P<0.01).

5. γ-H2AX foci induction in cell line (Immunofluorescence)

There are several experimental techniques to detect γ-H2AX foci in cultured cells. The most reliable one is immunofluorescent labelling of γ-H2AX, and nuclei followed by microscopy imaging and analysis. The most important advantage of this technique is the ability of providing quantitative information regarding to the number of foci in each cell and, hence, the number of DSBs. At this time, this approach has been considered as 'gold standard' in analytical methods and generally used for estimating the DNA damage due to external radiation exposures or other factors that induce DNA DSB (Lapytsko *et al.*, 2015).

Here, I stimulated DSB in DNA to analyse the number of γ-H2AX foci in all 4 different types of ovarian cancer cell line with BRCA-wild-type and mutant gene. In the final step, γ-H2AX foci were analysed and quantified after 1- hr exposures to H_2O_2, following 1- and 24-hrs incubation with fresh medium. Images are taken by Leica microscope. Results are consistent with previous data from Imagestream, which displays those cells with BRCA2-m (e.g., PEO1) cannot be repaired, due to homologous recombination deficiency but cells with intact BRCA2 (e.g., PEO4 and MDAH-2774) can be repaired after inducing DSB. However, some cells (e.g., SKOV3) demonstrate a similar pattern to those carry BRCA2-m. This might be due to cells exhibiting ''BRCAness'' which is having deficiency in other genes involved in HR pathway. This experiment was done 3 times for all cell lines. Figures 51-54 show the data and p-value for all cell lines.

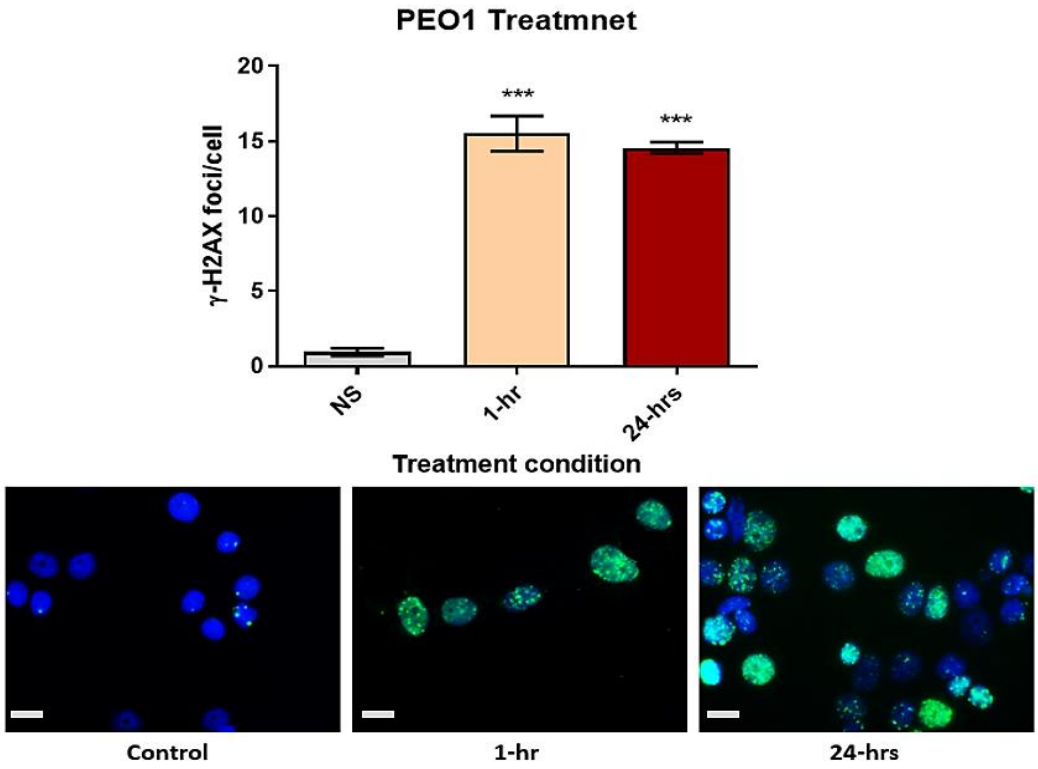

Figure 51. Number of γ-H2AX foci per cell in PEO1 after H_2O_2 treatment. This Figure shows the number of γ-H2AX foci per cell in PEO1 based on different condition of treatment. Error bars represent standard error of the mean (SEM). Significant change was seen between control and after 1-hr ($p<0.0001$), control and after 24-hrs ($p<0.0001$), (Bar scale: 10µM).

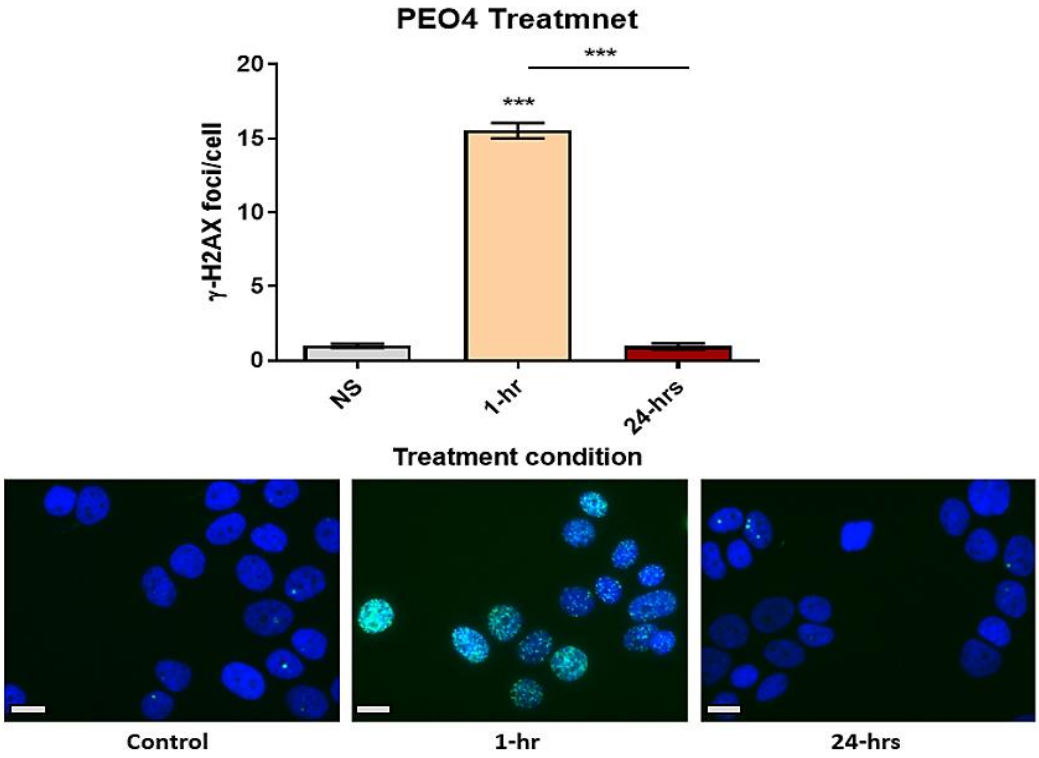

Figure 52. Number of γ-H2AX foci per cell in PEO4 after H_2O_2 treatment. This figure shows the number of γ-H2AX foci per cell in PEO4 based on different condition of treatment. Error bars represent standard error of the mean (SEM). Significant change was seen between control and after 1-hr ($p<0.0001$), after 1-hr and after 24-hrs ($p<0.0001$), (Bar scale: 10µM).

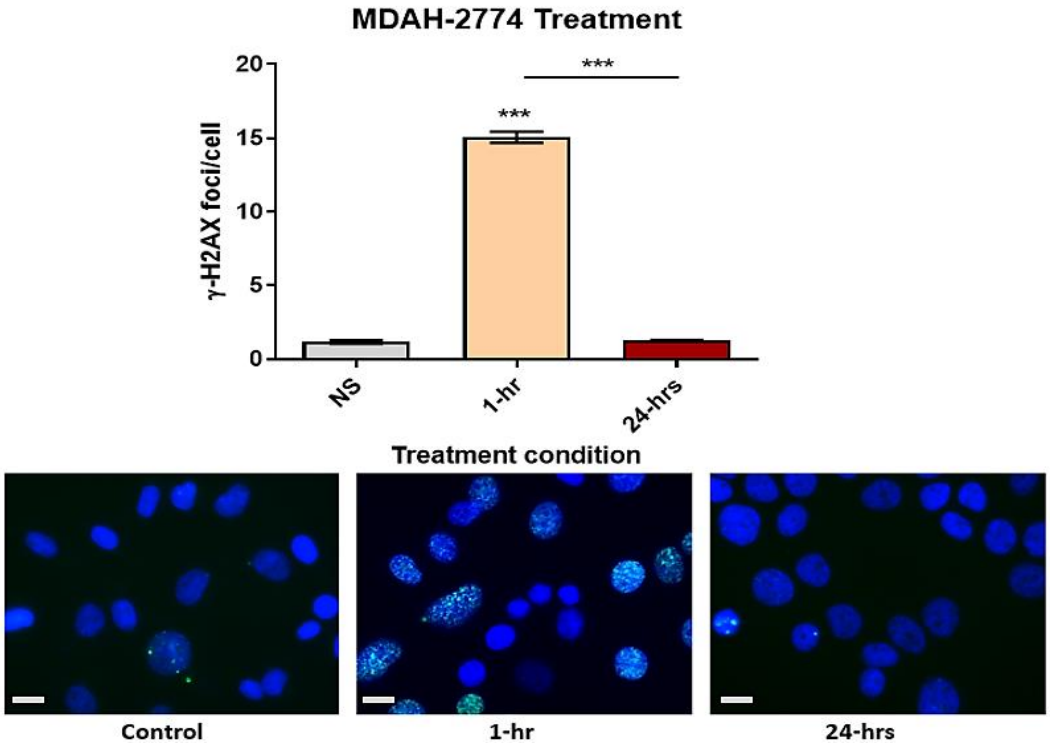

Figure 53. Number of γ-H2AX foci per cell in MDAH-2774 after H_2O_2 treatment. Figure above shows the number of γ-H2AX foci per cell in MDAH-2774 based on different condition of treatment. Error bars represent standard error of the mean (SEM). Significant change was seen between control and after 1-hr ($p<0.0001$), after 1-hr and after 24-hrs ($p<0.0001$), (Bar scale: 10µM).

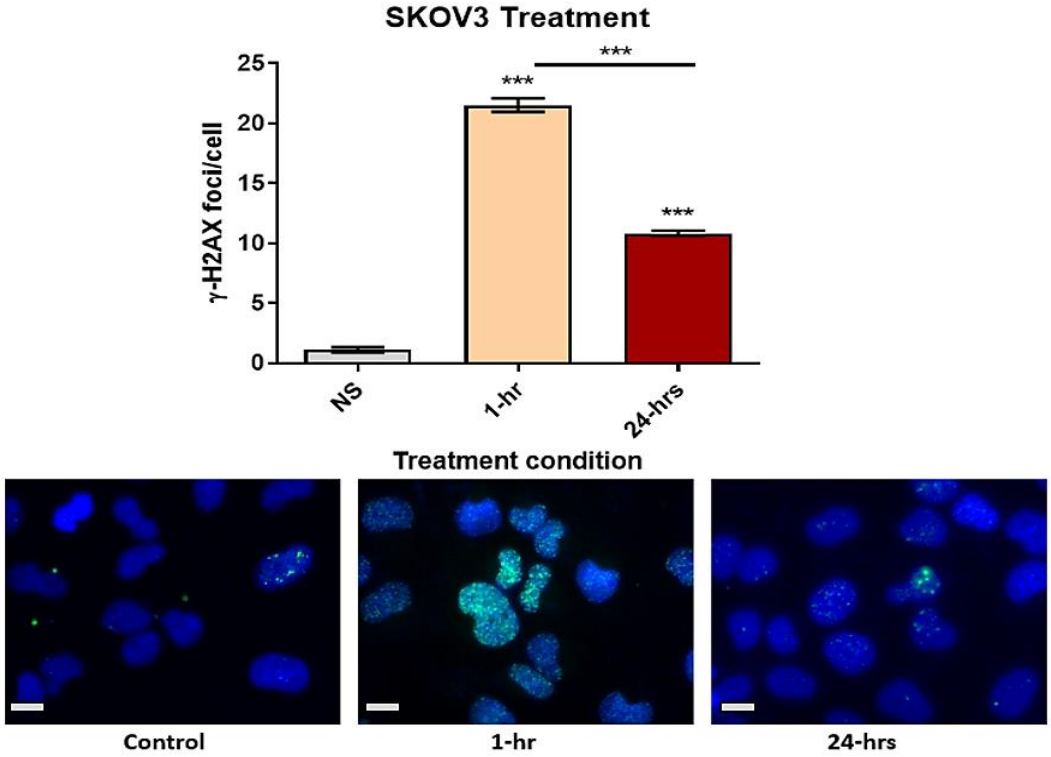

Figure 54. Number of γ-H2AX foci per cell in SKOV3 after H_2O_2 treatment. This figure shows the number of γ-H2AX foci per cell in SKOV3 based on different condition of treatment. Error bars represent standard error of the mean (SEM). Significant change was seen between control and after 1-hr ($p<0.0001$), control and after 24-hrs ($p<0.0001$) and after 1-hr and 24-hrs ($p<0.0001$), (Bar scale: 10µM).

Discussion

General discussion

As described before, both BRCA1 and BRCA2 are critical for the DNA repair process through HR, which is mainly involved in the repair of DNA lesions that postpone the creation of DNA replication forks, result in DSBs, and this has led to the development of therapeutic methods to target tumours with loss-of-function in mutated genes. They are essential proteins for high-fidelity repair of DSB of DNA through the HRR pathway. Around 20% of high-grade serous ovarian cancers have somatic or germline BRCA mutations and testing for BRCA-m should be combined to routine clinical practice. Despite the fact that, the integrity of BRCA proteins is central to effective HRR, other proteins are also essential for this process (Moynahan and Jasin, 2010).

In this chapter I examined the hypothesis that homologous recombination pathway can be affected by BRCA2 deficiency by validating the effect of this deficiency in a number of different OC cell lines. H_2O_2 exposure allowed us to analyse more precisely the possibility of correlation between the BRCA2 deficiency and effect on HR pathway. For this aim, I exposed a set of 3 BRCA2 proficient (PEO4, MDAH-2774, SKOV3) and one deficient (PEO1) cell line to hydrogen peroxide that induce double-strand break in DNA and then monitored DSBs repair using γ-H2AX assays. Monitoring DSBs with γ-H2AX assay showed a significant high level of DNA DSBs in PEO1 cell line (BRCA2-m) following 1- and 24-hrs H_2O_2 exposures, when compared to control. Likewise, SKOV3 (BRCA2-wildtype) cell line surprisingly displayed a high level of γ-H2AX in compared to control, which suggesting other defective genes, involved in HR pathway could result in disruption of HR repair mechanism. Although, in PEO4 and MDAH-2774 (BRCA2-silent mutation) cell lines, the number of γ-H2AX foci returned to near normal levels which indicating full DNA repair. These results indicate the lack of ability to fully repair of DNA damage in cancer cells with BRCA2-mutation. It is important that deficiencies in BRCA2 gene will affect genome stability.

It has been established that normal cells will repair DSBs within 24h after inducing DNA damage (Gordon *et al.,* 2002). In association with this, Vaurijoux *et al*., 2017 has showed that, after ionizing radiation, the peak of γ-H2AX foci number was at 30 minutes after exposure, and most of these damages disappear within hours of exposure (Vaurijoux *et al.,* 2017). These data corroborate previous studies, Rogakou *et al.,* 1999, which showed that DNA DSBs can be rapidly detected and marked in condensed chromosomes and in interphase

chromatin. They observed that after 30 minutes irradiation, DNA damage could be found and started to disappear after 24-hrs of exposure, due to DNA repair (Rogakou *et al.*, 1999).

In addition, in previous studies, it has been displayed that BRCA1/2 are involved in DNA DSBs repair through the HR pathway. For example, Adam-Zahir *et al.*, showed that, in A2780 (BRCA-wildtype) and A2780cis (BRCA1-m) cell lines, there was an enhanced level of γ-H2AX foci after exposure to 0.50 μg/ml HN2. However, foci formation in the A2780cis cell line was significantly increased in comparison to the A2780 cell line (Adam-Zahir *et al.*, 2015). In another study, it was found that MRC5 cell line with normal repair kinetic had lower number of γ-H2AX foci compared to AT5BIVA with ATM deficient and XP14BR with DNA-PKcs deficient. Ataxia telangiectasia mutated gene (ATM) has a major role in HR pathway and DNA-PKcs can cooperate with it during DNA damage checkpoints. These data show that, deficiency in genes involved in HR can lead to HR deficiency (Parris *et al.*, 2015).

HRD can happen through other mechanisms that lead to BRCA-like phenotype. The concept of "BRCAness" has been established to define this shared phenotype between sporadic and familial cancers with mutation in BRCA1/2 gene. Recently, it has been established that somatic mutations in other genes such as ATM, ATR, CDK12, CHEK2 and PALB2 which are involved in HR repair, has a role in development of tumours (Rigakos and Razis, 2012). It appears therefore, that tumours with BRCAness may also respond to similar therapeutic approaches as BRCA1/2-m tumours. Although, cancers with BRCA1/2 mutation and those with BRCAness indicate that small population of these cases, possibly restricting the therapeutic benefit of PARP-inhibitor monotherapy. Therefore, it seems to be a promising treatment strategy in BRCA-wildtype tumours and those without BRCAness that might result in HR deficiency and subsequent sensitization to PARP-inhibitors (Papadimitriou, Mountzios and Papadimitriou, 2018).

Conclusions

In summary, I used imaging flow cytometry and immunofluorescence to assess the effect of BRCA2 mutation on homologous recombination *in vitro*. Understanding of BRCA mutation status in OC patients is important in terms of managing individual risk and identifying other family members at risk. The status of BRCA1/2 in patients can help through treatment outcomes and with the development of PARP inhibitors, offers the potential for personalized anticancer treatment (Drew, 2015).

Chapter4: H2AX

Introduction

It is essential for normal cellular function and maintenance of genomic stability to recognise and subsequent repair of DNA damage. An acquired or inherited deficiency in DNA repair pathways in human, can lead to an increased lifetime risk of cancer. DNA double strand break (DSB) is the most lethal insult to the genome and if left unrepaired, can result in genomic instability and cell death (Ledermann, Drew and Kristeleit, 2016). Normal cells naturally have efficient mechanisms for DNA repair, which eventually remove almost all damage. Nevertheless, some people inherency has mutations that affect DNA repair pathways, and these people have higher risk of cancer. For instance, people born with mutant gene involved in NHEJ pathway are more sensitive to IR and have high risk of suffering from leukaemia and solid tumours.

Other examples of mutations in DNA repair genes which prompt cancer include BRCA1 and BRCA2. Mutation in these two well-characterized genes, could result in a significant risk of breast and ovarian cancer on carriers. Both genes are involved in HR which has a main role in DNA DSBs repair (O'Donovan and Livingston, 2010). HR uses a homologous DNA template to repair DSB which is started through end resection from the ends of DNA break to produce a long stretch of single-strand DNA for strand invasion. At first, HRD was identified in tumour cells carrying germline mutations in BRCA1 and BRCA2 genes as a tumour suppressor. Additionally, genetic and epigenetic inactivation of several components which has a role in HR, might lead to HRD in sporadic cancers, generally characterised BRCAness (Hoppe *et al.*, 2018).

In the last two decades, the significance of HR in the conservation of mammalian genome integrity has been emerged. HR is mostly responsible for DSBs repairing, as a result of replication fork stalling (in the late S phase). HR pathway includes nucleolytic processing, strand invasion, formation of Holliday junction and branch migration. DSBs can be visualized as local spot of repair protein accumulation which is called foci in the nucleus. There are some proteins which accumulate in foci, including 53BP1, RPA, RAD51 and γH2AX around the DSB. In the last decade, a new biomarker, the phosphorylated histone H2AX, has discovered as a powerful tool to monitor DNA DSBs in translational cancer research.

H2AX is one of the isoforms from the Histone H2A family protein which is distinguished from other isoforms through the presence of a short COOH terminal tail. H2AX can range

from between 2-25% of the H2A protein depending on the species of mammal. Before stop codon, the tail has a highly conserved sequence containing one serine at position 139 and one glutamine residue at position 140, known as the SQ motif. The phosphorylated form of H2AX on the Serine 139 residue located in the COOH tail, was named γ-H2AX because it was first detected in cells exposed to γ-rays and it is accumulated around the break in a 2Mb region (Kuo and Yang, 2008). Once DSB has taken place, H2AX molecules are rapidly phosphorylated via PI3-kinases, including ATM, ATR and DNA-PK, depending on the cause of DNA damage and timing. γH2AX generation is one of the earliest events discovered in cells due to exposure to DNA damaging agents. It appears within minutes and reaches maximum levels after 30 min (Ivashkevich *et al.*, 2012).

Furthermore, mice lacking H2AFX had shown more sensitivity to radiation and are less efficient at DSB repair which lead to high level of chromosomal abnormalities (Bassing *et al.*, 2002). This suggests a role for H2AX to prevent genomic instability related to cancer. Loss of one or both H2AX alleles in mice result in genomic integrity and high risk of tumour progression in a p53 null background (Bassing *et al.*, 2003)(Benton *et al.*, 2003).These findings imply a role of H2AX as a genome caretaker and the expression of both gene alleles is necessary for preventing tumorigenesis (Dickey *et al.*, 2009).

There are various genes mutations and polymorphisms involving in DNA damage response which have been reported in several human cancers. Although no significant risk involvement with a mutation or SNP has yet been determined. One possible reason can be that a mutant gene in isolation may have a minor effect on cancer risk, while combination with other gene mutations could become significant. The distal 11q arm harbours main DDR genes including ATM, MRE11A, CHEK1 and H2AFX. In this context, it might be interesting that loss of distal 11q arm is frequently detected in different cancers and result in tumour progression. In a considerable proportion of head and neck squamous cell carcinomas, Parikh et al. discovered partial deletions of the region on 11q23 containing H2AFX, suggesting a possible contribution of H2AFX in human cancers (Srivastava *et al.*, 2009). Furthermore, the study indicates that other tumours categorized by loss of the distal region of chromosome 11q need to be analysed for loss of DNA repair efficiency (Dickey *et al.*, 2009).

H2AX is a modified histone H2A to switch original H2A in a subset of nucleosomes. Due to nucleosomes wrap and compact DNA into chromatin, DNA accessibility is limited for the cellular pathways that use DNA as a template. By this means, histone has a crucial role in several mechanisms including transcription regulation, DNA repair, DNA replication and

chromosomal stability. DNA accessibility is controlled by histone code which is a complex set of histone post-translational modifications, and nucleosome remodelling. Furthermore, H2AX is essential for checkpoint-mediated arrest of cell cycle process after exposure to low doses of ionizing radiation and also for efficiency of DNA DSBs, particularly when altered through phosphorylation of C-terminal domain (UniProt, 2020).

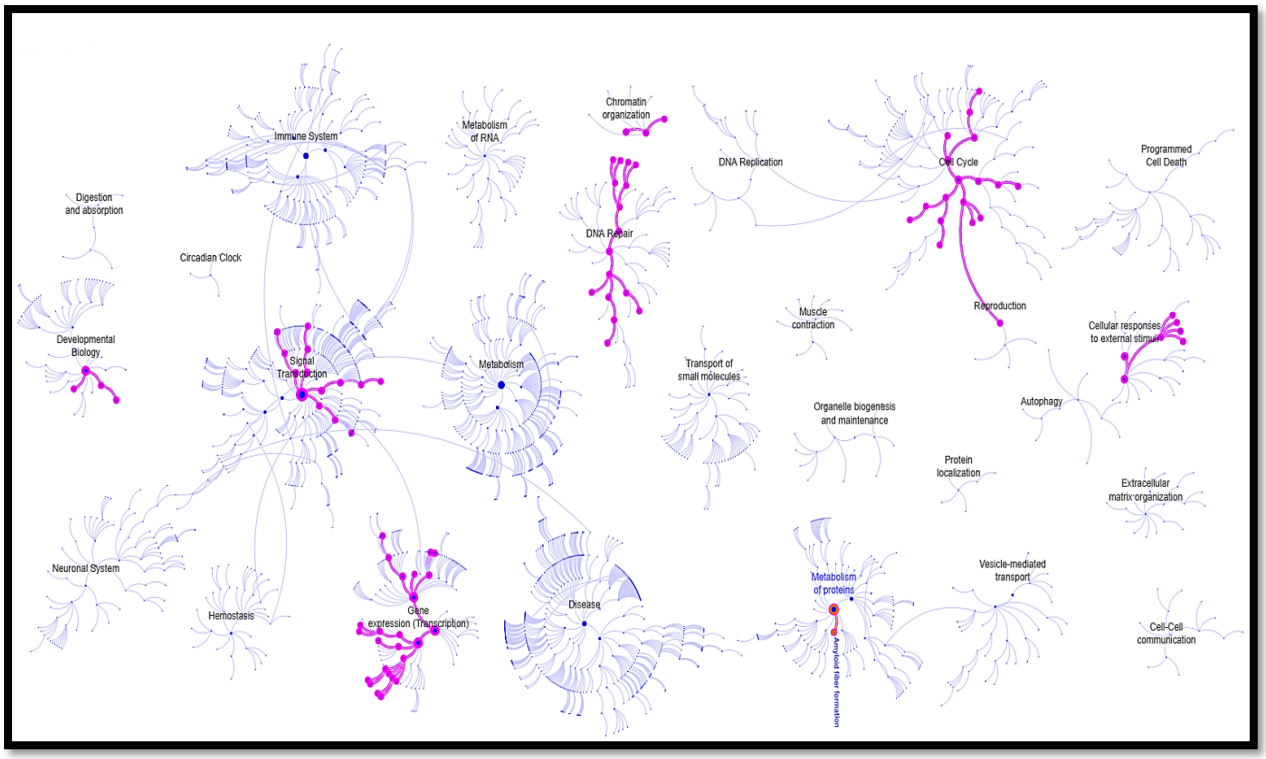

Figure 55. Signalling pathways that H2AX is generally involved. The main one is cell-cycle, DNA repair, gene expression (transcription) and signal transduction (Reactome, 2020).

In this study I assessed in detail the expression of H2AX in OC comprising of population sample and genotyping. I have provided a better insight into the protein expression using a tissue microarray and presented evidence of transcriptional changes based on the BRCA status.

Aims

- Look at the H2AX expression in OC using TCGA and validating our cancer patients' sample through qPCR.
- Using gene set enrichment analysis (GSEA) to study gene association of some genes involved in OC patients with high level of H2AX.
- Study of H2AX prognostic value by using KM plot in OC patients
- Assess the expression of H2AX in different type of OC with different stage by using tissue microarray.
- Compare the level of H2AX phosphorylation with gene expression.

Result

4.1. H2AFX is over-expressed in Ovarian Cancer and predicts survival

H2AX (H2AFX) expression was noticeably upregulated in primary and recurrent ovarian cancer patients when compared to healthy controls tissue in TCGA (Figure 56). qRT-PCR in a small cohort of stage III OC patients established high level of H2AX expression gene, in comparison to age matched controls (Figure 57).

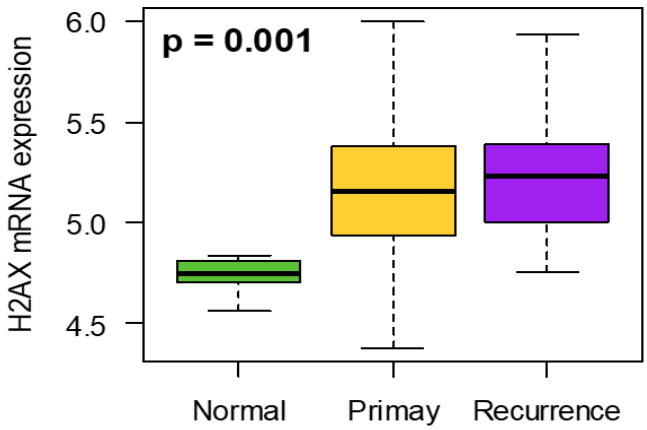

Figure 56.H2AX expression in OC tissues vs normal ones. H2AX is significantly (P=0.001) overexpressed in OC tissues (Primary: n=568, Recurrence: n=17) against normal tissues (n=8). Credit: TCGA .

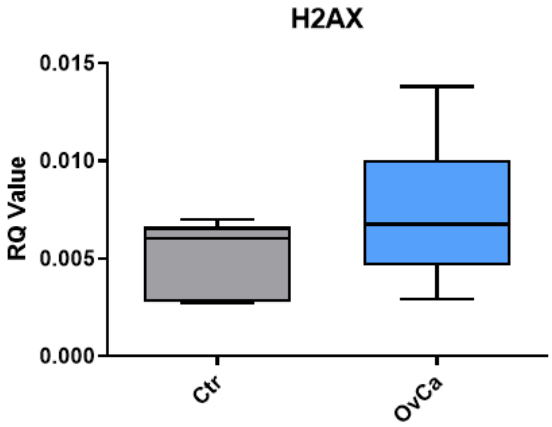

Figure 57.H2AX gene expressions quantified by qRT-PCR. H2AX is upregulated in stage III OC patients (n=10) compared to controls (n=6).

Gene Set Enrichment Analysis (GSEA) revealed that gene sets were also enriched in the H2AX highly expressing ovarian cancers. In G2/M checkpoint, E2F target and DNA repair processes, genes related to regulation of nucleobase, nucleoside, nucleotide, and nucleic acid metabolism were enriched.

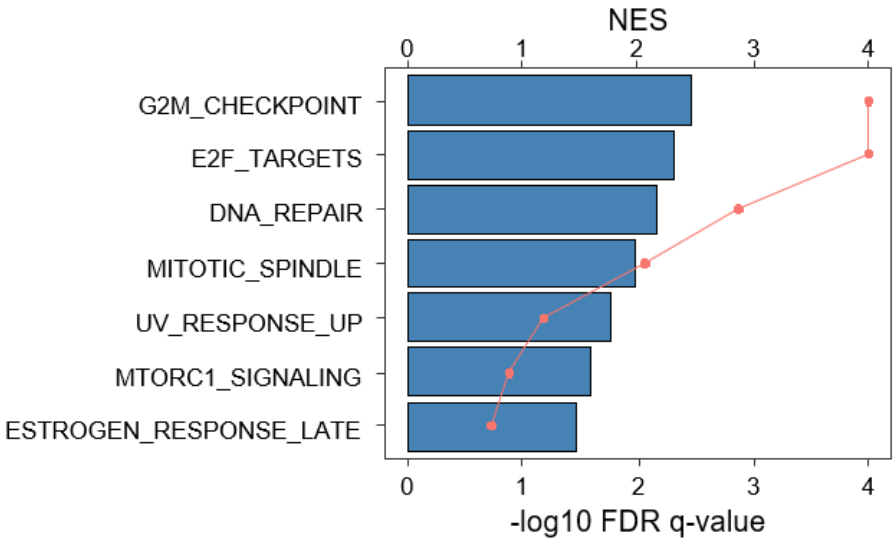

Figure 58. Hallmark gene sets enriched in OC patients expressing high levels of H2AX. (G2/M checkpoint: NES (normalized enrichment score) =2.46, p<0.001; E2F targets: NES=2.30, p<0.001; DNA repair: NES = 2.15, p < 0.001; Estrogen response: NES=1.46, p=0.048); mitotic spindle: NES = 1.98, p < 0.001; mTORC1 signalling: NES = 1.6; p = 0.047; and UV response: NES = 1.75, p = 0.004.

We then performed gene enrichment on genes significantly associated with the mentioned processes. The most significant **biological processes** were: **G2/M:** Regulation of nucleobase, nucleoside, nucleotide and nucleic acid metabolism, Signal transduction, cell communication. **E2F:** Regulation of nucleobase, nucleoside, nucleotide and nucleic acid metabolism, regulation of cell cycle, DNA replication, DNA repair. **DNA repair:** Regulation of nucleobase, nucleoside, nucleotide and nucleic acid metabolism, DNA replication. **Mitotic spindle:** Cell communication, Signal transduction. **mTORC1 signalling:** Energy pathways, Metabolism, Protein metabolism. **Estrogen response:** Metabolism, Energy pathways. Gene enrichment analysis was performed on these gene sets and data are shown in Figure 59-64.

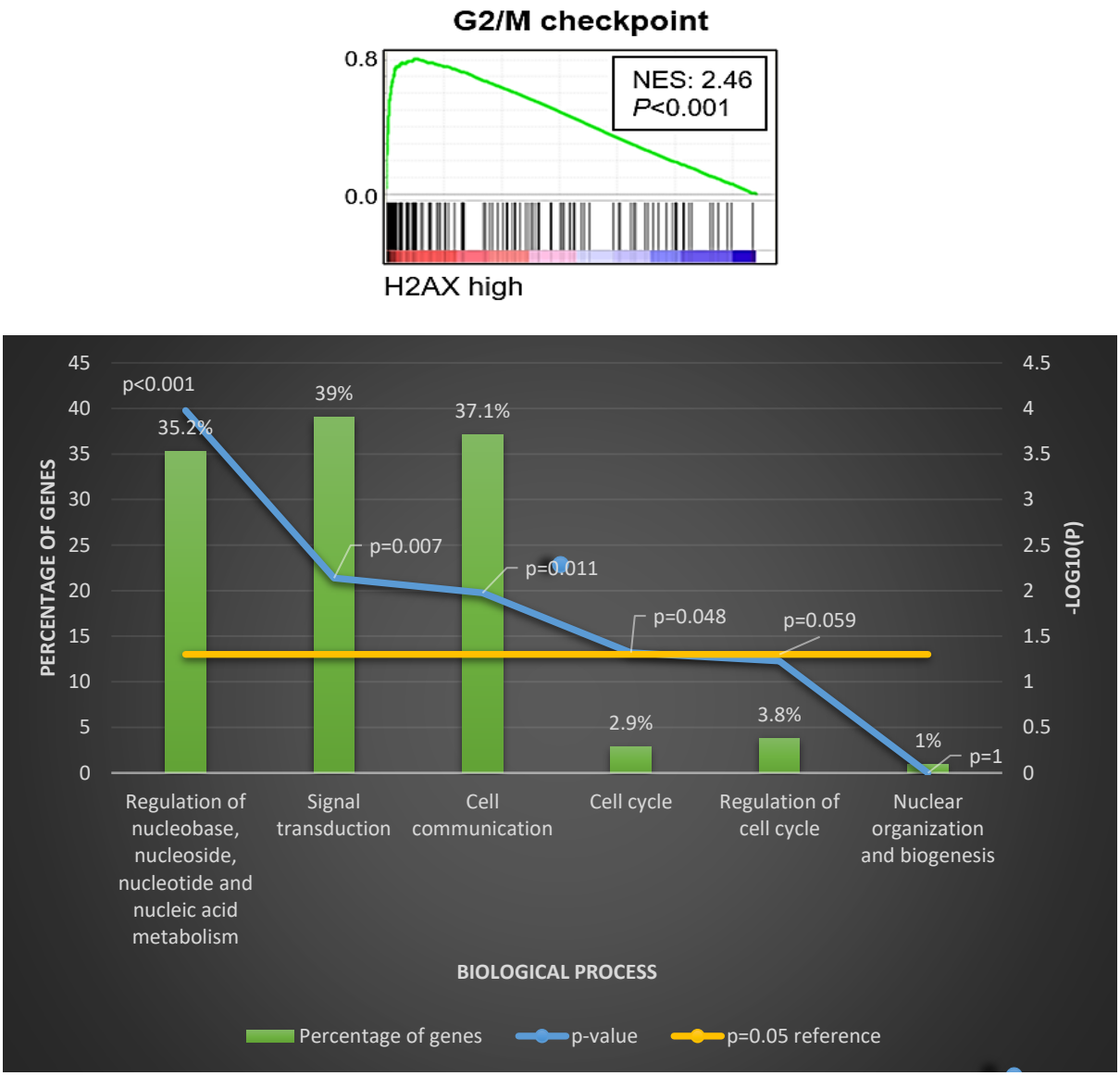

Figure 59. Gene enrichment analysis on G2/M checkpoint gene set. Gene enrichment on genes significantly associated with G2/M checkpoint with significant biological processes of regulation of nucleic acid metabolism, signal transduction and cell communication.

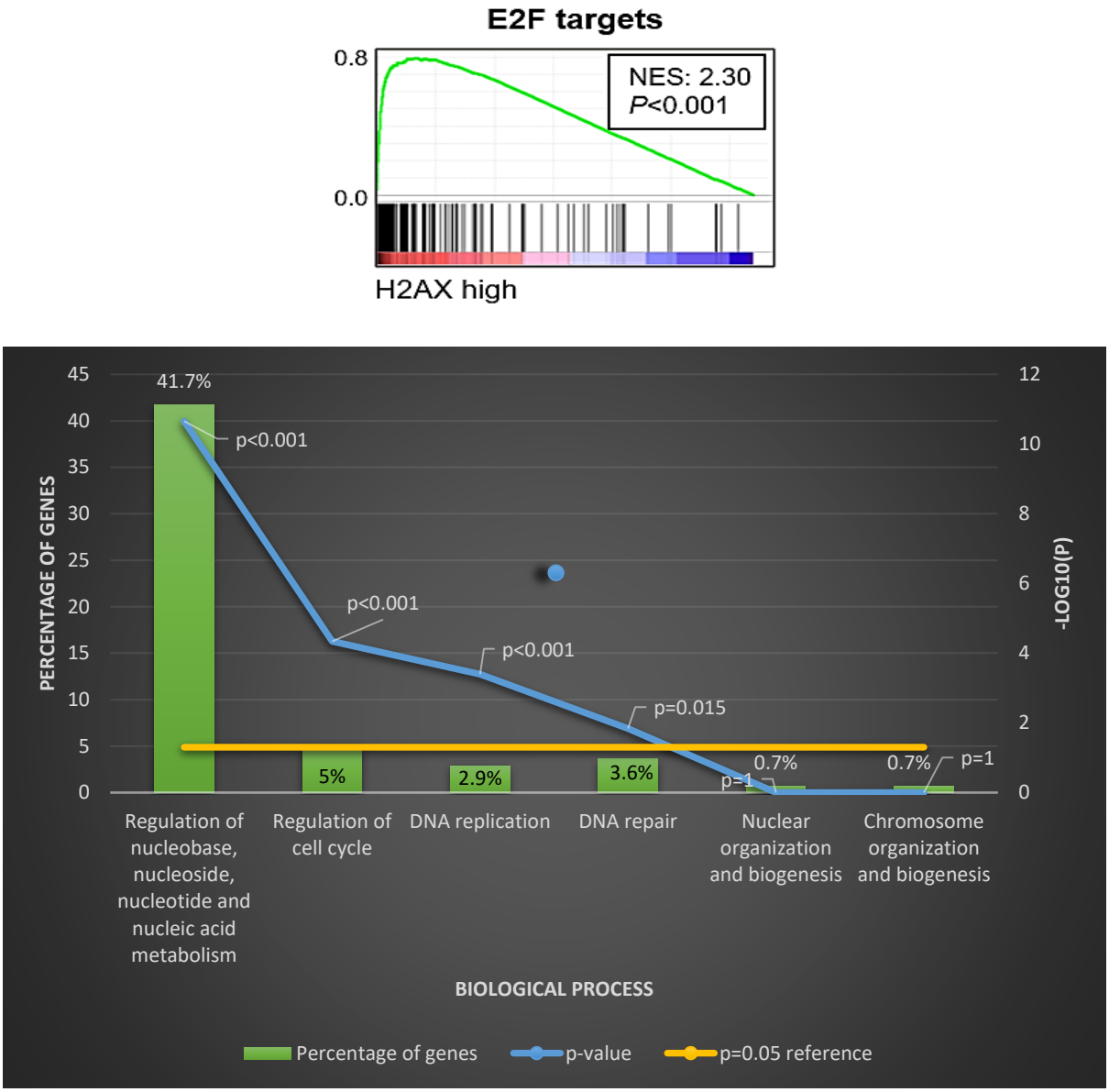

Figure 60. Gene enrichment analysis on E2/F targets gene set. Gene enrichment on genes significantly associated with E2F targets, with significant biological processes of and regulation of nuclei acid metabolism and cell cycle as well as DNA replication and repair.

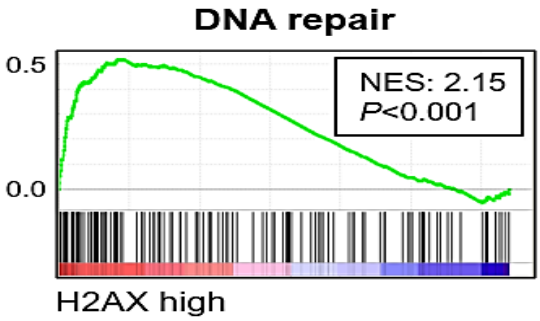

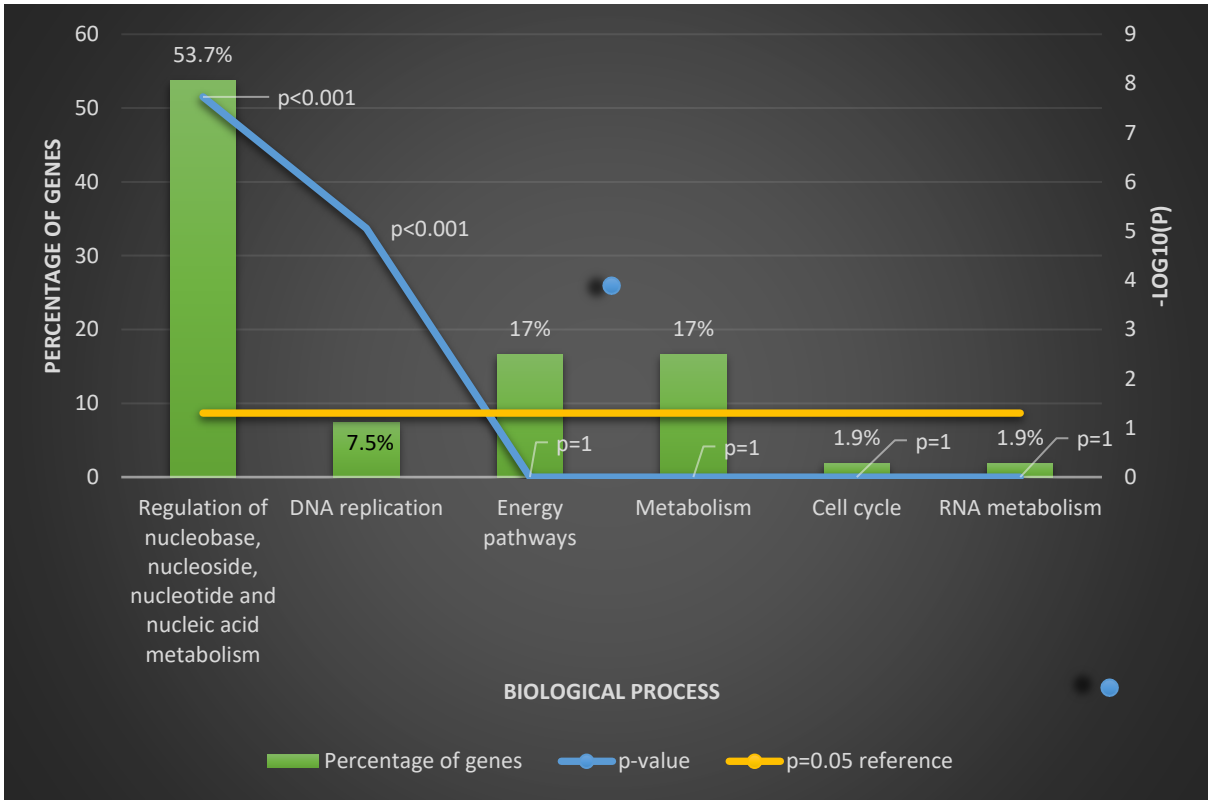

Figure 61. Gene enrichment analysis on DNA repair gene set. Gene enrichment on genes significantly associated with DNA repair with significant biological processes of regulation of nucleic acid metabolism and DNA replication.

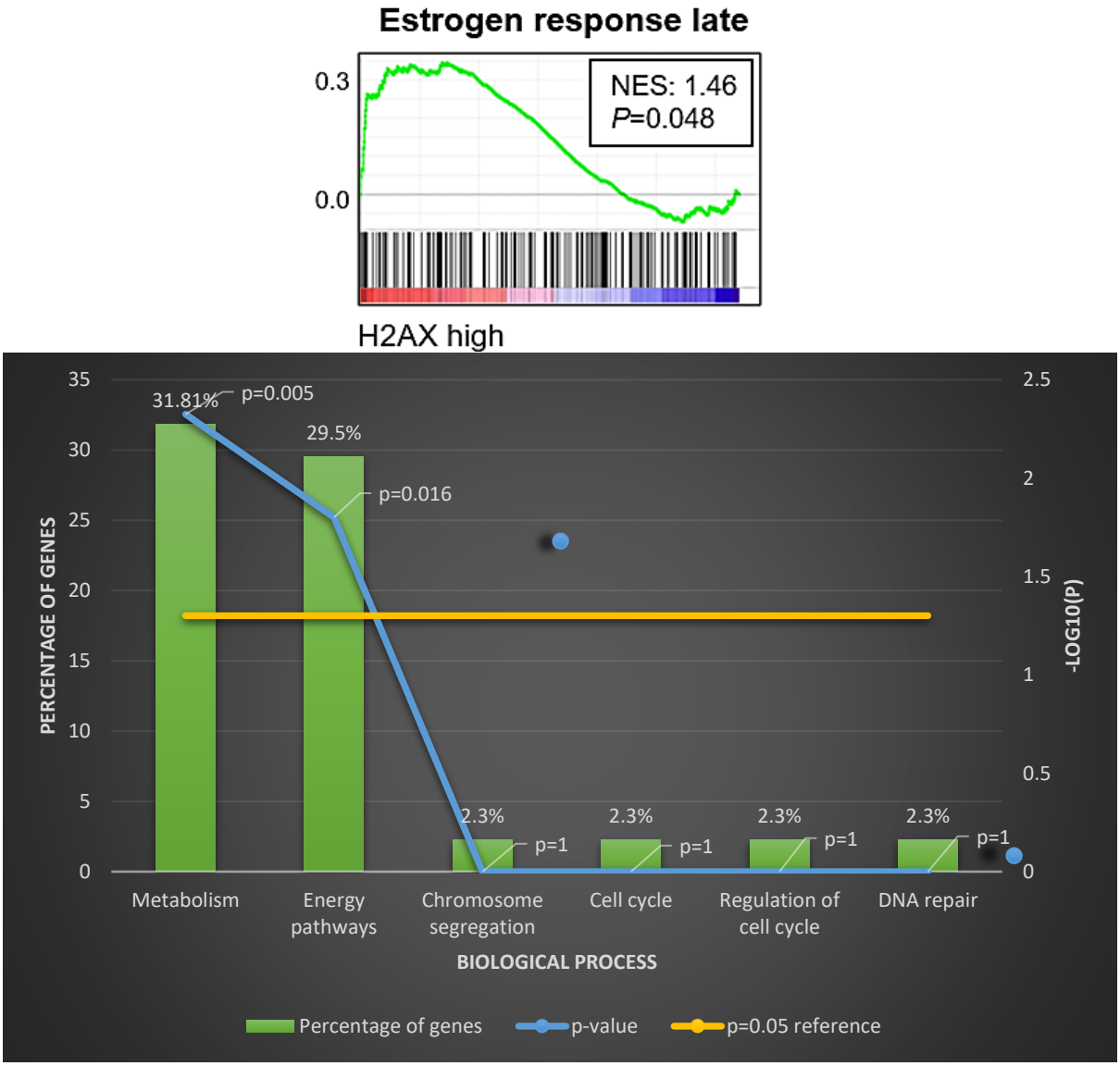

Figure 62. Gene enrichment analysis on Estrogen response gene set. Gene enrichment on genes significantly associated with Estrogen response (late) with significant biological processes of metabolism and energy pathways.

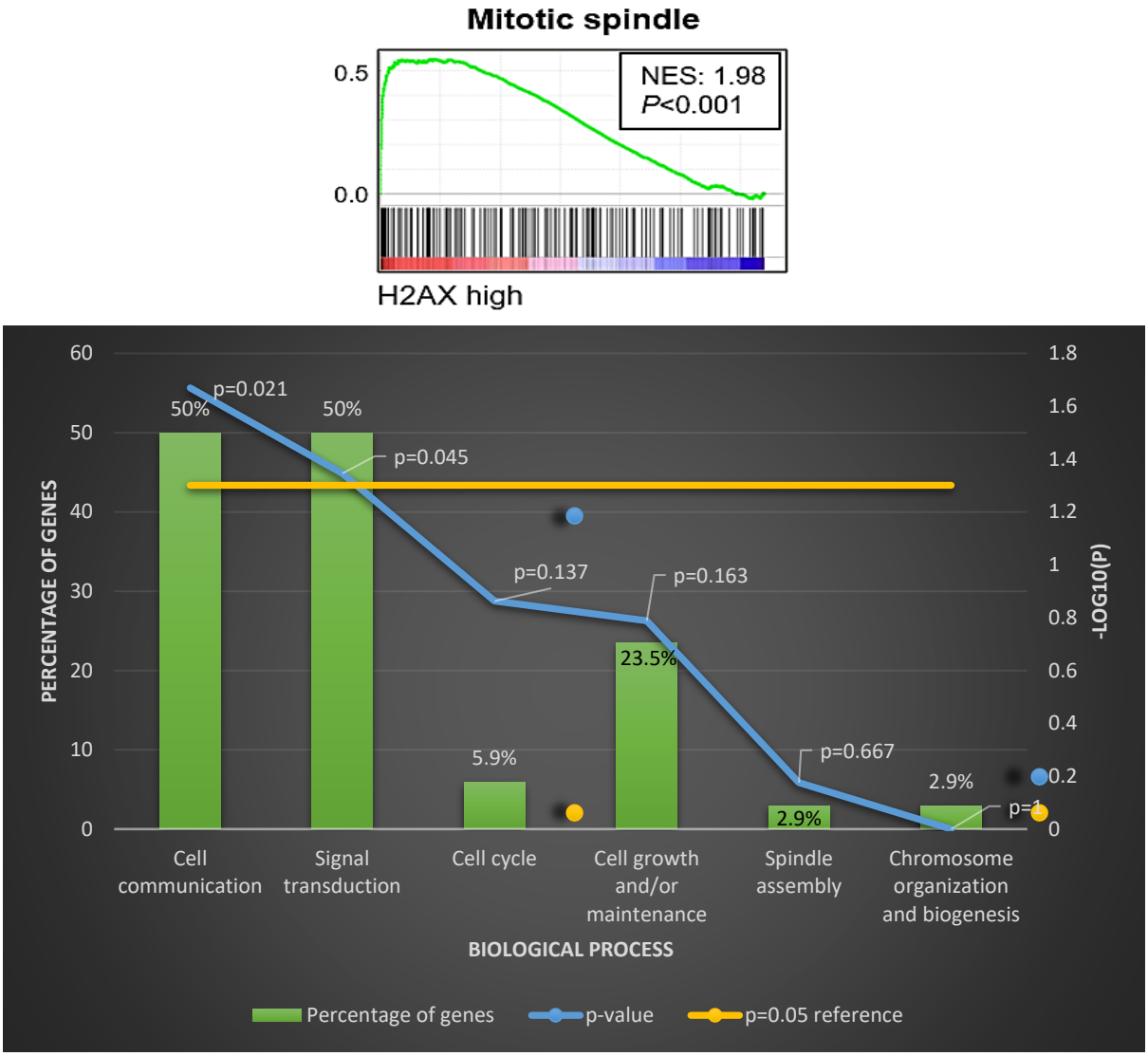

Figure 63. Gene enrichment analysis on Mitotic spindle gene set. Gene enrichment on genes significantly associated with Mitotic spindle with significant biological processes of signal transduction and cell communication.

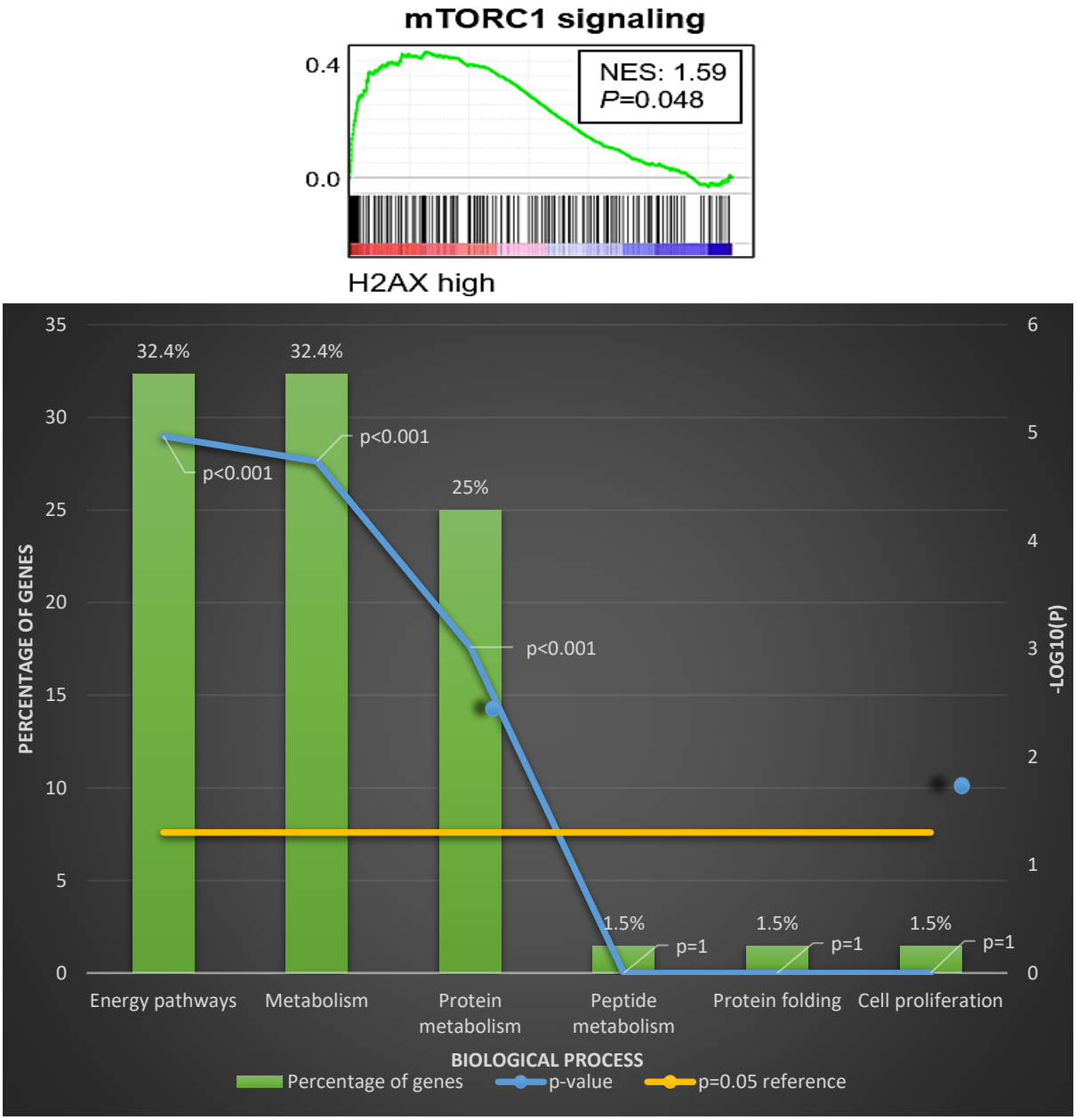

Figure 64. Gene enrichment analysis on mTORC1 signalling gene set. Gene enrichment on genes significantly associated with mTORC1 signalling, with significant biological processes of energy pathways, metabolism, and protein metabolism.

Moreover, signal transduction and cell communication genes were enhanced in the G2/M checkpoint set; cell cycle regulator and DNA replication/repair genes in the E2F gene set. From the estrogen response and mTORC1 signalling gene sets, metabolism (precisely protein metabolism for the mTORC1 set) and energy pathway genes were enriched. Lastly, from the mitotic spindle set, genes from cell communication and signal transduction pathways were enhanced (Saravi *et al.*, 2020).

I extended these observations through stratifying H2AX expression with genes expression which are responsible for phosphorylating H2AX due to DSBs, including ATM, ATR,

MDC1 and DNA-PK (Figure 65). Of these four genes, only MDC1 showed a significant upregulation in the high-H2AX expressing OC group.

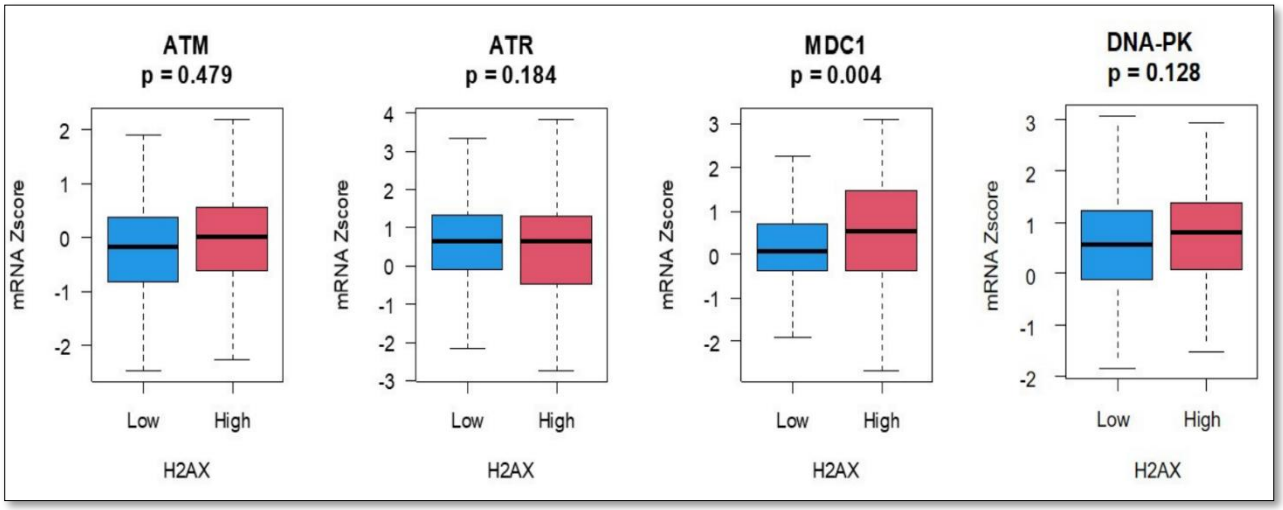

Figure 65.Differential expression of 4 key genes that change the H2AX phosphorylation status in response to DSBs upon stratification of ovarian cancer patients to low- and high-expressing H2AX groups. Only Mediator of DNA Damage Checkpoint 1 (MDC1) was significantly upregulated in the high-H2AX expressing group.

In terms of prognostic value, higher expression of H2AX was correlated with better overall survival (OS; p=0.010), whereas there was no apparent alteration on disease free survival (DFS) in the TCGA ovarian cancer cohort (Figure 66).

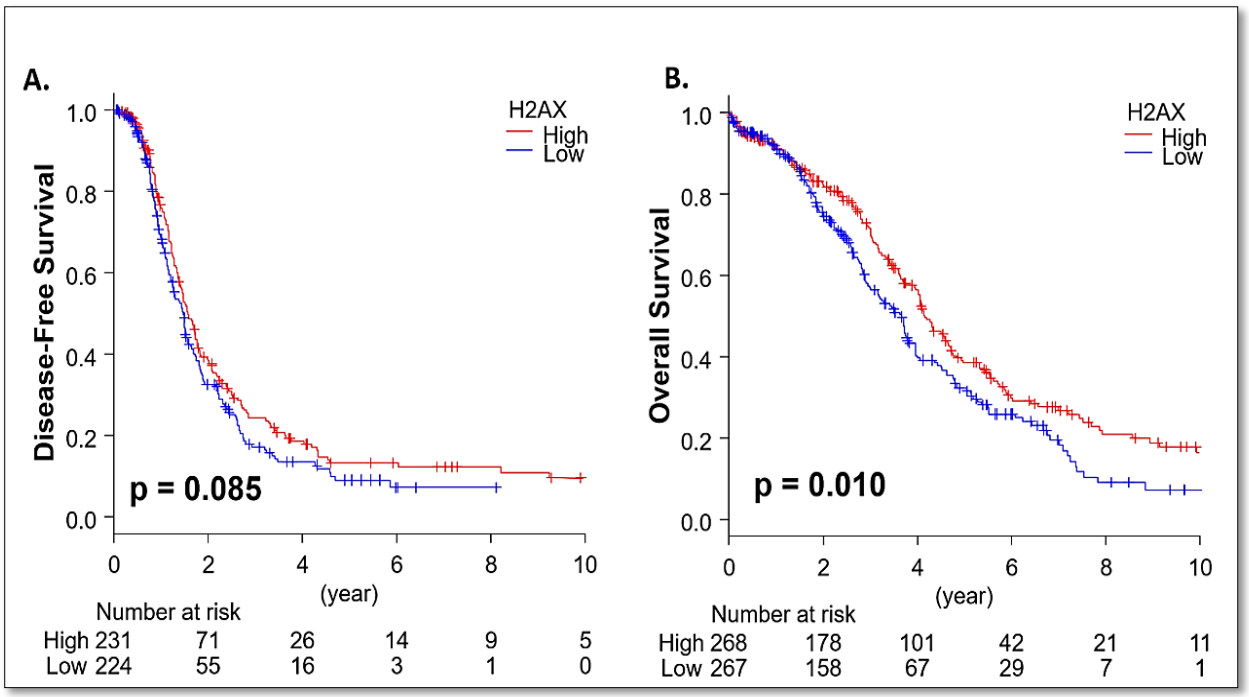

Figure 66. Kaplan-Meier (KM) plots for disease-free survival (A) and overall survival (B) in OC patients using the TCGA database.

4.2. H2AX protein is abundantly expressed in ovarian cancer tissues

Following *in silico* analysis of H2AFX in terms of expression and survival prediction, I studied the expression of H2AX protein in 100 cores of OC patients and adjacent tissue (Figure 67). H2AX protein was significantly expressed in both high- and low-grade serous samples, as well as in mucinous and endometrioid adenocarcinomas. Interestingly, normal adjacent control (NAT) ovarian tissue displayed greatly higher H2AX expression, compared to ovarian cancer cores. Lastly, a decrease in H2AX staining was remarked in patients with late-stage OC (stages II-IV, n=18) when compared to early-stages (I-II; n =62).

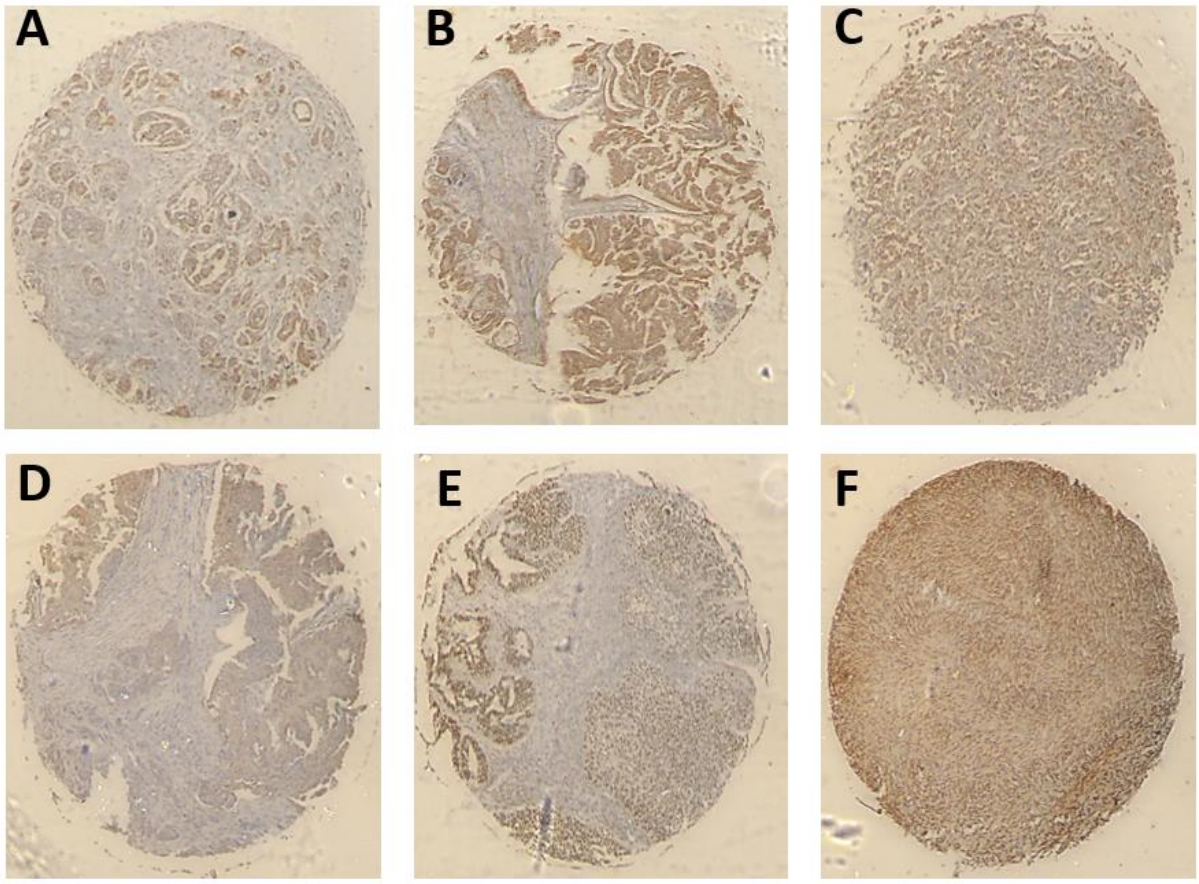

Figure 67. Staining of OC cores with H2AX. **(A)**: Low grade serous (LGS), **(B)**: High grade serous (HGS), **(C):** Mucinous adenocarcinoma (Adeno), **(D):** Metastatic serous carcinoma (MSC), **(E):** Endometrial adenocarcinoma, and **(F):** adjacent to tumour ovarian tissue (NAT). Abundance of staining was detected across all different OC types with a noted upregulation in NAT tissue.

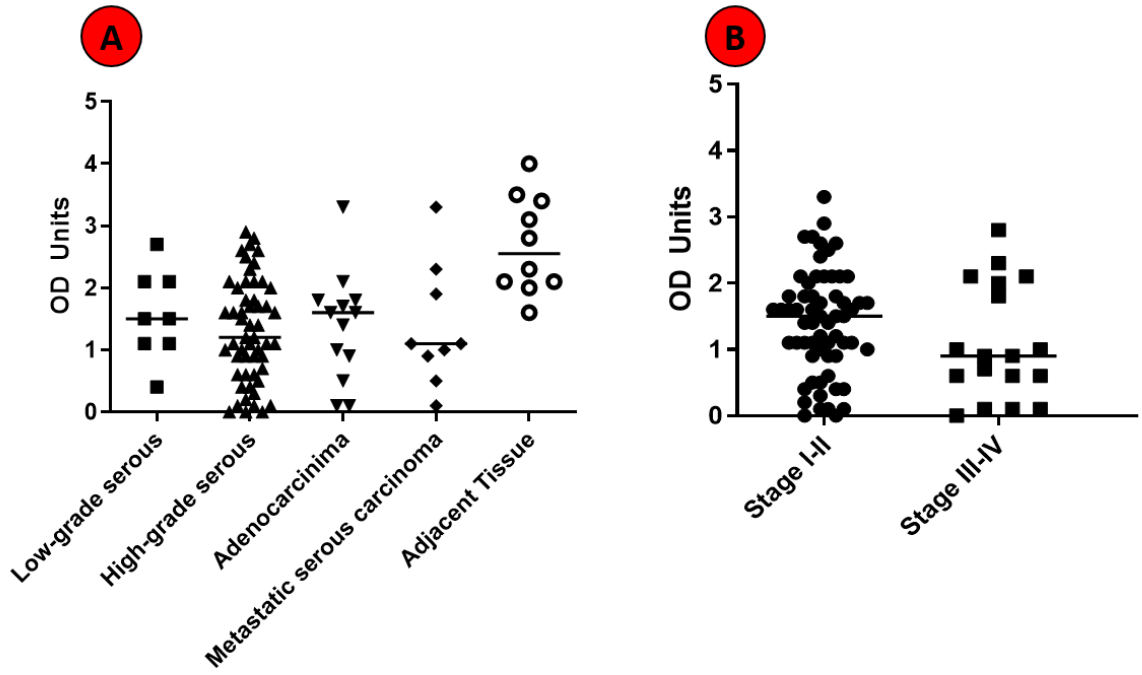

Figure 68. Individual values graph of IHC data **(A).** Abundance of staining was detected across all different OC types with an upregulation in NAT tissue **(B)**. Non-significant difference in H2AX staining in late stage (III and IV) when compared to early stage (I and II).

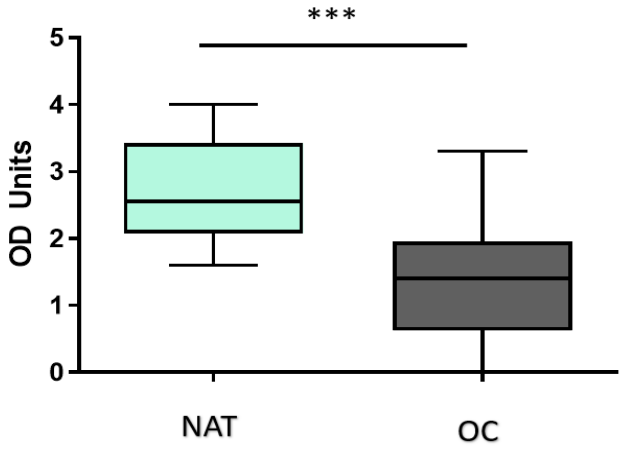

Figure 69. Data from IHC on microarray panel with 100 different ovarian cancer tissues. Significant protein upregulation of H2AX (*** P=0.0003) when all NAT cores were compared to OC.

4.3. Genome-wide association study (GWAS) for *H2AX*

This GWAS study was conducted by Dr Fotios Drenos, by using the 842 OC cases, at population level based on data from the UK Biobank in order to identify any associations of SNPs with cancer as well as 5-year overall survival, based on a localised Manhattan plot of Chromosome 11q23.3 (Figure 70). In total, 108 SNPs were studied. A Reference SNP cluster rs72997349 (C-T) demonstrated a significant increase of risk (p=0.005) for ovarian cancer (for the most common C-allele) with an odd of 1.4 (95% CIs 1.1-1.8) (Figure 70.A). We have expanded on these observations by using the 227 incident cases with 5-year overall survival, studying the same SNP cohort (Figure 70.B). The top association in terms of lowest p-value was rs10790282 (A-G) with p = 0.011 and a protective effect of 0.58 or for each G allele, or else an increasing OR of 1.72 per each A allele.

The UK Biobank is a large population study of approximately 500,000 individuals. These were recruited between 2006 and 2011 from 22 UK Biobank assessment centres throughout England, Wales and Scotland. The age range of the participants at the time of enrolment in the study was from 40 to 69 years, with a mean age of 56.5 years old. Females represent 54.4% of the sample.

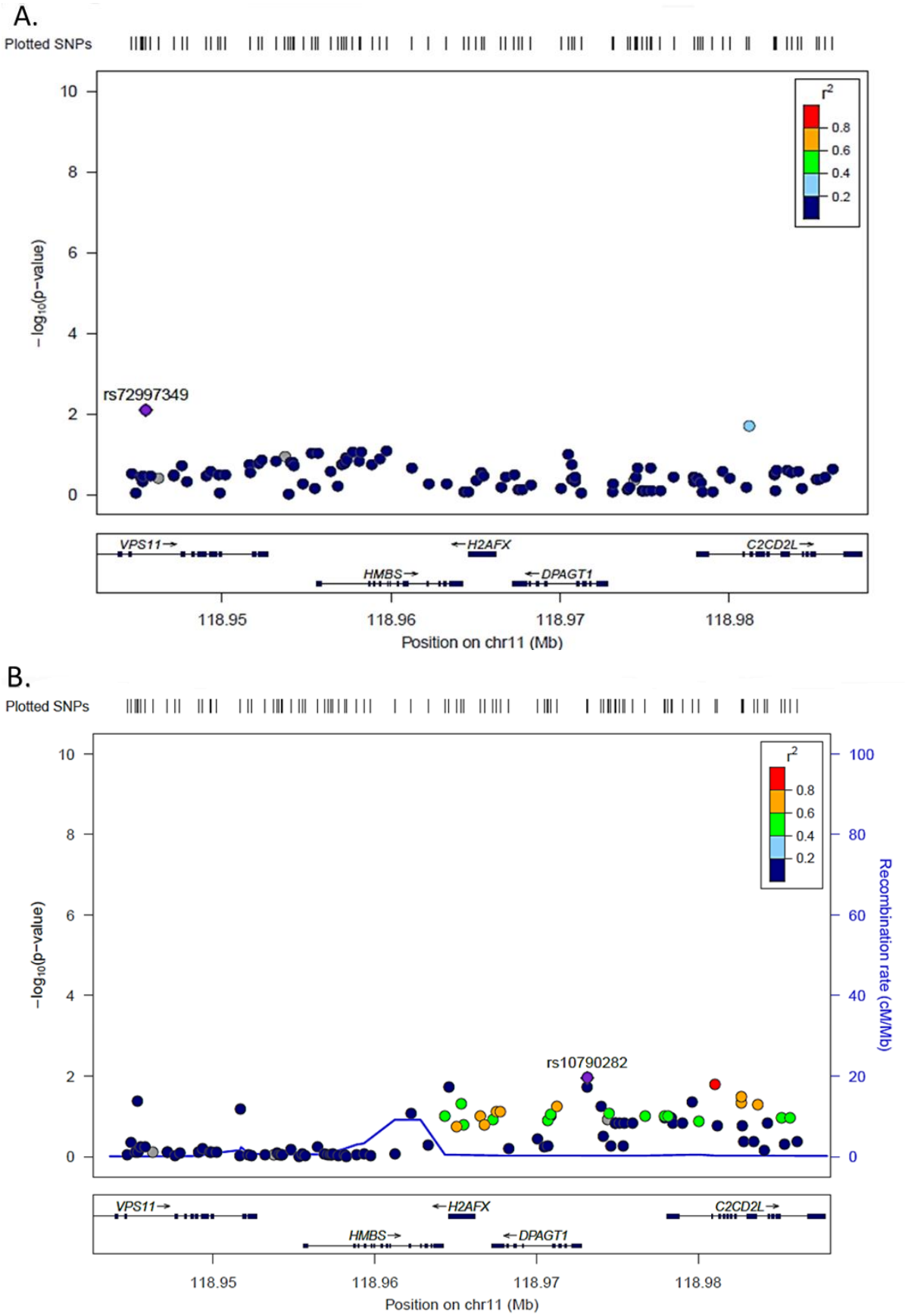

Figure 70.Genome-wide association study (GWAS) for H2AX. Reference SNP cluster rs72997349 (C-T) demonstrated a significant increase of risk for ovarian cancer (**A**), whereas Reference SNP cluster rs1079082 (A-G) demonstrated a significant increase in overall survival (**B**).

4.4. H2AFX expression correlates with γ-H2AX staining *in vitro*

Here I have studied whether transcriptional changes of the H2AX gene associate with changes in γ-H2AX foci following induced DNA damage using H_2O_2 in BRCA wild-type and BRCA mutant cell lines. For this, I have used 4 ovarian cancer cell lines as *in vitro* models: SKOV3 (BRCA wild-type), PEO1 (BRCA2-mutant), PEO4 (BRCA2-Silent mutant) and MDAH-2774 (BRCA2-Silent mutant). I measured the number of γ-H2AX foci by using immunofluorescence technique. Prior to the experiment, I analysed the number of γ-H2AX foci in BRCA2 wild-type and mutant ovarian cancer cell lines to examine whether BRCA2 status will impact HR deficiency and effective repair of ds-DNA break *in vitro*.

I compared changes in gene expression to γ-H2AX staining in the above-mentioned cell lines treated with H_2O_2 to see if there is any correlation between mRNA expression and phosphorylation of the protein. It was shown that PEO1 (BRCA2-mutant cell line) had a higher number of γ-H2AX foci when compared to BRCA-wild type cell lines and in particular, PEO4 that a direct comparison can be drawn. The alteration of γ-H2AX in the cell lines is consistent with the change of H2AX gene expression. The data are shown in Figure 71.

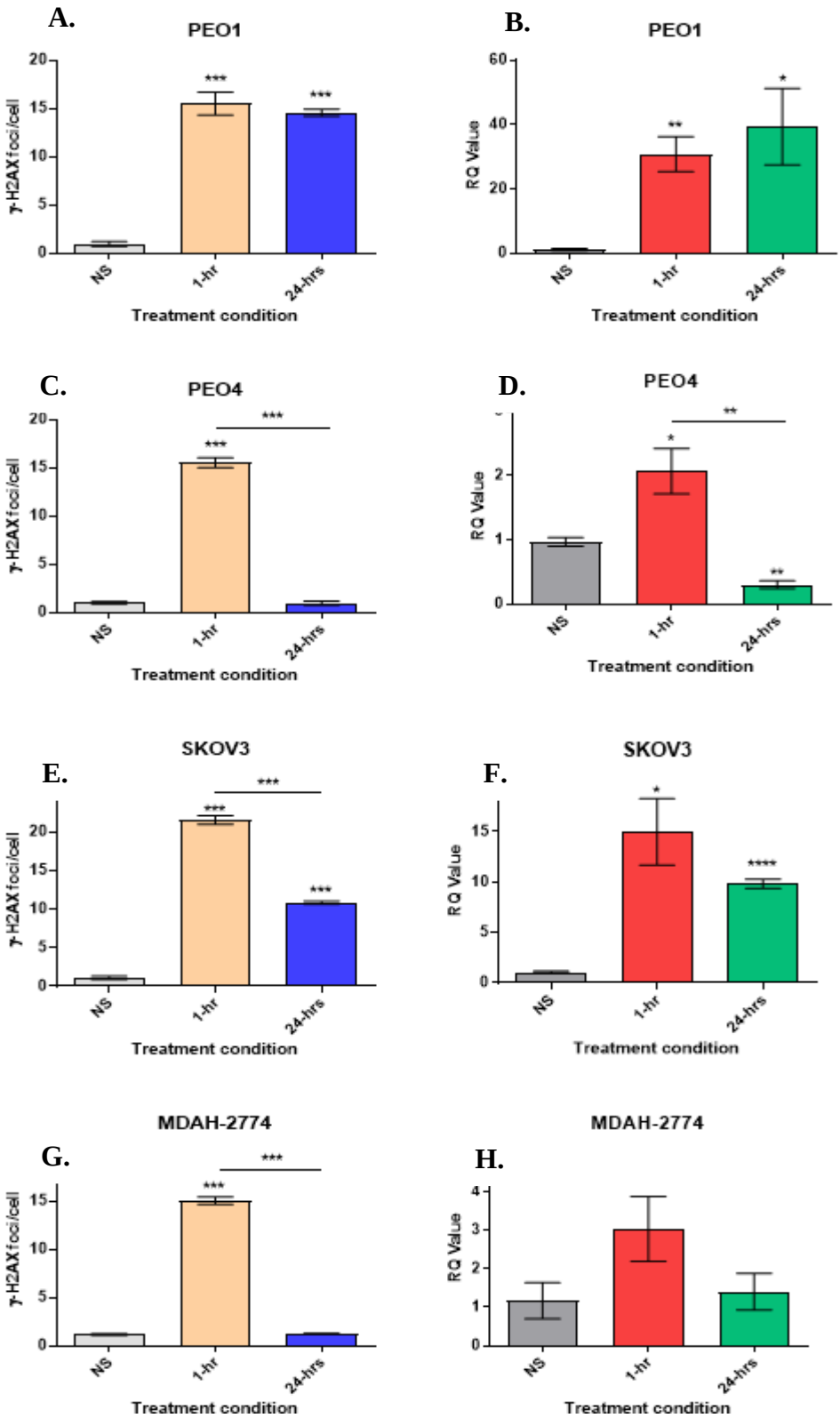

Figure 71. Treatment of cell lines with H2O2 and measurement of γ-H2AX foci (A,C,E,G) and H2AX gene expression (B,D,F,H) in BRCA2 mutant PEO1 cell line (A,B), in comparison with BRCA2 silent mutant cell line PEO4 (C,D) and BRCA2 wild type SKOV3 (E,F) and MDAH-2774 (G,H). NS; No Supplement. Panel A. 1-hr: *** $p < 0.0001$, 24-hrs: *** $p < 0.0001$ (compared to NS). Panel B. 1-hr: ** $p = 0.0056$, 24-hrs: * $p = 0.0322$ (compared to NS). Panel C. 1-hr: *** $p < 0.0001$ (compared to NS). *** $p < 0.0001$ (1-hr compared to 24-hrs). Panel D. 1-hr: * $p = 0.0375$, 24-hrs: ** $p = 0.0016$ (compared to NS). ** $p = 0.0078$ (1-hr compared to 24-hrs). Panel E. 1-hr: *** $p < 0.0001$, 24-hrs: *** $p < 0.0001$ (compared to NS). *** $p < 0.0001$ (1-hr compared to 24-hrs). Panel F. 1-hr: * $p = 0.0134$, 24-hrs: *** $p < 0.0001$ (compared to NS). Panel G. 1-hr: *** $p < 0.0001$ (compared to NS). *** $p < 0.0001$ (1-hr compared to 24-hrs).

Discussion

In this study I presented a complete overview of the alterations at gene and protein level of H2AX in OC and suggest a potential predictive biomarker. In silico analysis using the TCGA databases revealed that H2AX is overexpressed in OC in comparison to controls. Interestingly, H2AX showed to be upregulated in most cancers, compared to controls except for acute myeloid leukaemia. It has been demonstrated that H2AX expression level is significantly higher in triple negative breast cancers (TNBC) than non-TNBC and in HER2 positive tumours against tumours without HER2 overexpression (Katsuta *et al.*, 2018).

In terms of prognostic value, I established that higher expression of H2AX is related to better overall survival (OS), whereas there was no apparent difference on disease free interval (DFI) in the ovarian cancer cohort. This is in contrast with renal and liver cancer, where high expression of H2AX is an unfavourable prognostic marker (Protein Atlas, 2021). Similarly, H2AX high expressing breast tumours showed significantly worse OS (p=0.007) as well as DFS (p=0.001) and this was the case only in advanced stages (Stage I vs Stage II/III/IV, p=0.029). In a similar study using a qualitative protein expression scoring system for γ-H2AX reported a significantly reduced disease-free interval amongst patients with high γ-H2AX expression while it has been shown that there is no significant correlation with the OS in 63 OC patients (Mei *et al.*, 2015).

I have then performed gene set enrichment analysis on the OC population with high H2AX expression and have identified G2/M checkpoint, E2F targets, DNA repair, estrogen response, mitotic spindle, mTORC1 and UV response gene sets associated with this population. This fits well with the widely reported roles for H2AX as a major protein in DNA repair processes. I established that the OC population with high H2AX expression is correlated with upregulation of different biological pathways, such as PI3K/AKT/mTOR, activated in ~50% serous OC (Altomare *et al.*, 2004). This pathway, and primarily the mTORC1 complex, provides a balance between cellular resources, including amino acids and/or cellular stressors such as hypoxia to control cellular behaviour (Rogers-Broadway *et al.*, 2019). Emerging data also connects mTOR with the aetiopathogenesis of ovarian cancer. My group has previously indicated that inhibition of the mTOR pathway using rapamycin, and rapalogues can lead to cytostatic effect on preclinical models of ovarian cancer (Rogers-Broadway *et al.*, 2016).

As anticipated, I prove high level of H2AX expression in high-grade serous OC, mucinous adenocarcinomas, and clear cell carcinomas. Surprisingly, I also demonstrate high expression

in low-grade serous ovarian cancer. I also showed no correlation between H2AX overexpression and FIGO stage, supporting the study of 87 epithelial OC (EOC) patients, where γ-H2AX immunostaining was not significantly connected with age, histopathological type, tumour differentiation, lymph node metastasis, FIGO stage or size of residual disease (Mei *et al.*, 2015). Low grade serous OC is generally characterised as Grade 1, only 8 of the 100 cores included in the microarray sere described as G1/2 serous tumours. Historically, the 'G2' assigned serous cancers are now recognised a high-grade (G3) which could account for this variation as the numbers of true G1 (low grade) cases were possibly too small for comparison.

The most remarkable observation from the IHC study is the significant overexpression of H2AX in the normal adjacent tissue (NAT) in comparison to the actual malignant area in all histopathological types of ovarian cancer. This finding raises several questions as to how "normal" this tissue can be. Indeed, histologically normal tissue, normally taken from the surrounding area (<2cm) of the malignant cells, is usually used as a control in cancer research. Although, until recently, there was a little information about its transcriptomic profile, how it might be affected by the malignant cells and how it might compare with healthy control tissue, either taken from some distance away such as an unaffected ovary or an age-matched healthy control.

In a latest study using an cancers array including uterus and breast, it was displayed that NAT tissue is different from both healthy and tumour tissues when they compared NAT, GTEX and TCGA transcriptomics from 8 cancer types (Aran *et al.*, 2017). NAT tissue undergoes several processes comprising of extracellular matrix remodelling, wound healing-like processes, fibrosis, and an EMT (Loret *et al.*, 2019). It might be possible that the upregulation I have seen in H2AX is connected to crosstalk with the cancer microenvironment, ostensibly preconditioning the adjacent normal tissue. There is another possibility for the differences between NAT, tumour and control tissues which is the potential involvement of microRNAs (miRNAs). For instance, miR-24 upregulation in terminally differentiated blood cells, can lead to decreasing of H2AX level (Lal *et al.*, 2009). Therefore, it might be possible that this miRNA targets H2AX transcripts, since it seems to be present at ovarian level (Ludwig *et al.*, 2016), based on the human miRNA tissue atlas. Importantly, targeting miR-24 (along with miR-192-5p, miR-139-5p and miR-155-5p) could be counted as a valuable tool towards reducing or reversing cisplatin resistance (Liu *et al.*, 2017).

I developed my observations by involving data at population level, making use of the UK Biobank. I have discovered two distinct clusters in the region of Chromosome 11q23.3 of

ovarian cancer patients which associates to increase in prevalence and poor prognosis. This is a chromosomal region that has been linked to LOH in ovarian cancer. For instance, it has been shown that 11q22.3-q25 LOH has been connected to more aggressive disease in OC (Launonen *et al.*, 1998). This was further supported by another study implying that LOH of 11q23.3-q24 (D11S1340 and D11S912), was also related to an adverse disease course (Launonen *et al.*, 2000). It should be considered that alterations in this region are not fully unique to ovarian cancer.

I have then performed IHC using a tissue microarray of OC patients and 10 adjacent tissues to OC in attempt to dissect further the expression of H2AX at protein level in different types of OCs and stages. I have shown that H2AX is abundantly expressed in high- and low-grade serous OC, mucinous adenocarcinomas, metastatic serous carcinomas and clear cell carcinomas. This is in agreement with RNAseq data demonstrating substantial expression across different types of OCs (Hendrix *et al.*, 2006). There were no apparent significant differences in the protein expression amongst these subtypes. This agrees with a study of 87 EOC patients where γ-H2AX immunostaining was not significantly correlated with age, histopathological type, tumour differentiation, lymph node metastasis, FIGO stage or size of resident lesion (Mei *et al.*, 2015). This is in contrast to what it has been observed in breast cancer where, there were more H2AX high tumours with advancement of Stage (Stage I: 2.8%, Stage II: 5.5%, Stage III/IV 7.4%). One of the limitations of this study was the low number of stage IV samples as well as the lack of OC cores from patients resistant to chemotherapy. This should be investigated further, since significant correlation was noted in the response to the chemotherapy and γ-H2AX immunostaining in EOC patients (Mei *et al.*, 2015).

Lastly, γ-H2AX staining has been displayed that to be significantly higher in BRCA1/2 mutation-positive fallopian tube epithelium in comparison to control (BRCA wild-type) fallopian tube epithelium (Staff *et al.*, 2014). Here I showed a good connection between the phosphorylation level of γ-H2AX foci and the H2AX gene expression, in appropriate cell lines *in vitro*. I recommend that H_2O_2, as a DNA damaging agent can trigger the cellular transcription machinery to produce H2AX proteins for phosphorylation to support DNA repair. These molecular events may possibly be required in order to provide a steady state of H2AX protein. For example, it has been indicated that oncogenic transformation of human breast cancer epithelial cells leads to a decrease in abundance of proteins (Lamond *et al.*, 2018).

Comparison of the BRCA2 mutant cell line (PEO1) with the BRCA wild-type OC cell line (SKOV3) and those with a silent BRCA2 mutation (PEO4, MDAH-2774) can underlines the importance of BRCA2 in repair of dsDNA. The intriguing increase in H2AX 24 hours after H_2O_2 exposure in SKOV3 cells suggests that this line may present a type of 'BRCAness'. This refers to EOC (up to 50% of HGS) that show a defective phenotype of HRR without BRCA mutations (Turner, Tutt and Ashworth, 2004) (Ping Lin *et al.*, 2018). Notably, SKOV3 has 3 other genes mutated participating in HRR (Beaufort *et al.*, 2014).

Chapter5: Effect of the latest PARP inhibitors Rucaparib in ovarian cancer using preclinical *in vitro* models

Introduction

As mentioned in the introduction chapter, there are two tumour suppressor genes which are highly penetrant in ovarian cancer, BRCA1 and BRCA2. Most patients carrying BRCA1/2 mutation acquire loss of heterozygosity (LOH) of the BRCA1/2 wild-type allele (Ramus *et al.*, 2003) and are considered HR deficient (Venkitaraman, 2004). A novel target in cancer therapy is targeting the PARP-1/2 enzymes which play significant roles in ssDNA breaks in base excision repair (BER) pathway.

One critical function of PARP1 enzyme is supporting the repair of single-strand DNA in BER pathway. PARP1 plays a role as a first responder to detect DNA damage and assist choice of DNA repair pathway. In conjunction with BRCA2 that has a role in dsDNA repair pathway; due to deficiency in BRCA2, PARP1 takes over the BRCA2 roles which are necessary for the function of HR pathway. Cells with BRCA2 mutation have been shown to be highly sensitive to PARP1 inhibition that can lead to cell death by apoptosis, in contrast to those with efficient/wild-type BRCA2 (Bryant *et al.*, 2005).

Synthetic lethality is a concept of, when two non-lethal genetic mutations which are harmless by itself, present in combination, will lead to cell death. Cancer therapy intends to develop this concept through exposing tumour cells carrying one deficient gene DNA repair pathway to an agent which targets its synthetically lethal partner pathway, which result in selective cancer cell death (O'Neil, Bailey and Hieter, 2017). While non-cancer cells are expected to be efficient in both DNA repair pathways, remain intact and diminish systemic side-effects (Drew *et al.*, 2011).

PARP inhibition leads to accumulation of SSB which will convert to DSB and, unless repaired by HR, it will cause cell death. This concept led to development of PARP inhibitors which have been shown to be 100-1000-fold more sensitive in tumour cells with BRCA1/2 defective, compared to those with wild-type BRCA1/2. In addition, other than BRCA1/2, mutation in other genes involved in HR can affect on it and some of these mutations are sensitive to PARP inhibitors treatment (Bryant *et al.*, 2007).

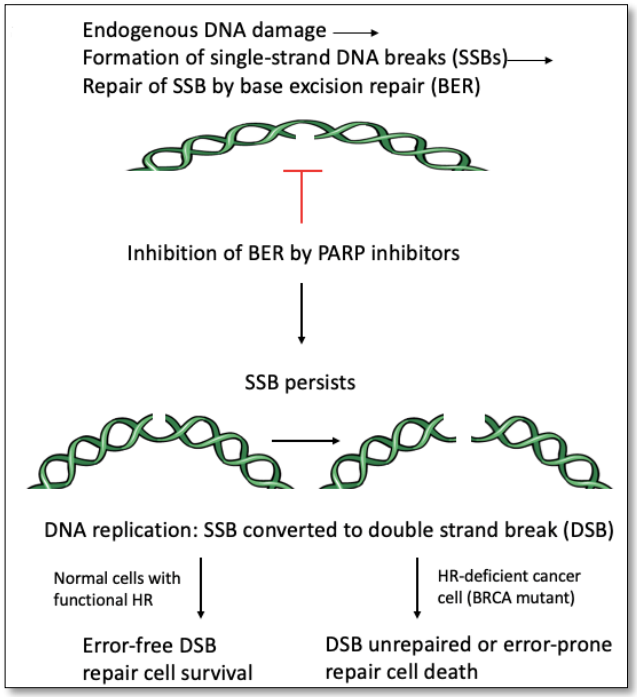

Figure 72. Schematic figure of synthetic lethality. Synthetic lethality of PARP inhibitors in BRCA-deficient cells. Adapted from (Drew, 2015).

Additionally, PARPi sensitivity has been established in cancer cells with mutations in other genes involved in HR pathway including ATM, Rad51, Rad54, RPA1, NBS1, ATR, CHK1, CHK2 and FANC group. Data from The Cancer Genome Atlas Research Network (TCGA) has shown the deficiency of HR pathway in up to 50% of high-grade serous ovarian cancer (The Cancer Genome Atlas Research Network, 2011).

Rucaparib is a new PARP-i that inhibits PARP1, PARP2 and PARP3 enzymes and has been examined its efficiency in OC patients with BRCA1 and BRCA2 mutant (Colomba *et al.*, 2019). Rucaparib has been studied in combination with other chemotherapeutic agents and act as a single agent in a 3rd line and beyond therapy, whereas it has not received approval as a maintenance strategy. Additionally, PARP inhibitors, has been validated through the double-blind phase II trial in patients who were platinum-sensitive relapsed with epithelial ovarian cancer (Ledermann *et al.*, 2014).

Pennington et al established that 31% of OC patients carry a deleterious germline (24%) and/or somatic (9%) mutation in one or more of 13 homologous recombination genes, comprising of BRCA1, BRCA2, ATM, BARD1, BRIP1, CHEK1, CHEK2, FAM175A, MRE11A, NBN, PALB2, Rad51C, and Rad51D (Pennington *et al.*, 2014). It has demonstrated that up to 50% of sporadic EOC are defective in homologous recombination pathway (Prakash *et al.*, 2015). Therefore, depending on BRCA mutations status, or even genomic sequencing of all gene participating in HR, it could be underestimated that 20-35%

of patients with HR deficiency would respond to PARP-inhibitors treatment. Interestingly, emerging data suggest that new PARP inhibitors might also exert a beneficial effect on both BRCA wild-type and BRCA-mutant patients. However, the mechanisms involved are still not fully elucidated (Curtin, 2014).

Aims

- Use different ovarian cancer cell lines that are BRCA2-wildtype (SKOV3), BRCA2-m (PEO1) and BRCA2-silent mutant (PEO4, MDAH) to assess the effects of Rucaparib *in vitro.*
- Use liquid biopsies from a clinical trial of ovarian cancer patients treated with Rucaparib (in collaboration with MVCC) to assess the effect of Rucaparib on CTC enumeration and expression of key proteins.

Result

5.1. PARP1 assay

Here I examined the expression of PARP1 enzyme after DNA damage to assess the effect of Rucaparib in different ovarian cancer cell lines with BRCA2-wildtype (SKOV3), BRCA2-m (PEO1) and BRCA2-silent mutant (PEO4, MDAH). According to clonogenic assays, it has been established that 10μM of Rucaparib is cytotoxic based on IC_{50} results (Nile *et al.*, 2016). In all cell lines, incubation with 10 μM Rucaparib resulted in a 50 % reduction in endogenous PARP-1 activity in comparison to those which were treated only with the DMSO as a drug vehicle. In contrast, PARP-1 expression was considerably increased by treatment with the DNA damaging agent hydrogen peroxide (H_2O_2) at 20 mM. This was shown by a 28.8-fold for PEO1, 5-fold for PEO4, 12.5-fold for MDAH-2774 and 15.3-fold for SKOV3 increase in PARP-1 activity compared to untreated cells. However, the H_2O_2-induced increase in PARP-1 activity was decreased to levels similar to untreated cells after co-treatment with 10 μM Rucaparib in all cell lines. Figure 73 displays the images taken from treated cells and Figure 74-75 show statistical analysis of this experiment.

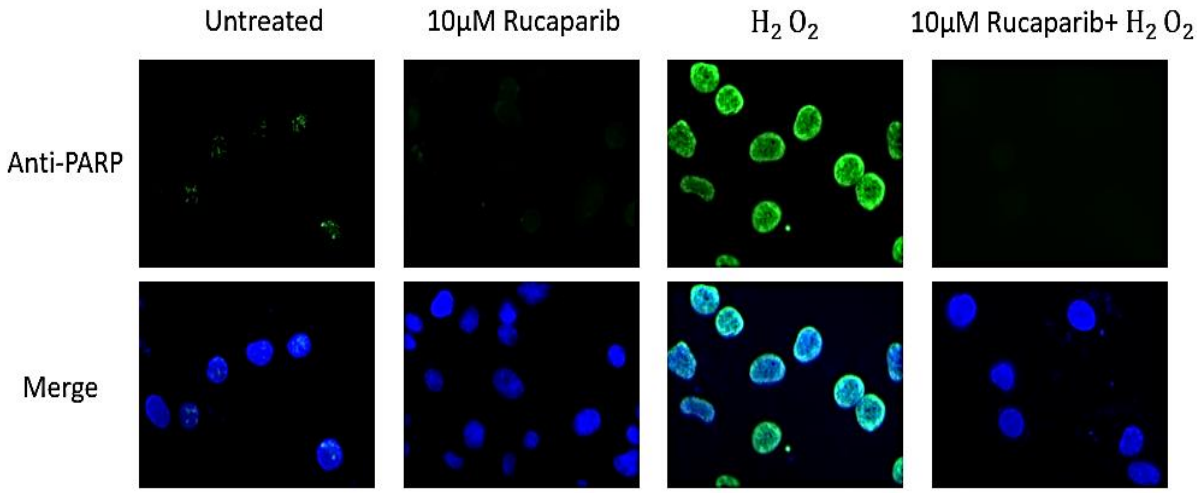

Figure 73. Representative figure of PEO1 cell line, the effect of Rucaparib on PARP1 activity. Cells were treated with 20mM H_2O_2 in order to accelerate PARP1 activity in the presence or absence of the Rucaparib. Poly (ADP-ribose) (PAR) chain creation was spotted using an anti-PAR monoclonal Alexa-Fluor 488-conjugated antibody (green). The nucleus was visualised using DAPI (blue).

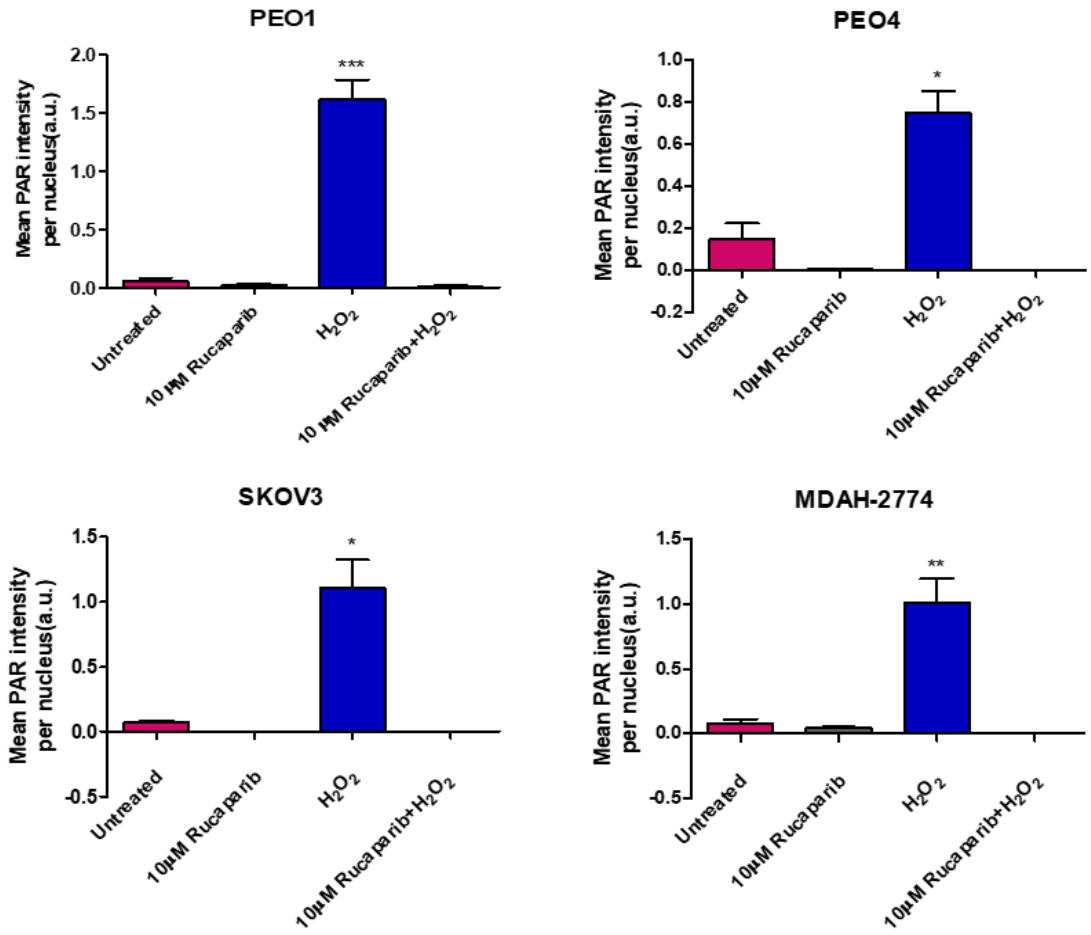

Figure 74. The effect of Rucaparib on PARP1 activity. Fluorescence intensity for AF-488 was calculated using ImageJ software and normalised to DAPI fluorescence intensity in all cell lines. Drug vehicles were DMSO for Rucaparib. Untreated cells were exposed to 0.1 % (v/v) DMSO diluted in culture medium. The designation '10μM Rucaparib' shows that cells were treated with 10μM Rucaparib in the absence of H_2O_2. The designation 'H_2O_2' implies that cells were treated with 20 mM H_2O_2 alone, in the absence of Rucaparib. Data are means ± SEM, n = 3; PE04: p=0.0017, PEO1: p<0.0001, MDAH-2774: p=0.0010, SKOV3: p=0.0016, compared to H_2O_2 alone.

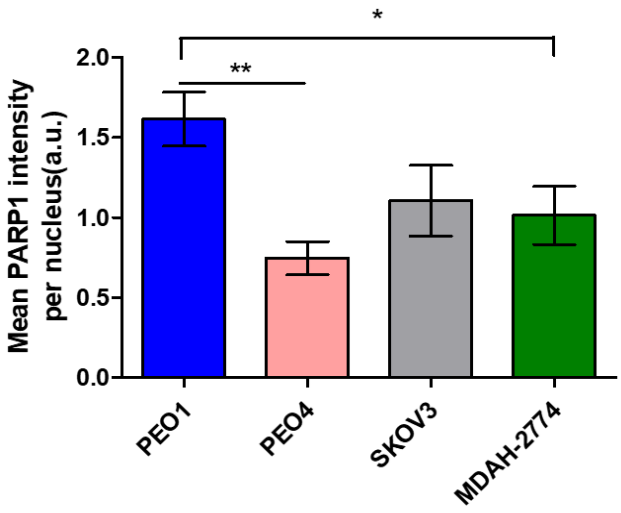

Figure 75. PARP1 assay results. The figure displays the intensity of PARP1 enzyme in all cell lines treated with H_2O_2 alone. PEO1: ** p=0.0024 (compared to PEO4), PEO1: * p=0.0424 (compared to MDAH-2774). Data are means ± SEM.

5.2. Wound healing assay

Here, the migratory and proliferative capacity of ovarian cancer cells was examined before and after treatment with Rucaparib at 10µM. Wound healing assays were conducted to visualise cells' migratory and proliferative capacity spatially *in vitro*. All control cell lines (treated with 0.1% DMSO), showed a marked and faster growth into the wound compared to treated cell lines with Rucaparib. The images (Figure 77) showed the extent of scratch closure developed under control conditions compared to those treated with Rucaparib. PEO4 and MDAH-2774 (BRCA2-silent mutant) showed that the gap was closing but not as fast as the control where the gap was 80-90% closed. SKOV3 (BRCA2-wildtype) cells revealed the gap closing but also less, in comparison to PEO4 and MDAH-2774. However, in PEO1 which is a BRCA2-m, the gap did not close as much as other cell lines, during 72-hrs treatment with Rucaparib, but also the gap size was increased. One of the reasons for this can be the cell death due to the cytotoxic effect of Rucaparib. In general, treatment with PARP inhibitor (Rucaparib) on OC led to a decrease in cell growth and affected cell proliferation.

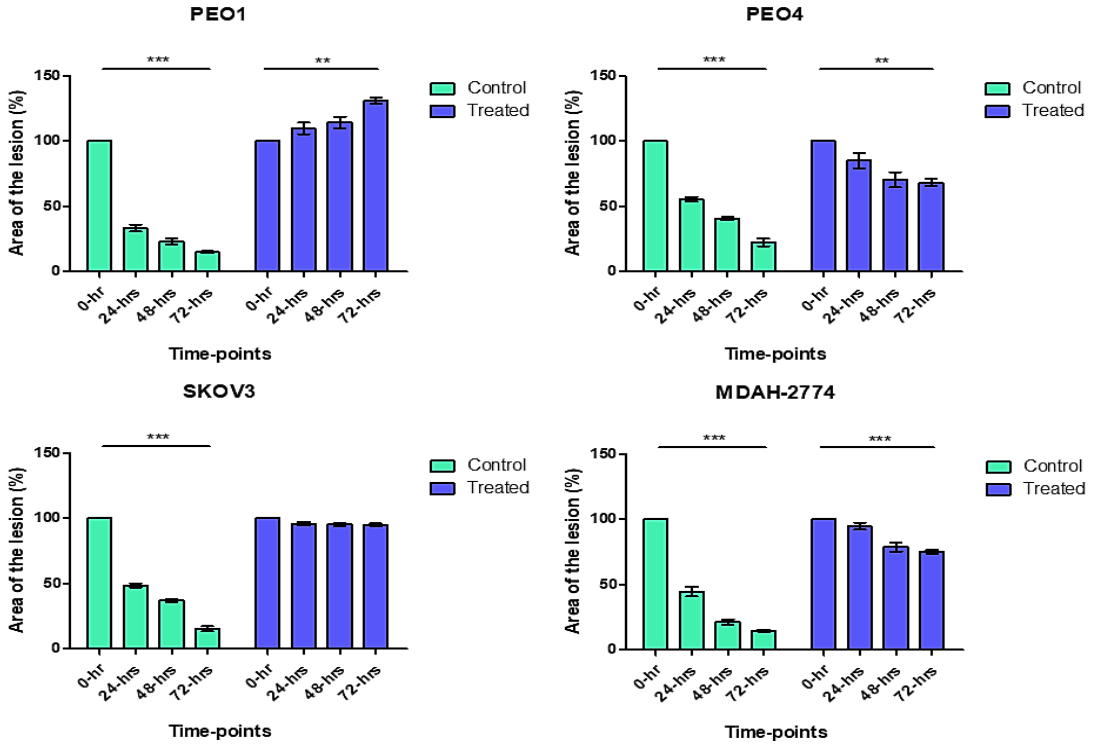

Figure 76. Gap size analysis after Rucaparib treatment. Figure above displays the analysis of gap size which was conducted by ImageJ software. As it can be seen, control samples in all cell lines show a decrease in gap size whereas after Rucaparib treatment there was an increased level of gap size in BRCA2-m cell line (PEO1). One-way ANOVA was performed with GraphPad Prism® and the statistic was: **PEO4:** control:*** p<0.0001, treated:**p=0.0059. **PEO1:** control:***p<0.0001, treated:**p=0.0018. **MDAH-2774:** control:***p<0.0001, treated:***p=0.0006. **SKOV3:** control:***p<0.0001, treated: p=0.1088.

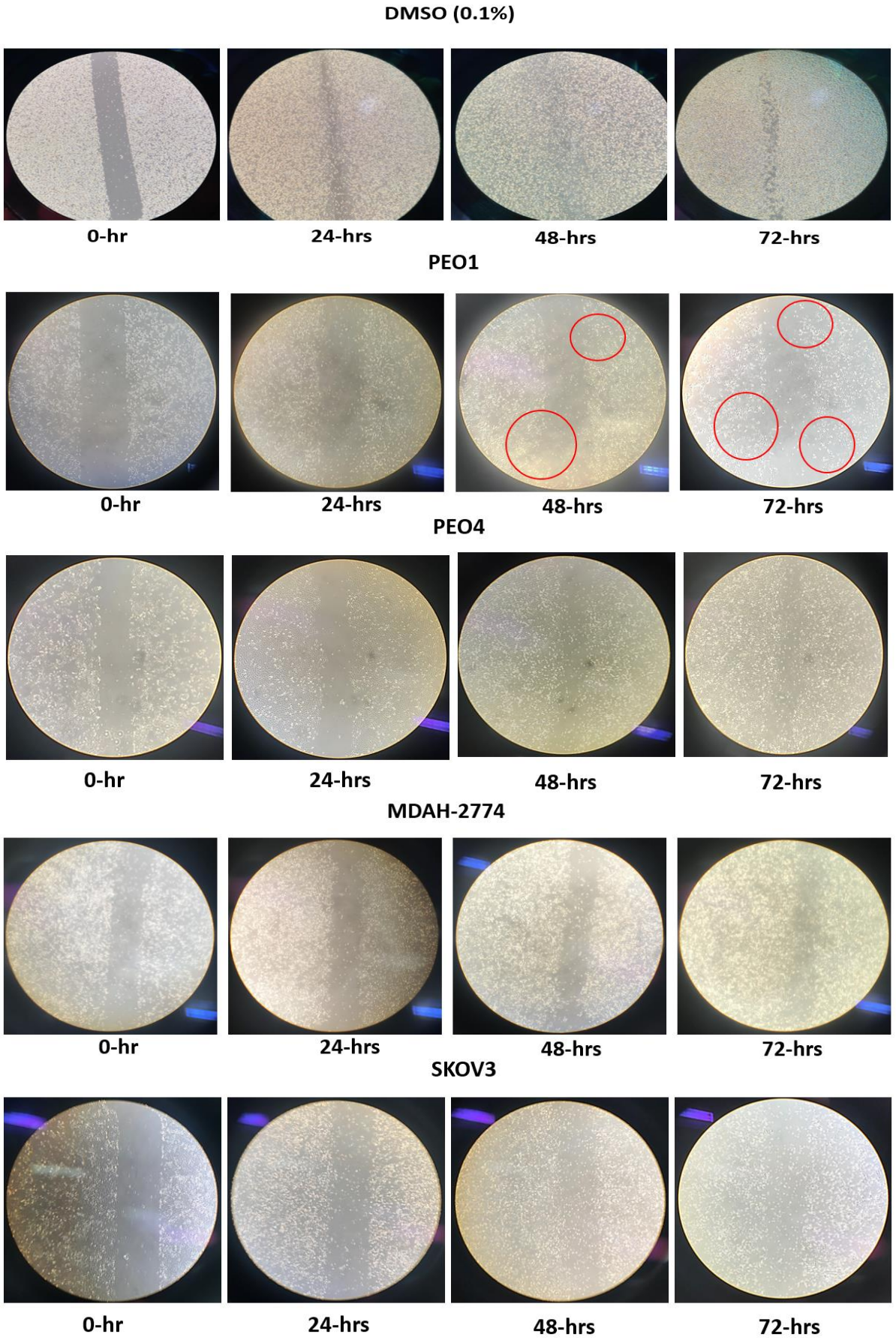

Figure 77.Schematic representation showing the artificial wound created on all cell lines surfaces (40x magnification). The figure shows the cells before(0-hr) and after treatment at (24-, 48- and 72-hrs).

5.3. Proliferation assay

Here I analysed the number of live cells and dead cells treated with Rucaparib in different time-points. This experiment was performed to analyse the effect of Rucaparib on cell viability, following the wound healing assay findings. As it can be seen in Figure 78, in all cell lines treated with DMSO (i.e., control), there is no difference in live cells percentage, and it displays a steady and stable graph. However, in those cells treated with Rucaparib, there is a decrease in the number of live cells, with a different trend in each cell line.

In BRCA2-m cells (PEO1) the number of live cells after 72-hrs DMSO (0.1%) exposure was around 95% while in cells with Rucaparib treatment the number decreased to less than 60%. In PEO4 and MDAH-2774 cell line (BRCA2-silnet mutation) the level of cell viability was 94% and 95% respectively after DMSO treatment (72-hrs). However, after 72-hrs Rucaparib treatment the number of live cells decreased to 76% and 80% respectively. Moreover, SKOV3 cell line showed the same level of live cells after 72-hrs DMSO treatment which was 96% while the Rucaparib treated cells showed the cell viability level of 70%. In general, Rucaparib treatment led to lower number of live cells in BRCA2-m cells, compared to other cells with BRCA2 wild-type or BRCA2-silent mutation which can be related to sensitivity of BRCA2-m cells to PARP-inhibitors.

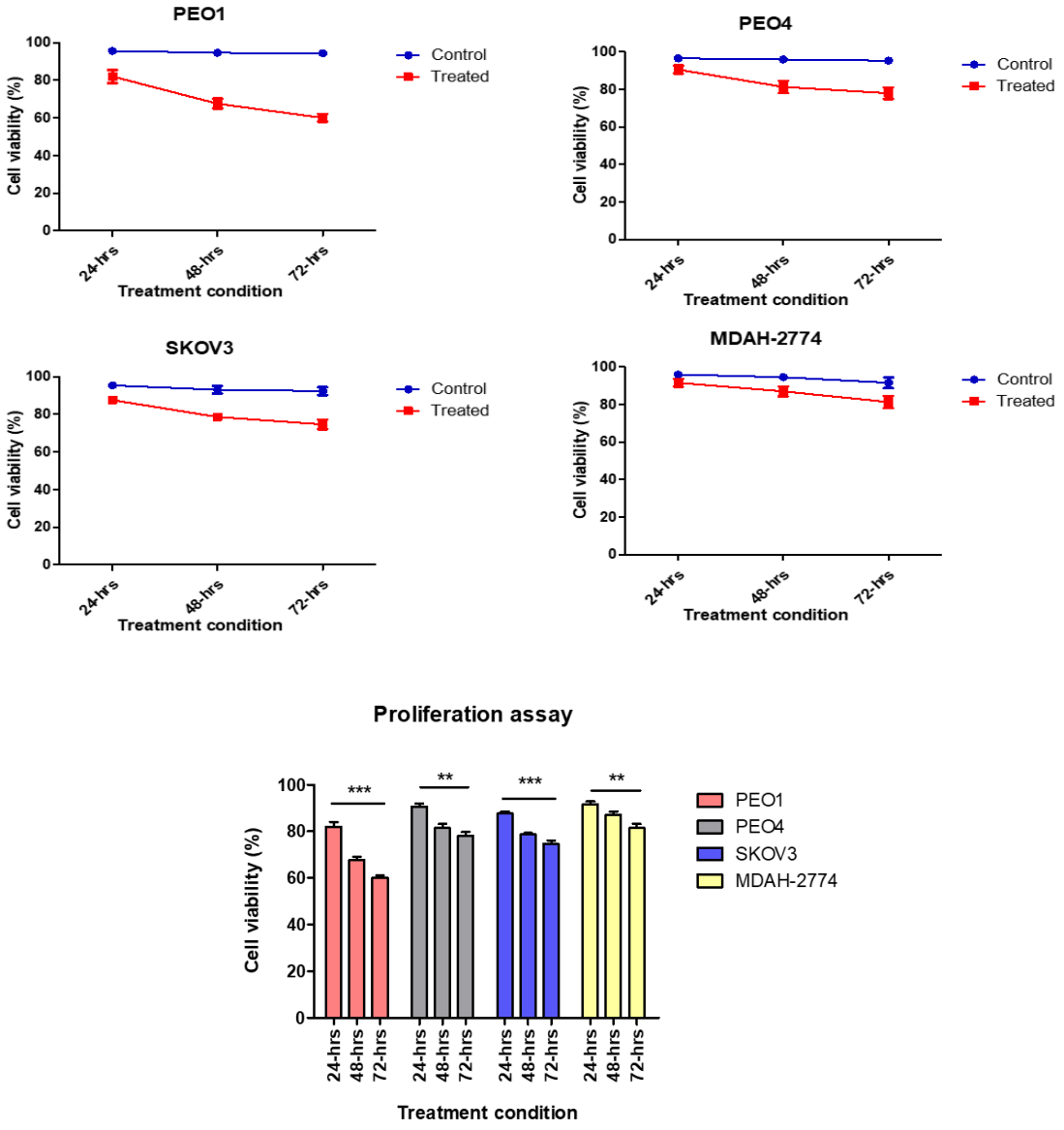

Figure 78. Proliferation assay results. The figure above represents the percentage of live cells (cell viability) in all cell lines, after Rucaparib treatment in different time-points. As it can be seen in the figure, the PEO1 (BRCA2-m) cells showed high level of decrease in cell viability after 72-hrs treatment with Rucaparib in compared to other cell lines. However, the decrease level of cell viability in SKOV3 (BRCA2-wildtype) was still higher than PEO4 and MDAH-2774 (BRCA2-silent mutant) which can be referred to 'BRCAness' term. One-way ANOVA was performed with GraphPad Prism® and the statistic was: **PEO1:** *** p=0.0002. **PEO4:** **p=0.0037. **MDAH-2774:** **p=0.0096. **SKOV3:** ***p=0.0003.

5.4. Apoptotic assay (Annexin V assay)

Based on the theory that PARP inhibition makes cancer cells sensitive to genotoxic agents; I assessed the effects of a Rucaparib treatment on different ovarian cancer cells with BRCA2-m or BRCA2-wt gene. As I can see from previous section (5.3) Rucaparib treatment inhibited proliferation of OC cells, particularly it decreased the cell growth significantly in PEO1 cell line which is BRCA2-mutant compared to BRCA2-wildtype cell lines. Annexin V/PI double staining results suggest that all control cell lines, treated with 0.1% DMSO (48-/72-hrs) show

more than 95% of cell viability. However, after 48-hrs exposure to Rucaparib, PEO1 (BRCA2-m) cells displayed more than 10% of dead cells which increased to 19% after 72-hrs treatment. Furthermore, after 48-hrs treatment, more than 95% of SKOV3 (BRCA2-wildtype) cells went through apoptotic which led to 4% dead cell after 72-hrs treatment that can be referred to 'BRCAness' term. Although, in PEO4 (BRCA2-silent mutant) and MDAH-2774 (BRCA2-silent mutant), after 48-hrs treatment, the number of live cells was 43.5% and 39.3% respectively and the number of dead cells was less than 1% for both cell lines. Moreover, after 72-hrs treatment, the number of dead cells was significantly lower than other cell lines (less than 1%). As shown in Figures 79-83, Rucaparib treatment alone can trigger the apoptotic pathways in OC cell lines. In addition, PEO1 (BRCA2-mutant) had a significantly higher level of cell death after 72-hrs treatment with Rucaparib, compared to other cell lines which are wild-type for BRCA2, and it can be concluded that BRCA2 cancer cells are more sensitive to Rucaparib.

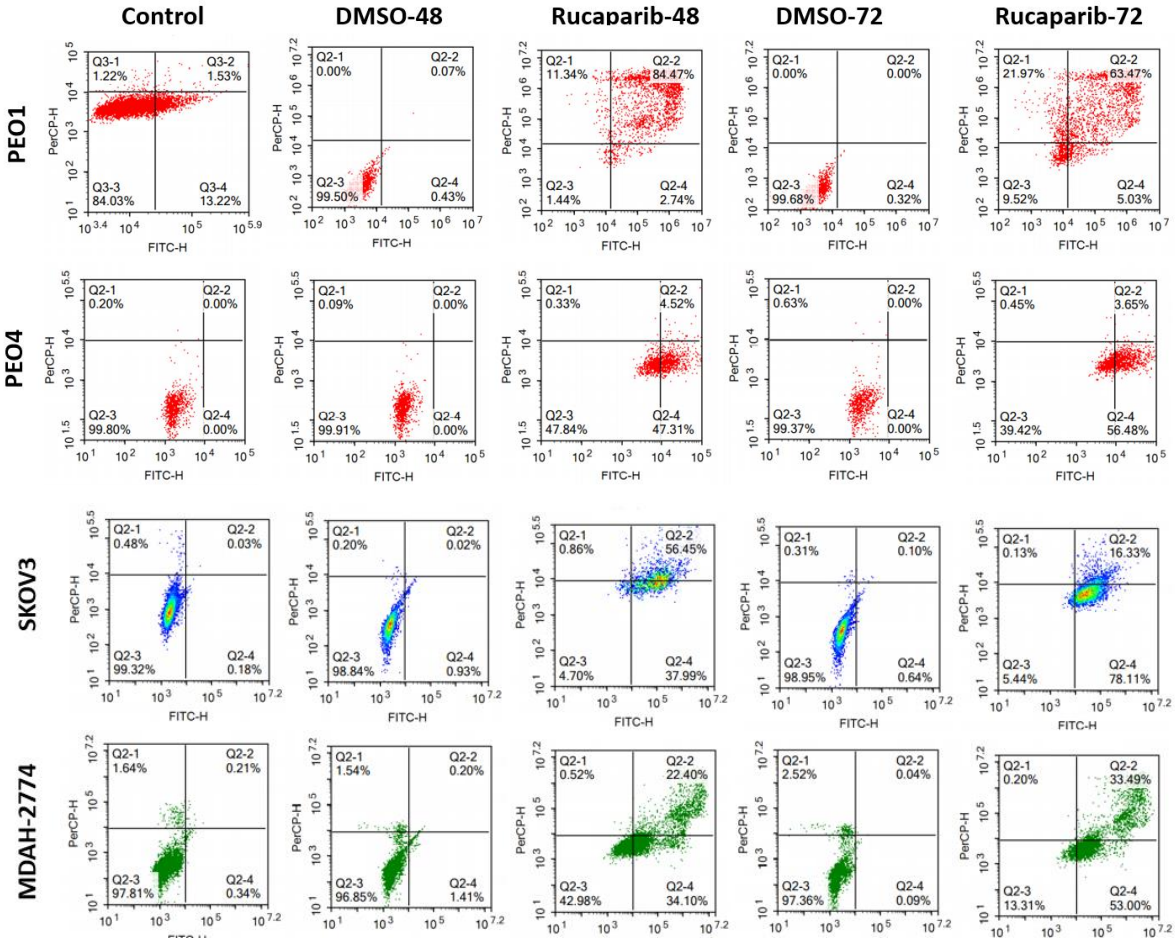

Figure 79.Flow cytometry analysis with annexin V and propidium iodide staining in PEO1, PEO4, MDAH-2774 and SKOV3 cells showed a significant increase of apoptotic population (early apoptosis; annexin V+/PI−, late apoptosis; annexin V+/PI+) with treatment of 10 μM Rucaparib. Flow cytometry analysis was performed 48-hrs and 72-hrs after treatment of Rucaparib.

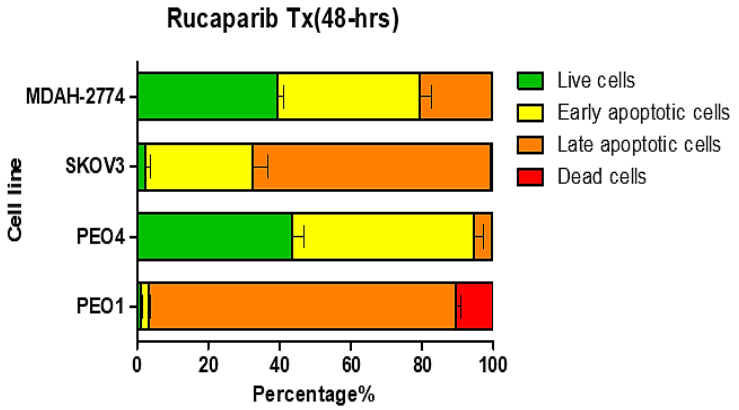

	PEO1	PEO4	SKOV3	MDAH-2774
Live	1.2%	43.5%	2.5%	39.3%
Early Apoptotic	2.15%	50.8%	29.9%	40%
Late Apoptotic	86.15%	5.1%	66.9%	20.3%
Dead	10.5%	0.6%	0.7%	0.4%

Figure 80. Annexin V assay. The figure shows the different number of cells in 4 categories including live cells, early apoptotic cells, late apoptotic cells, and dead cell, after 48-hrs Rucaparib treatment in all cell lines.

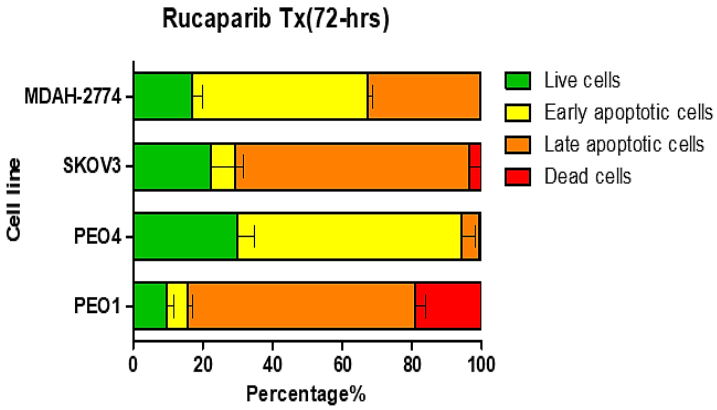

	PEO1	PEO4	SKOV3	MDAH-2774
Live	9.7%	29.8%	22.45%	17%
Early Apoptotic	6.1%	64.35%	6.9%	50.4%
Late Apoptotic	65.3%	5.3%	66.9%	32.3%
Dead	18.9%	0.55%	3.75%	0.3%

Figure 81.Annexin V assay. The figure shows the different number of cells in 4 categories including live cells, early apoptotic cells, late apoptotic cells, and dead cell, after 72-hrs Rucaparib treatment in all cell lines.

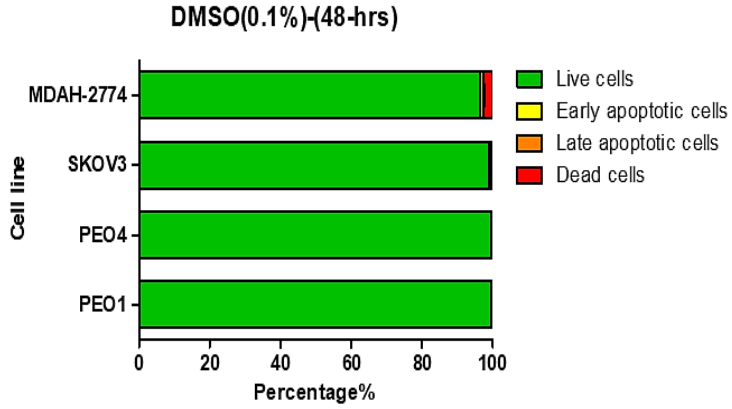

	PEO1	PEO4	SKOV3	MDAH-2774
Live	99.7%	99.7%	98.9%	96.5%
Early Apoptotic	0.2%	0.1%	0.9%	1%
Late Apoptotic	0.1%	0.1%	0%	0%
Dead	0%	0.1%	0.2%	2.5%

Figure 82. Annexin V assay. The figure shows the different number of cells in 4 categories including live cells, early apoptotic cells, late apoptotic cells, and dead cell, after 48-hrs treatment with DMSO (0.1%) in all cell lines.

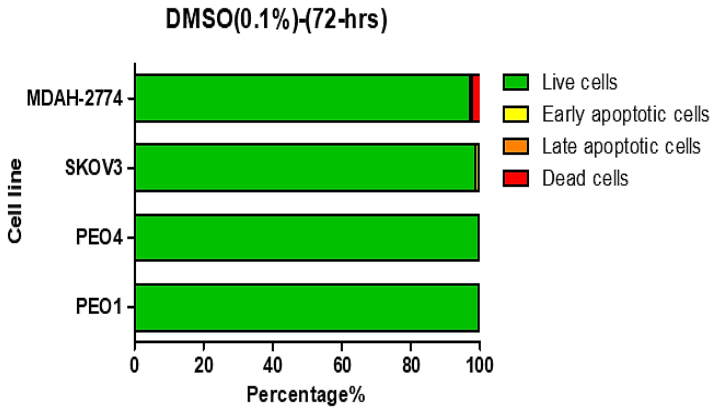

	PEO1	PEO4	SKOV3	MDAH-2774
Live	99.6%	99.6%	98.8%	97%
Early Apoptotic	0.4%	0%	0.8%	0.4%
Late Apoptotic	0%	0%	0%	0%
Dead	0%	0.4%	0.4%	2.6%

Figure 83. Annexin V assay. The figure shows the different number of cells in 4 categories including live cells, early apoptotic cells, late apoptotic cells, and dead cell, after 72-hrs treatment with DMSO (0.1%) in all cell lines.

5.5. γ-H2AX assay

The generation of γ-H2AX foci at the site of DNA double strand breaks follows phosphorylation of the H2AX histone variant protein at serine residue 139 upon DNA damage. γ-H2AX foci were detected with an γ-H2AX antibody (Alexa Fluor 488-conjugated antibody). γ-H2AX foci co-localised with the DAPI which confirms the nuclear localisation of γ-H2AX. My results (Figure 84) showed that Rucaparib treatment significantly increased DNA damage as indicated by an increased number of γ-H2AX foci after 1-hour treatment, 20.3-fold for MDAH-2774, following a decrease trend 12.2-fold after 24-hrs, 12-fold after 48-hrs and 11.8-fold after 72-hrs in compared to drug vehicle ones. A similar trend observed in PEO4 which was 21.9-fold after 1-hr, 15.6-fold after 24-hrs, 10.5-fold after 48-hrs and 12.6-fold after 72-hrs. In addition, Rucaparib treatment produced a considerably greater amount of DNA damage in PEO1 and SKOV3 when compared to PEO4 and MDAH-2774. In PEO1, it was 27.6-fold after 1-hr, 18.8-fold after 24-hrs, then it raised to 20.7-fold after 48-hrs and the dropped to 15.2-fold after 72-hrs. Similarly, in SKOV3 cell line, it was 27.1-fold after 1-hr, 32.3-fold after 24-hrs followed by a significant decrease to 8.7-fold after 48-hrs and 8.9-fold after 72-hrs treatment. Therefore, Rucaparib can lead to inhibition of DNA damage repair in ovarian cancer cells with BRCA2-m.

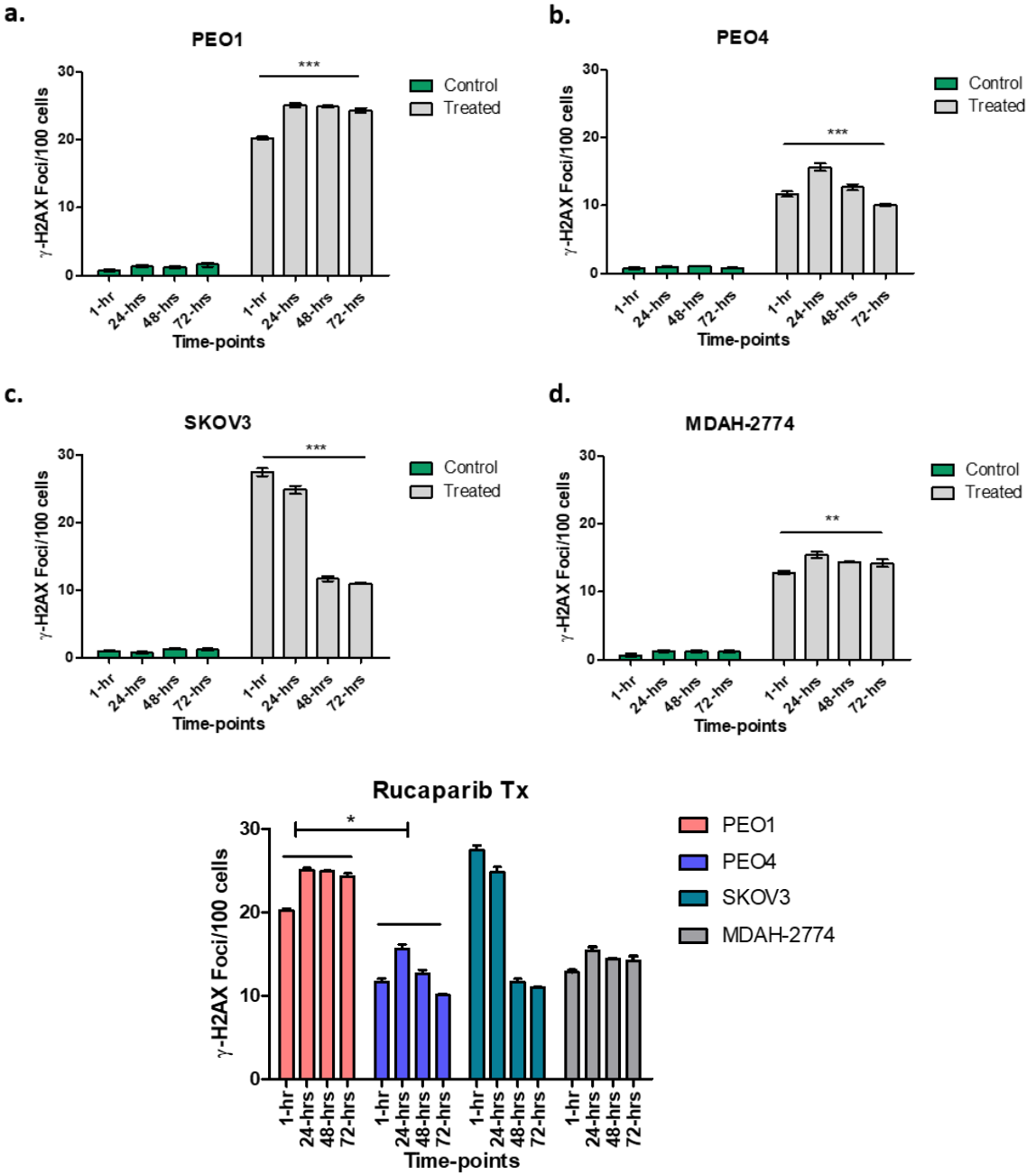

Figure 84. γ-H2AX assay results. The figure represents the number of γ-H2AX foci after Rucaparib treatment in different time-points. Cells were treated with 10 μM Rucaparib as single agents. Cells were harvested 1-hr, 24-hrs, 48-hrs and 72-hrs after 10μM Rucaparib exposure and the total number of γ-H2AX positive cells was analysed using immunofluorescence. One-way ANOVA was performed with GraphPad Prism® and the statistic was: **PEO1:** control: p=0.1061, treated:***p<0.0001. **PEO4:** control: p=0.1372, treated:***p<0.0001. **SKOV3:** control: p=0.0697, treated: ***p<0.0001. **MDAH-2774:** control: p=0.1247, treated:**p=0.0095. All Rucaparib treated was compared together with two-way ANOVA which PEO4 and PEO1 has a significant different (*) with p=0.0224.

5.6. Gene expression after Rucaparib treatment

I expanded on my previous results, by assessing the relative expression of some specific genes after 48-hrs and 72-hrs treatment with Rucaparib. These genes have a role in pro-apoptotic pathway (BAX), pro-metastatic pathway (SNAI1), H2AX and mTOR complex (mTOR, Raptor and Rictor). qPCR for these genes was carried out using the reference gene YWHAZ in triplicate on cDNA synthesised from the extracted RNA from PEO1, PEO4, MDAH-2774 and SKOV3 cell lines after Rucaparib exposure. Biological and technical triplicates were performed for each experiment.

BAX is a member of the BCL2 family member, and it has a role as pro-apoptotic regulators which are involved in several cellular activities. When BAX forms a heterodimer with BCL2, it acts as an apoptotic activator (Zhang *et al.,* 2016). Snail is a family member of transcription factors which act as a repressor of the adhesion molecule E-cadherin to control EMT during embryonic development. The EMT has been defined as an crucial mechanism supporting invasion and can lead to cancer metastasis as a result of gaining migration and invasion ability of the cell (Lu *et al.,* 2012).

The mTOR pathway is a crucial regulator for several pathways including growth, proliferation, apoptosis, and angiogenesis to provide balance between cellular resources comprising of amino acids and growth factors; and stresses such as hypoxia to regulate the cellular behaviour. The function of this pathways is controlled by the mTOR complex 1 (mTORC1) and mTOR complex 2 (mTORC2). mTORC1 includes mTOR, Raptor, DEPTOR, GBL and PRAS 40. mTORC2 includes mTOR, Rictor, DEPTOR and GBL. mTOR is a serine/threonine kinase and is the main catalytic factor of mTORC1 and mTORC2. DEPTOR is a key regulator of both mTORC1 and mTORC2 complexes. Raptor is a protein component of mTORC1 only and regulates the activity of mTOR kinase. Rictor is a component of mTORC2 only and due to its contribution in growth factor, energy sensing, its impact on protein synthesis and cell cycle progression, the mTOR pathway is involved in a wide range of malignancies (Rogers-Broadway *et al.,* 2019).

The expression of BAX (pro-apoptotic gene) was increased after 72-hrs Rucaparib treatment in PEO1 (BRCA2-m). Increased apoptosis of PEO1 cell line from previous data, apoptotic assay, was associated with increased expression of BAX. Although in other cell lines with BRCA2-wildtype (SKOV3) and BRCA2-silent mutant (PEO4 and MDAH-2774), the expression of BAX was decreased after 72-hrs exposure to Rucaparib. Moreover, there was a decrease in SNAI1 expression (pro-metastatic gene) in PEO4, MDAH-2774 and SKOV3 while it was increased in PEO1 (BRCA2-m) cell line. SNAI1 downregulates the EMT

pathway that is an essential pathway for metastasis and upregulation of this gene in PEO1 after Rucaparib treatment can be related to that BRCA-m cell lines are more sensitive to PARP-inhibitors. All these data are shown in Figure 85.

H2AX is one of the isoforms from the Histone H2A family protein which is essential for checkpoint-mediated arrest of cell cycle process and for efficiency of DNA DSBs, particularly when altered through phosphorylation of C-terminal domain. This suggests a role for H2AX which can prevent genomic instability related to cancer (Saravi *et al.*, 2020). In order to gain better insight, I expanded my observations on the expression of H2AX and compared it to the number of γ-H2AX foci from previous data to see if there is a connection between the expression of H2AX protein and its phosphorylation. I have showed that the change of γ-H2AX is consistent with the alteration in H2AX gene expression in OC cell lines treated with H_2O_2 (Saravi *et al.*, 2020).

As it can be seen in the Figure 86, PEO1 (BRCA2-m) shows an increase in the expression of H2AX which is consistent with the high number of γ-H2AX foci after 48- and 72-hrs treatment with Rucaparib. However, in PEO4 (BRCA2-silent mutant) there was a significant decrease in both γ-H2AX foci number and H2AX expression after 72-hrs treatment. Additionally, there is a decrease trend in MDAH-2774 and SKOV3 cell lines after 72-hrs exposure to Rucaparib. These data can be in association with efficiency of PARP-inhibitors on BRCA2-m cell line.

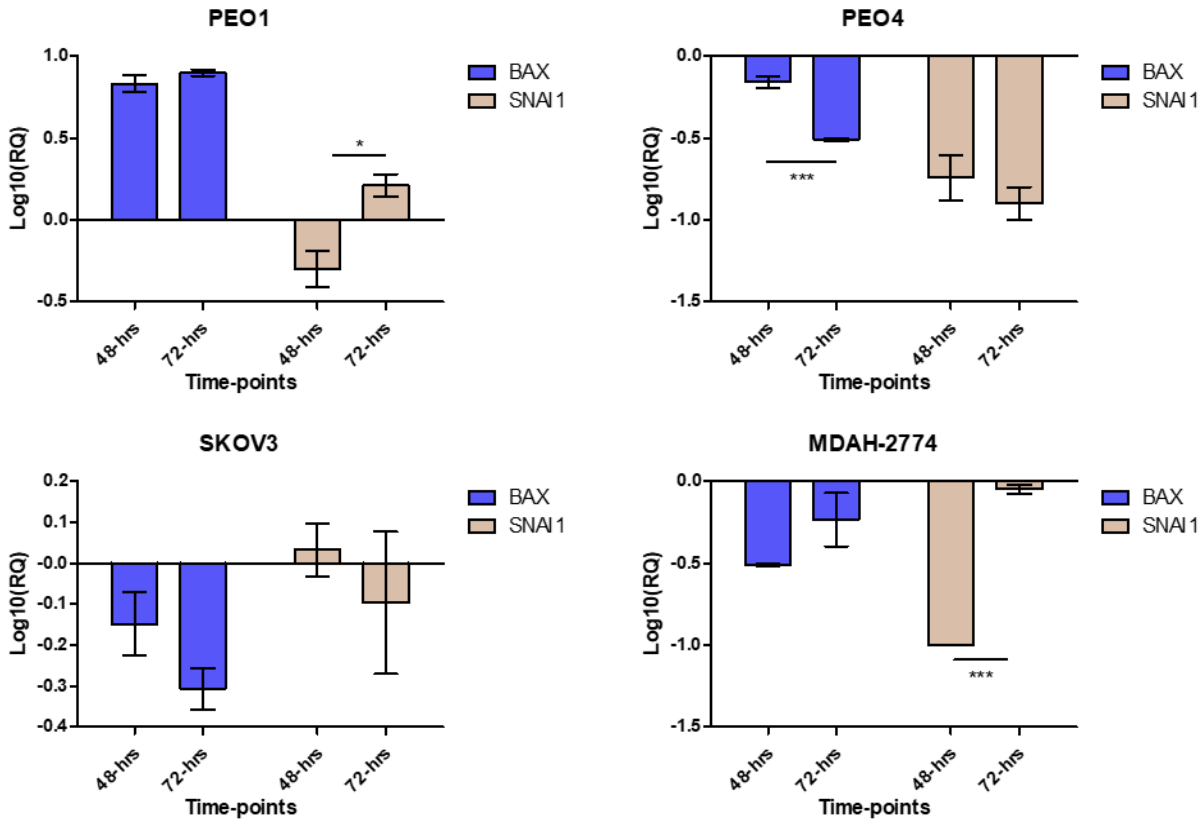

Figure 85. Gene expression analysis after Rucaparib treatment. The figure represents the expression of different genes after Rucaparib treatment in different time-points. Cells were treated with 10 µM Rucaparib as single agents. Cells were harvested 48-hrs and 72-hrs after 10µM Rucaparib exposure. The gene expression was assessed by qPCR and log10(RQ) and T-test was performed with GraphPad Prism®, between 48- and 72-hrs treatment, and the statistic was: **PEO1:** BAX: p=0.2743, SNAI1: * p=0.0181. **PEO4:** BAX: *** p=0.0007, SNAI1: p=0.4067. **SKOV3:** BAX: p=0.1629, SNAI1: p=0.5255. **MDAH-2774:** BAX: p=0.1681, SNAI1: *** p=0.0001.

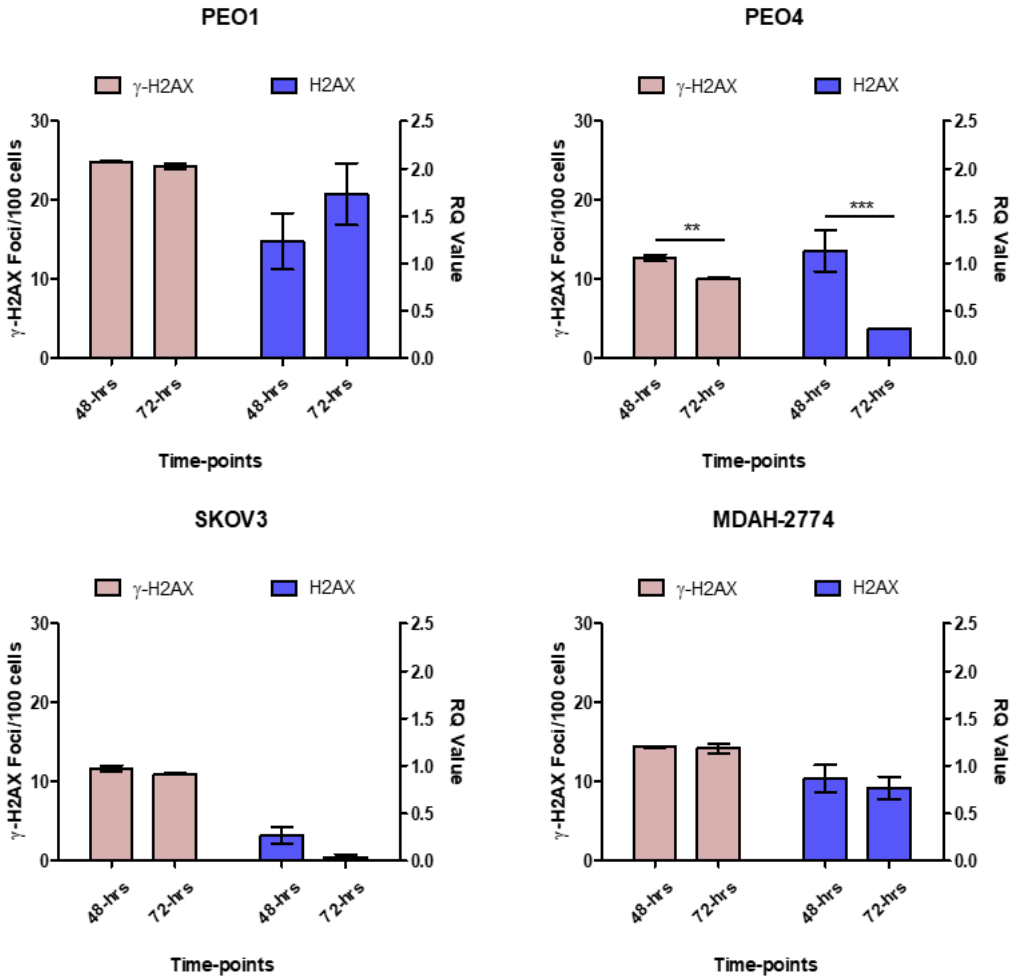

Figure 86. Comparison of alteration of γ-H2AX foci and H2AX protein expression after Rucaparib treatment. The figure represents the number of γ-H2AX foci and H2AX protein expression after Rucaparib treatment in different time-points. Cells were treated with 10 μM Rucaparib as single agents. Cells were harvested 48-hrs and 72-hrs after 10μM Rucaparib exposure. The total number of γ-H2AX foci in 100 cells was analysed using immunofluorescence and the expression of H2AX protein was assessed by qPCR. T-test was performed with GraphPad Prism®, between 48- and 72-hrs treatment, and the statistic was: **PEO1:** γ-H2AX foci: p=0.2037, H2AX protein: p=0.3214. **PEO4:** γ-H2AX foci:** p=0.0045, H2AX protein:***p=0.0005. **SKOV3:** γ-H2AX foci: p=0.1543, H2AX protein: p=0.0686. **MDAH-2774:** γ-H2AX foci: p=0.7473, H2AX protein: p=0.6240.

As it displayed in Figure 87, in PEO1 (BRCA-m) cell line, mTOR, Raptor, and Rictor showed a decrease in expression. PEO4 (BRCA2-silent mutant) and MDAH-2774 (BRCA2-silent mutant) displayed a decrease in mTOR and Rictor but an increase in Raptor expression. However, SKOV3 represented an increase in mTOR expression but a decrease in Raptor and Rictor expression. A common feature for all cell lines was the downregulation of DEPTOR after treatment with rucaparib, reaching statistical significance in the PEO4 cell line. Based on my findings, I hypothesise that, using Rucaparib (latest PARP-inhibitors) on PEO1 which has a mutant BRCA2 gene, counteracts the activity mTOR complex genes compared to those cell lines with BRCA2-wildtype (SKOV3) and with BRCA2-silent mutation (PEO4 and MDAH-2774).

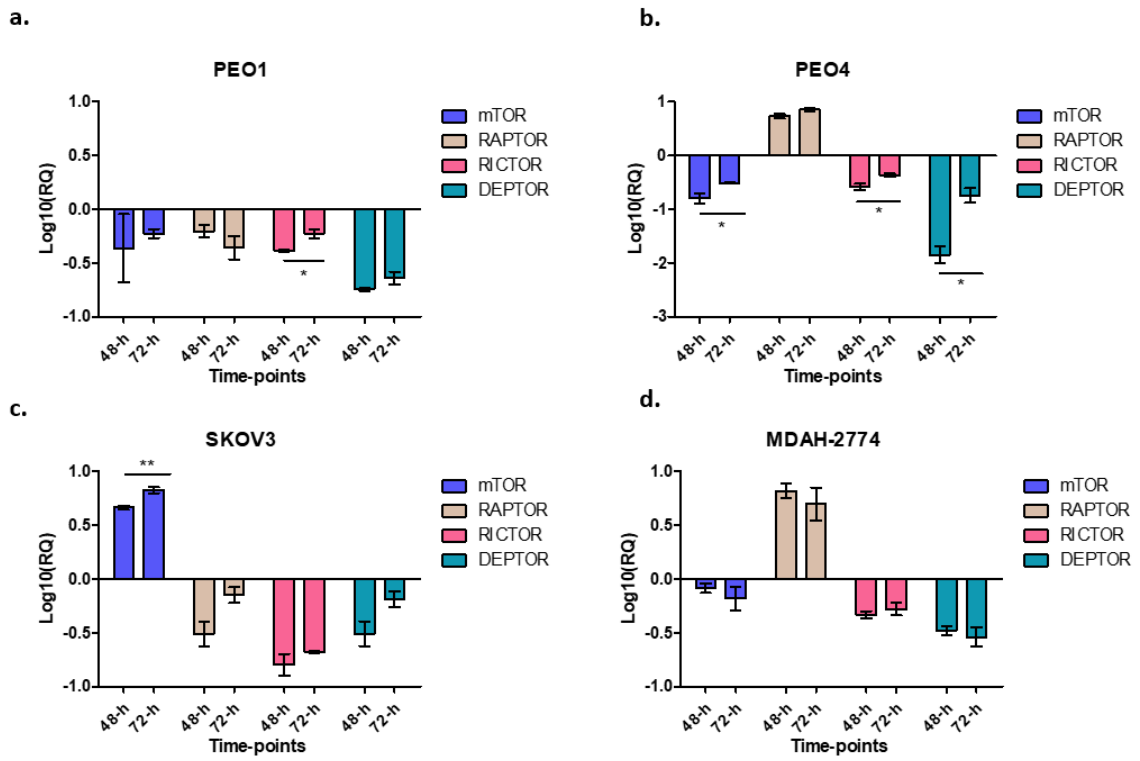

Figure 87. Gene expression analysis after Rucaparib treatment. The figure represents the expression of different genes after Rucaparib treatment in different time-points. Cells were treated with 10 μM Rucaparib as single agents. Cells were harvested 48-hrs and 72-hrs after 10μM Rucaparib exposure. The gene expression was assessed by qPCR and log10(RQ) and T-test was performed with GraphPad Prism®, between 48- and 72-hrs treatment, and the statistic was: **PEO1:** mTOR: p=0.6895, Raptor: p=0.2852, Rictor: * p=0.0194, DEPTOR: p=0.1900. **PEO4:** mTOR: * p=0.0447, Raptor: p=0.0881, Rictor: * p=0.0322, DEPTOR: *p=0.0136. **SKOV3:** mTOR: ** p=0.0092, Raptor: p=0.0582, Rictor: p=0.2966, DEPTOR: p=0.089. **MDAH-2774:** mTOR: p=0.4632, Raptor: p=0.4579, Rictor: p=0.4748, DEPTOR: p=0.6433.

5.7. A pilot study

PARP inhibitors can result in an accumulation of ds-DNA breaks which cannot be repaired by ovarian cancer cells with HRD. High-grade serous ovarian cancers (HGSOCs), is the most common histological subtype of EOC, which have been presented to harbour a deleterious germline (24%) and/or somatic (9%) mutation in one or more genes in the HR pathway, with the most prevalent having a mutation in BRCA1 (19%) or BRCA2 (6%) (Pennington *et al.*, 2014). Therapeutical options for recurrent ovarian cancer patients who have received two or more prior lines of chemotherapy have lately extended with the U.S. Food and Drug Administration (FDA) and European Commission (EC) approvals of the new PARP inhibitor. Rucaparib (Drew *et al.*, 2020).

In this part of the study, the number of γ-H2AX (as a DNA biomarker) and WT1 (as an ovarian cancer biomarker/CTC) was measured in liquid biopsies from ovarian cancer patients with BRCA-wildtype or -mutated who have been treated with three or more prior lines of chemotherapy before the beginning of Centurion trial and then treated with Rucaparib drug combined with immunotherapy. I have only measured a limited number of patients, so no definitive conclusions can be drawn. However, there is a decreasing trend of the number of γ-H2AX and WT1 in samples during treatment. In general, the number of γ-H2AX-positive CTCs decreased in patients treated with Rucaparib. Additionally, it represents the better result in those patients who were BRCA-m (as it is shown in the Figure 88, P-1 and P-2), which is decreasing in the number of γ-H2AX and WT1 due to the Rucaparib treatment, despite other patients who were not BRCA-m (as it is shown in the Figure 88, P-6 and P-7). This data suggest that BRCA-m patients can be more sensitive to treatment with PARP inhibitors.

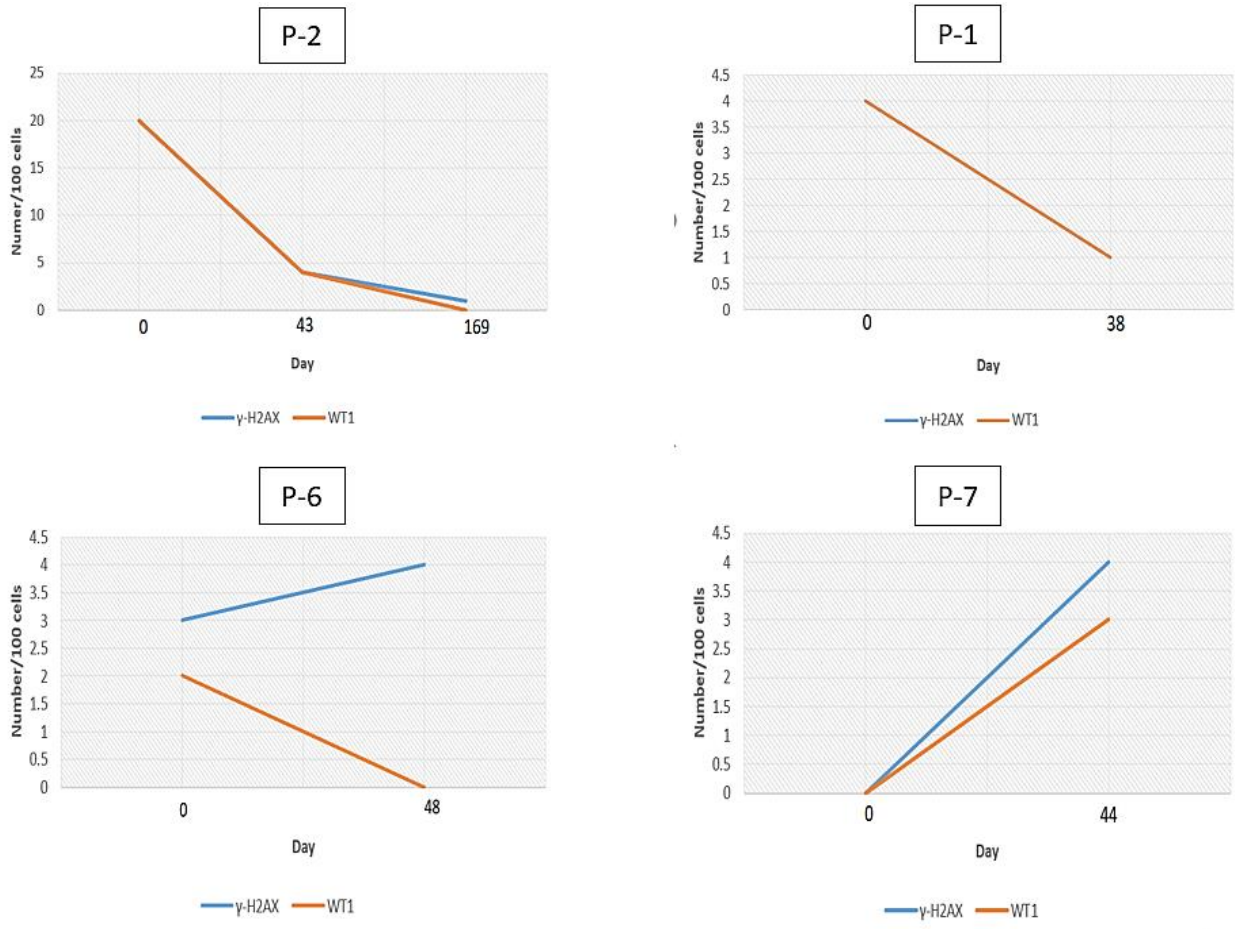

Figure 88. Figure of individual OC patients who treated with Rucaparib. As it can be seen, P-2 and P-1 who are both BRCA-m patients, show a decreased level of both γ-H2AX and WT1 number during Rucaparib treatment. However, P-6 who was not BRCA-m, represent the increasing level of γ-H2AX number but decreasing level of WT1 number during treatment. in the other hand, P-7 who was not BRCA-m, shows an increasing level of both γ-H2AX and WT1 number during Rucaparib treatment.

Discussion

General discussion

In this part of the study, I concentrated to dissect the effect of Rucaparib (PARP-inhibitor) *in vitro*. I have indicated that PARP1-targetted therapy may possibly be effective in the treatment of ovarian cancer patients with BRCA2-m gene. In OC cell lines, inhibition of PARP enzyme was significantly associated with decrease in cell proliferation and increase in apoptosis which is indicatives of potential cytotoxic effects of Rucaparib. Moreover, it induces DNA damage which trigger the DNA repair pathways and lead to express the high level of DNA damage biomarker, γ-H2AX (Saravi *et al.*, 2021).

In addition, my results are in agreement with data from Carey *et al.*, 2019, which showed that in BRCA-mutant/sporadic triple negative breast cancer (TNBC) patients, using PARP inhibitor (Niraparib) remarkably led to increased DNA damage, downregulate HR and subsequent downregulation of the EMT (Carey *et al.*, 2019).

Based on my data, after comparing two BRCA2-m ovarian cancer cell lines, PEO1 which is a BRCA2-m and PEO4 which is BRCA2-silent mutant (expected to work as a wild-type BRCA2), it has been showed that Rucaparib treatment on PEO1 had a more cytotoxic effect compared to PEO4. These results are in correlation with the data from Centurion trial which displayed that BRCA-m patients might have a better response to Rucaparib treatment compared to non-BRCA-m ones. While this investigation was ongoing, another study reported the clinical benefit of Rucaparib maintenance treatment in the post-progression period for patients with recurrent ovarian cancer. ARIEL3 was designed to register around 560 patients and consist of 180–200 patients with a BRCA-m in their carcinoma and up to 360 patients without BRCA-m. Most of the patients in ARIEL3 trial had received two previous platinum-based chemotherapy regimens. 375 of patients received Rucaparib and 189 of them received Placebo. It has displayed that the median CFI (chemotherapy-free interval) was significantly longer for patients who received Rucaparib maintenance treatment which directed to the point that patients receiving Rucaparib treatment were able to postpone the start of further anticancer therapy, possibly letting them to have more time for recovery from previous negative side-effects of chemotherapy and delay additional side-effects related to anticancer therapy (Ledermann *et al.*, 2020). These data support the hypothesis that OC patients with BRCA mutation have the higher likelihood of benefiting from treatment with PARP inhibitors.

Moreover, in this study I provided evidence of differential expression of pro-apoptotic gene (BAX), pro-metastatic gene (SNAI1), and mTOR complex genes in OC cell lines with BRCA2-wt/m, and how PARP-inhibitors can change the expression of these gens. After 72-hrs Rucaparib treatment, PEO1 cell line (BRCA2-m), compared to other cell lines SKOV3 (BRCA2-wt), PEO4 and MDAH-2774 (BRCA2-silent mutation), showed an up-regulation of BAX and down-regulation of SNAI1 genes' expression which can be related to the efficiency of PARP inhibition on BRCA2 defective OC. Regarding to mTOR complex genes, in PEO1 (BRCA2-m) there was a significant decrease in the expression of mTOR, Raptor and Rictor as compared to the controls.

In regards to DEPTOR, its precise role in malignancies is still controversial. DEPTOR seems to develop a dual role, acting as a tumour suppressor in some cancers and as an oncogene in others. Studies have demonstrated that DEPTOR inhibits mTORC1, while it can also activate the Akt pathway (through phosphorylation at S437 and T308 residues) which leads to cell proliferation (Catena and Fanciulli, 2017). For instance, in cervical squamous cell carcinoma cells DEPTOR induced cell survival, and overexpression of DEPTOR associated with poor prognosis in differentiated thyroid carcinoma (Srinivas *et al.*, 2016)(Pei *et al.*, 2011)(Peterson *et al.*, 2009). However, when silenced, DEPTOR stimulates apoptosis through downregulation of PI3K/AKT pathway (Catena and Fanciulli, 2017). It is possible that Rucaparib affect the expression and subsequent activity of mTOR pathway. My results showed that PARP inhibition alters the mTOR complex genes ratio. My study opens prospects for using these different genes to be used as potential biomarkers (Saravi *et al.*, 2021).

Lately, by using targeted next generation sequencing, has been shown that the PI3K-AKT-mTOR pathway can possibly stimulate cancer cell transformation towards endometriosis-associated ovarian cancer (Er *et al.*, 2016). This is consistent with Cardnell *et al.*, 2016 study, which investigated the proteomic changes in PI3K/mTOR pathways that happen following treatment with PAPR inhibitors including Olaparib and Rucaparib on small cell lung cancer. They have found that proteins involved in the PI3K/mTOR pathway were significantly upregulated after PARP inhibition (Cardnell *et al.*, 2016).

In summary, PARP inhibition can be a promising strategy for the treatment of ovarian cancer patients, especially those with HR deficiency and/or BRCA-m gene. In tumours with BRCA deficient gene, PARP inhibitor monotherapy is already an effective therapeutic method that supports the synthetic lethality concept. However, using of PARP inhibitors as a monotherapy is unlikely to induce cancer cell death in BRCA-proficient tumours but the ideal

treatment method for the future remains the combination of PARP inhibition with either cytotoxic DNA-damaging chemotherapeutic agents (such as platinum-analogues) or with molecular targeted agents that also damage the mechanisms of DNA repair.

Chapter6: Expression of γ-H2AX in clinical samples - CICATRIX Clinical Study

Introduction

In this chapter, I focused on the analysis of circulating tumour cells (CTCs) from OC patients that have joined the CICATRIX clinical study. As mentioned in introduction, CTCs can be of prognostic value in various cancers such as colorectal (Tan and Wu, 2018) and breast cancer (Diaz and Bardelli, 2014), but their value in ovarian cancer is still under intense investigation. To date, detection of small populations of CTCs from blood signifies a technical challenge. There are several CTCs detection techniques such as flow-cytometry and other methods including the use of antibody enrichment techniques, thought to be more sensitive (Hou *et al.*, 2012). Although, analysis of CTCs has been restricted by some factors such as biological heterogeneity and the absence of surface signals on CTCs as differed to static cells (Gorges *et al.*, 2012). Most analyses established for CTC identification, depend on a common cell surface marker, epithelial cell adhesion molecule (EpCAM), however CTCs may express low/no levels of EpCAM, due to the epithelial-to-mesenchymal transition (EMT; (Schneck *et al.*, 2015)).

Detection of γ-H2AX expression in CTCs, as an accepted marker of DNA damage, can be used to demonstrate response to treatment, early after chemotherapy in OC patients (Toss *et al.*, 2014). Here I determine the practicality of γ-H2AX quantification as a predictive biomarker of response in CTCs in OC (Mah, El-Osta and Karagiannis, 2010). Currently, many techniques are used to detect γ-H2AX, including constant or pulsed field gel electrophoresis, comet-assays, flow-cytometry, western-blot, and immunofluorescence with antibodies directed against both H2AX and γ-H2AX. However, fluorescence microscopy is the most sensitive and preferred method to detect γ-H2AX (Saggese, 2018).

γ-H2AX formation has recently been examined in cancer cell lines treated with different targeted and chemotherapy agents and in CTCs from patient blood samples processed using γ-H2AX antibody staining in immunofluorescence method. Garcia-villa *et al.*, 2012 successfully demonstrated the presence of γ-H2AX expression on CTCs from metastatic breast cancer patients, receiving carboplatin, a DNA damaging chemotherapeutic agent (Garcia-Villa *et al.*, 2012). Additionally, Wang *et al.*, 2010 showed that, the percentage of γ-H2AX-positive CTCs, taken from patients with variety of advanced malignancies, was enhanced in a concentration-dependent manner in cells treated with topotecan *ex vivo* in therapeutically relevant concentrations (Wang *et al.*, 2010a).

It is still unknown if there is a clinical value between γ-H2AX-positive foci in CTCs during chemotherapy and disease progression. Here I studied γ-H2AX in OC patients, using WT1, an accepted immunohistochemical marker for serous ovarian cancer, to identify ovarian cancer CTCs. I have developed a method for sample preparation, positive identification, quantification, and characterisation of CTCs from whole blood taken from OC patients during treatment.

Aims

- To study the γ-H2AX expression and assess γ-H2AX in CTCs as a predictive biomarker of treatment response.
- To assess any correlations between γ-H2AX foci, WT1 and CA125 levels and clinical outcomes of OC patients receiving chemotherapy.

Result

1. Proof of principle experiment

A proof of principle experiment was performed to test the efficiency of the fluorescence microscopy method using liquid biopsies**.** This was carried out with using healthy blood donated from 3 volunteers. Blood was split into 4 tubes (1ml in each tube), then mixed with BRCA2-wildtype ovarian cancer cells (SKOV3) in serial dilutions (Fig. 89). Samples were stained with γ-H2AX and WT1 antibodies as described in section 3.2 and visualised under Leica microscope.

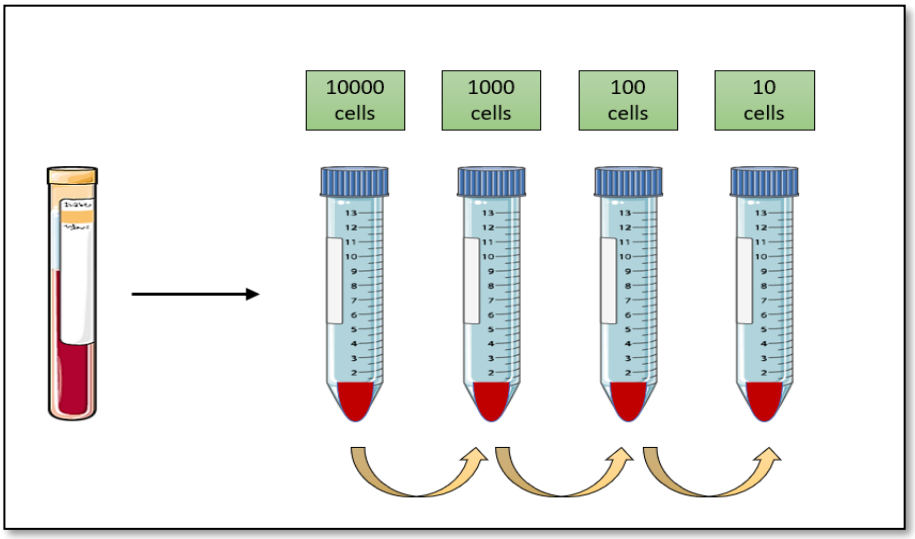

Figure 89. Schematic figure of the serial dilution process. Each tube contains 1ml blood from healthy volunteer, mixed with SKOV3 cell line in serial dilutions, followed by γ-H2AX and WT1 antibody staining.

Both γ-H2AX and WT1 were successfully identified in volunteer whole blood. However, as expected for healthy volunteer blood, numbers of γ-H2AX positive cells were very low, as neither the SKOV3 nor the volunteer blood had been knowingly exposed to DNA damaging strategies. There were more WT1 positive cells present, denoting the spiked SKOV3 cells. No γ-H2AX foci were captured at 0.01 and 0.1 dilutions. It was slightly increased at 1 and 10 dilutions with average cell number of 0.6 and 2.6, respectively. Similarly, larger number of WT1 positive stained cells were identified in the samples with more spiked SKOV3 cells (0.3 at 0.01, 3.6 at 0.1, 8.6 at 1 and 15 at 10 cell per ml dilutions) (Fig 91).

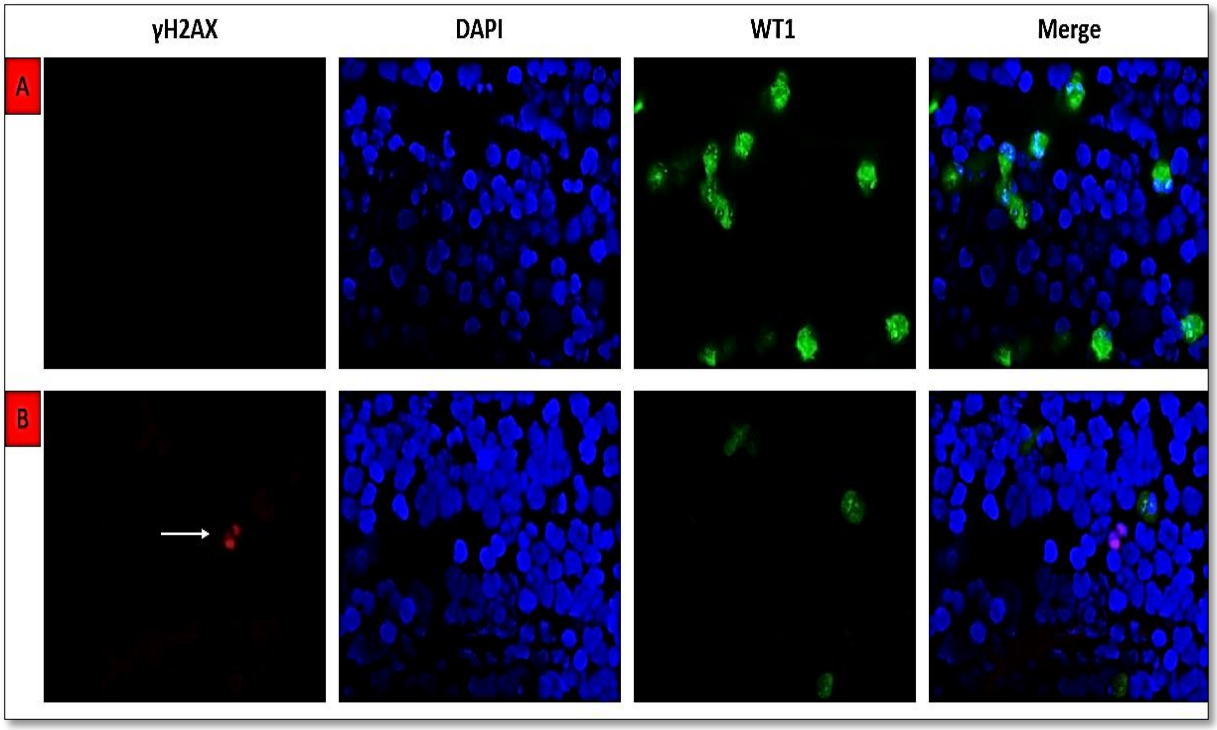

Figure 90. Representative figure of healthy blood cells mixed with SKOV3 cell line. This figure displays (red) γ-H2AX (marked with white arrow), stained with AF-647; WT1 (green), stained with AF-488; and nucleus (blue) stained with DAPI, in blood taken from healthy individuals spiked with SKOV3 cells. A and B show example images captured from 1000 cell per 1ml dilutions. There was a low number of detected foci for γ-H2AX whereas higher number of WT1 positive staining was observed, in increasing dilution.

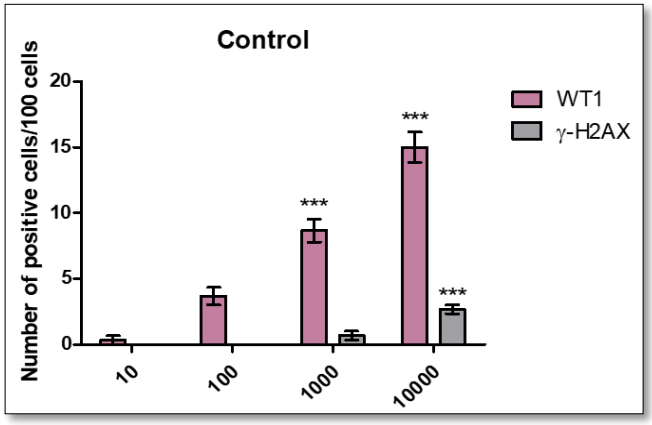

Figure 91. The graph represents the trend of γ-H2AX and WT1 in different serial dilutions of SKOV3 cells in control blood (1.0 mL). As it can be seen, the number of positive staining for γ-H2AX is very low as they are healthy cells and not expected to have a significant DSB DNA damage. One-way ANOVA was performed with GraphPad Prism®, between different concentrations. *** Significantly higher compared to 10-concentration ($p<0.0001$).

2. Analysis of ovarian cancer blood samples

Patient blood samples were collected from ovarian cancer patients kindly participating in the CICATRIX study at Mount Vernon Cancer Centre; ethical approval was granted by the West Midlands-South Birmingham committee (16-WM-0196). Samples were taken at different time-points during the patient's initial treatment at diagnosis.

Patients were categorised to one of 3 groups: neo-adjuvant chemotherapy (NACT), primary surgery, and relapse. Standard treatment for advanced epithelial OC is primary cytoreductive surgery (PCS) followed by adjuvant chemotherapy with carboplatin / paclitaxel and sometimes maintenance bevacizumab or a PARP inhibitor. Patient who are not suitable for initial surgery are treated with neoadjuvant chemotherapy (NACT). Some of these patients then become fit enough for interval surgery (IDS group) whilst others never have surgery. Therefore, cohorts comprised of two further subcategories which are a) NACT interval surgery and b) NACT no surgery. The first group of NACT includes upfront chemotherapy followed by interval cytoreductive surgery and further post-operative chemotherapy (IDS). Patients with comorbidities representing more risky surgery, or very extensive cancer (e.g. Stage IV disease) where it would be impossible to remove it all, fall into this category. (Rauh-Hein *et al.*, 2015). Patients in the no surgery group either do not respond to the NACT (platinum resistant disease) or have multiple significant comorbidities which render it impossible to ever operate safely. NACT consists of 3-4 cycles of chemotherapy (every three weeks) prior to repeating the CT scan to assess whether the patient can undergo IDS. 2-3 cycles of the same chemotherapy are delivered post operatively making 6 cycles in total. These patients are likely to be on maintenance bevacizumab (a VEGF inhibitor) treatments afterwards.

Patients undergoing primary debulking surgery have 6 cycles of the same adjuvant chemotherapy and for patients where there was residual disease, maintenance bevacizumab (three weekly) for 18 cycles in total. Patients with BRCA mutations, either germline or somatic, or other homologous repair deficiencies (HRD) will have additional PARP inhibitor maintenance until disease progression. Remaining patients will be followed up off all treatment.

The final category is relapsed patients, where their OC has returned. Such patients face another line of chemotherapy and sometimes maintenance treatments such as PARP inhibitors (Olaparib, Niraparib, Rucaparib) afterwards. (Rauh-Hein *et al.*, 2015). Relapsed patients are divided, for communicative convenience into - platinum sensitive (at least 6 months from last platinum treatment) or platinum resistant (<6 months since last platinum treatment).

Table 14. The number of patients in each group.

Category	NACT	Primary Surgery	Relapse
Number of patients	43	30	33

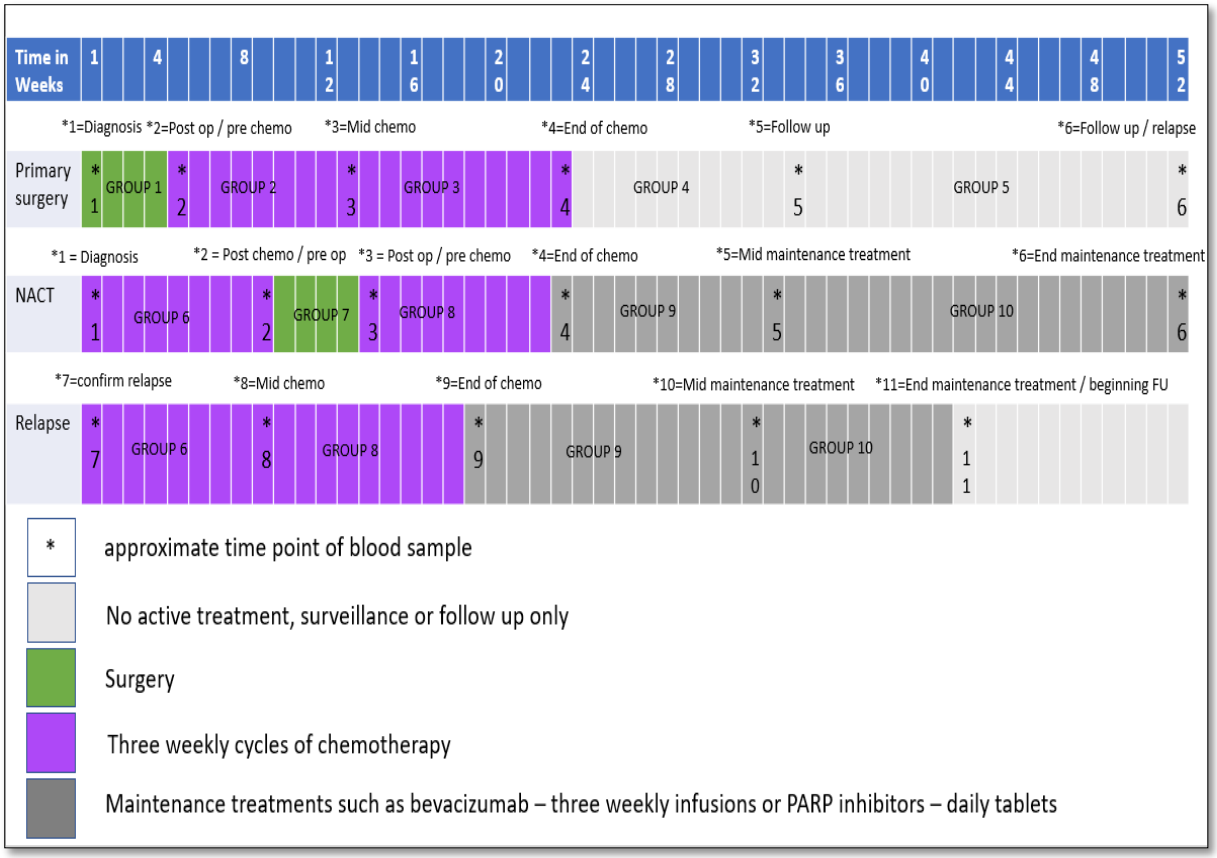

Figure 92.Timeline of patient's treatment. Figure above shows the time and process of patient's treatment for all 3 categories of patients including primary surgery, NACT and relapse.

All blood samples were analysed using fluorescent microscopy. Quantification was calculated as positive cells per 100 cells. In summary, I measured the number of γH2AX, WT1 compared to CA125 levels at different stage of treatment. My results show that overall, the level of CTCs with positive γ-H2AX staining was highest prior to chemotherapy treatment and fell during treatment to the lowest at the end of treatment.

To begin with, I combined all the groups where patients have received chemotherapy (n=22)- irrespective of agent. Interestingly it showed that patients had responded well to the treatment, which might be signified by the initial spike in number of γ-H2AX, WT1 and CA125, eluding to a response due to tumour necrosis and thus further CTC shedding, followed by decreasing in CTC counts as the patient continues to do well on the treatment (Figure 93). There was a significant positive correlation between γ-H2AX and WT1 in the early group.

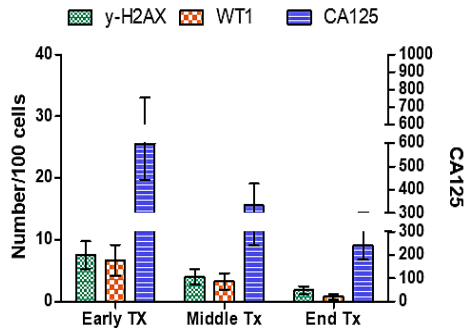

Figure 93. The graph of all patients received chemotherapy. The average number of positive-γH2AX staining was 7.5 (per 100 cells), at the early stage of treatment, then decreased at the middle and end treatment which were 4 and 1.8, respectively. Additionally, WT1 displayed the similar changes as γ-H2AX. The average number of positive-WT1 staining was 6.6 at the early treatment which was dropped at the middle and end of treatment, 3.2 and 0.7, respectively. All WT1-positive staining cells were positive for γ-H2AX staining. Moreover, CA125 levels showed a decreasing trend from early treatment to end treatment which was consistent with γ-H2AX and WT1 results. The average number of CA125 was 598.2 for early Tx, 333.2 for middle Tx and 240.9 for end Tx.

Following the initial overview of the trajectories of γ-H2AX, WT1 and CA125, I have dissected those responses further. For example, Figure 94 relates to the five patients who had primary surgery and demonstrate differences in average numbers of cells with WT1/γ-H2AX, seen prior to start of therapy with the end of treatment and compared with the changes in CA125 levels assayed routinely in the hospital laboratory. Cells positive for WT1 fell from 8.6 at the beginning to 2.6 at the end of treatment. This mirrored a similar drop in cells positive for γ-H2AX (11.4 - 4.6) as well as CA125 levels (1716 – 14.3) at the same time-points.

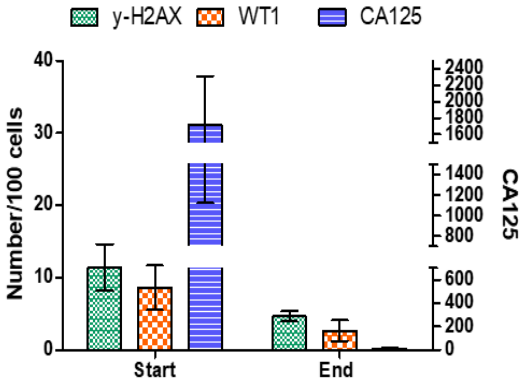

Figure 94.The graph of primary surgery patients comparing start of the treatment with end of the treatment. There is a decrease in the level of positive-γ-H2AX staining cells same as positive-WT1 staining cells, at the start of the treatment in comparison to the end. All WT1-positive staining cells were positive for γ-H2AX staining. Likewise, the count of CA125 presented a decreasing trend from start of the treatment to the end treatment which was consistent with γ-H2AX and WT1 results.

Evaluation of the numbers of cells from before to after the adjuvant chemotherapy for this primary surgery cohort (n=6) also showed a decrease in the number of γ-H2AX, WT1 and CA125 in early-, mid-, and late- treatment samples but this failed to reach significance (Fig

95). There was a significant positive correlation between γH2AX and WT1 in the early group.

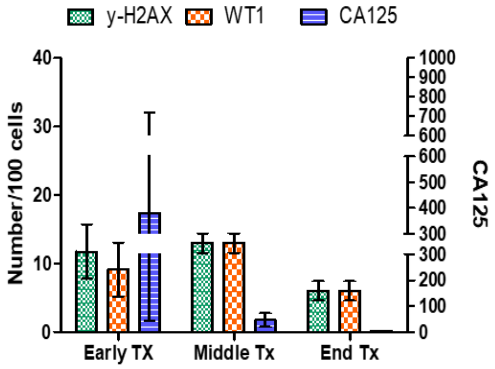

Figure 95.The graph of primary surgery group patients, to assess the effect of chemotherapy after surgery. The average number of positive-γ-H2AX stained cells was 11.7 (per 100 cells), early / pre-treatment, increasing to 13 mid-treatment and decreasing to 6 at the end treatment sample. WT1 showed similar changes, 9.1 early treatment, 13 mid-treatment, 6 at the end of treatment. All WT1-positive staining cells were positive for γ-H2AX staining. Average CA125 levels corroborated, but decreased throughout treatment, 381.7 for early, 46.5 for middle and 5 for end of treatment timepoints.

For NACT/IDS group I looked at the effects of chemotherapy before interval debulking surgery (n=8) and post-operative chemotherapy (n=5). As shown in Fig 96, the average CA125 values reduced steadily across the process of treatment. However, the average numbers of γ-H2AX and WT1 stained circulating cells after surgery was higher than before surgery although they decreased to lower levels than initially, by the end of adjuvant chemotherapy.

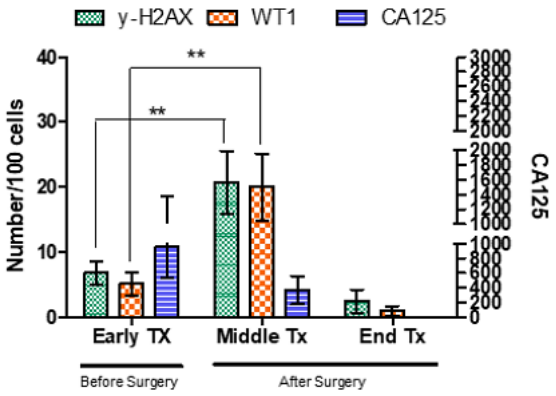

Figure 96.The graph of all NACT patients received chemotherapy. The average number of positive-γ-H2AX staining was 6.8 (per 100 cells), at the early stage and before the surgery, then increased to 20.7 at the middle Tx which was after the surgery. Finally, it was reduced to 2.5 at the end of the treatment. Moreover, WT1 indicated the parallel changes as γ-H2AX. The average number of positive-WT1 staining was 5.1 before the surgery, at the early Tx. After the surgery, it was increased at the middle Tx to 20 and finally dropped to 1 at the end of treatment. All WT1-positive staining cells were positive for γ-H2AX staining. Also, the count of CA125 showed a decreasing trend from early treatment to end treatment with average number of 951.9 for early Tx, 371.4 for middle Tx and 8 for end Tx. ** γ-H2AX p=0.0093, ** WT1 p=0.0089, CA125 p=0.4751.

There was no significant difference in the mean numbers of γ-H2AX and WT1 positive cells between the NACT/surgery and NACT alone groups, suggesting that the rise post-operatively could simply reflect a higher circulating cancer cell burden arising from surgical damage. There was a significant positive correlation between γ-H2AX and WT1 in both groups.

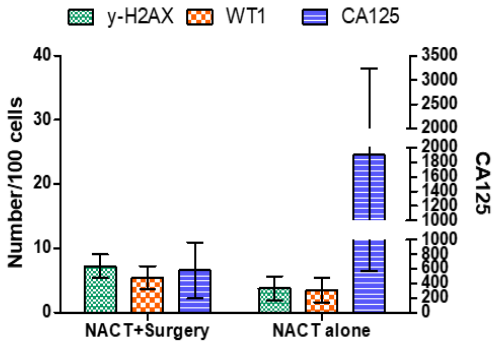

Figure 97.The graph of NACT patients with/without surgery. In those NACT patients who received surgery (n=7), the average number of positive-γ-H2AX staining and positive-WT1 staining were 7.2 and 5.4, respectively while those NACT patient who did not receive the surgery (n=2) displayed a lower average number of positive staining for γ-H2AX and WT1 which were 3.7 and 3.5, respectively. However, the change of CA125 was different in comparison to γ-H2AX and WT1. The average number of CA125 was 581.3 in NACT patients with surgery and higher number in NACT patients with no surgery which was 1905.

Figure 98 displays the effect of maintenance bevacizumab on WT1, γ-H2AX in CTCs. The groups (4,5,6) represent samples taken at 3 different timepoints: **4** is where chemotherapy has ended and bevacizumab alone begins, **5** are samples taken in the middle of maintenance bevacizumab and **6** at the end of bevacizumab. The numbers of γ-H2AX and WT1 staining cells were lowest at the end of maintenance bevacizumab treatment. There was a significant positive correlation between γ-H2AX and WT1 in group 5, i.e., all cells staining for γ-H2AX also stained for WT1. This is very interesting given that the CA125, reflecting disease progression has, as expected, mostly risen over the period of bevacizumab maintenance therapy. Possibly this is because the antiangiogenic action of bevacizumab obstructs entry to the circulatory system for cancer-associated cells.

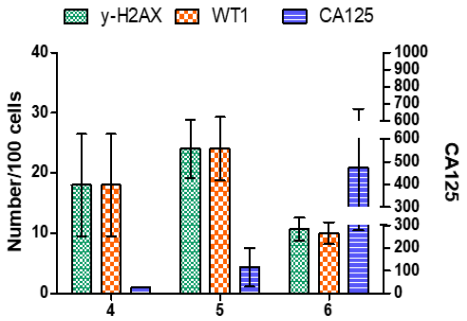

Figure 98.The graph of NACT patients (n=18) to evaluate the effect of maintenance Bevacizumab. The average number of positive-γ-H2AX staining was 18 (per 100 cells), at group 4, then increased to 24 at group 5. Finally, it was reduced to 10.6 at the end of treatment, group 6. Moreover, WT1 indicated the similar changes as γ-H2AX. The average number of positive-WT1 staining was 18 (per 100 cells), at group 4, then increased to 24 at group 5 and finally, it was decreased to 10.6 at the end of treatment, group 6. All WT1-positive staining cells were positive for γ-H2AX staining. Although, the average number of CA125 indicated an increasing trend from the end of chemotherapy to end of maintenance treatment with average number of 26 for group 4, 114.9 for group 5, and 473.8 for group 6.

For the relapse patients I looked at the changes in relation to different chemotherapy schedules / drugs. Responding patients (n=7) treated with combination carboplatin and caelyx seemed to fall into 2 groups, those who had clear responses, and those who had stable disease. There was a decreasing trend in number of γ-H2AX, WT1 stained cells and CA125 before and after chemotherapy in this group. As expected, some patients did not respond to carboplatin caelyx treatment. There was a significant positive correlation between γ-H2AX and WT1 in the early group.

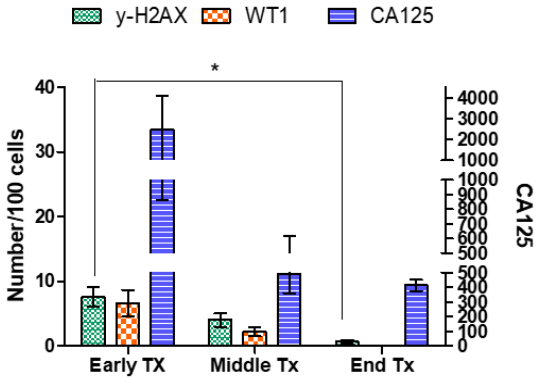

Figure 99.The graph of Relapse patients treated with Carboplatin and Caelyx. The average number of positive-γ-H2AX staining was 7.6 (per 100 cells), at the early stage of treatment, then decreased at the middle and end treatment which were 4 and 0.6 respectively. Significant change was seen between γ-H2AX early and end (*, p=0.0253). Additionally, WT1 displayed the similar changes as γ-H2AX. The average number of positive-WT1 staining was 6.6 at the early treatment which was dropped at the middle and end of treatment, 2.2 and 0 respectively. All WT1-positive staining cells were positive for γ-H2AX staining. Furthermore, the level of CA125 displayed a decreasing trend from early treatment to end treatment which was consistent with γ-H2AX and WT1 results. The average number of CA125 was 677.5 for early Tx, 543.5 for middle Tx and 374 for end Tx.

There were too few patients (n=4) receiving an alternative relapse treatment, carboplatin with gemcitabine, to assess any changes properly as there was only one patient who had had an

end of treatment sample taken. Although, Fig 100 demonstrates a reduction in number of γH2AX, WT1 stained cells mid treatment corroborating the decreasing CA125 levels.

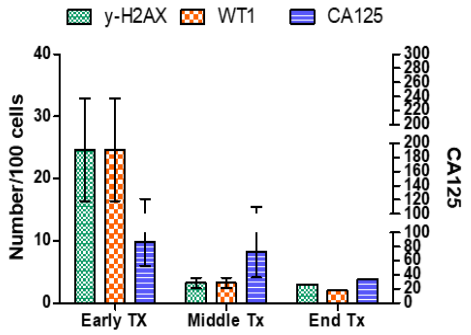

Figure 100.The graph of Relapse patients treated with Carboplatin and Gemicitabine. The average number of positive-γ-H2AX staining was 24.6 (per 100 cells), at the early stage of treatment, then decreased at the middle and end treatment which were 3.2 and 3 respectively. Moreover, WT1 showed the similar changes as γ-H2AX. The average number of positive-WT1 staining was 24.6 at the early treatment which was dropped at the middle and end of treatment, 3.2 and 2 respectively. All WT1-positive staining cells were positive for γ-H2AX staining. Likewise, the number of CA125 was decreased from early treatment to end treatment which was consistent with γ-H2AX and WT1 results. The average number of CA125 was 87 for early Tx, 73.2 for middle Tx and 34 for end Tx.

One of the last lines of therapy for relapsed OC is weekly paclitaxel. Patients in this group (n=7) exhibited a reduction in CA125 levels by the end of treatment, although the average numbers of γ-H2AX and WT1 stained cells increased mid-treatment before disappearing.

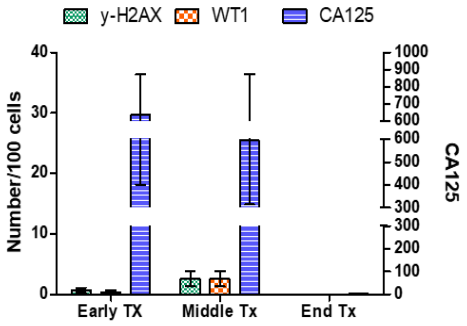

Figure 101.The graph of Relapse patients treated with Taxol. The average number of positive-γ-H2AX staining was 0.6 (per 100 cells), at the early stage of treatment, then slightly increased at the middle of treatment which was 2.6 and decreased to 0 at the end of treatment. Additionally, WT1 indicated the similar changes as γ-H2AX. The average number of positive-WT1 staining was 0.3 at the early treatment which was enhanced at the middle to 2.6 and again decreased to 0 at the end of the treatment. All WT1-positive staining cells were positive for γ-H2AX staining. The average number of CA125 was decreased from early treatment to end treatment, which was 636 for early Tx, 594.7 for middle Tx and 1 for end Tx.

Finally, I looked at the effect of PARP-inhibitor (niraparib) maintenance in BRCA wildtype patients with relapsed OC (n=6). Interestingly, the number of γ-H2AX and WT1 stained cells fell throughout maintenance niraparib being the lowest when niraparib was stopped. In contrast, as with the maintenance bevacizumab, CA125 levels rose steadily and were higher

at the end of treatment suggesting that the patient was no longer responding to niraparib. Again, there was a significant positive correlation between γ-H2AX and WT1.

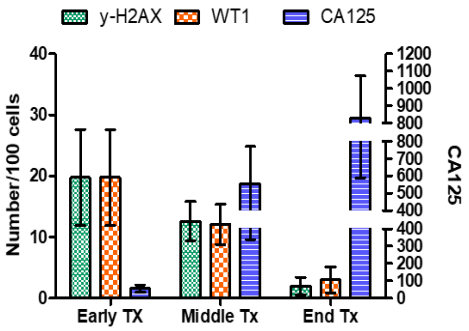

Figure 102.The graph of Relapse patients treated with PARP-inhibitors. The average number of positive-γ-H2AX staining was 19.7 (per 100 cells), at the early stage of treatment, then decreased at the middle and end treatment which were 12.6 and 2 respectively. Moreover, WT1 showed the similar changes as γ-H2AX. The average number of positive-WT1 staining was 19.7 at the early treatment which was dropped at the middle and end of treatment, 12.1 and 3, respectively. All WT1-positive staining cells were positive for γ-H2AX staining. However, the number of CA125 was increased from early treatment to end treatment. The average number of CA125 was 55.6 for early Tx, then increased to 555.5 for middle Tx and 831.5 for end Tx.

The statistical analysis including correlation coefficient and p-values, was performed through GraphPad Prism® and can be found in table15.

Table 15. Table of statistical values. This table displays the correlation coefficient and p values for each category of our result.

Patients group	Number of patients	Marker/Stage Tx	Correlation coefficient	Significant p value
All patients received chemotherapy	22	γ-H2AX/WT1 early	0.76	0.00012
		γ-H2AX/WT1 end	0.70	0.009
Primary surgery comparing start with end of Tx	5	γ-H2AX/WT1 end	0.70	0.009
		WT1/CA125 early	-0.79	
Primary group effect of chemotherapy after surgery	6	γ-H2AX/WT1 early	0.99	0.000005
NACT received chemotherapy comparing before and after surgery	Before: 8	γ-H2AX/WT1 early	0.78	0.0009
	After: 5	γ-H2AX/WT1 middle	0.99	0.0000011
NACT with/without surgery	With:7	γ-H2AX/WT1 with surgery	0.77	0.0018
		γ-H2AX/WT1 without surgery	0.99	0.0062
	Without: 2	γ-H2AX/CA125 without surgery	0.91	
		WT1/CA125 without surgery	0.94	
NACT with maintenance Bevacizumab	18	γ-H2AX/WT1 group 5	0.99	P<0.0001
		γ-H2AX/WT1 group 6	1.00	
		γ-H2AX/CA125 group 6	0.78	
		WT1/CA125 group 6	0.78	
Relapse patients/treated with Carboplatin+Caelyx	7	γ-H2AX/WT1 early	0.91	
Relapse patients/treated with Carboplatin+Gemicitabine	4	γ-H2AX/WT1 middle	1.00	
Relapse patients/treated with Taxol	7	γ-H2AX/WT1 middle	1.00	
Relapse patients/treated with PARP inhibitors	6	γ-H2AX/WT1 early	1.00	
		γ-H2AX/WT1 middle	0.99	P<0.0001

Changes in cellular localisation of γ-H2AX

There are several reports regarding the presence of not just canonical "foci" staining, but also the existence of an "apoptotic ring" (Solier and Pommier, 2014) which looks very similar to the staining I have observed in some of my patients' samples. As the name indicates, Solier and Pommier, describe a staining pattern of γ-H2AX around the nucleus and link this to the apoptotic process and implied such γ-H2AX staining as another apoptosis marker (Solier and Pommier, 2014).

Interestingly, staining discrepancies were noticed in some cells, stained with γ-H2AX. Figure 103 is a representative figure of different -γH2AX staining, taken from different OC patients. It was shown that, in addition to sighted common staining which was a diffuse staining for both γ-H2AX and WT1 (Fig 103-b), I also detected CTCs with significant apoptotic ring for γ-H2AX staining (Fig 103-c, d) and foci staining for both γ-H2AX and WT1 (Fig 103-a). Therefore, preliminary evidence indicates that there might be more than just the presence or absence of γ-H2AX in CTCs and the cellular distribution could also have clinical relevance.

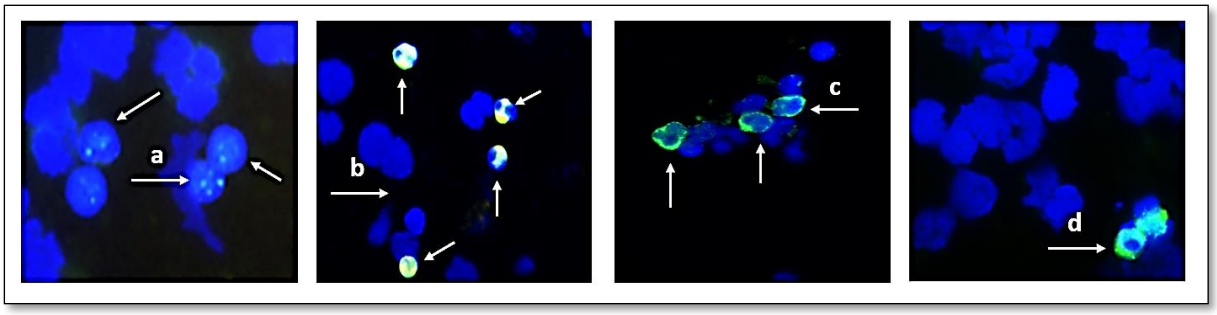

Figure 103. γ-H2AX formation and detection in ovarian cancer patient's blood cells. Using of a specific γ-H2AX antibody allows to visualize the DSBs as discrete foci (a). In some cells, DSB formation can lead to apoptosis and increase formation of both DSBs and γ-H2AX which show different pattern of staining including, γ-H2AX diffuse staining (b), γ-H2AX staining of apoptotic bodies that appear as an apoptotic ring (c-d). Blue: DNA; Green: γ-H2AX.

In my study, I have found only 22 samples (out of 122) of patients in different stage of treatment which displayed different pattern of γ-H2AX staining (see Appendix A). Figure 104 shows some of these images for diffuse, foci and apoptotic ring staining in γ-H2AX and WT1.

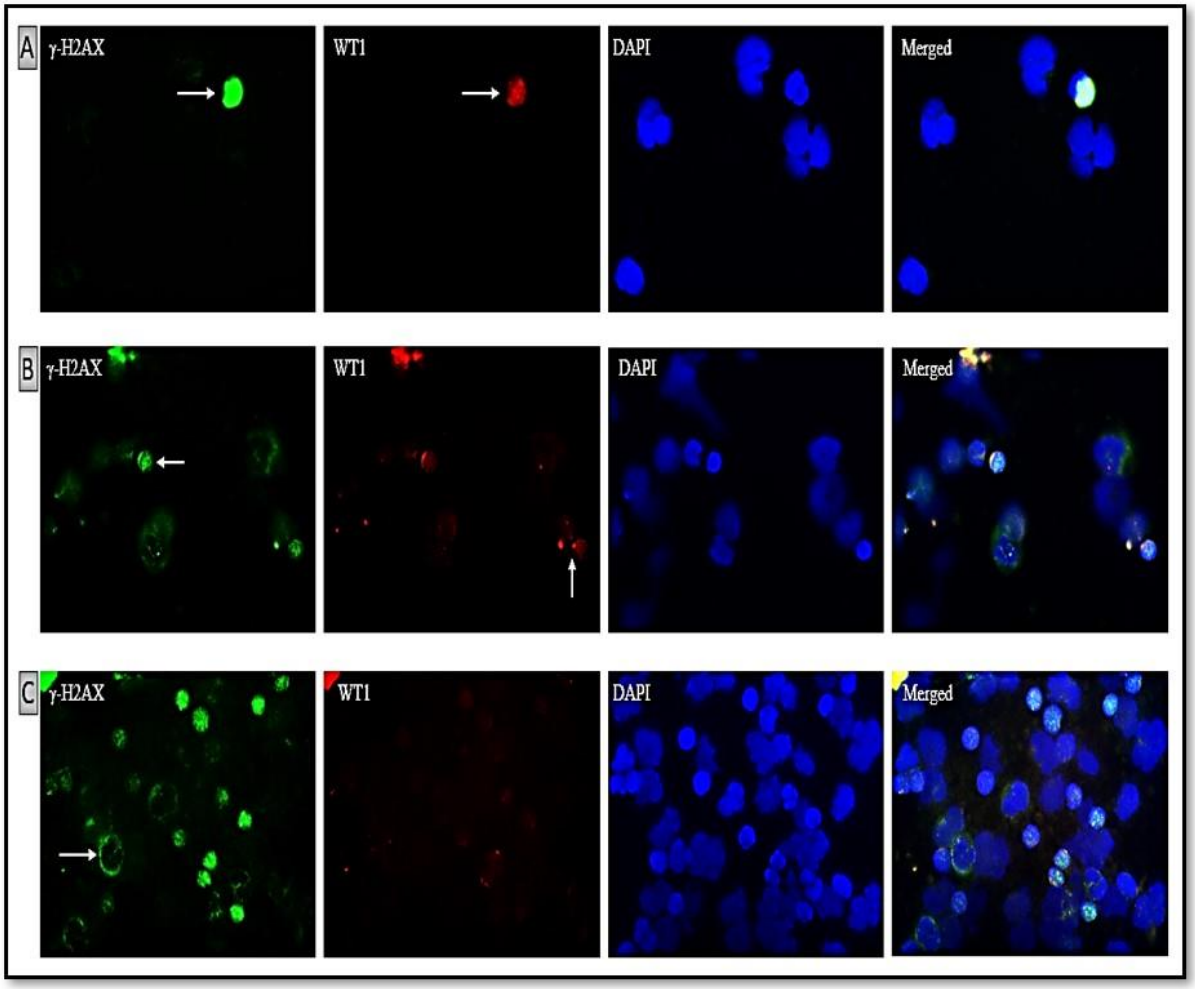

Figure 104. γ-H2AX and WT1 staining in blood samples from OC patients. (A) diffuse staining for both γ-H2AX and WT1, (B) foci stating for both γ-H2AX and WT1 which was indicated in different cells, (C) apoptotic ring staining for γ-H2AX.

Discussion

Several anticancer treatments, such as radiotherapy and chemotherapy, work through DNA damage and inducing sufficient DSB numbers in tumour cells which result in destructive lesions, impeding cell function, proliferation and finally cell death. An early response to ds-DNA damage is accumulation of γ-H2AX, which has been proposed as a sensitive indicator of drug efficiency (Redon *et al.*, 2012). DNA damage monitoring can be used to predict tumour cell survival after exposure to cytotoxic drugs (Shah *et al.*, 2015). CTCs in this work were identified with cytokeratin and WT1 markers. These cells also showed positive γ-H2AX staining presumably reflecting DNA damage seen as a consequence of the chromosomal instability of HGSOC as well as surges presumed to be related to drug-induced DNA insults. By determination of both numbers of CTCs and level of γ-H2AX expression before and after treatment, I have tried to determine if the patient is responding to their therapeutic regimen. I have compared the CTC numbers and level of γ-H2AX to CA125, a routinely used clinical biomarker for HGSOC, taken at similar time points.

My results indicate that the level of CTCs with positive γ-H2AX and WT1 staining declined following chemotherapy treatment. For example, relapse patients, treated with different chemotherapeutic agents including carboplatin, Caelyx, gemcitabine and paclitaxel, displayed a drop in the number of γ-H2AX and WT1 positive cells during chemotherapeutic treatments which mirrored a similar fall in CA125 and response to treatment. The opposite was true for a few patients who had progressive disease – i.e., a rise in the number of γ-H2AX and WT1 positive cells aligning with a rise in CA125. The effects of maintenance therapies such as antiangiogenics (bevacizumab) and PARP-inhibitors (niraparib) in relapsed OC patients was also explored. Interestingly in both maintenance situations, a trend of decreasing levels of γ-H2AX and WT1 during and following treatment, was not supported by a decrease in CA125 which rose towards the end of the maintenance phase indicating disease relapse. It is not clear why there should be fewer CTCs with ds DNA damage following maintenance therapy but in the context of cancer progression, antiangiogenic therapy may reflect an inability of cancer cells to access the circulatory system as easily – as these drugs distorted neo-vasculature development.

There are many other reasons for changes in γ-H2AX levels under certain circumstances such as increased ROS from anaesthesia in post-op patients (Rothkamm *et al.*, 2015). Cytotoxic agents themselves are very likely to increase γ-H2AX e.g., paclitaxel, a microtubule stabiliser, Caelyx, an alkylating agent which promotes cross-linking of DNA strands, as does

platinum, all of which will cause an increase in ds DNA breaks due to their actions. gemcitabine, however is an nucleoside analogue which substitutes in place of another base and provokes chain termination but not necessarily generating DNA-DSB (Rothkamm *et al.*, 2015).

My results are in agreement with Wang *et al.*,2010 study which demonstrated changes in γ-H2AX level in CTCs from patients undergoing chemotherapy treatment. Data from limited number of patients in their study has indicated the percentage of γH2AX-positive CTCs was increased following administration of topotecan which is a topo 1 isomerase inhibitor and as such may be acting to elevate H2AX levels via transcription as well as directly causing DNA-DSB (Wang *et al.*, 2010b). This change was measured after a single day of receiving drug and quantified from a mean of 2% at baseline (range 0%–6%) to a mean of 38% (range 22%–64%). However, this increase was regardless of increases or decreases in the total number of CTCs (Wang *et al.*, 2010b). Additionally, an increase in the number of CTCs positive for γ-H2AX in patients treated with topotecan and ABT-888 (PARP-inhibitors) has also been observed in patients with refractory solid tumours and lymphomas. The level of γ-H2AX was increased from 16% at baseline to 100%, suggesting a significant DNA damage response to drug treatment (Kummar *et al.*, 2011).

Assessment of γ-H2AX staining in CTCs could be an additional biomarker of response to treatment and may play a role in "personalising" cancer therapy by allowing rapid assessments of ongoing response to specific treatments (Olive, Banáth and Sinnott, 2004). Future studies with much larger cohorts will be needed to provide further insight into its clinical utility as biomarker. Apart from the changes in the levels of γ-H2AX over treatment, changes in the cellular distribution patterns of this protein might be of equal importance, when studying apoptotic events.

In this study, I show for first time different pattern of γ-H2AX staining in CTCs including diffuse staining, foci staining and apoptotic ring staining. Solier and Pommier 2014 displayed γ-H2AX apoptotic ring versus γ-H2AX DDR foci in HCT116 human colon carcinoma cell line which was treated with TRAIL (TNF-related apoptosis-inducing ligand) (Solier and Pommier, 2014). Consistent with my data, Mukherjee *et al*., 2006 displayed evidence that γ-H2AX is phosphorylated through the procedure of apoptotic DNA fragmentation. Their study revealed that H2AX is phosphorylated during apoptotic DNA fragmentation in Chinese hamster ovary, and human fibroblast cell line which were treated with Staurosporine to trigger apoptosis. The phosphorylation process occurs late and can be associated with chromatin condensation (Mukherjee *et al.*, 2006). The mechanisms and relevance of the

differences in γ-H2AX staining patterns requires further delineation. For instance, cells that display apoptotic ring staining in my cohort, could have been circulating in the patient for several days, or longer, and may originally have shown the more commonly identified focal staining (Garcia-Villa *et al.*, 2012). Broad evaluations of the various γ-H2AX staining patterns in the context of patient responses to treatment are also required.

Chapter7: Discussion

7.1. Impact and importance

Over the past four decades, cancer diagnosis and treatment has come a long way; despite this, survival rates remain low in many cancers such as ovarian cancers, where ten-year survival rates is only 35% (CRUK, 2019c). 71.7% of ovarian cancer patients survive for at least one year, which drops to 42.6% surviving for five years or more (CRUK, 2019c).

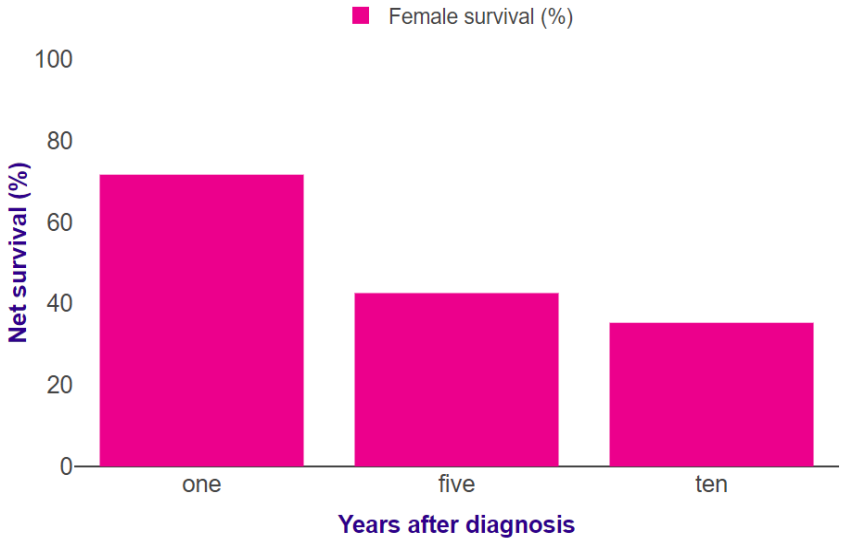

Figure 105. Ovarian Cancer Age-Standardised One-, Five- and Ten-Year Net Survival, Adults (Aged 15-99), England, 2013-2017. This graph displays one- and five-year net survival and predicted ten-year net survival, with 95% confidence intervals. Ovarian cancer survival continues to drop after five years of diagnosis and 35.3% of patients are expected to survive for ten years or more. Credit: (CRUK, 2019c).

Late diagnosis is a significant contributing factor to such low survival rates. Except in the case of advanced illness, signs are often unclear, which resulting in most of the patients being diagnosed only at a late stage (e.g., III and IV which is usually the case with ovarian cancer). Additionally, it is well-known that cancer prognosis is linked to staging, with early diagnosis providing more treatment choices and improved chances of survival. To further complicate matters, the limited understanding of interpatient variability, which determines the condition and modulates the response to therapy, is also an important concern for clinicians in the care of patients.

7.2. Rucaparib: a recently approved PARP inhibitor for ovarian cancer treatment and maintenance

A great deal of attention is now focusing on 'precision medicine' or customized therapy, whereby individual patients receive tailored care to their condition, considering their individual genetic profile and possible therapeutic responses. This allows the identification of appropriate treatment for the patient based on their exact needs.

The main findings of my study can be summarized as follows: Defective BRCA2 causes HRR dysfunction, which results in the DSB-DNA damage being left unrepaired and leads to cell death. Increased γ-H2AX foci in BRCA2-m cell line is consistent with the idea that BRCA2 has a crucial role in HR pathway (Rigakos and Razis, 2012). Here, I assessed the effect of Rucaparib *in vitro*. In OC cell lines with defective BRCA2 gene, inhibition of PARP enzyme was significantly related to a decrease in cell proliferation and increase in apoptosis. Additionally, DNA repair pathways are activated and express a high level of the DNA damage biomarker, γ-H2AX. In line with the results in my study, the expression pattern of the DDR molecules including PARP1, γ-H2AX and BRCA2 have been related to the progression of many cancers, such as breast cancer (Rojo *et al.*, 2012), ovarian cancer (Cho *et al.*, 2015) (Gan *et al.*, 2013), and glioblastoma (Galia *et al.*, 2012). Comparison of the BRCA2 mutant cell line (PEO1) with the BRCA wild-type OC cell line (SKOV3) and those with a silent BRCA2 mutation (PEO4, MDAH-2774) underlined the importance of BRCA2 in repair of dsDNA. The intriguing increase in γ-H2AX, 24 hours after H_2O_2 exposure in SKOV3 cells suggests that this cell line may represent a model of 'BRCAness'. This refers to EOC (up to 50% of HGS) that show a defective phenotype of HRR without BRCA mutations (Turner, Tutt and Ashworth, 2004) (Ping Lin *et al.*, 2018). Notably, SKOV3 has 3 other genes mutated participating in HRR (Beaufort *et al.*, 2014). These findings are born out in clinical practice where patients with BRCA mutations make up a distinct subset of the high grade serous ovarian cancer population.7.2.1. Rucaparib Clinical Trials

Rucaparib has been evaluated in clinical trials, focussing on ovarian cancer patients with BRCA mutations. As with most other PARP inhibitors, rucaparib cannot be used in combination with other chemotherapeutic agents as the toxicity to too great. It is however licensed for use as a single agent in patients with platinum sensitive recurrence (Grignani *et al.*, 2020) (Colomba *et al.*, 2019).

The ARIEL3 study reported the clinical benefit of rucaparib maintenance treatment following chemotherapy in patients with recurrent ovarian cancer. Most of the patients in this trial had received two previous platinum-based chemotherapy regimens; they were randomised 2:1 to receive rucaparib or placebo maintenance, provided they had had a response to their relapse chemotherapy. Time to the next relapse was longer in those receiving rucaparib (HR 0.32) and this was greatest for those with BRCA mutations (either somatic or germline) (Coleman *et al.*, 2017). A subsequent trial (ARIEL 4) has shown that rucaparib can be used to treat ovarian cancer patients with BRCA mutations, i.e., without cytotoxic chemotherapy. There was a significant benefit in progression free survival for rucaparib when compared to

standard chemotherapy (HR 0.64) (Kristeleit *et al.*, 2021). PARP inhibitors, like rucaparib, are now an integral part of the management of most patients with high grade serous ovarian cancer.

7.3. H2AX: upregulated in OC and demonstrates utility as a prognostic biomarker in terms of overall survival

H2AX is well recognised as a biomarker of DNA damage. I have explored alterations at gene and protein level of H2AX in OC to evaluate its' role as a potential predictive biomarker. In silico analysis using the TCGA databases revealed that H2AX is overexpressed in OC in comparison to controls. In terms of prognostic value, I established that higher expression of H2AX is related to better overall survival (OS), although there was no apparent difference on disease free interval (DFI), in the ovarian cancer cohort.

I have then performed IHC using a tissue microarray of OC patients and 10 adjacent tissues to OC in attempt to dissect further the expression of H2AX at protein level in different types of OCs and stages. I have shown that H2AX is abundantly expressed in high- and low-grade serous OC, mucinous adenocarcinomas, metastatic serous carcinomas, and clear cell carcinomas. Lastly, γ-H2AX staining has been shown to be significantly higher in BRCA1/2 mutation-positive fallopian tube epithelium in comparison to control (BRCA wild-type) fallopian tube epithelium (Staff *et al.*, 2014). Here I document a correlation between the phosphorylation level of γ-H2AX foci and the H2AX gene expression, in appropriate cell lines *in vitro*.

One intriguing proposal is that H2AX gene could be a good candidate to indicate susceptibility to different cancers such as lymphomas and leukaemia (Dickey *et al.*, 2009). A study by Novik et al. revealed a population-based group of H2AX genetic variants in non-Hodgkins lymphoma (NHL), which is known as one of the most commonly diagnosed cancers worldwide (Novik *et al.*, 2007). A further study has indicated changes in H2AX gene copy number in 37% of breast cancer tumour samples (25/65 cases). Moreover, the breast cancer cell line MCF7, displayed a two-fold deletion in H2AFX gene copy number. This finding implies that the deletion in the H2AFX gene copy number may possibly have a role in breast carcinogenesis (Srivastava *et al.*, 2008). In conclusion, H2AX appears to have a role in structural and functional part of DSB response, and participating in the process of DNA-DSB through the retention of particular factors such as ATM and DNA-PK (Turinetto and Giachino, 2015). These molecular events may possibly be necessary in order to provide a steady state of H2AX protein which could be a surrogate biomarker to γ-H2AX.

7.4. The clinical utility of CTCs as a liquid biomarker in OC

Currently, a large body of work is concentrating in the identification of robust 'liquid biopsy' biomarkers to support further precision medicine. 'Liquid biopsy' intends to enhance and maybe replace the classic invasive tissue biopsy in certain cases. It is believed that blood samples may more accurately represent the genetic diversity of a tumour profile and serve as a surrogate biomarker to help diagnose and treat cancer, an early warning of pending resistance, and perhaps consecutive monitoring of patients undergoing several cycles of treatment. (Chudasama *et al.*, 2019). Identification and evaluation of novel liquid biomarkers may also allow the development of new therapeutic targets and enhance our understanding of the biology of cancer spread.

Several elements are available for analysis: circulating tumour cells (CTCs), circulating free nucleic acids (ctNAs) (i.e., DNA and RNA) and other genomic material (e.g., exosomes) in whole blood. Here, I examined these biomarkers, evaluate their effectiveness, and assess their clinical utility and significance in identifying biomarkers for use in a population of patients with high grade ovarian cancer. I have compared these potential markers with standard clinical markers, CA125 and outcomes from imaging and clinical assessments. Evolutionary pressure imposed by treatments leads to the adaptation of cancer cells over time and makes them resistant to drugs (Friedman, 2016). Therefore, it could be important to identify biomarkers to characterise and provide real time data on the response of cancer to current therapies.

Discovery of γ-H2AX expression in CTCs, can potentially be used to determine response to treatment, early after chemotherapy in OC patients (Toss *et al.*, 2014). Accumulation of γ-H2AX is an early response to DSB-DNA damage and a sensitive indicator of drug efficiency (Redon *et al.*, 2012). By monitoring the DNA damage, it is possible to predict tumour cell survival after cytotoxin drugs exposure *in situ* (Shah *et al.*, 2015). Additionally, it is possible to find out if the patient is responding to the therapeutic regime using sequential sampling that is non-invasive, through evaluation of both numbers of CTCs and level of γ-H2AX expression before and after treatment. The feasibility of γ-H2AX quantification as a predictive biomarker of response in CTCs in OC has been attempted here. My preliminary results show that the CTCs level with positive γ-H2AX and WT1 staining dropped following chemotherapy treatment including carboplatin, liposomal doxorubicin, gemcitabine and paclitaxel, most likely indicating a reduction in circulating cancer-associated cells. Additionally, the effect of PARP-inhibitors in relapsed OC patients was investigated and

again a reduction in levels of γ-H2AX and WT1 positive cells was observed, following niraparib treatment. The presence of WT1 in the same cells with increased γ-H2AX, confirms that these are most likely to be cancer-associated cells with drug-induced DNA damage.

Furthermore, accurate confirmation and validatory studies in vitro and in vivo would be needed but γ-H2AX is a potential pharmacodynamic biomarker which can be used to define the genotoxic ability of novel anti-cancer drugs in patients. Thus γ-H2AX assays may facilitate personalized cancer management where such changes could allow immediate proof of efficacy / futility of the current therapy and the ability to rapidly alter treatment regimens where required.

In summary, the two main goals for clinical use of γ-H2AX monitoring in cancer therapy includes first, γ-H2AX is a potential pharmacodynamic biomarker which can be used to define the genotoxic ability of novel anti-cancer drugs in patients. The second one is, γ-H2AX assays that might possibly allow to personalize the treatment which is the next step in cancer treatment. Moreover, identification and evaluation of new liquid biomarkers can allow to develop new therapeutic targets and enlighten the biology of cancer spread. Additionally, real-time measurements of liquid biomarkers, can possibly assist to identify variations in the cancer biology, mainly during drug treatment where these alterations could provide an ineffectiveness of patients' treatment, applying rapid modifications regarding to therapeutic regimes. In that matter, it has been established that liquid biomarkers have a huge potential in a clinical setting. By predicting and monitoring patient treatment, it is possible to determine the best drugs for the patient based on their genomic profile, along with an effective treatment update due to drug resistance for example which can lead to poor response.

Here, I created a pipeline to identify robust liquid biomarkers, as shown in Fig 106.

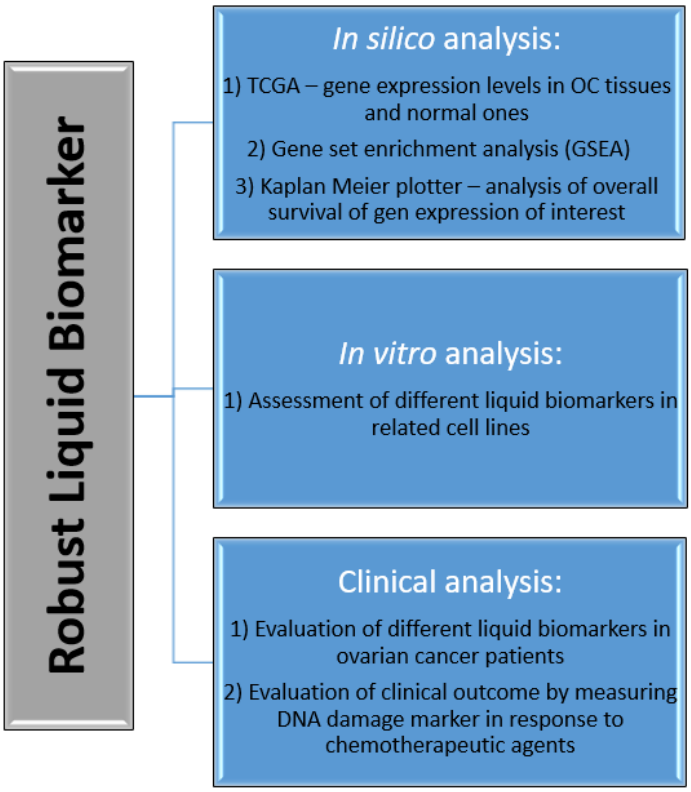

Figure 106. Flow diagram of liquid biopsy identification. Discovery of liquid biomarker is defined by *in silico*, *in vitro* and clinical analysis.

7.5. Limitations of the study

7.5.1. *In vitro*-related limitation

There are number of limitations in this work. I did not assess γ-H2AX and WT1 in BRCA1-m OC cell lines such as IGROV-1 and SNU-251, to evaluate the effect of BRCA1 mutation on homologous recombination efficiency. Given the differing clinical attributes of patients with BRCA1 and 2 mutations, and the differing locations of these genes, it is likely that there will be differences, possibly of great interest. The lack of a normal ovarian cancer cell line as a control is another major limitation. Normal human ovarian surface epithelial (OSE) cells, the source of most human ovarian carcinomas, have a very limited lifespan in culture. Creation of immortalized OSE cell lines requires inactivation of pRb and p53 protein function which regularly result in an enhanced chromosome instability during prolonged culture (Li *et al.*, 2007). Due to ethical restrictions, I were unable to obtain normal tissue and generate primary cell cultures.

7.5.2. Technological limitations

Major challenges have been encountered in attempting to develop reliable methods to capture and enumerate CTCs. CELLSEARCH® is the first FDA-approved and standardised system

to detect and quantify CTCs of epithelial origin including CD45-, EpCAM+ and Cytokeratins8/18+/19+, from 7.5 mL blood sample. Although the cell numbers are extremely low, it claims to show a high level of sensitivity and specificity in certain tumour types – e.g. breast and prostate cancer (Cell Search, 2021). Other methodologies, such as Parsortix and ISET, have varying results and have not been evaluated here but should be taken into consideration for further studies. ImageStream, whilst allowing for the quantification of large number of cells has limited resolution for the quantification of γ-H2AX foci. *In situ* fluorescence microscopy is considerably more accurate in this respect (Parris *et al.*, 2015).

There are some challenges regarding to count the foci in each cell and distinguishing between diffuse staining and foci staining in samples taken from OC patients. Pairing γ-H2AX with additional biomarkers could be potentially useful to differentiate γ-H2AX foci from apoptotic γ-H2AX. Colocalization of γ-H2AX with histone H2B phosphorylation on serine 14 (Solier *et al.*, 2009), phosphorylated Hsp90α (Solier *et al.*, 2012), and MDC1 (or 53-BP1) (Solier and Pommier, 2011) could improve recognition of the differences (Solier and Pommier, 2014).

Although there are several methods to detect DNA damage, including immunohistochemistry and γ-H2AX immunofluorescence, not all methods are suitable for routine clinical use. For example, while FACS analysis of γ-H2AX has a high sensitivity level compared to the alkaline comet assay (Ismail, Wadhra and Hammarsten, 2007), it does not separate CTCs from normal blood cells(Olive *et al.*, 1999). Furthermore, it has a low sensitivity to distinguish CTCs, even if it could detect them. In comparison to other techniques, the combination of CTCs with nuclear γ-H2AX detection is not only a distinctive and enhanced approach, but also practical to be used in clinical trials of molecular-targeted oncology drugs (Wang *et al.*, 2010a). However, the methods can be labour- and time-intensive which limits their applicability in terms of clinical use for monitoring tumour response after chemotherapy treatment (Wang *et al.*, 2010b).

7.5.3. Clinical limitations

There are also further limitations in my study, relating to the small number of clinical samples available for validation using qRT-PCR. It might be possible to gain better insight by comparing γ-H2AX immunostaining with benign ovarian tissue from normal age-matched controls instead of NAT tissue as well. It is essential to overcome the shortfalls before considering clinical application, along with more larger sample size testing. Further

unreliability also comes from using a single broad-spectrum marker rather than multiple specific markers to detect CTCs. Current systems of CTC assay are limited to cell membrane antigens including HER2, MUC1, and EGFR, none of which are specifically relevant for high grade ovarian cancer which is associated with intracellular mutant p53 and WT1 proteins. Using such multiple and highly specific markers for ovarian cancer cells may allow verification of cells with uncertain cytokeratin staining.

There are many ongoing scientific discussions in the field, regarding to the biological meaning of residual DNA damage foci which might continue for many days following high/low dose of irradiation (Ahmed *et al.*, 2012). Many different mechanisms have been examined that possibly contribute to this effect, including delayed or ineffective γ-H2AX dephosphorylation (Grudzenski *et al.*, 2010); the induction of secondary, bystander-type foci which exists much longer compared to directly induced foci (Ojima *et al.*, 2011) and DNA damage foci accumulation in senescent cells (Sedelnikova *et al.*, 2004) where they might be related to telomeres (Fumagalli *et al.*, 2013).

Fumagalli *et al.*, 2013 suggested that when cells are exposed to DNA damage sources including exogenous or endogenous, it generates DSBs, leading to trigger DDR foci formation. Most lesions will be repaired over time, which I have shown in vitro. DNA damage foci, and particularly γ-H2AX, have been used widely as a DNA damage marker or repair in research studies (Valdiglesias *et al.*, 2013). For example, detection of γ-H2AX was used to show that Radium 223 decreases the number of CTCs in prostate cancer patients, on the CellSearch platform (NIH, 2021a). Some chemotherapeutic agents may lead to an accumulation of γ-H2AX which is unrelated to ds breaks e.g., topo 1 inhibitors, alternative nuclear biomarkers would be required to develop this approach (Smirnov *et al.*, 2005). However DSBs that appear at telomeres will not be repaired and this leads to continual DDR foci formation which resulting in the constant activated DNA damage-induced checkpoint state which is known as cellular senescence (Fumagalli *et al.*, 2013). The examination that DNA damage created at telomeres resists repair is certainly of relevance for ageing studies with accumulating DNA damage (Herbig *et al.*, 2006) but there is less evidence in cancer.

7.6. Future work

Metastatic cancer is often difficult to biopsy and uncomfortable for patients. Therapy is inevitably based on analysis of cancer cells from a diagnostic biopsy or primary surgery. This may not be representative of any active metastatic clones. This is part of the attraction of a liquid biopsy where theoretically cells from the most active neoplastic clone are represented

(Dent *et al.*, 2016). Homologous recombination deficiency (HRD) has recently been recognised as an important factor in determining optimal management of patients with high grade serous ovarian cancer. Those with BRCA 1 and 2 and other more common genetic mutations such as RAD51 and PALB2 genes (Lord and Ashworth, 2012b) are readily identified by sequencing but ~30% of this population harbour HRD with no observable genetic mutations. Currently there are 2 licensed commercial tests which evaluate HRD in patients. Both require DNA from cancer tissue, and neither are fully reliable. If a 'liquid biopsy' could identify the patients with HRD, this would be a major step forward.

My work with γ-H2AX in CTCs lends itself to this approach but there is much to be done. Measurements of alterations in histone post-translational modifications (PTMs), including but not limited to γ-H2AX, require investigation as do the detection of HRR deficiencies at the mRNA/protein level. RAD51 has a key role in HR repair and mediates pairing of homologous DNA sequences and strand invasion (Baumann and West, 1998) (Tarsounas, Davies and West, 2004) RAD51 is overexpressed in different cancer cell lines and correlated with resistance to DNA damaging treatment (Klein, 2008) (Adam-Zahir *et al.*, 2015). Identification of concomitant repair genes such as RAD51 and RAD51AP1 would consolidate my work with the γ-H2AX findings demarcating HR damage. This can be of particular interest for personalised medicine approaches, since tumour cells display deficiencies in HRR, and are thus vulnerable to particular anticancer drugs (Gachechiladze *et al.*, 2017).

Genetic instability is a hallmark of ovarian cancer and approximately 50% of OC patients harbour homologous recombination repair deficiencies (HRD). HRD has been successfully exploited using PARP inhibitors (PARPi) in patients with germline BRCA1/2 mutations (BRCAm). Approximately 80% patients with relapsed OC (ROC) are BRCA1/2 wildtype (BRCAwt), but many also respond to PARPi for shorter periods of time. Interestingly, clinical trials have also shown that a further significant cohort of patients who do not bear these HRD 'scars' nor have BRCA mutations also respond to PARPi. Current FDA approved tests for HRD are time-consuming and require quantities of tumour DNA which is not available in ~30% of patients. Liquid biopsies allow easily accessible serial monitoring in ovarian cancer, possibly from cells with more representative and immediately threatening molecular profiles than found in tissue samples. Liquid biopsies allow easily accessible serial monitoring in ovarian cancer, possibly from cells with more representative and immediately threatening molecular profiles than found in tissue samples. We hypothesise that the

formation of γ-H2AX in response to DNA double stranded breaks (DSBs) in non-haematopoetic circulating cells (circulating tumour cells, CTCs) could provide the basis for a sensitive non-invasive assay. Ultimately, this would enable more effective treatment planning and the development of tactics to prevent resistance (Colomba *et al.*, 2019).

Developing novel HRD biomarkers for ovarian cancer based on liquid biopsies, will have profound implications in healthcare. The total amount of OC costs in UK (NHS) is £460million/year, with the cost per patient being £65,740. Earlier detection and better treatment will lead to savings of £16 million/year (source: CRUK). Data obtained from this study will provide benefits to OC healthcare providers by: providing a more accurate tool for monitoring therapeutic response and repeated longitudinal sampling to assess changes in cancer will be easier using 'circulating' liquid biopsies. Ultimately, this will lead to improvements in attempting earlier diagnosis of ovarian cancer and reductions in mortality.

Appendix A

A.1. Extended Tables

Table 16.Patient information. Details of patients used in this study.

Patient Trial ID	Cycle	y-H2AX/100 cell	WT1/100 cell	y-H2AX + WT1/100 cell	BRCA-Positive
P023	end	4	4+2(dots)	4	No
LP020	EOT	1(cytoplasmic)	0	0	No
LP041	EOT	2+3(dots)	2	2	BRCA2
P114	mid	16+2(dots)	16	16	No
P203	start	1+2(cytoplasmic)	0	0	No
P196	mid-b	4(dots)	0	0	No
P110	EOT	2+2(ring)	0	0	YES
P149	mid-b	3+2(apoptotic ring)	3	3	No
P051	FU4	12+1(apoptotic ring)	12	12	No
P046	2 4	2+1(dots) 2+2(dots)	2 0	2 0	No
LP022	FU	1(cytoplasmic)	0	0	No
P234	start	12+1(dots)	12	12	BRCA VUS (may not behave like true BRCA-m
	mid-b	6+4(cytoplasmic)	6	6	
P239	Visit-3	5 (dots)+3	3	3	No
P240	EOT	1+1(dots)+1(ring)	1(dots)+1	1	YES(BRCA1)
P241	early MID	2+1(dots) 13+ 4(ring)	2 13	2 13	No
P080	FU2	3(ring)+4	0	0	No
P244	SCR	17 (1 with dots)	16	16	No
P248	SCR	11+2(dots)	4	4	No
P255	SCR	4+2(dots)	0	0	No
P256	SCR	1(apoptotic ring)	0	0	No
P265	SCR	2(cytoplasmic)+2+2(foci)	2	2	No
P273	SCR	9+3 foci	9	9	No

Table 17. 19 ongoing or recruiting trials on OC using Rucaparib (NIH, 2021b).

Row	Status	Study title	Conditions	Interventions
1	Completed	A Study of Oral Rucaparib in Patients with a Solid Tumour (Phase I) or with gBRCA Mutation	• Ovarian Cancer • Fallopian Tube Cancer	Drug: Rucaparib

		Ovarian Cancer (Phase II)	• Peritoneal Cancer • Advanced Solid Tumour with Evidence of Germline or Somatic BRCA	
2	Not yet recruiting	Rucaparib maintenance After Bevacizumab Maintenance Following Carboplatin Based First Line Chemotherapy in Ovarian Cancer Patients	• Ovarian Cancer • Fallopian Tube Cancer • Primary Peritoneal Cancer • Clear Cell Carcinoma	Drug: Rucaparib Drug: Placebos
3	Active, not recruiting	A Study of Rucaparib as Switch Maintenance Following Platinum-Based Chemotherapy in Patients with Platinum-Sensitive, High-Grade Serous or Endometrioid Epithelial Ovarian, Primary Peritoneal or Fallopian Tube Cancer	• Ovarian Cancer • Fallopian Tube Cancer • Peritoneal Cancer	Drug: Rucaparib Drug: Placebos
4	Active, not recruiting	A Study in Ovarian Cancer Patients Evaluating Rucaparib and Nivolumab as Maintenance Treatment Following Response to Front-Line Platinum-Based Chemotherapy	• Epithelial Ovarian Cancer • Primary Peritoneal • Fallopian Tube Cancer • Newly diagnosed • FIGO Stage III-IV • Partial Response • Complete Response	Drug: Rucaparib Drug: Nivolumab Drug: Placebo Oral Tablet Drug: Placebo IV Infusion
5	Active, not recruiting	A Study Evaluating the Safety, Pharmacokinetics and Efficacy of Ipatasertib Administered in Combination with Rucaparib in Participants with Advanced Breast, Ovarian Cancer, and Prostate Cancer.	• Breast Cancer • Prostate Cancer • Ovarian Cancer	Drug: Part 1, Dose Level 1 and Dose Level 2a: Ipatasertib Drug: Part 1, Dose level 2b and dose level 3: Ipatasertib Drug: Part 1, Dose Level 1 and Dose Level 2b: Rucaparib Drug: Part 1, Dose Level 2a and Dose Level 3: Rucaparib
6	Active, not recruiting	ARIEL4: A Study of Rucaparib Versus Chemotherapy BRCA Mutant Ovarian, Fallopian Tube, or Primary Peritoneal Cancer Patients	• Ovarian Cancer • Epithelial Ovarian Cancer • Fallopian Tube Cancer • Peritoneal Cancer	Drug: Chemotherapy Drug: Rucaparib
7	Completed	Rucaparib (CO-338; Formally Called AG-014699 or PF-0136738) in Treating Patients with Locally Advanced or Metastatic Breast Cancer or Advanced Ovarian Cancer	• BRCA1 Mutation Carrier • BRCA2 Mutation Carrier • Breast Cancer • Ovarian Cancer	Drug: rucaparib (CO-338; formally AG-014699 or PF-01367338) Genetic: protein expression analysis Genetic: western blotting Other: immunohistochemistry staining method Other: liquid chromatography

				Other: mass spectrometry Other: pharmacological study
8	Recruiting	A Phase II Study of Nivolumab/Bevacizumab/Rucaparib	• Peritoneal Cancer • Ovarian Cancer • Fallopian Tube Cancer	Drug: Bevacizumab Drug: Nivolumab Drug: Rucaparib
9	Active, not recruiting	A Study of Rucaparib in Patients with Platinum-Sensitive, Relapsed, High-Grade Epithelial Ovarian, Fallopian Tube, or Primary Peritoneal Cancer (ARIEL2)	• Ovarian Cancer • Epithelial Ovarian Cancer • Fallopian Tube Cancer • Peritoneal Cancer	Drug: Oral rucaparib
10	Recruiting	Analysis of the Clinical Experience with Rucaparib in the Rucaparib Access Program (RAP) in Spain - A GEICO Study	• Epithelial Ovarian Cancer • Fallopian Tube Cancer • Primary Peritoneal Cancer	Drug: Rucaparib
11	Enrolling by invitation	CATCH-R: A Rollover Study to Provide Continued Access to Rucaparib	• Metastatic Castration-Resistant Prostate Cancer • Ovarian Cancer • Epithelial Ovarian Cancer • Fallopian Tube Cancer • Peritoneal Cancer • Other Solid Tumour	Drug: Rucaparib
12	Active, not recruiting	A Study to Evaluate Rucaparib in Combination with Other Anticancer Agents in Patients with a Solid Tumor (SEASTAR)	• Ovarian Cancer • Triple-negative Breast Cancer • Urothelial Carcinoma • Solid Tumour	Drug: Rucaparib Drug: Lucitanib Drug: Sacituzumab govitecan
13	Terminated	A Study to Evaluate Rucaparib in Combination with Nivolumab in Patients with Selected Solid Tumours (ARIES)	• Epithelial Ovarian Cancer • Fallopian Tube Cancer • Primary Peritoneal Carcinoma • High Grade Serous Carcinoma • Endometrioid Adenocarcinoma	Drug: Rucaparib Drug: Nivolumab
14	Recruiting	Chk2 Inhibitor for Recurrent Epithelial Peritoneal, Fallopian or Ovarian Cancer (CREATIVE Phase IA Trial)	• Platinum-resistant Ovarian Cancer • Platinum-refractory Ovarian Carcinoma • Platinum-Resistant Fallopian Tube Carcinoma • Platinum-Resistant Primary Peritoneal Carcinoma	Drug: PHI-101 administration

15	Active, not recruiting	Mirvetuximab Soravtansine and Rucaparib Camsylate in Treating Participants with Recurrent Endometrial, Ovarian, Fallopian Tube or Primary Peritoneal Cancer	• BRCA1 Gene Mutation • BRCA2 Gene Mutation • Folate Receptor Alpha Positive • Recurrent Fallopian Tube Carcinoma • Recurrent Ovarian Carcinoma • Recurrent Primary Peritoneal Carcinoma • Recurrent Uterine Corpus Carcinoma • Recurrent Uterine Serous Carcinoma • Recurrent Uterine Carcinosarcoma • Platinum Resistant Ovarian Cancer	Other: Laboratory Biomarker Analysis Biological: Mirvetuximab Soravtansine Other: Pharmacokinetic Study Drug: Rucaparib Camsylate
16	Recruiting	Microdevice In Ovarian, Fallopian Tube, And Peritoneal Cancer	• Ovarian Cancer • Fallopian Tube Cancer • Peritoneal Cancer • Ovarian Cancer • Fallopian Tube Cancer • Peritoneal Cancer	Combination Product: Microdevice
17	Recruiting	A Study to Evaluate Rucaparib in Patients with Solid Tumours and With Deleterious Mutations in HRR Genes	• Solid Tumour	Drug: Rucaparib
18	Recruiting	Carboplatin-Paclitaxel-Bevacizumab vs Carbo-Pacli-Beva-Rucaparib vs Carbo-Pacli-Ruca, Selected According to HRD Status, in Patients with Advanced Ovarian, Primary Peritoneal and Fallopian Tube Cancer, Preceded by a Phase I Dose Escalation Study on Ruca-Beva Combination	• Advanced (Stage IIIB-C-IV) Ovarian, Primary Peritoneal and Fallopian Tube Cancer	Drug: Carboplatin Drug: Paclitaxel Drug: Bevacizumab Drug: Rucaparib
19	Terminated	Open-Label Safety and Tolerability Study of INCB057643 in Subjects with Advanced Malignancies	• Solid Tumour	Drug: INCB057643 Drug: Gemcitabine Drug: Paclitaxel Drug: Rucaparib Drug: Abiraterone Drug: Ruxolitinib Drug: Azacitidine

Bibliography

Abaji, C., Cousineau, I. and Belmaaza, A. (2005) 'BRCA2 regulates homologous recombination in response to DNA damage: Implications for genome stability and carcinogenesis', *Cancer Research*, 65(10), pp. 4117–4125. doi: 10.1158/0008-5472.CAN-04-3071.

Al Abo, M. *et al.* (2014) 'Compensatory functions and interdependency of the DNABinding domain of BRCA2 with the BRCA1-PALB2-BRCA2 complex', *Cancer Research*, 74(3), pp. 797–807. doi: 10.1158/0008-5472.CAN-13-1443.

ACS (2018) *Sign annd Symptoms of Ovarian Cancer, American cancer society*. Available at: https://www.cancer.org/cancer/ovarian-cancer/detection-diagnosis-staging/signs-and-symptoms.html.

Adalsteinsson, V. A. *et al.* (2017) 'Scalable whole-exome sequencing of cell-free DNA reveals high concordance with metastatic tumors', *Nature Communications*, 8(1). doi: 10.1038/s41467-017-00965-y.

Adam-Zahir, S. *et al.* (2015) 'Increased γ-H2AX and Rad51 DNA Repair Biomarker Expression in Human Cell Lines Resistant to the Chemotherapeutic Agents Nitrogen Mustard and Cisplatin', *Chemotherapy*, 60(5–6), pp. 310–320. doi: 10.1159/000430086.

Ahmed, E. A. *et al.* (2012) 'Persistent DNA damage after high dose in vivo Gamma exposure of Minipig skin', *PLoS ONE*, 7(6). doi: 10.1371/journal.pone.0039521.

Aktas, B. *et al.* (2011) 'Molecular profiling and prognostic relevance of circulating tumor cells in the blood of ovarian cancer patients at primary diagnosis and after platinum-based chemotherapy', *International Journal of Gynecological Cancer*, 21(5), pp. 822–830. doi: 10.1097/IGC.0b013e318216cb91.

Alemar, J. and Schuur, E. R. (2013) 'Progress in using circulating tumor cell information to improve metastatic breast cancer therapy', *Journal of Oncology*, 2013. doi: 10.1155/2013/702732.

Alix-Panabieѐres, C. and Pantel, K. (2013) 'Circulating tumor cells: Liquid biopsy of cancer', *Clinical Chemistry*, 59(1), pp. 110–118. doi: 10.1373/clinchem.2012.194258.

Alix-Panabières, C. and Pantel, K. (2016) 'Clinical applications of circulating tumor cells and circulating tumor DNA as liquid biopsy', *Cancer Discovery*, 6(5), pp. 479–491. doi: 10.1158/2159-8290.CD-15-1483.

Alphametrix (2015) *EVE™ Automatic Cell Counter*. Available at: http://www.alphametrix.de/page/index.php?category=cellanalytic&pageid=156 (Accessed: 15 October 2018).

Alsop, K. *et al.* (2012) 'BRCA mutation frequency and patterns of treatment response in BRCA mutation-positive women with ovarian cancer: A report from the Australian ovarian cancer study group', *Journal of Clinical Oncology*, 30(21), pp. 2654–2663. doi: 10.1200/JCO.2011.39.8545.

Altomare, D. A. *et al.* (2004) 'AKT and mTOR phosphorylation is frequently detected in ovarian cancer and can be targeted to disrupt ovarian tumor cell growth', *Oncogene*, 23(34), pp. 5853–5857. doi: 10.1038/sj.onc.1207721.

Andorfer, P. *et al.* (2016) 'Vascular endothelial growth factor A as predictive marker for mTOR inhibition in relapsing high-grade serous ovarian cancer', *BMC Systems Biology*, 10(1), pp. 1–12. doi: 10.1186/S12918-016-0278-Z.

Aran, D. *et al.* (2017) 'Comprehensive analysis of normal adjacent to tumor transcriptomes', *Nature Communications*, 8(1), pp. 1–13. doi: 10.1038/s41467-017-01027-z.

Arora, S. *et al.* (2021) 'FDA Approval Summary: Olaparib Monotherapy or in Combination with Bevacizumab for the Maintenance Treatment of Patients with Advanced Ovarian

Cancer', *Oncologist*, 26(1), pp. e164–e172. doi: 10.1002/onco.13551.
ATCC (2016) *SK-OV-3 [SKOV-3; SKOV3] (ATCC® HTB-77™), ATCC*. Available at: https://www.lgcstandards-atcc.org/Products/All/HTB-77.aspx?geo_country=gb# (Accessed: 21 October 2018).
Attard, G. and de Bono, J. S. (2011) 'Utilizing circulating tumor cells: Challenges and pitfalls', *Current Opinion in Genetics and Development*, 21(1), pp. 50–58. doi: 10.1016/j.gde.2010.10.010.
Avastin (2021) *What are the benefits and risks of Avastin for ovarian cancer (OC)?* Available at: https://www.avastin.com/patient/ovar/treatment/benefits-risks.html (Accessed: 5 July 2021).
Balmus, G. *et al.* (2019) 'ATM orchestrates the DNA-damage response to counter toxic non-homologous end-joining at broken replication forks', *Nature Communications*, 10(1), pp. 1–18. doi: 10.1038/s41467-018-07729-2.
Banerjee, S. and Gore, M. (2009) 'The Future of Targeted Therapies in Ovarian Cancer', *The Oncologist*, 14(7), pp. 706–716. doi: 10.1634/theoncologist.2009-0013.
Banys-Paluchowski, M. *et al.* (2020) 'Clinical relevance of circulating tumor cells in ovarian, fallopian tube and peritoneal cancer', *Archives of Gynecology and Obstetrics*, 301(4), pp. 1027–1035. doi: 10.1007/s00404-020-05477-7.
Bassing, C. H. *et al.* (2002) 'Increased ionizing radiation sensitivity and genomic instability in the absence of histone H2AX', *Proceedings of the National Academy of Sciences of the United States of America*, 99(12), pp. 8173–8178. doi: 10.1073/pnas.122228699.
Bassing, C. H. *et al.* (2003) 'Histone H2AX: A dosage-dependent suppressor of oncogenic translocations and tumors', *Cell*, 114(3), pp. 359–370. doi: 10.1016/S0092-8674(03)00566-X.
Baumann, P. and West, S. C. (1998) 'Role of the human RAD51 protein in homologous recombination and double- stranded-break repair', *Trends in Biochemical Sciences*, 23(7), pp. 247–251. doi: 10.1016/S0968-0004(98)01232-8.
Beaufort, C. M. *et al.* (2014) 'Ovarian cancer cell line panel (OCCP): Clinical importance of in vitro morphological subtypes', *PLoS ONE*, 9(9). doi: 10.1371/journal.pone.0103988.
Benafif, S. and Hall, M. (2015) 'An update on PARP inhibitors for the treatment of cancer', *OncoTargets and Therapy*, 8, pp. 519–528. doi: 10.2147/OTT.S30793.
Benton, C. B. *et al.* (2003) 'H2AX Haploinsufficiency Modifies Genomic Stability and Tumor Susceptibility', *Cell*, 114(3), pp. 371–383. doi: 10.1016/j.critrevonc.2015.03.002.Chronic.
Bettegowda, C. *et al.* (2014) 'Detection of circulating tumor DNA in early- and late-stage human malignancies', *Science Translational Medicine*, 6(224). doi: 10.1126/scitranslmed.3007094.
BetterthanBRCA (2019) *11 Facts You Need To Know About BRCA And Genetic Breast Cancer*. Available at: https://www.betterthanbrca.com/en/11-facts-about-brca-genetic-mutation-breast-cancer/ (Accessed: 16 December 2020).
Biobank (2014) 'Integrating electronic health records into the UK Biobank Resource'. Available at: http://biobank.ctsu.ox.ac.uk/crystal/crystal/docs/DataLinkageProcess.pdf.
Blassl, C. *et al.* (2016) 'Gene expression profiling of single circulating tumor cells in ovarian cancer – Establishment of a multi-marker gene panel', *Molecular Oncology*, 10(7), pp. 1030–1042. doi: 10.1016/j.molonc.2016.04.002.
Bonner, W. M. *et al.* (2008) 'γH2AX and cancer', *Nature Reviews Cancer*, 8(12), pp. 957–967. doi: 10.1038/nrc2523.
Brabletz, T. (2012) 'EMT and MET in Metastasis: Where Are the Cancer Stem Cells?', *Cancer Cell*, 22(6), pp. 699–701. doi: 10.1016/j.ccr.2012.11.009.
Brandsma, I. and Gent, D. C. (2012) 'Pathway choice in DNA double strand break repair:

Observations of a balancing act', *Genome Integrity*, 3, pp. 1–10. doi: 10.1186/2041-9414-3-9.
Brown, J. S., Kaye, S. B. and Yap, T. A. (2016) 'PARP inhibitors: The race is on', *British Journal of Cancer*, 114(7), pp. 713–715. doi: 10.1038/bjc.2016.67.
Bryant, H. E. *et al.* (2005) 'Specific killing of BRCA2-deficient tumours with inhibitors of poly(ADP-ribose) polymerase', *Nature*, 434(7035), pp. 913–917. Available at: file:///C:/Users/sayeh/Dropbox/My PC (LAPTOP-VSN7VDJR)/Desktop/PhD/Thesis Data(1)/Chapter-2(Rucaparib)/PARP paper/New folder/nature03443.pdf.
Bryant, H. E. *et al.* (2007) 'Erratum: Specific killing of BRCA2-deficient tumours with inhibitors of poly(ADP-ribose) polymerase (Nature (2005) 434, (913-917))', *Nature*, 447(7142), p. 346. doi: 10.1038/nature05789.
Buis, J. *et al.* (2012) 'Mre11 regulates CtIP-dependent double-strand break repair by interaction with CDK2', *Nature Structural and Molecular Biology*, 19(2), pp. 246–253. doi: 10.1038/nsmb.2212.
Bunnell, A. E. *et al.* (2017) 'The Clinical Utility of Next Generation Sequencing Results in a Community-Based Hereditary Cancer Risk Program', *Journal of Genetic Counseling*, 26(1), pp. 105–112. doi: 10.1007/s10897-016-9985-2.
Bunting, S. F. *et al.* (2012) 'BRCA1 Functions Independently of Homologous Recombination in DNA Interstrand Crosslink Repair', *Molecular Cell*, 46(2), pp. 125–135. doi: 10.1016/j.molcel.2012.02.015.
Buys, S. S. *et al.* (2011) 'Effect of screening on ovarian cancer mortality: The Prostate, Lung, Colorectal and Ovarian (PLCO) cancer screening randomized controlled trial', *JAMA - Journal of the American Medical Association*, 305(22), pp. 2295–2302. doi: 10.1001/jama.2011.766.
Bycroft, C. *et al.* (2018) 'The UK Biobank resource with deep phenotyping and genomic data', *Nature*, 562(7726), pp. 203–209. doi: 10.1038/s41586-018-0579-z.
Capizzi, E. *et al.* (2008) 'Quantification of free plasma DNA before and after chemotherapy in patients with advanced epithelial ovarian cancer', *Diagnostic Molecular Pathology*, 17(1), pp. 34–38. doi: 10.1097/PDM.0b013e3181359e1f.
Cardnell, R. J. *et al.* (2016) 'Activation of the PI3K/mTOR pathway following PARP inhibition in small cell lung cancer', *PLoS ONE*, 11(4), pp. 1–17. doi: 10.1371/journal.pone.0152584.
Carey, J. P. W. *et al.* (2019) 'cancer', 78(3), pp. 742–757. doi: 10.1158/0008-5472.CAN-17-1494.Synthetic.
Cassidy, L. D., Liau, S. S. and Venkitaraman, A. R. (2014) 'Chromosome instability and carcinogenesis: Insights from murine models of human pancreatic cancer associated with BRCA2 inactivation', *Molecular Oncology*, 8(2), pp. 161–168. doi: 10.1016/j.molonc.2013.10.005.
Catena, V. and Fanciulli, M. (2017) 'Deptor: Not only a mTOR inhibitor', *Journal of Experimental and Clinical Cancer Research*, 36(1), pp. 1–9. doi: 10.1186/s13046-016-0484-y.
cBioPortal (2021) *BRCA2 mutations*. Available at: https://www.cbioportal.org/results/mutations?case_set_id=all&gene_list=BRCA2&cancer_study_list=5c8a7d55e4b046111fee2296&mutations_gene=BRCA2 (Accessed: 17 July 2021).
Ceccaldi, R., Rondinelli, B. and D'Andrea, A. D. (2016) 'Repair Pathway Choices and Consequences at the Double-Strand Break', *Trends in Cell Biology*, 26(1), pp. 52–64. doi: 10.1016/j.tcb.2015.07.009.
Cell Search (2021) *The CELLSEARCH® System—Explore Our Platform*. Available at: https://www.cellsearchctc.com/product-systems-overview (Accessed: 3 September 2021).
Cerbinskaite, A. *et al.* (2012) 'Defective homologous recombination in human cancers', *Cancer Treatment Reviews*, 38(2), pp. 89–100. doi: 10.1016/j.ctrv.2011.04.015.

Chapman, J. R. *et al.* (2013) 'RIF1 Is Essential for 53BP1-Dependent Nonhomologous End Joining and Suppression of DNA Double-Strand Break Resection', *Molecular Cell*, 49(5), pp. 858–871. doi: 10.1016/j.molcel.2013.01.002.
Chatterjee, N., Walker, G. C. (2017) 'Mechanisms of DNA damage, repair, and mutagenesis. Environmental and molecular mutagenesis', *Physiology & behavior*, 58(5), pp. 235–263. doi: 10.1002/em.22087.Mechanisms.
Chen, S. and Parmigiani, G. (2007) 'Meta-analysis of BRCA1 and BRCA2 penetrance', *Journal of Clinical Oncology*, 25(11), pp. 1329–1333. doi: 10.1200/JCO.2006.09.1066.
Cheng, X. *et al.* (2017) 'Circulating cell-free DNA and circulating tumor cells, the "liquid biopsies" in ovarian cancer', *Journal of Ovarian Research*, 10(1), pp. 1–10. doi: 10.1186/s13048-017-0369-5.
Cho, D. H. *et al.* (2015) 'The expression of DBC1/CCAR2 is associated with poor prognosis of ovarian carcinoma', *Journal of Ovarian Research*, 8(1), pp. 1–11. doi: 10.1186/s13048-015-0129-3.
Chudasama, D. *et al.* (2019) 'Liquid biopsies in lung cancer: Four emerging technologies and potential clinical applications', *Cancers*, 11(3), pp. 1–20. doi: 10.3390/cancers11030331.
Chun, J., Buechelmaier, E. S. and Powell, S. N. (2013) 'Rad51 Paralog Complexes BCDX2 and CX3 Act at Different Stages in the BRCA1-BRCA2-Dependent Homologous Recombination Pathway', *Molecular and Cellular Biology*, 33(2), pp. 387–395. doi: 10.1128/mcb.00465-12.
Clamp, A. R. *et al.* (2019) 'Weekly dose-dense chemotherapy in first-line epithelial ovarian, fallopian tube, or primary peritoneal carcinoma treatment (ICON8): primary progression free survival analysis results from a GCIG phase 3 randomised controlled trial', *The Lancet*, 394(10214), pp. 2084–2095. doi: 10.1016/S0140-6736(19)32259-7.
Coleman, K. A. and Greenberg, R. A. (2011) 'The BRCA1-RAP80 complex regulates DNA repair mechanism utilization by restricting end resection', *Journal of Biological Chemistry*, 286(15), pp. 13669–13680. doi: 10.1074/jbc.M110.213728.
Coleman, R. L. *et al.* (2017) 'Rucaparib maintenance treatment for recurrent ovarian carcinoma after response to platinum therapy (ARIEL3): a randomised, double-blind, placebo-controlled, phase 3 trial', *The Lancet*, 390(10106), pp. 1949–1961. doi: 10.1016/S0140-6736(17)32440-6.
Colomba, E. *et al.* (2019) 'Rucaparib in the landscape of PARP inhibition in ovarian cancer', *Expert Review of Anticancer Therapy*, 19(6), pp. 437–446. doi: 10.1080/14737140.2019.1607302.
Cooper, G. M. (2000) *The Cell: A Molecular Approach*. 2nd Editio, *The Eukaryotic Cell Cycle*. 2nd Editio. Sinauer Associates. Available at: https://www.ncbi.nlm.nih.gov/books/NBK9876/.
Cousineau, I. and Belmaaza, A. (2011) 'EMSY overexpression disrupts the BRCA2/RAD51 pathway in the DNA-damage response: Implications for chromosomal instability/recombination syndromes as checkpoint diseases', *Molecular Genetics and Genomics*, 285(4), pp. 325–340. doi: 10.1007/s00438-011-0612-5.
CRUK (2018a) *Ovarian cancer incidence statistics*, *Cancer Research UK*. Available at: https://www.cancerresearchuk.org/health-professional/cancer-statistics/statistics-by-cancer-type/ovarian-cancer#heading-Zero.
CRUK (2018b) *Ovarian cancer risk*, *Cancer Research UK*. Available at: https://www.cancerresearchuk.org/health-professional/cancer-statistics/statistics-by-cancer-type/ovarian-cancer/risk-factors.
CRUK (2019a) *About stages and grades*, *Cancer Research*. Available at: https://www.cancerresearchuk.org/about-cancer/ovarian-cancer/stages-grades/about-stages-and-grades.

CRUK (2019b) *Epithelial ovarian cancer, Cancer Research UK*. Available at: https://www.cancerresearchuk.org/about-cancer/ovarian-cancer/types/epithelial-ovarian-cancers/epithelial#:~:text=Doctors now think that most,to the ovary and grow.
CRUK (2019c) *Ovarian cancer survival statistics, Cancer Research UK*. Available at: https://www.cancerresearchuk.org/health-professional/cancer-statistics/statistics-by-cancer-type/ovarian-cancer/survival (Accessed: 16 November 2020).
CRUK (2019d) *Stage 1, Cancer Research*. Available at: https://www.cancerresearchuk.org/about-cancer/ovarian-cancer/stages-grades/stage-1.
CRUK (2019e) *Stage 2, Cancer Research*. Available at: https://www.cancerresearchuk.org/about-cancer/ovarian-cancer/stages-grades/stage-2.
CRUK (2019f) *Stage 3, Cancer Research*.
CRUK (2019g) *Stage 4, Cancer Research*. Available at: https://www.cancerresearchuk.org/about-cancer/ovarian-cancer/stages-grades/stage-4.
Curtin, N. (2014) 'PARP inhibitors for anticancer therapy', *Biochemical Society Transactions*, 42(1), pp. 82–88. doi: 10.1042/BST20130187.
Dann, R. B. *et al.* (2012) 'BRCA1/2 mutations and expression: Response to platinum chemotherapy in patients with advanced stage epithelial ovarian cancer', *Gynecologic Oncology*, 125(3), pp. 677–682. doi: 10.1016/j.ygyno.2012.03.006.
Dasgupta, A., Lim, A. R. and Ghajar, C. M. (2017) 'Circulating and disseminated tumor cells: harbingers or initiators of metastasis?', *Molecular oncology*, 11(1), pp. 40–61. doi: 10.1002/1878-0261.12022.
Deb, S. *et al.* (2014) 'Mutational profiling of familial male breast cancers reveals similarities with luminal A female breast cancer with rare TP53 mutations', *British Journal of Cancer*, 111(12), pp. 2351–2360. doi: 10.1038/bjc.2014.511.
Dent, B. M. *et al.* (2016) 'High-resolution imaging for the detection and characterisation of circulating tumour cells from patients with oesophageal, hepatocellular, thyroid and ovarian cancers', *International Journal of Cancer*, 138(1), pp. 206–216. doi: 10.1002/ijc.29680.
Diaz, L. A. and Bardelli, A. (2014) 'Liquid biopsies: Genotyping circulating tumor DNA', *Journal of Clinical Oncology*, 32(6), pp. 579–586. doi: 10.1200/JCO.2012.45.2011.
Dickey, J. S. *et al.* (2009) 'H2AX: Functional roles and potential applications', *Chromosoma*, 118(6), pp. 683–692. doi: 10.1007/s00412-009-0234-4.
Doubeni, C. A., Doubeni, A. and Myers, A. E. (2016) 'Diagnosis and Management of Ovarian Cancer', *Am Fam Physician*, 93(11), pp. 937–44. Available at: https://www.aafp.org/afp/2016/0601/p937.html.
Drew, Y. *et al.* (2011) 'Therapeutic potential of poly(ADP-ribose) polymerase inhibitor AG014699 in human cancers with mutated or methylated BRCA1 or BRCA2', *Journal of the National Cancer Institute*, 103(4), pp. 334–346. doi: 10.1093/jnci/djq509.
Drew, Y. (2015) 'The development of PARP inhibitors in ovarian cancer: From bench to bedside', *British Journal of Cancer*, 113(S1), pp. S3–S9. doi: 10.1038/bjc.2015.394.
Drew, Y. *et al.* (2020) 'Real-World Delivery of Rucaparib to Patients with Ovarian Cancer: Recommendations Based on an Integrated Safety Analysis of ARIEL2 and Study 10', *The Oncologist*, 25(1). doi: 10.1634/theoncologist.2019-0229.
Drost, R. *et al.* (2011) 'BRCA1 RING function is essential for tumor suppression but dispensable for therapy resistance', *Cancer Cell*, 20(6), pp. 797–809. doi: 10.1016/j.ccr.2011.11.014.
ECACC (2020a) *PEO1, Public Health England*. Available at: https://www.phe-culturecollections.org.uk/products/celllines/generalcell/detail.jsp?refId=10032308&collection=ecacc_gc (Accessed: 20 April 2020).
ECACC (2020b) *PEO4, Public Health England*. Available at: https://www.phe-culturecollections.org.uk/products/celllines/generalcell/detail.jsp?refId=10032309&collection

=ecacc_gc (Accessed: 20 April 2020).
Elazezy, M. and Joosse, S. A. (2018) 'Techniques of using circulating tumor DNA as a liquid biopsy component in cancer management', *Computational and Structural Biotechnology Journal*, 16, pp. 370–378. doi: 10.1016/j.csbj.2018.10.002.
Er, T. K. *et al.* (2016) 'Targeted next-generation sequencing for molecular diagnosis of endometriosis-associated ovarian cancer', *Journal of Molecular Medicine*, 94(7), pp. 835–847. doi: 10.1007/s00109-016-1395-2.
Expasy (2020) *Cellosaurus MDAH 2774 (CVCL_0420)*. Available at: https://web.expasy.org/cellosaurus/CVCL_0420 (Accessed: 27 June 2020).
Francis, J. C. *et al.* (2010) 'Brca2 and Trp53 deficiency cooperate in the progression of mouse prostate tumourigenesis', *PLoS Genetics*, 6(6), pp. 1–9. doi: 10.1371/journal.pgen.1000995.
Freidin, M. B. *et al.* (2015) 'Circulating tumor DNA outperforms circulating tumor cells for KRAS mutation detection in thoracic malignancies', *Clinical Chemistry*, 61(10), pp. 1299–1304. doi: 10.1373/clinchem.2015.242453.
Friedman, R. (2016) 'Drug resistance in cancer: Molecular evolution and compensatory proliferation', *Oncotarget*, 7(11), pp. 11746–11755. doi: 10.18632/oncotarget.7459.
Fumagalli, M. *et al.* (2013) 'NIH Public Access', 14(4), pp. 355–365. doi: 10.1038/ncb2466.Telomeric.
Gachechiladze, M. *et al.* (2017) 'RAD51 as a potential surrogate marker for DNA repair capacity in solid malignancies', *International Journal of Cancer*, 141(7), pp. 1286–1294. doi: 10.1002/ijc.30764.
Gaitskell, K. *et al.* (2018) 'Histological subtypes of ovarian cancer associated with parity and breastfeeding in the prospective Million Women Study', *International Journal of Cancer*, 142(2), pp. 281–289. doi: 10.1002/ijc.31063.
Galia, A. *et al.* (2012) 'PARP-1 protein expression in glioblastoma multiforme', *European Journal of Histochemistry*, 56(1), pp. 45–48. doi: 10.4081/ejh.2012.e9.
Gan, A. *et al.* (2013) 'Poly(adenosine diphosphate-ribose) polymerase expression in BRCA-proficient ovarian high-grade serous carcinoma; Association with patient survival', *Human Pathology*, 44(8), pp. 1638–1647. doi: 10.1016/j.humpath.2013.01.015.
Gao, J. *et al.* (2013) 'Integrative analysis of complex cancer genomics and clinical profiles using the cBioPortal', *Science Signaling*, 6(269). doi: 10.1126/scisignal.2004088.
Garcia-Villa, A. *et al.* (2012) 'Assessment of γ-H2AX levels in circulating tumor cells from patients receiving chemotherapy', *Frontiers in Oncology*, 2(October), pp. 1–7. doi: 10.3389/fonc.2012.00128.
Garm, C. *et al.* (2013) 'Genetic and environmental influence on DNA strand break repair: A twin study', *Environmental and Molecular Mutagenesis*, 54(6), pp. 414–420. doi: 10.1002/em.21791.
Gelmon, K. A. *et al.* (2011) 'Olaparib in patients with recurrent high-grade serous or poorly differentiated ovarian carcinoma or triple-negative breast cancer: A phase 2, multicentre, open-label, non-randomised study', *The Lancet Oncology*, 12(9), pp. 852–861. doi: 10.1016/S1470-2045(11)70214-5.
George, A. (2015) 'UK BRCA mutation testing in patients with ovarian cancer', *British Journal of Cancer*, 113(S1), pp. S17–S21. doi: 10.1038/bjc.2015.396.
Gordon, W. C. *et al.* (2002) 'DNA damage and repair in light-induced photoreceptor degeneration', *Investigative Ophthalmology and Visual Science*, 43(11), pp. 3511–3521.
Gorges, T. M. *et al.* (2012) 'Circulating tumour cells escape from EpCAM-based detection due to epithelial-to-mesenchymal transition', *BMC Cancer*, 12(1), p. 1. doi: 10.1186/1471-2407-12-178.
Van Gorp, T. *et al.* (2011) 'HE4 and CA125 as a diagnostic test in ovarian cancer:

Prospective validation of the Risk of Ovarian Malignancy Algorithm', *British Journal of Cancer*, 104(5), pp. 863–870. doi: 10.1038/sj.bjc.6606092.
Grignani, G. *et al.* (2020) 'Delving into PARP inhibition from bench to bedside and back', *Pharmacology and Therapeutics*, 206, p. 107446. doi: 10.1016/j.pharmthera.2019.107446.
Grudzenski, S. *et al.* (2010) 'Inducible response required for repair of low-dose radiation damage in human fibroblasts', *Proceedings of the National Academy of Sciences of the United States of America*, 107(32), pp. 14205–14210. doi: 10.1073/pnas.1002213107.
Grunewald, T. and Ledermann, J. A. (2017) 'Targeted Therapies for Ovarian Cancer', *Best Practice and Research: Clinical Obstetrics and Gynaecology*, 41, pp. 139–152. doi: 10.1016/j.bpobgyn.2016.12.001.
GSEA (2021) *No Title*. Available at: http: //software.broadinstitute.org/gsea/index.jsp (Accessed: 20 January 2020).
Gudmundsdottir, K. and Ashworth, A. (2006) 'The roles of BRCA1 and BRCA2 and associated proteins in the maintenance of genomic stability', *Oncogene*, 25(43), pp. 5864–5874. doi: 10.1038/sj.onc.1209874.
Hacker, N. F. and Rao, A. (2017) 'Surgery for advanced epithelial ovarian cancer', *Best Practice and Research: Clinical Obstetrics and Gynaecology*, 41, pp. 71–87. doi: 10.1016/j.bpobgyn.2016.10.007.
Hauck, Z. (2020) *How Your Hormones Affect Athletic Performance and Why You Need to Start Testing, ZRT Laboratory Blog*. Available at: https://www.zrtlab.com/blog/archive/how-your-hormones-affect-athletic-performance/ (Accessed: 3 July 2021).
Hendrix, N. D. *et al.* (2006) 'Fibroblast growth factor 9 has oncogenic activity and is a downstream target of Wnt signaling in ovarian endometrioid adenocarcinomas', *Cancer Research*, 66(3), pp. 1354–1362. doi: 10.1158/0008-5472.CAN-05-3694.
Herbig, U. *et al.* (2006) 'Cellular Senescence in Aging Primates Published by : American Association for the Advancement of Science Linked references are available on JSTOR for this article : Cellular Senescence in Aging Primates', 311(5765), p. 1257.
Hiltermann, T. J. N., van der Wekken, A. J. and Groen, H. J. M. (2012) 'Moving forward with circulating tumor cells and lung cancer', *Journal of Thoracic Disease*, 4(5), pp. 440–441. doi: 10.3978/j.issn.2072-1439.2012.08.08.
Ho, S. M. (2003) 'Estrogen, progesterone and epithelial ovarian cancer', *Reproductive Biology and Endocrinology*, 1, pp. 1–8. doi: 10.1186/1477-7827-1-73.
Hoeijmakers, J. H. J. (2001) 'Genome maintenance mechanisms for preventing cancer', *Nature*, 411(6835), pp. 366–374. doi: 10.1038/35077232.
Hong, Y., Fang, F. and Zhang, Q. (2016) 'Circulating tumor cell clusters: What we know and what we expect (Review)', *International Journal of Oncology*, 49(6), pp. 2206–2216. doi: 10.3892/ijo.2016.3747.
Hoppe, M. M. *et al.* (2018) 'Biomarkers for homologous recombination deficiency in cancer', *Journal of the National Cancer Institute*, 110(7), pp. 704–713. doi: 10.1093/jnci/djy085.
Hou, J. M. *et al.* (2012) 'Clinical significance and molecular characteristics of circulating tumor cells and circulating tumor microemboli in patients with small-cell lung cancer', *Journal of Clinical Oncology*, 30(5), pp. 525–532. doi: 10.1200/JCO.2010.33.3716.
Hou, W. H., Chen, S. H. and Yu, X. (2019) 'Poly-ADP ribosylation in DNA damage response and cancer therapy', *Mutation Research - Reviews in Mutation Research*, 780(September), pp. 82–91. doi: 10.1016/j.mrrev.2017.09.004.
Howard, S. M., Yanez, D. A. and Stark, J. M. (2015) 'DNA Damage Response Factors from Diverse Pathways, Including DNA Crosslink Repair, Mediate Alternative End Joining', *PLoS Genetics*, 11(1), pp. 1–26. doi: 10.1371/journal.pgen.1004943.
Huang, B. *et al.* (2018) 'Exosomes derived from human adipose mesenchymal stem cells

improve ovary function of premature ovarian insufficiency by targeting SMAD', *Stem Cell Research and Therapy*, 9(1), pp. 1–12. doi: 10.1186/s13287-018-0953-7.
Huang, F. and Mazin, A. V. (2014) 'Targeting the homologous recombination pathway by small molecule modulators', *Bioorganic and Medicinal Chemistry Letters*, 24(14), pp. 3006–3013. doi: 10.1016/j.bmcl.2014.04.088.
Huang, W. L. *et al.* (2017) 'Liquid biopsy genotyping in lung cancer: Ready for clinical utility?', *Oncotarget*, 8(11), pp. 18590–18608. doi: 10.18632/oncotarget.14613.
Ismail, I. H., Wadhra, T. I. and Hammarsten, O. (2007) 'An optimized method for detecting gamma-H2AX in blood cells reveals a significant interindividual variation in the gamma-H2AX response among humans', *Nucleic Acids Research*, 35(5). doi: 10.1093/nar/gkl1169.
Ivashkevich, A. *et al.* (2012) 'Use of the γ-H2AX assay to monitor DNA damage and repair in translational cancer research', *Cancer Letters*, 327(1–2), pp. 123–133. doi: 10.1016/j.canlet.2011.12.025.
Jacot, W. *et al.* (2013) 'BRCA1 promoter hypermethylation, 53BP1 protein expression and PARP-1 activity as biomarkers of DNA repair deficit in breast cancer', *BMC Cancer*, 13, pp. 1–11. doi: 10.1186/1471-2407-13-523.
Ji, J. *et al.* (2017) 'Phosphorylated fraction of H2AX as a measurement for DNA damage in cancer cells and potential applications of a novel assay', *PLoS ONE*, 12(2), pp. 1–18. doi: 10.1371/journal.pone.0171582.
Kang, S. (2015) 'Neoadjuvant chemotherapy for ovarian cancer: Do we have enough evidence?', *The Lancet*, 386(9990), pp. 223–224. doi: 10.1016/S0140-6736(14)62259-5.
Kapeleris, J. *et al.* (2018) 'The prognostic role of circulating tumor cells (CTCs) in lung cancer', *Frontiers in Oncology*, 8(AUG), pp. 1–13. doi: 10.3389/fonc.2018.00311.
Katopodis, P. *et al.* (2019) 'Kinase inhibitors and ovarian cancer', *Cancers*, 11(9), pp. 1–17. doi: 10.3390/cancers11091357.
Katsuta, E. *et al.* (2018) *Abstract 3216: H2AX is a novel prognostic marker of breast cancer*, *American Association for Cancer Research*. doi: 10.1158/1538-7445.AM2018-3216 Published July 2018.
Khoo, B. L. *et al.* (2016) 'Liquid biopsy and therapeutic response: Circulating tumor cell cultures for evaluation of anticancer treatment', *Science Advances*, 2(7), pp. 1–15. doi: 10.1126/sciadv.1600274.
Kim, S. *et al.* (2003) 'BRCA status, molecular markers, and clinical variables in early, conservatively managed breast cancer', *Breast Journal*, 9(3), pp. 167–174. doi: 10.1046/j.1524-4741.2003.09307.x.
Kimura, S. and Suzuki, T. (2009) 'Fine-tuning of the ribosomal decoding center by conserved methyl-modifications in the Escherichia coli 16S rRNA', *Nucleic Acids Research*, 38(4), pp. 1341–1352. doi: 10.1093/nar/gkp1073.
Klein, H. L. (2008) 'The consequences of Rad51 overexpression for normal and tumor cells', *DNA Repair*, 7(5), pp. 686–693. doi: 10.1016/j.dnarep.2007.12.008.
Krebs, M. G. *et al.* (2010) 'Circulating tumour cells: Their utility in cancer management and predicting outcomes', *Therapeutic Advances in Medical Oncology*, 2(6), pp. 351–365. doi: 10.1177/1758834010378414.
Krebs, M. G. *et al.* (2014) 'Molecular analysis of circulating tumour cells - Biology and biomarkers', *Nature Reviews Clinical Oncology*, 11(3), pp. 129–144. doi: 10.1038/nrclinonc.2013.253.
Kristeleit, R. *et al.* (2021) '1Rucaparib versus chemotherapy in patients with advanced, relapsed ovarian cancer and a deleterious BRCA mutation: efficacy and safety from ARIEL4, a randomized phase III study', *Gynecologic Oncology*, 162, pp. S3–S4. doi: 10.1016/s0090-8258(21)00656-9.
Kukolj, E. *et al.* (2017) 'PARP inhibition causes premature loss of cohesion in cancer cells',

Oncotarget, 8(61), pp. 103931–103951. doi: 10.18632/oncotarget.21879.
Kummar, S. *et al.* (2011) 'Phase I study of PARP inhibitor ABT-888 in combination with topotecan in adults with refractory solid tumors and lymphomas', *Cancer Research*, 71(17), pp. 5626–5634. doi: 10.1158/0008-5472.CAN-11-1227.
Kuo, L. J. and Yang, L. X. (2008) 'γ-H2AX- A novel biomaker for DNA double-strand breaks', *In Vivo*, 22(3), pp. 305–310.
Kurman, R. J. and Shih, I. M. (2016) 'The dualistic model of ovarian carcinogenesis revisited, revised, and expanded', *American Journal of Pathology*, 186(4), pp. 733–747. doi: 10.1016/j.ajpath.2015.11.011.
Kustanovich, A. *et al.* (2019) 'Life and death of circulating cell-free DNA', *Cancer Biology and Therapy*, 20(8), pp. 1057–1067. doi: 10.1080/15384047.2019.1598759.
Kyo, S. *et al.* (2020) 'The fallopian tube as origin of ovarian cancer: Change of diagnostic and preventive strategies', *Cancer Medicine*, 9(2), pp. 421–431. doi: 10.1002/cam4.2725.
Lal, A. *et al.* (2009) 'MiR-24-mediated downregulation of H2AX suppresses DNA repair in terminally differentiated blood cells', *Nature Structural and Molecular Biology*, 16(5), pp. 492–498. doi: 10.1038/nsmb.1589.
Lamond, A. I. *et al.* (2018) 'Proteome-wide analysis of protein abundance and turnover remodelling during oncogenic transformation of human breast epithelial cells [version 1; referees: 2 approved, 1 approved with reservations]', *Wellcome Open Research*, 3(May), pp. 1–48. doi: 10.12688/wellcomeopenres.14392.1.
Langelier, M. *et al.* (2012) 'Structural Basis for DNA', *Structure*, 728(May), pp. 728–733.
Lanman, R. B. *et al.* (2015) 'Analytical and clinical validation of a digital sequencing panel for quantitative, highly accurate evaluation of cell-free circulating tumor DNA', *PLoS ONE*, 10(10), pp. 1–27. doi: 10.1371/journal.pone.0140712.
Lapytsko, A. *et al.* (2015) 'FoCo: A simple and robust quantification algorithm of nuclear foci', *BMC Bioinformatics*, 16(1), pp. 17–19. doi: 10.1186/s12859-015-0816-5.
Launonen, V. *et al.* (1998) 'Chromosome 11q22.3-q25 LOH in ovarian cancer: Association with a more aggressive disease course and involved subregions', *Gynecologic Oncology*, 71(2), pp. 299–304. doi: 10.1006/gyno.1998.5186.
Launonen, V. *et al.* (2000) 'and 17 in Ovarian Cancer : Correlation To Clinicopathological Variables', *Cancer Genetics and Cytogenetics*, 122, pp. 49–54.
Ledermann, J. *et al.* (2012) 'Olaparib Maintenance Therapy in Patients With Platinum-Sensitive Relapsed Serous Ovarian Cancer', *Obstetrical & Gynecological Survey*, 69(10), pp. 594–596. doi: 10.1097/ogx.0000000000000107.
Ledermann, J. *et al.* (2014) 'Olaparib Maintenance Therapy in Patients With Platinum-Sensitive Relapsed Serous Ovarian Cancer', *Obstetrical & Gynecological Survey*, 69(10), pp. 594–596. doi: 10.1097/ogx.0000000000000107.
Ledermann, J. A. *et al.* (2020) 'Rucaparib for patients with platinum-sensitive, recurrent ovarian carcinoma (ARIEL3): post-progression outcomes and updated safety results from a randomised, placebo-controlled, phase 3 trial', *The Lancet Oncology*, 21(5), pp. 710–722. doi: 10.1016/S1470-2045(20)30061-9.
Ledermann, J. A., Drew, Y. and Kristeleit, R. S. (2016) 'Homologous recombination deficiency and ovarian cancer', *European Journal of Cancer*, 60, pp. 49–58. doi: 10.1016/j.ejca.2016.03.005.
Lee, Y. W., Ha, M. S. and Kim, Y. K. (2001) 'H2O2-induced cell death in human glioma cells: Role of lipid peroxidation and PARP activation', *Neurochemical Research*, 26(4), pp. 337–343. doi: 10.1023/A:1010993428770.
Leung, A. W. Y. *et al.* (2016) 'Synthetic lethality in lung cancer and translation to clinical therapies', *Molecular Cancer*, 15(1), pp. 1–16. doi: 10.1186/s12943-016-0546-y.
Li, C. *et al.* (2006) 'Genetic variants of the ADPRT, XRCC1 and APE1 genes and risk of

cutaneous melanoma', *Carcinogenesis*, 27(9), pp. 1894–1901. doi: 10.1093/carcin/bgl042.
Li, M. *et al.* (2016) ' 53 BP 1 ablation rescues genomic instability in mice expressing " RING -less" BRCA 1 ', *EMBO reports*, 17(11), pp. 1532–1541. doi: 10.15252/embr.201642497.
Li, N. F. *et al.* (2007) 'Human ovarian surface epithelial cells immortalized with hTERT maintain functional pRb and p53 expression', *Cell Proliferation*, 40(5), pp. 780–794. doi: 10.1111/j.1365-2184.2007.00462.x.
Lidder, P. and Sonnino, A. (2012) 'Chapter 1 - Biotechnologies for the Management of Genetic Resources for Food and Agriculture', *ELSEVIER*, 78, pp. 1–167. doi: https://doi.org/10.1016/B978-0-12-394394-1.00001-8.
Liede, A. *et al.* (2002) 'Contribution of BRCA1 and BRCA2 mutations to breast and ovarian cancer in Pakistan', *American Journal of Human Genetics*, 71(3), pp. 595–606. doi: 10.1086/342506.
Lim, D. S. and Hasty, P. (1996) 'A mutation in mouse rad51 results in an early embryonic lethal that is suppressed by a mutation in p53.', *Molecular and Cellular Biology*, 16(12), pp. 7133–7143. doi: 10.1128/mcb.16.12.7133.
Liu, W. *et al.* (2017) 'A systems biology approach to identify microRNAs contributing to cisplatin resistance in human ovarian cancer cells', *Molecular BioSystems*, 13(11), pp. 2268–2276. doi: 10.1039/c7mb00362e.
Lord, C. J. and Ashworth, A. (2012a) 'The DNA damage response and cancer therapy', *Nature*, 481(7381), pp. 287–294. doi: 10.1038/nature10760.
Lord, C. J. and Ashworth, A. (2012b) 'The DNA damage response and cancer therapy', *Nature*, 481(7381), pp. 287–294. doi: 10.1038/nature10760.
Lord, C. J. and Ashworth, A. (2017) 'PARP inhibitors: Synthetic lethality in the clinic', *Science*, 355(6330), pp. 1152–1158. doi: 10.1126/science.aam7344.
Lorente, D., Mateo, J. and de Bono, J. S. (2014) 'Molecular Characterization and Clinical Utility of Circulating Tumor Cells in the Treatment of Prostate Cancer', *American Society of Clinical Oncology Educational Book*, (34), pp. e197–e203. doi: 10.14694/edbook_am.2014.34.e197.
Loret, N. *et al.* (2019) 'The role of epithelial-to-mesenchymal plasticity in ovarian cancer progression and therapy resistance', *Cancers*, 11(6), pp. 1–22. doi: 10.3390/cancers11060838.
Lu, Z. Y. *et al.* (2012) 'SNAI1 overexpression induces stemness and promotes ovarian cancer cell invasion and metastasis', *Oncology Reports*, 27(5), pp. 1587–1591. doi: 10.3892/or.2012.1685.
Ludwig, N. *et al.* (2016) 'Distribution of miRNA expression across human tissues', *Nucleic Acids Research*, 44(8), pp. 3865–3877. doi: 10.1093/nar/gkw116.
Mah, L. J., El-Osta, A. and Karagiannis, T. C. (2010) 'γh2AX: A sensitive molecular marker of DNA damage and repair', *Leukemia*, 24(4), pp. 679–686. doi: 10.1038/leu.2010.6.
Mahdian-shakib, A. *et al.* (2016) 'Differential role of microRNAs in prognosis, diagnosis, and therapy of ovarian cancer', *Biomedicine and Pharmacotherapy*, 84, pp. 592–600. doi: 10.1016/j.biopha.2016.09.087.
Mari, R. *et al.* (2019) 'Liquid biopsies for ovarian carcinoma: How blood tests may improve the clinical management of a deadly disease', *Cancers*, 11(6), pp. 1–23. doi: 10.3390/cancers11060774.
McCluggage, W. G. (2011) 'Morphological subtypes of ovarian carcinoma: A review with emphasis on new developments and pathogenesis', *Pathology*, 43(5), pp. 420–432. doi: 10.1097/PAT.0b013e328348a6e7.
McGlynn, P. and Lloyd, R. G. (2002) 'Recombinational repair and restart of damaged replication forks', *Nature Reviews Molecular Cell Biology*, 3(11), pp. 859–870. doi: 10.1038/nrm951.

Mcvey, M. *et al.* (2017) 'MMEJ repair of double-strand breaks: deleted sequences and alternative endings', *Trends Genet.*, 24(11), pp. 529–538. doi: 10.1016/j.tig.2008.08.007.MMEJ.
Medicalexpress (2017) *N*. Available at: https://medicalxpress.com/news/2016-06-liquid-biopsy-techniquesedge-cancer.html (Accessed: 29 May 2020).
Mehta, A. and Haber, J. E. (2014) 'Sources of DNA double-strand breaks and models of recombinational DNA repair', *Cold Spring Harbor Perspectives in Biology*, 6(9). doi: 10.1101/cshperspect.a016428.
Mei, L. *et al.* (2015) 'Phospho-histone H2AX is a diagnostic and prognostic marker for epithelial ovarian cancer', *International Journal of Clinical and Experimental Pathology*, 8(5), pp. 5597–5602.
Miyamoto, D. T. *et al.* (2012) 'Androgen receptor signaling in circulating tumor cells as a marker of hormonally responsive prostate cancer', *Cancer Discovery*, 2(11), pp. 995–1003. doi: 10.1158/2159-8290.CD-12-0222.
Moujaber, T. *et al.* (2018) 'BRAF Mutations in Low-Grade Serous Ovarian Cancer and Response to BRAF Inhibition', *JCO Precision Oncology*, (2), pp. 1–14. doi: 10.1200/po.17.00221.
Mouliere, F. *et al.* (2018) 'Enhanced detection of circulating tumor DNA by fragment size analysis', *Science Translational Medicine*, 10(466), pp. 1–14. doi: 10.1126/scitranslmed.aat4921.
Moynahan, M. E. and Jasin, M. (2010) 'Mitotic homologous recombination maintains genomic stability and suppresses tumorigenesis', *Nature Reviews Molecular Cell Biology*, 11(3), pp. 196–207. doi: 10.1038/nrm2851.
Mukherjee, B. *et al.* (2006) 'DNA-PK phosphorylates histone H2AX during apoptotic DNA fragmentation in mammalian cells', *DNA Repair*, 5(5), pp. 575–590. doi: 10.1016/j.dnarep.2006.01.011.
Munzone, E. *et al.* (2010) 'Changes of HER2 status in circulating tumor cells compared with the primary tumor during treatment for advanced breast cancer', *Clinical Breast Cancer*, 10(5), pp. 392–397. doi: 10.3816/CBC.2010.n.052.
Murray, A. J. and Davies, D. M. (2013) 'The genetics of breast cancer', *Surgery (United Kingdom)*, 31(1), pp. 1–3. doi: 10.1016/j.mpsur.2012.10.019.
National Institutes of Health (2015) 'Genetics Home Reference BRCA2 gene', *U.S. National Library of Medicine*. Available at: https://ghr.nlm.nih.gov/gene/BRCA2#conditions.
Neff, R. T., Senter, L. and Salani, R. (2017) 'BRCA mutation in ovarian cancer: testing, implications and treatment considerations', *Therapeutic Advances in Medical Oncology*, 9(8), pp. 519–531. doi: 10.1177/ 1758834017714993.
Nepomuceno, T. C. *et al.* (2020) 'PALB2 Variants: Protein Domains and Cancer Susceptibility', *Trends in Cancer*, pp. 1–10. doi: 10.1016/j.trecan.2020.10.002.
Newman, E. A. *et al.* (2015) 'Alternative NHEJ pathway components are therapeutic targets in high-risk neuroblastoma', *Molecular Cancer Research*, 13(3), pp. 470–482. doi: 10.1158/1541-7786.MCR-14-0337.
NHS (2020) *Symptoms*. Available at: https://www.nhs.uk/conditions/ovarian-cancer/symptoms/.
NICE (2011) *Ovarian cancer: recognition and initial management, National Institue for Health and Care Excellence*. Available at: https://www.nice.org.uk/guidance/cg122/chapter/1-guidance (Accessed: 4 July 2021).
NICE (2013) *Familial breast cancer: classification, care and managing breast cancer and related risks in people with a family history of breast cancer, Clinical Guideline CG164*. Available at: https://www.nice.org.uk/guidance/cg164 (Accessed: 8 February 2021).
NIH (2019) *PARP Inhibitors Show Promise as Initial Treatment for Ovarian Cancer*.

Available at: https://www.cancer.gov/news-events/cancer-currents-blog/2019/parp-inhibitors-ovarian-cancer-initial-treatment (Accessed: 10 June 2021).
NIH (2021a) *Assess Gamma H2AX Positivity in Circulating Prostate Cancer Cells Before and After Radium 223*. Available at: https://clinicaltrials.gov/ct2/show/NCT02981797?term=gamma+H2AX&cond=Cancer&draw=2&rank=1 (Accessed: 7 September 2021).
NIH (2021b) *No Title*. Available at: https://clinicaltrials.gov/ct2/results?cond=Ovarian+Cancer&term=rucaparib&cntry=&state=&city=&dist= (Accessed: 4 September 2021).
Nijman, S. M. B. (2011) 'Synthetic lethality: General principles, utility and detection using genetic screens in human cells', *FEBS Letters*, 585(1), pp. 1–6. doi: 10.1016/j.febslet.2010.11.024.
Nile, D. L. *et al.* (2016) 'An evaluation in vitro of PARP-1 inhibitors, rucaparib and olaparib, as radiosensitisers for the treatment of neuroblastoma', *BMC Cancer*, 16(1), pp. 1–13. doi: 10.1186/s12885-016-2656-8.
Novik, K. L. *et al.* (2007) 'Genetic variation in H2AFX contributes to risk of non-Hodgkin lymphoma', *Cancer Epidemiology Biomarkers and Prevention*, 16(6), pp. 1098–1106. doi: 10.1158/1055-9965.EPI-06-0639.
Nowacka-Zawisza, M. *et al.* (2008) 'Dinucleotide repeat polymorphisms of RAD51, BRCA1, BRCA2 gene regions in breast cancer: Original Article', *Pathology International*, 58(5), pp. 275–281. doi: 10.1111/j.1440-1827.2008.02223.x.
O'Donovan, P. J. and Livingston, D. M. (2010) 'BRCA1 and BRCA2: Breast/ovarian cancer susceptibility gene products and participants in DNA double-strand break repair', *Carcinogenesis*, 31(6), pp. 961–967. doi: 10.1093/carcin/bgq069.
O'Driscoll, M. and Jeggo, P. A. (2006) 'The role of double-strand break repair - Insights from human genetics', *Nature Reviews Genetics*, 7(1), pp. 45–54. doi: 10.1038/nrg1746.
O'Neil, N. J., Bailey, M. L. and Hieter, P. (2017) 'Synthetic lethality and cancer', *Nature Reviews Genetics*, 18(10), pp. 613–623. doi: 10.1038/nrg.2017.47.
Ojima, M. *et al.* (2011) 'Persistence of DNA double-strand breaks in normal human cells induced by radiation-induced bystander effect', *Radiation Research*, 175(1), pp. 90–96. doi: 10.1667/RR2223.1.
Olive, P. L. *et al.* (1999) 'The comet assay in clinical practice', *Acta Oncologica*, 38(7), pp. 839–844. doi: 10.1080/028418699432527.
Olive, P. L., Banáth, J. P. and Sinnott, L. T. (2004) 'Phosphorylated histone H2AX in spheroids, tumors, and tissues of mice exposed to etoposide and 3-amino-1,2,4-benzotriazine-1,3-dioxide', *Cancer Research*, 64(15), pp. 5363–5369. doi: 10.1158/0008-5472.CAN-04-0729.
Papadimitriou, M., Mountzios, G. and Papadimitriou, C. A. (2018) 'The role of PARP inhibition in triple-negative breast cancer: Unraveling the wide spectrum of synthetic lethality', *Cancer Treatment Reviews*, 67, pp. 34–44. doi: 10.1016/j.ctrv.2018.04.010.
Paracchini, L., D'incalci, M. and Marchini, S. (2021) 'Liquid biopsy in the clinical management of high-grade serous epithelial ovarian cancer—current use and future opportunities', *Cancers*, 13(10). doi: 10.3390/cancers13102386.
Parris, C. N. *et al.* (2015) 'Enhanced γ-H2AX DNA damage foci detection using multimagnification and extended depth of field in imaging flow cytometry', *Cytometry Part A*, 87(8), pp. 717–723. doi: 10.1002/cyto.a.22697.
Patel, A. G., Sarkaria, J. N. and Kaufmann, S. H. (2011) 'Nonhomologous end joining drives poly(ADP-ribose) polymerase (PARP) inhibitor lethality in homologous recombination-deficient cells', *Proceedings of the National Academy of Sciences of the United States of America*, 108(8), pp. 3406–3411. doi: 10.1073/pnas.1013715108.

Pei, L. *et al.* (2011) 'Overexpression of DEP domain containing mTOR-interacting protein correlates with poor prognosis in differentiated thyroid carcinoma', *Molecular Medicine Reports*, 4(5), pp. 817–823. doi: 10.3892/mmr.2011.503.
Pennington, K. P. *et al.* (2014) 'Germline and somatic mutations in homologous recombination genes predict platinum response and survival in ovarian, fallopian tube, and peritoneal carcinomas', *Clinical Cancer Research*, 20(3), pp. 764–775. doi: 10.1158/1078-0432.CCR-13-2287.
Peterson, T. R. *et al.* (2009) 'DEPTOR Is an mTOR Inhibitor Frequently Overexpressed in Multiple Myeloma Cells and Required for Their Survival', *Cell*, 137(5), pp. 873–886. doi: 10.1016/j.cell.2009.03.046.
Pfisterer, J. *et al.* (2005) 'Combination therapy with gemcitabine and carboplatin in recurrent ovarian cancer', *International Journal of Gynecological Cancer*, 15(SUPPL. 1), pp. 36–41. doi: 10.1111/j.1525-1438.2005.15355.x.
Piha-Paul, S. A. *et al.* (2014) 'Advanced gynecologic malignancies treated with a combination of the VEGF inhibitor bevacizumab and the mTOR inhibitor temsirolimus', *Oncotarget*, 5(7), pp. 1846–1855. doi: 10.18632/oncotarget.1834.
Ping Lin, Z. *et al.* (2018) 'Combination of triapine, olaparib, and cediranib suppresses progression of BRCA-wild type and PARP inhibitor-resistant epithelial ovarian cancer', *PLoS ONE*, 13(11), pp. 1–24. doi: 10.1371/journal.pone.0207399.
Pisano, M. *et al.* (2000) 'Identification of a founder BRCA2 mutation in Sardinia', *British Journal of Cancer*, 82(3), pp. 553–559. doi: 10.1054/bjoc.1999.0963.
Plummer, R. *et al.* (2013) 'A phase II study of the potent PARP inhibitor, Rucaparib (PF-01367338, AG014699), with temozolomide in patients with metastatic melanoma demonstrating evidence of chemopotentiation', *Cancer Chemotherapy and Pharmacology*, 71(5), pp. 1191–1199. doi: 10.1007/s00280-013-2113-1.
Podhorecka, M., Skladanowski, A. and Bozko, P. (2010) 'H2AX phosphorylation: Its role in DNA damage response and cancer therapy', *Journal of Nucleic Acids*, 2010. doi: 10.4061/2010/920161.
Poveda, A. *et al.* (2011) 'Circulating tumor cells predict progression free survival and overall survival in patients with relapsed/recurrent advanced ovarian cancer', *Gynecologic Oncology*, 122(3), pp. 567–572. doi: 10.1016/j.ygyno.2011.05.028.
Powell, S. N. and Kachnic, L. A. (2003) 'Roles of BRCA1 and BRCA2 in homologous recombination, DNA replication fidelity and the cellular response to ionizing radiation', *Oncogene*, 22(37 REV. ISS. 3), pp. 5784–5791. doi: 10.1038/sj.onc.1206678.
Prakash, R. *et al.* (2015) 'Homologous recombination and human health: The roles of BRCA1, BRCA2, and associated proteins', *Cold Spring Harbor Perspectives in Biology*, 7(4), pp. 1–27. doi: 10.1101/cshperspect.a016600.
Protein Atlas (2021) *Pr*. Available at: https://www.proteinatlas.org/ (Accessed: 20 January 2020).
Pruim, R. J. *et al.* (2011) 'LocusZoom: Regional visualization of genome-wide association scan results', *Bioinformatics*, 27(13), pp. 2336–2337. doi: 10.1093/bioinformatics/btq419.
R Project (2021) *No Title*. Available at: http:///www.r-project.org/.
Ramus, S. J. *et al.* (2003) 'BRCA1/2 mutation status influences somatic genetic progression in inherited and sporadic epithelial ovarian cancer cases', *Cancer Research*, 63(2), pp. 417–423.
Rastogi, R. P. *et al.* (2010) 'Molecular mechanisms of ultraviolet radiation-induced DNA damage and repair', *Journal of Nucleic Acids*, 2010. doi: 10.4061/2010/592980.
Rauh-Hein, A. *et al.* (2015) 'NACT compared with PDS in EOC', *Clinics and Research in Hepatology and Gastroenterology*, 39(1), pp. 9–19. doi: 10.1001/jamaoncol.2016.4411.Neoadjuvant.

Reactome (2020) *No Title*. Available at: https://reactome.org/PathwayBrowser/#/ (Accessed: 12 October 2020).
Reczek, C. R. *et al.* (2013) 'The interaction between CtIP and BRCA1 is not essential for resection-mediated DNA repair or tumor suppression', *Journal of Cell Biology*, 201(5), pp. 693–707. doi: 10.1083/jcb.201302145.
Redon, C. E. *et al.* (2012) 'γ-H2AX and other histone post-translational modifications in the clinic', *Biochimica et Biophysica Acta - Gene Regulatory Mechanisms*, 1819(7), pp. 743–756. doi: 10.1016/j.bbagrm.2012.02.021.
Rigakos, G. and Razis, E. (2012) 'BRCAness: Finding the Achilles Heel in Ovarian Cancer', *The Oncologist*, 17(7), pp. 956–962. doi: 10.1634/theoncologist.2012-0028.
Risch, H. A. *et al.* (2001) 'Prevalence and penetrance of germline BRCA1 and BRCA2 mutations in a population series of 649 women with ovarian cancer', *American Journal of Human Genetics*, 68(3), pp. 700–710. doi: 10.1086/318787.
Rogakou, E. P. *et al.* (1999) 'Megabase chromatin domains involved in DNA double-strand breaks in vivo', *Journal of Cell Biology*, 146(5), pp. 905–915. doi: 10.1083/jcb.146.5.905.
Rogers-Broadway, K. R. *et al.* (2016) 'Differential effects of rapalogues, dual kinase inhibitors on human ovarian carcinoma cells in vitro', *International Journal of Oncology*, 49(1), pp. 133–143. doi: 10.3892/ijo.2016.3531.
Rogers-Broadway, K. R. *et al.* (2019) 'Differential expression of mTOR components in endometriosis and ovarian cancer: Effects of rapalogues and dual kinase inhibitors on mTORC1 and mTORC2 stoichiometry', *International Journal of Molecular Medicine*, 43(1), pp. 47–56. doi: 10.3892/ijmm.2018.3967.
Rojas, V. *et al.* (2016) 'Molecular characterization of epithelial ovarian cancer: Implications for diagnosis and treatment', *International Journal of Molecular Sciences*, 17(12). doi: 10.3390/ijms17122113.
Rojo, F. *et al.* (2012) 'Nuclear PARP-1 protein overexpression is associated with poor overall survival in early breast cancer', *Annals of Oncology*, 23(5), pp. 1156–1164. doi: 10.1093/annonc/mdr361.
Rossi, M. and La Vecchia, C. (2014) 'Flavonoids and the risk of ovarian cancer', *American Journal of Clinical Nutrition*, 100(5), pp. 1217–1219. doi: 10.3945/ajcn.114.098285.
Rothkamm, K. *et al.* (2015) 'Review Article,DNA Damage Foci: Meaning and Significance', *Environmental and Molecular Mutagenesis*, 56(6), pp. 491–504. doi: 10.1002/em.21944.
Russo, A. *et al.* (2009) 'Hereditary ovarian cancer', *Critical Reviews in Oncology/Hematology*, 69(1), pp. 28–44. doi: 10.1016/j.critrevonc.2008.06.003.
Ryan, E. L., Hollingworth, R. and Grand, R. J. (2016) 'Activation of the DNA damage response by RNA viruses', *Biomolecules*, 6(1), pp. 2–24. doi: 10.3390/biom6010002.
Saggese, M. (2018) 'A novel method to quantify gamma H2AX foci in circulating tumour cells in patients receiving chemotherapy for colorectal cancer', (November). Available at: http://discovery.ucl.ac.uk/id/eprint/10049500.
Sakai, W. *et al.* (2009) 'Functional restoration of BRCA2 protein by secondary BRCA2 mutations in BRCA2-mutated ovarian carcinoma', *Cancer Research*, 69(16), pp. 6381–6386. doi: 10.1158/0008-5472.CAN-09-1178.
Sakai, W. *et al.* (2010) 'NIH Public Access', 69(16), pp. 6381–6386. doi: 10.1158/0008-5472.CAN-09-1178.Functional.
Saravi, S. *et al.* (2020) 'H2A Histone Family Member X (H2AX) Is Upregulated in Ovarian Cancer and Demonstrates Utility as a Prognostic Biomarker in Terms of Overall Survival', *Journal of Clinical Medicine*, 9(9), p. 2844. doi: 10.3390/jcm9092844.
Saravi, S. *et al.* (2021) 'Preclinical Studies on the Effect of Rucaparib in Ovarian Cancer : Impact of BRCA2 Status', pp. 1–13.
Schneck, H. *et al.* (2015) 'EpCAM-independent enrichment of circulating tumor cells in

metastatic breast cancer', *PLoS ONE*, 10(12), pp. 1–23. doi: 10.1371/journal.pone.0144535.
Sedelnikova, O. A. *et al.* (2004) 'Senescing human cells and ageing mice accumulate DNA lesions with unrepairable double-strand breaks', *Nature Cell Biology*, 6(2), pp. 168–170. doi: 10.1038/ncb1095.
Sedelnikova, O. A. and Bonner, W. M. (2006) 'γH2AX in cancer cells: A potential biomarker for cancer diagnostics, prediction and recurrence', *Cell Cycle*, 5(24), pp. 2909–2913. doi: 10.4161/cc.5.24.3569.
Sekiguchi, J. A. M. and Ferguson, D. O. (2006) 'DNA double-strand break repair: A relentless hunt uncovers new prey', *Cell*, 124(2), pp. 260–262. doi: 10.1016/j.cell.2006.01.010.
Sevinc, A. *et al.* (2007) 'Benign causes of increased serum CA-125 concentration', *Lancet Oncology*, 8(12), pp. 1054–1055. doi: 10.1016/S1470-2045(07)70357-1.
Shah, K. *et al.* (2015) 'γH2AX expression in cytological specimens as a biomarker of response to radiotherapy in solid malignancies', *Diagnostic Cytopathology*, 44(2), pp. 141–146.
Sharma, V. *et al.* (2016) 'Methods Used in Economic Evaluations of Testing and Diagnosis for Ovarian Cancer: A Systematic Review', *International Journal of Gynecological Cancer*, 26(5), pp. 865–872. doi: 10.1097/IGC.0000000000000699.
Smirnov, D. A. *et al.* (2005) 'Global gene expression profiling of circulating tumor cells', *Cancer Research*, 65(12), pp. 4993–4997. doi: 10.1158/0008-5472.CAN-04-4330.
Smits, S. *et al.* (2017) 'Influences on anticipated time to ovarian cancer symptom presentation in women at increased risk compared to population risk of ovarian cancer', *BMC Cancer*, 17(1), pp. 1–11. doi: 10.1186/s12885-017-3835-y.
Solier, S. *et al.* (2009) 'Death Receptor-Induced Activation of the Chk2- and Histone H2AX-Associated DNA Damage Response Pathways', *Molecular and Cellular Biology*, 29(1), pp. 68–82. doi: 10.1128/mcb.00581-08.
Solier, S. *et al.* (2012) 'Heat shock protein 90α (HSP90α), a substrate and chaperone of DNA-PK necessary for the apoptotic response', *Proceedings of the National Academy of Sciences of the United States of America*, 109(32), pp. 12866–12872. doi: 10.1073/pnas.1203617109.
Solier, S. and Pommier, Y. (2011) 'MDC1 cleavage by caspase-3: A novel mechanism for inactivating the DNA damage response during apoptosis', *Cancer Research*, 71(3), pp. 906–913. doi: 10.1158/0008-5472.CAN-10-3297.
Solier, S. and Pommier, Y. (2014) 'The nuclear γ-H2AX apoptotic ring: Implications for cancers and autoimmune diseases', *Cellular and Molecular Life Sciences*, 71(12), pp. 2289–2297. doi: 10.1007/s00018-013-1555-2.
Srinivas, K. P. *et al.* (2016) 'DEPTOR promotes survival of cervical squamous cell carcinoma cells and its silencing induces apoptosis through downregulating PI3K/AKT and by up-regulating p38 MAP kinase', *Oncotarget*, 7(17), pp. 24154–24171. doi: 10.18632/oncotarget.8131.
Srivastava, N. *et al.* (2008) 'Copy number alterations of the H2AFX gene in sporadic breast cancer patients', *Cancer Genetics and Cytogenetics*, 180(2), pp. 121–128. doi: 10.1016/j.cancergencyto.2007.09.024.
Srivastava, N. *et al.* (2009) 'Role of H2AX in DNA damage response and human cancers', *Mutation Research - Reviews in Mutation Research*, 681(2–3), pp. 180–188. doi: 10.1016/j.mrrev.2008.08.003.
Staff, S. *et al.* (2014) 'Quantitative analysis of γ-H2AX and p53 nuclear expression levels in ovarian and fallopian tube epithelium from risk-reducing salpingo-oophorectomies in BRCA1 and BRCA2 mutation carriers', *International Journal of Gynecological Pathology*, 33(3), pp. 309–316. doi: 10.1097/PGP.0b013e31829c673b.

Steel, C. M. (2003) 'BRCA1 and BRCA2 mutations in Scotland and Northern Ireland', *British Journal of Cancer*, 88(8), pp. 1256–1262. doi: 10.1038/sj.bjc.6600840.
Stroun, M. *et al.* (1989) 'Neoplastic characteristics of the DNA found in the plasma of cancer patients', *ONCOLOGY*, 46(5), pp. 318–322. doi: 10.1159/000226740.
Su, H. *et al.* (2017) 'Arabidopsis RAD51, RAD51C and XRCC3 proteins form a complex and facilitate RAD51 localization on chromosomes for meiotic recombination', *PLoS Genetics*, 13(5), pp. 1–27. doi: 10.1371/journal.pgen.1006827.
Sudlow, C. *et al.* (2015) 'UK Biobank: An Open Access Resource for Identifying the Causes of a Wide Range of Complex Diseases of Middle and Old Age', *PLoS Medicine*, 12(3), pp. 1–10. doi: 10.1371/journal.pmed.1001779.
Sun, J. *et al.* (2013) 'Effects of nanotoxicity on female reproductivity and fetal development in animal models', *International Journal of Molecular Sciences*, 14(5), pp. 9319–9337. doi: 10.3390/ijms14059319.
Sun, Z. *et al.* (2016) 'Estimating the Prevalence of Ovarian Cancer Symptoms in Women Aged 50 Years or Older: Problems and Possibilities', *American Journal of Epidemiology*, 184(9), pp. 670–680. doi: 10.1093/aje/kww086.
Tan, Y. and Wu, H. (2018) 'The significant prognostic value of circulating tumor cells in colorectal cancer: A systematic review and meta-analysis', *Current Problems in Cancer*, 42(1), pp. 95–106. doi: 10.1016/j.currproblcancer.2017.11.002.
Tarsounas, M., Davies, A. A. and West, S. C. (2004) 'RAD51 localization and activation following DNA damage', *Philosophical Transactions of the Royal Society B: Biological Sciences*, 359(1441), pp. 87–93. doi: 10.1098/rstb.2003.1368.
Telli, M. L. and Ford, J. M. (2010) 'Novel treatment approaches for triple-negative breast cancer', *Clinical Breast Cancer*, 10(SUPPL. 1), pp. E16–E22. doi: 10.3816/CBC.2010.s.003.
The Cancer Genome Atlas Research Network (2011) 'Integrated Genomic Analyses of Ovarian Carcinoma The Cancer Genome Atlas Research Network', *Nature*, 474(7353), pp. 609–615. doi: 10.1038/nature10166.Integrated.
Thorlacius, S. *et al.* (1997) 'Study of a single BRCA2 mutation with high carrier frequency in a small population', *American Journal of Human Genetics*, 60(5), pp. 1079–1084.
Tortora, G. J. and Derrickson, B. (2017) *Tortora's principles of anatomy and physiology*. Global edi.
Tortora, G. J., Derrickson, B. and Nielsen, M. (2011) *Principles of anatomy & physiology: Vol. 1, Organization, support and movement, and control systems of the human body*. 13th edn. International student version.
Toss, A. *et al.* (2014) 'CTC enumeration and characterization: Moving toward personalized medicine', *Annals of Translational Medicine*, 2(11). doi: 10.3978/j.issn.2305-5839.2014.09.06.
Towler, W. I. *et al.* (2013) 'Analysis of BRCA1 Variants in Double-Strand Break Repair by Homologous Recombination and Single-Strand Annealing', *Human Mutation*, 34(3), pp. 439–445. doi: 10.1002/humu.22251.
Turinetto, V. and Giachino, C. (2015) 'Survey and summary multiple facets of histone variant H2AX: A DNA double-strand-break marker with several biological functions', *Nucleic Acids Research*, 43(5), pp. 2489–2498. doi: 10.1093/nar/gkv061.
Turner, N., Tutt, A. and Ashworth, A. (2004) 'Hallmarks of "BRCAness" in Sporadic Cancers', *Nat Rev Cancer*, 4(10), pp. 814–9. doi: 10.1038/nrc1457.
UCSC Xena (2021) *No Title*. Available at: https://xena.ucsc.edu/ (Accessed: 19 January 2020).
UniProt (2020) *UniProtKB - P16104 (H2AX_HUMAN)*. Available at: https://www.uniprot.org/uniprot/P16104 (Accessed: 10 April 2020).
Valdiglesias, V. *et al.* (2013) 'γH2AX as a marker of DNA double strand breaks and genomic

instability in human population studies', *Mutation Research - Reviews in Mutation Research*, 753(1), pp. 24–40. doi: 10.1016/j.mrrev.2013.02.001.
Vaurijoux, A. *et al.* (2017) 'Transmission of persistent ionizing radiation-induced foci through cell division in human primary cells', *Mutation Research - Fundamental and Molecular Mechanisms of Mutagenesis*, 797–799, pp. 15–25. doi: 10.1016/j.mrfmmm.2017.03.003.
Venkitaraman, A. R. (2001) 'Functions of BRCA1 and BRCA2 in the biological response to DNA damage', *Journal of Cell Science*, 114(20), pp. 3591–3598.
Venkitaraman, A. R. (2004) 'Tracing the network connecting BRCA and Fanconi anaemia proteins', *Nature Reviews Cancer*, 4(4), pp. 266–276. doi: 10.1038/nrc1321.
Verhoog, L. C. *et al.* (2001) 'Large regional differences in the frequency of distinct BRCA1/BRCA2 mutations in 517 Dutch breast and/or ovarian cancer families', *European Journal of Cancer*, 37(16), pp. 2082–2090. doi: 10.1016/S0959-8049(01)00244-1.
Vymetalkova, V. *et al.* (2018) 'Circulating cell-free dna and colorectal cancer: A systematic review', *International Journal of Molecular Sciences*, 19(11). doi: 10.3390/ijms19113356.
Wang, L. H. *et al.* (2010a) 'Monitoring drug-induced γH2AX as a pharmacodynamic biomarker in individual circulating tumor cells', *Clinical Cancer Research*, 16(3), pp. 1073–1084. doi: 10.1158/1078-0432.CCR-09-2799.
Wang, L. H. *et al.* (2010b) 'Monitoring drug-induced γH2AX as a pharmacodynamic biomarker in individual circulating tumor cells', *Clinical Cancer Research*, 16(3), pp. 1073–1084. doi: 10.1158/1078-0432.CCR-09-2799.
Wang, L. H. *et al.* (2013) 'Abstract 1472: Assessment of CTC-based pharmacodynamic biomarkers in NCI clinical trials of targeted anticancer therapeutics.', *Cancer research*, 73(8), pp. 1472–1472. doi: 10.1158/1538-7445.AM2013-1472.
Webb, P. M. and Jordan, S. J. (2017) 'Epidemiology of epithelial ovarian cancer', *Best Practice and Research: Clinical Obstetrics and Gynaecology*, 41, pp. 3–14. doi: 10.1016/j.bpobgyn.2016.08.006.
WHEC (2014) *Current Ovarian Cancer Management*. Available at: http://www.womenshealthsection.com/content/gyno/gyno026.php3.
Wicha, M. S. and Hayes, D. F. (2011) 'Circulating tumor cells: Not all detected cells are bad and not all bad cells are detected', *Journal of Clinical Oncology*, 29(12), pp. 1508–1511. doi: 10.1200/JCO.2010.34.0026.
WorldAtlas (2017) *Countries With The Highest Incidence Of Ovarian Cancer In The World*. Available at: https://www.worldatlas.com/articles/countries-with-the-highest-incidence-of-ovarian-cancer-in-the-world.html (Accessed: 3 July 2021).
Xia, B. *et al.* (2006) 'Control of BRCA2 Cellular and Clinical Functions by a Nuclear Partner, PALB2', *Molecular Cell*, 22(6), pp. 719–729. doi: 10.1016/j.molcel.2006.05.022.
Ximbio (2018a) *PEO1 Cell Line*. Available at: https://ximbio.com/reagent/151672/peo1-cell-line#references (Accessed: 21 October 2018).
Ximbio (2018b) *PEO4 Cell Line*. Available at: https://ximbio.com/reagent/151673/peo4-cell-line (Accessed: 21 October 2018).
Xu, Y. *et al.* (2017) '53BP1 and BRCA1 control pathway choice for stalled replication restart', *eLife*, 6, pp. 1–24. doi: 10.7554/eLife.30523.
Yelamos, J. *et al.* (2011) 'PARP-1 and PARP-2: New players in tumour development.', *American journal of cancer research*, 1(3), pp. 328–346. Available at: http://www.ncbi.nlm.nih.gov/pubmed/21968702%0Ahttp://www.pubmedcentral.nih.gov/articlerender.fcgi?artid=PMC3180065.
Yun, M. H. and Hiom, K. (2009) 'CtIP-BRCA1 modulates the choice of DNA double-strand-break repair pathway throughout the cell cycle', *Nature*, 459(7245), pp. 460–463. doi: 10.1038/nature07955.

Zelensky, A., Kanaar, R. and Wyman, C. (2014) 'Mediators of homologous DNA pairing', *Cold Spring Harbor Perspectives in Biology*, 6(12), pp. 1–16. doi: 10.1101/cshperspect.a016451.
Zhang, F. *et al.* (2015) 'Poly(ADP-Ribose) Mediates the BRCA2-Dependent Early DNA Damage Response', *Cell Reports*, 13(4), pp. 678–689. doi: 10.1016/j.celrep.2015.09.040.
Zhang, L. *et al.* (2016) 'Linked references are available on JSTOR for this article : Role of BAX in the Apoptotic Response to Anticancer Agents', 290(5493), pp. 989–992.
Zhang, X. *et al.* (2018) 'Analysis of Circulating Tumor Cells in Ovarian Cancer and Their Clinical Value as a Biomarker', *Cellular Physiology and Biochemistry*, 48(5), pp. 1983–1994. doi: 10.1159/000492521.
Zhou, Y. *et al.* (2015) 'Prognostic value of circulating tumor cells in ovarian cancer: A meta-analysis', *PLoS ONE*, 10(6), pp. 1–14. doi: 10.1371/journal.pone.0130873.